Northumbria Research Link

Citation: Vlasits, Tamas (1997) Modelling and application of a cross-aperture coupled single feed circularly polarised patch antenna. Doctoral thesis, University of Northumbria at Newcastle.

This version was downloaded from Northumbria Research Link: http://nrl.northumbria.ac.uk/id/eprint/15678/

Northumbria University has developed Northumbria Research Link (NRL) to enable users to access the University's research output. Copyright © and moral rights for items on NRL are retained by the individual author(s) and/or other copyright owners. Single copies of full items can be reproduced, displayed or performed, and given to third parties in any format or medium for personal research or study, educational, or not-for-profit purposes without prior permission or charge, provided the authors, title and full bibliographic details are given, as well as a hyperlink and/or URL to the original metadata page. The content must not be changed in any way. Full items must not be sold commercially in any format or medium without formal permission of the copyright holder. The full policy is available online: http://nrl.northumbria.ac.uk/policies.html

Some theses deposited to NRL up to and including 2006 were digitised by the British Library and made available online through the EThOS e-thesis online service. These records were added to NRL to maintain a central record of the University's research theses, as well as still appearing through the British Library's service. For more information about Northumbria University research theses, please visit University Library Online.

Northumbria University NEWCASTLE

UniversityLibrary

MODELLING AND APPLICATION OF A CROSS-APERTURE COUPLED SINGLE FEED CIRCULARLY POLARISED PATCH ANTENNA

TAMÁS VLASITS

Division of Electrical and Electronic Engineering

School of Engineering

University of Northumbria at Newcastle, UK

This thesis has been submitted to the University of Northumbria at Newcastle for the degree of Doctor of Philosophy

March 1997

ABSTRACT

This thesis presents the results of the research that has been carried out in order to design an improved microstrip antenna for a two-way microwave based digital communication link for communication between a road-side unit and a vehicle. The system is to be used for traffic applications such as automatic motorway tolling.

The research has mainly concentrated on the theoretical and practical investigation of a novel type of circularly polarised (CP) microstrip antenna in order to obtain an in-vehicle unit with simple structure using inexpensive materials, such as the normal fibre-glass printed circuit board. An equivalent modelling circuit has been derived for the proposed cross-aperture coupled patch antenna based on transmission line modelling. The antenna has also been analysed using the resonant cavity method and the results of the two techniques have been compared with each other and with practical and computer simulation results. Since this antenna, as do other single feed CP patches, exhibits insufficient axial ratio bandwidth, the strip-slot-foam-inverted patch construction method has been used to improve the axial ratio performance and allow the manufacturing tolerance of the antenna to be relaxed. Based on this investigation, a novel type of in-vehicle unit antenna has been realised with an appropriate bandwidth, and which requires only inexpensive materials to fabricate. The antenna has then been incorporated in the in-vehicle unit and on test showed superior performance when compared with the previously used dual feed antenna.

Also experiments have been carried out in order to determine the kind of polarisation that should be implemented in the communication system to reduce interference in the traffic environment where strong multi-path reflections occur. It was found that the best option in order to minimise interference is circular polarisation of the same sense for both the vehicle-to-roadside and roadside-to-vehicle links. This allowed the design of a low complexity in-vehicle unit requiring a single diode for both ASK detection and PSK modulation.

As a result of this work research papers have been published in the Microwave Journal (Vol. 38, No7, July 1995), the IEE Electronics Letters (Vol. 32. No7, 28 March 1996 and Vol. 32. No21, 10 October 1996), and in the proceedings of the 24th European Microwave Conference (5-8 September 1994, Nice), the Eight International Conference on Road Traffic Monitoring and Control (23-25 April 1996, London) and the Second and Third Communications Network Symposium (10-11 July 1995, Manchester and 8-9 July 1996, Manchester).

ACKNOWLEDGEMENTS

I would like to express my sincere thanks to my director of studies Professor E. Korolkiewicz, my second supervisor Dr. A. Sambell, and, Mr. Stan Scott for their continued guidance, technical advice and encouragement throughout this project.

Special thanks are also due to Julia Relle and her family for their invaluable support and encouragement throughout my PhD studies.

Finally, I would like to thank my mother and father, to whom I dedicate this achievement, for having the belief and confidence in me, and, for their sacrifices which enabled my education.

ABBREVIATIONS

ADS	Automatic Debiting Systems
ADEPT	Automatic Debiting and Payment for Transport
AR	Axial Ratio
ASK	Amplitude Shift Keying
BER	Bit Error Rate
BW	Bandwidth
CEPT	Committee of European Post and Telecommunications
CP	Circularly Polarised
CRC	Cyclic Redundancy Check
CW	Continuos Wave
DPSK	Differential Phase Shift Keying
DRIVE	Dedicated Road Infrastructure for Vehicle Safety in Europe
DRO	Dielectric Resonator Oscillator
EIRP	Effective Isotropic Radiated Power
ETC	Electronic Toll Collection
HDLC	High-Level Data Link Control
IF	Intermediate Frequency
IRM	Image Rejection Mixer
LHCP	Left-Hand Circularly Polarised
OBU	On-Board Unit
PSK	Phase Shift Keying
RHCP	Right-Hand Circularly Polarised
RSU	Road-Side Unit
SSFIP	Strip-Slot-Foam-Inverted Patch
SWR	Standing Wave Ratio
TSS	Tangential SenSitivity

TABLE OF CONTENTS

CHAPTER 1.

INTRODUCTION AND REVIEW OF THESIS

1.1 BACKGROUND

Increasing traffic volumes in urban areas and on main link routes is one of the major problems governments face in the developed and developing countries all over the world. If it is not addressed it will have a detrimental impact on the environment, economy and safety of road users. It is estimated that the cost of congestion in the European Union is 120bn Ecu per year [Nuttall 1995a]. Since building new roads presents high economic and environmental costs for society, the best and economical solution to the problem is to use the existing road network more efficiently by the application of the new technology of Road Transport Informatics. This may include Traffic Information Broadcasting, Route Guidance, Urban Traffic Control and Automatic Debiting Systems (ADS).

For many years road-toll facilities have been in operation for revenue collection on major highways, tunnels and bridges and used to finance the construction and maintenance of these new facilities.

However, nearly all road toll system requires that the drivers stop their cars and find the correct coins or a valid card before the barrier is opened so that they can then continue their journey. The toll charge levied rarely if ever takes into account type of journey, time of day, prevailing traffic conditions and other relevant factors and only the type of vehicle is considered.

A versatile tolling system that does not require the vehicle to stop and may vary the charges according to many or all of these factors can be implemented by the use of Automatic Debiting Systems based on a two-way data communication between road-side equipment and an in-vehicle unit.

One of the main advantages of Automatic Debiting Systems is that they can apply a variable charge, which can depend upon the time of day, which is related to the degree of congestion. Variable charging is usually used only in urban areas but it can also be introduced on inter-urban routes. In this way the use of certain busy areas and particular time-slots can be discouraged and better alternatives encouraged, thus distributing the road-load system in space and time.

Installing non-stop toll collection systems on motorways can increase the vehicle processing capability of a single toll lane by up to three-fold [Foote 1981]. The subsequent reduction in congestion at the site would, in turn, reduce journey times. Moreover, toll-site operators would realise an increase in revenue, as other drivers are encouraged to use the facility when the congestion is reduced. The reduction in toll-site congestion may also have a positive effect on the environment as there will be a reduction in noise and air pollution around the site as vehicle queuing decreases.

1.1.1 TECHNOLOGIES ADOPTED FOR TRAFFIC APPLICATIONS

The operation of Automatic Debiting Systems is based on a secure two-way data communication between a so called in-vehicle, or, on-board unit (OBU) installed in the vehicle and a road-side unit (RSU) usually mounted on an overhead gantry. For the realisation of the data communication there are three different methods currently available [Blythe 1992]. These are the Inductive, Optical, and the, Radio technologies which are described briefly below.

Inductive

The communication is realised through inductive coupling between a loop buried under the road surface and an on-board unit placed on the underside of the vehicle. The data is modulated on a low frequency (50KHz-300KHz) carrier. These systems are usually used with post-payment method, where the on-board unit transmits a unique fixed identification code to the interrogating road-side beacon. An Automatic Debiting System was realised with the use of inductive communication in the centre of Hong Kong for a pilot test in 1988 with a cordon pricing scheme in post-payment mode [Blythe 1989]. The system operated without any technical problem but was however not introduced due to social objections related to collecting and storing data on the personal movements of an individual.

The inductive loop system has a low data transmission rate and requires a relatively large-size of on-board unit. A further disadvantage is that roads must be dug up in order to position the inductive loops. However, the communication is not affected by environmental conditions and the inductive loops can be used to detect the position of vehicles accurately and also their speeds.

Optical

Optical systems operate with infrared diodes to transmit an on- and off-keying modulated beam and with photo-diodes to receive. These systems are able to transmit data at high bit-rates (100KBit/s-1MBit/s) and they have a long communication range (~60m). Their disadvantage is the sensitivity to various environmental conditions [Korolkiewicz 1989].

Radio Systems

Transponders which operate in the radio frequency and microwave frequency bands offer the best performance and flexibility of operation for automatic tolling and road-pricing applications. Their advantages include reliability, robustness against weather conditions and high data-rate.

1.1.2 RECENT DEVELOPMENTS IN ROAD TRAFFIC INFORMATICS

The European Community has agreed to the introduction of route-related motorway fees in all member states from 1998 and a number of trials have taken place. In Germany ten systems using infrared, radio and microwave technology were tested from May 1994 to April 1995 [Zimmermann and Neumeyer 1995]. The tests showed good reliability but was not sufficiently good for the German authorities who require further improvements in the effectiveness and accuracy of Electronic Toll Collection (ETC) systems [Nuttall 1996]. The French authorities are currently rigorously testing a microwave based (5.8GHz) tolling system in both the laboratory and traffic environment [Malbrunot 1995].

The employment of ETC systems are also being considered in the USA [Nuttall 1995b], Canada [Nuttall 1995c], Malaysia, Singapore and Japan [Murakoshi 1995]. Evaluation tests were carried out in the centre of Singapore in 1993 and 1994 [Nuttall 1995d] where a 2.45GHz microwave system has been selected for implementation in 1997. The system can support data transmission speeds of 1.5Mbps with vehicles travelling at up to 120km/h. The payment system works with a universal smart card which can also be used for public telephone calls and shopping.

ETC systems can only be used on motorways on a large scale if they are able to provide a secure means of toll collection and enforcement without causing any disruption in the free flow of traffic in several lanes with high vehicle speeds. This is a technically demanding task and one of the most promising solution uses video cameras to follow the positions of all the vehicles in the toll zone [Blythe 1996]. The data communication system is constructed so that it is able to localise the in-vehicle units which have paid correctly. By matching the vehicle data with the in-vehicle unit data, the vehicles not completing a valid transaction can be identified. This system using a 5.8GHz data link is being tested with 2000 vehicles on the A10 motorway near Salzburg. The target is to detect at least 85% of violators and to send only one in 10,000 violation letters in error.

The implementation of a world-wide electronic tolling system also raises the issue of data protection and security [Clough 1995]. Powerful encryption and data protection measures must be implemented on both the road-side to vehicle communication link and in the ETC management centre to minimise the risk of fraud and misuse of data on individuals.

In Europe, USA and Japan it is now being increasingly recognised that the microwave technology offers distinct advantages for realising a short two-way communication link between a road-side beacon and a moving vehicle [Newmann and Barink, 1996]. There is considerable world-wide interest and technical investigation has been devoted to the development of short range microwave communication links to be used for traffic applications.

In Europe the main initiative to develop a standardised data communication between a road-side unit and an in-vehicle unit is the ADEPT project (Automatic Debiting and Electronic Payment for Transport). ADEPT is part of the European Community DRIVE program (Dedicated Road Infrastructure for Vehicle Safety in Europe), which was approved by the European Councils of Ministers. Over three years funds of about 60 million ECU were made available to support the research [Walker, 1990]. Currently the system developed during this period is being tested at several test-sites in Europe [Vierth and Källström 1994].

The Centre for Communication Systems Research at the University of Northumbria was a member of the ADEPT consortium being responsible for the research and development of the 5.8GHz microwave data-link. As part of this research several detailed studies have been carried out by the members of the Research Group. These include the investigation of integrating microwave patch antennas with vehicle windscreens [Lowes 1995], design of patch antenna arrays for the road-side unit [Chan 1994] and the modelling of single feed slot antennas to be used in the on-board unit [Lim 1996]. This thesis is concerned with the optimum design of the communication system and with the investigation of a new type of circularly polarised aperture coupled antenna for the on-board unit.

1.2 REVIEW OF THE THESIS

For the reception and transmission of the microwave signal the on-board unit uses a circularly polarised microwave antenna, which was initially realised by a double feed square patch antenna with an external polariser built on a special microwave substrate material with low dielectric loss. However, this material is expensive as the structure occupies a relatively large surface area. The main focus of the research has therefore concentrated on designing a new type of circularly polarised antenna structure, which facilitates the realisation of the on-board unit without the need for an expensive substrate, and, which will occupy less board space.

Another part of the research presented in this thesis has concentrated on establishing the system parameters of the 5.8GHz microwave communication link which is to be used for traffic applications. A prototype system has been then developed and tested.

In Chapter two the work carried out regarding the communication system is reviewed. Due to the possible interference between adjacent communication systems, initially, parameters affecting the type of polarisation for down- and up-links were investigated. This has been carried out by examining the reflected signal levels from road-surface and different vehicles. The measurement has been performed in co-operation with Micro Design AS (a member of the ADEPT consortium) in Trondheim, Norway. It was found that interference can be significantly reduced by the use of circular polarisation, of the same sense, for both the road-side-to-vehicle (down-link) and vehicle-to-road-side (up-link) transmission. Based on this finding an on-board unit with a single diode acting as ASK detector and PSK modulator has been designed and also the associated road-side equipment has been developed.

The work on the communication system has been published in the Microwave Journal (Vol. 38, No.7, July 1995) and in the proceedings of the Second Communications Network Symposium (10-11 July 1995, Manchester).

In Chapter three a review of the current state of microstrip antenna theory and technology and of the various methods to generate circular polarisation is given. The importance of wide bandwidth for single feed CP antennas is highlighted and it is shown how this can be improved. A novel cross-aperture coupled single feed CP antenna is proposed for theoretical and practical investigation with a suitable simple structure for use in the OBU. This structure exhibits an improved bandwidth when implemented using a thick air substrate which allows the manufacturing tolerance requirements to be met.

An investigation demonstrating the excellent performance of the cross-aperture coupled patch antenna with air substrate has been published in the IEE Electronics Letters (Vol. 32, No.7, 28 March 1996).

Chapter four describes how the transmission line model has been developed for the circularly polarised cross-aperture coupled patch antenna. Initially the transition between a microstrip line and a cross-shaped aperture in its ground plane has been investigated theoretically and by computer simulation. Based on the result of this work a transmission line equivalent circuit of the cross-aperture coupled antenna has been developed with the associated theory.

The work described in Chapter four has also been published in the IEE Electronics Letters (Vol32. No. 21, 10 October 1996).

In Chapter five an original analysis of the proposed cross-aperture coupled circularly polarised patch antenna is given based on the resonant cavity method. This method is computationally more complex than the transmission line method, but usually also provides more accurate results.

In Chapter six the evaluation and comparison of the two theoretical models developed in Chapters four and five is presented. The input impedance and axial ratio as predicted by the two new theoretical models is compared to that given by computer simulation and measurements.

In Chapter seven it is described how the new on-board unit has been implemented using the cross-aperture coupled antenna with air substrate. The performance of the new on-board unit has been measured and a significant improvement has been found when compared to the OBU using the previous dual feed antenna design.

The design and evaluation of the new on-board unit antenna has been presented at the International IEE Conference on Road Traffic Monitoring and Control (23-35 April 1996, London) and at the Third Communications Network Symposium (8-9 July 1996, Manchester).

In Chapter eight the results of the assessment of the communication system carried out in co-operation with Sumitomo Electric Industries in Osaka, Japan is summarised. These tests include sensitivity measurements of both the road-side and on-board units and signal level and bit-error rate measurements performed using a gantry for the RSU and a vehicle for the OBU.

Chapter nine summarises the conclusions of the research and also identifies the areas for further work.

CHAPTER 2.

DESIGN OF THE COMMUNICATIONS LINK

2.1 INTRODUCTION

This chapter presents the work associated with the 5.8GHz short range microwave data communication system, which was carried out in a European Community research project called DRIVE II ADEPT (Dedicated Road Infrastructure for Vehicle Safety in Europe; Automatic Debiting and Electronic Payment for Transport). After establishing the communication mode and modulation method used, the type of polarisation to be assigned to either to the up/down links has been decided upon by both calculation and measurement in order to minimize interference between adjacent road-side units. A simple on-board unit has been designed based upon an investigation of the properties of a microwave diode. The modulation and demodulation circuits for the road-side unit have also been developed. The results of this work for the ADEPT project have also been published in the Microwave Journal (Vol. 38, No.7 July 1995). Finally, in this chapter, the design specifications for a new on-board unit antenna are identified.

2.2 COMMUNICATIONS SYSTEM SPECIFICATION

The main objective of the design of the microwave link is to ensure that the on-board unit (OBU) has a low profile and is inexpensive [Korolkiewicz 1989]. To make the on-board unit (OBU) inexpensive a talk and listen technique has been used, so that it is not necessary to have a local oscillator in the OBU as shown in Figure 2.1.

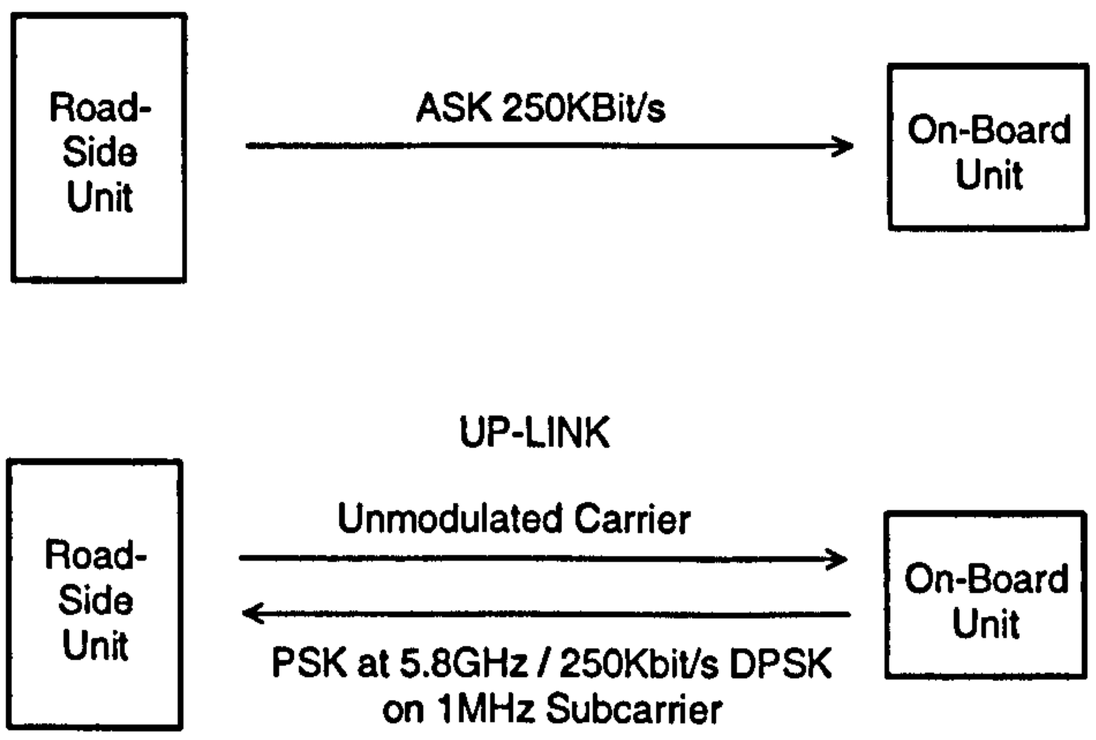

Figure 2.1. Operation of the microwave link

For transmission of information from the RSU to the OBU (called the down-link) the RSU talks and the OBU listens. To transmit information from the OBU to the RSU (called the up-link), the RSU sends a continuous wave (CW) signal which is modulated at the OBU, and the modulated signal is then re-transmitted back to the RSU by reflection.

The 5.795-5.805GHz frequency band has been designated by CEPT (Conference of European Post and Telecommunications) for the road-to-vehicle communication systems. An additional sub-band (5.805-5.815GHz) may also be used on a national basis to meet the requirements of multi-lane road junctions [Meinel 1992]. These two bands are divided into 6 channels with their centre frequencies being: 5.797, 5.800, 5.803, 5.806, 5.809, and 5.812GHz. The channel centre frequencies have been chosen so that they have equal spacing to ensure that intermodulation products do not fall into the receive band of any RSU [Korolkiewicz 1994]. A 1MHz bandwidth around the centre frequencies of each channel is reserved for the down-link signal, while two 1MHz wide side-bands adjacent to this band are designated for the up-link spectrum. The resulting allocated frequency spectrum for three communications channels is shown in Figure 2.2.

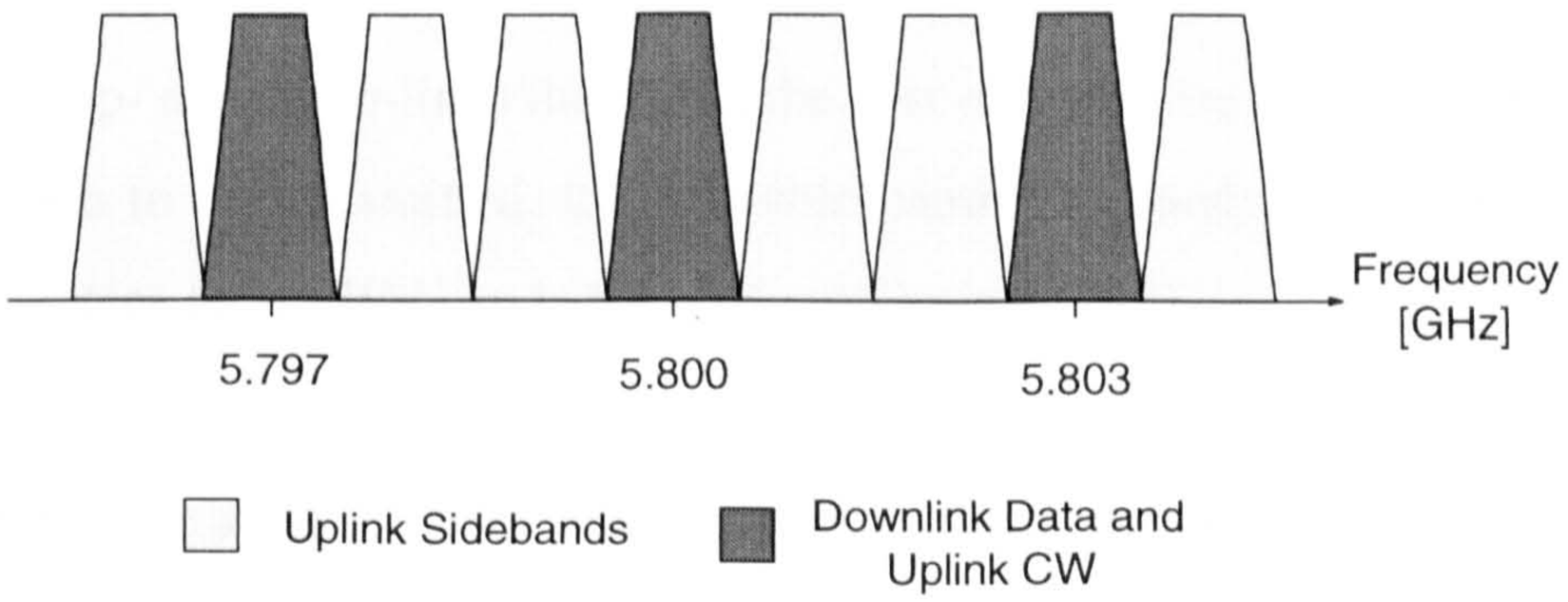

Figure 2.2. Down and up-link bands.

The maximum allowed EIRP is 2W or 33dBm. Circular polarisation is used as this minimizes the effect of multi-path reflections from vehicles. However, whether the same or opposite rotation is used for the up- and the down-links influences the level of interference between adjacent RSUs. This issue has been investigated theoretically and by measurement and is discussed in detail in the following section.

As shown in Figure 2.1, the system uses a half-duplex communication mode which reduces the complexity and therefore the cost of the on-board unit. The transmission mode of the system is synchronous as this is an efficient means of transmitting information at high data rates and is compatible with the computer control of the communication system based on the High-level Data Link Control (HDLC) protocol [Korolkiewicz 1994].

The length of the communication zone depends upon the amount of information that is required to be transmitted between the road-side unit and the on-board unit. For vehicle speeds of up to 160km/h a 6m long communication zone is required [Korolkiewicz 1994]. This means that the communication range of the system should be at least 11m if a typical mounting of the road-side unit is assumed to be at a height of up to 6m.

Based on the time available for the transaction, it was decided to use a 250kbit/s data rate for both up- and down-links this being the best compromise considering the amount of information to be transmitted, the available bandwidth, and, compatibility with the clock frequencies on the RSU and OBU [Micro Design 1993]

In order to provide a basis for the determination of the communication zone a maximum raw bit-error rate (BER) of 10^{-6} has been chosen. This implies a bit-error rate of 10^{-9} after error checking which is performed by the Cyclic Redundancy Check (CRC) code of the HDLC protocol.

Amplitude Shift Keying (ASK) modulation has been selected for the down-link modulation method, since it can be detected on the OBU with a low complexity unit consisting of a diode detector. The clock information required for the synchronous protocol is transmitted in the data signal by using Manchester encoding. This doubles the required bandwidth for the down-link signal to 500KHz, but it can still be fitted in the available 1MHz bandwidth reserved for down-link (see Figure 2.2).

In order to separate the up- and down-link bands to avoid interference, the up-link data transfer works with a subcarrier. The subcarrier is a DPSK modulated 1MHz signal, which is in turn used to PSK modulate the carrier. PSK modulation is used on the carrier as it is efficient and can easily be generated using a diode phase shifter. This modulation process produces an up-link spectrum which fits into the two side-bands reserved for the up-link as shown in Figure 2.2.

2.3 POLARISATION OPTIONS OF THE SYSTEM

The parameters which can affect interference between RSUs are mainly the physical separation between them and the type of polarisation that is being used. This section describes the nature of the interference produced by reflections and direct coupling. Results of reflection measurements are then examined to decide which polarisation arrangement should be used.

2.3.1 PARAMETERS OF MULTILANE INSTALLATIONS

The main objective is to achieve a technical solution where it is possible for different manufacturers to install their road-side equipment relatively close to each other without the danger of interference. The following are the requirements that need to be met for the multi-channel situation shown in Figure 2.3 [Micro Design 1993].

- Interference must not be a problem if two road-side units, B and C are situated on adjacent lanes 10m apart so that side-lobe interference may result.
- Co-channel interference must not be a problem if two RSUs are separated by a minimum distance of 1000m.
- Interference between adjacent RSUs (A and B) using different channels must be minimal.

2.3.2 POLARISATION OPTIONS CONSIDERED

The two possible polarisation options available when using a single patch antenna on the OBU are:

<u>Polarisation Option 1:</u>

a. Downlink: Left-hand circular.

b. Uplink: CW from RSU to OBU: Right -hand circular;

Reflected PSK modulated carrier: Right-hand circular.

Polarisation Option 2:

a. Downlink: Left-hand circular.

b. Uplink: CW from RSU to OBU: Left-hand circular;

Reflected PSK modulated carrier: Left-hand circular.

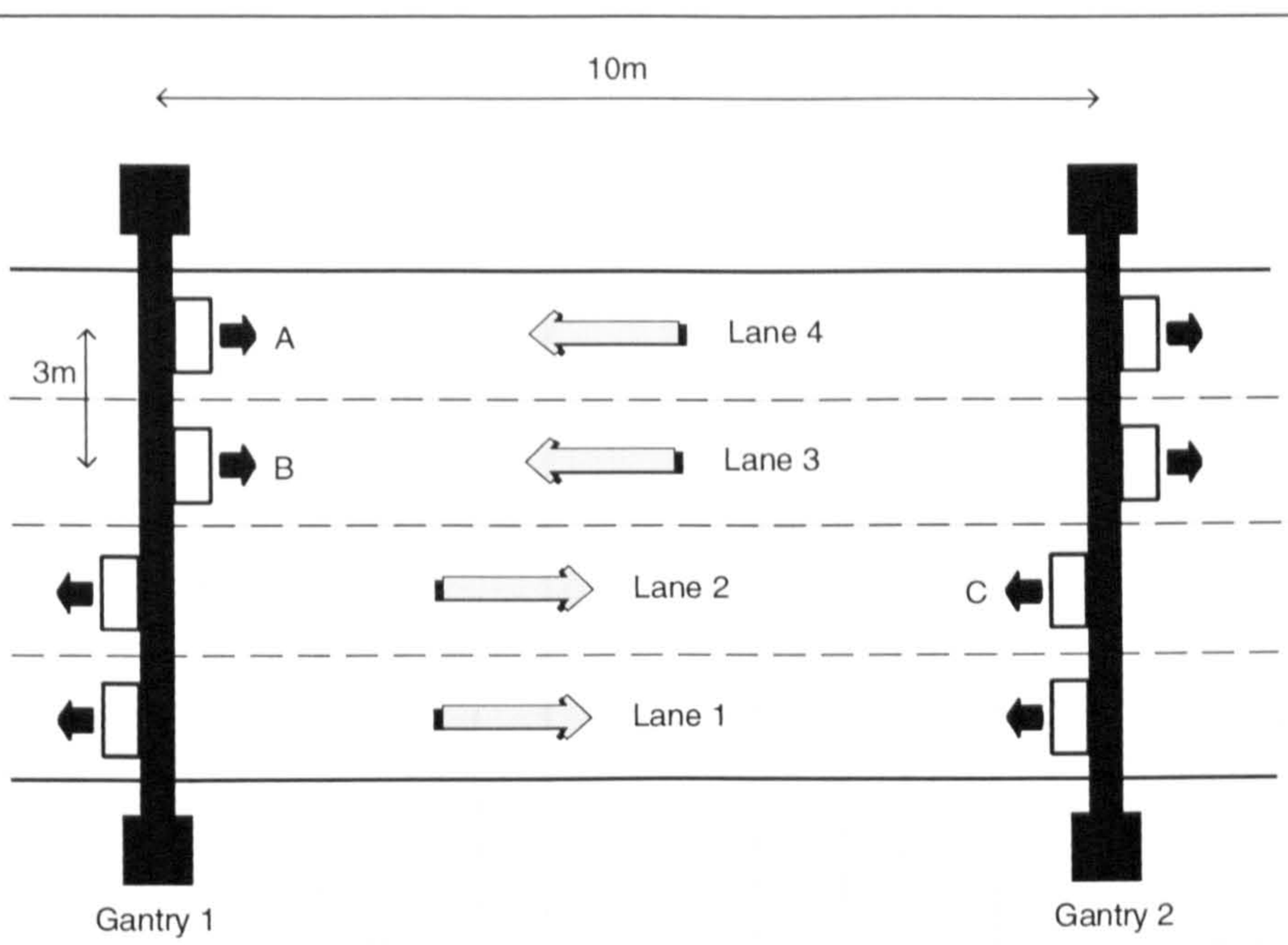

Figure 2.3. Multilane configuration.

2.3.3 RSU-RSU INTERFERENCE IN MULTILANE ENVIRONMENT

Interference Between RSUs A and B

Figure 2.4 illustrates how the interference due to reflections from road surface and/or vehicle bodies occurs, between RSUs A and B as shown in Figure 2.4.

The RSUs in Figure 2.4.a are operating with polarisation option 1. RSU A is communicating in the up-link mode with OBU1. RSU B is in communication with OBU2 in the down-link mode by transmitting an ASK modulated signal. This ASK signal can be reflected from the body of the vehicle and causes its rotation to invert [Balanis 1982]. A fraction of the down-link signal will therefore be reflected with right-hand polarisation which can be received by RSU A. This signal can interfere with the up-link signal of OBU1, because it is also right hand circularly polarised.

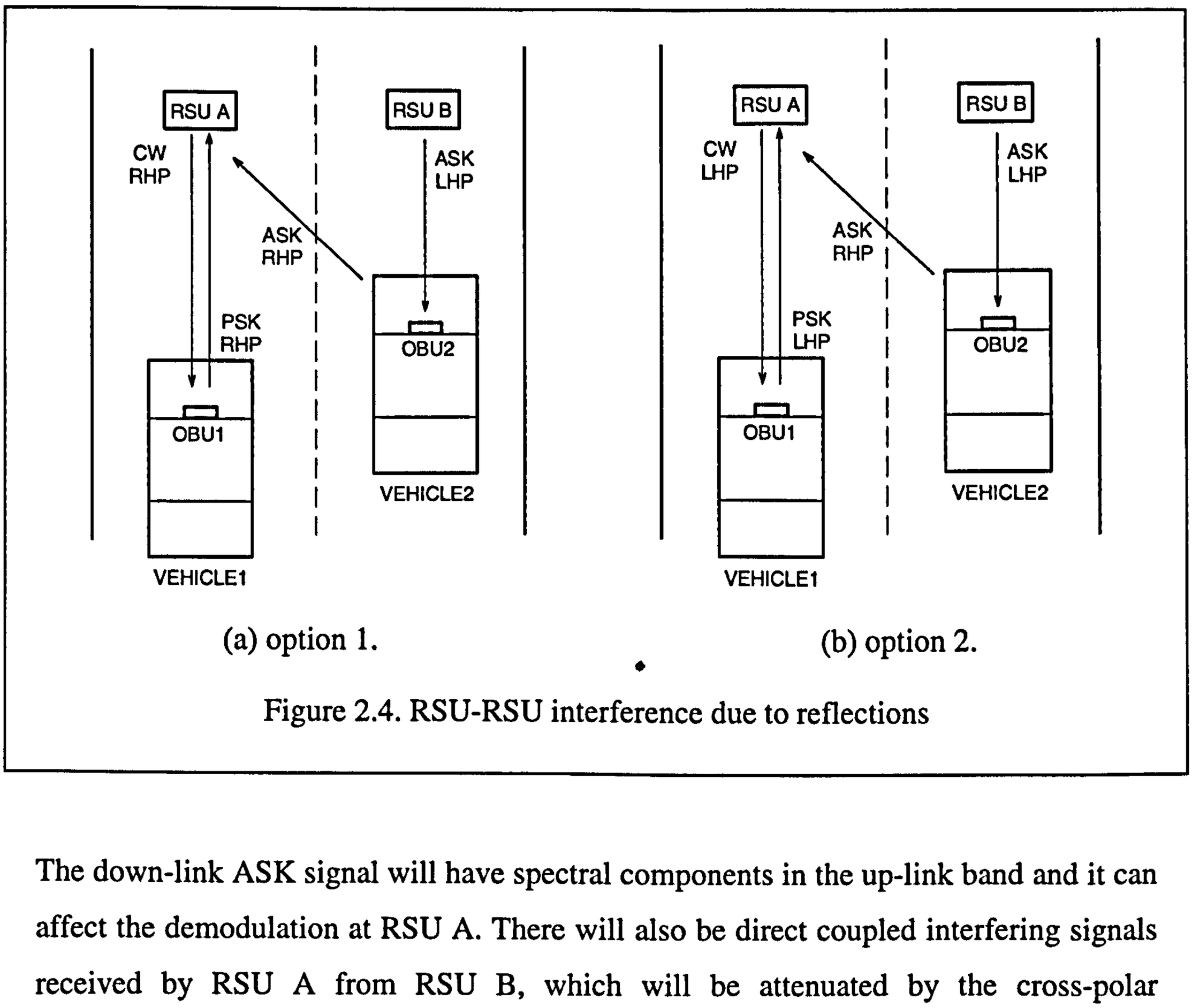

(a) option 1. (b) option 2.

Figure 2.4. RSU-RSU interference due to reflections

The down-link ASK signal will have spectral components in the up-link band and it can affect the demodulation at RSU A. There will also be direct coupled interfering signals received by RSU A from RSU B, which will be attenuated by the cross-polar discrimination of the antenna.

Figure 2.4.b illustrates the situation when the two RSUs use polarisation option 2. In this configuration the originally left-hand polarised ASK signal is reflected from the vehicle body with right hand polarisation. Since RSU A receives the down-link signal with left hand polarisation, the interfering reflected signal will be reduced by the cross-polar attenuation of the RSU antenna. Using this polarisation option the direct coupled signals will not be attenuated due to the cross-polar discrimination of the antennas.

Interference Between RSUs B and C

With reference to RSUs B and C in Figure 2.3 the interference is shown in Figure 2.5.

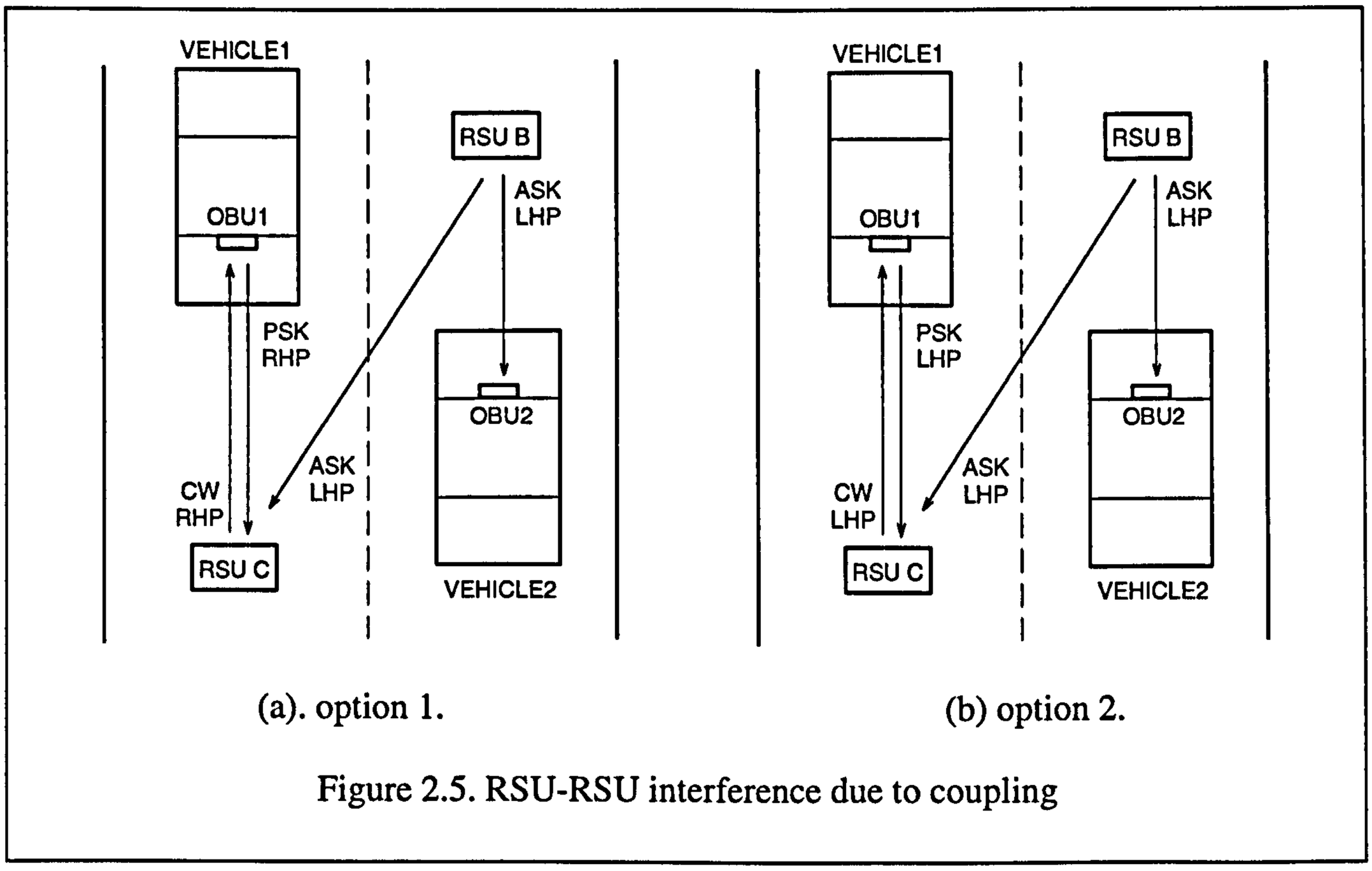

Figure 2.5. RSU-RSU interference due to coupling

Due to the side-lobe of the antenna there is an interfering signal transmitted directly from one RSU to the other. In this case the coupled interfering signal is attenuated more when using polarisation option 1, because of the opposite rotation of the desired and disturbing signals.

However, in this configuration interference might also occur due to reflected signals propagating from RSU B towards RSU C for which the polarisation arrangement 2 is to be preferred.

2.3.4 CALCULATION OF CO- AND CROSS-POLAR INTERFERING SIGNAL LEVELS

As can be seen from the previous examples, there are always two effects which can cause interferences, reflections and the direct coupling of signals. If the cross-polarised interfering signal (due to reflections) is stronger then it is preferable to use polarisation option 2, while in the other case (co-polar component due to direct coupling is stronger) option 1 would prove to be more beneficial.

Therefore, the main question is whether the co- or cross-polarised interfering signal is stronger in average in a real traffic situation. To examine the two options it was decided to estimate theoretically and experimentally the levels of the interfering signals.

In the theoretical calculations a simple model has been used with the reflecting object being a perfect mirror, 1.5m above the road surface. The antenna polar pattern plot was used to determine the side-lobe attenuation at different angles. The transmitting and receiving angle as well as the distance for the free space attenuation were calculated from the geometrical parameters of the multilane setup. The RSUs were assumed to be placed 5.5m above the road, pointing downwards at an angle of 45° with respect to the horizontal.

The power of the interfering signal (P_I) was calculated as given by the transmission formula in [Kraus 1991]

$$P_I[dBm] = P_T[dBm] + 20\log\left(\frac{\lambda}{4\pi R}\right) + G_R[dB] + L_S[dB] \qquad (2.1)$$

where, P_T is the radiated power (EIRP) from the transmitting road-side unit,

λ is the wave-length of the 5.8GHz carrier,

R is the length of signal path,

G_R is the gain of the receiving road-side unit antenna and

L_S is the side-lobe attenuation due to the direction of transmitting and receiving.

In order to obtain the co-polar interfering signal level through reflection and the cross-polar signal level through direct coupling, the value of cross-polar discrimination of the RSU antenna (15dB) has to be deducted from the value given by (2.1).

1. Reflected Signals Between RSUs A and B:

Transmitter EIRP	+33dBm
Free space attenuation (11.7m)	-69dB
Receiver antenna gain	+16dB
Side-lobe attenuation (15°)	2 X -11dB
(Cross-polar discrimination	15dB)
Received co-polar level	-57dBm
Received cross-polar level	-42dBm

2. Direct Coupled Signals Between RSUs A and B:

Transmitter EIRP	+33dBm
Free space attenuation (3m)	-57dB
Receiver antenna gain	+16dB
Side lobe attenuation (90°)	2 X -30dB
(Cross-polar discrimination	15dB)
Received co-polar level	-68dBm
Received cross-polar level	-83dBm

3. Reflected Signals Between RSUs B and C:

Transmitter EIRP	+33dBm
Free space attenuation (13.2m)	-70dB
Receiver antenna gain	+16dB
Side-lobe attenuation (16°)	2 X -11dB
(Cross-polar discrimination	15dB)
Received co-polar level	-58dBm
Received cross-polar level	-43dBm

4. Direct Coupled Signals Between RSUs B and C:

Transmitter EIRP	+33dBm
Free space attenuation (10.44m)	-68dB
Receiver antenna gain	+16dB
Side-lobe attenuation (46°)	2 X -25dB
(Cross-polar discrimination)	15dB
Received co-polar level	-69dBm
Received cross-polar level	-84dBm

It can be seen from the above calculations that the reflected signals have greater power level than that of the signals through direct coupling. Therefore it is expected that the cross-polar interfering signals will be stronger.

2.3.5 MEASUREMENT OF CO- AND CROSS-POLAR SIGNAL LEVELS

The level of interference depends on a number of parameters, e.g. antenna polar pattern, vehicle type, position of vehicle, etc., hence it is difficult to generalise from the calculations in the previous section. It was, therefore decided that for a variety of vehicles the maximum value of the co- and cross-polar signals would be measured in a traffic-like situation.

The tests were carried in co-operation with a ADEPT consortium member, Micro-Design AS in Trondheim, Norway. The test configurations viewed from above are shown in Figures 2.6 and 2.7 corresponding to the general multi-lane arrangement shown in Figure 2.3.

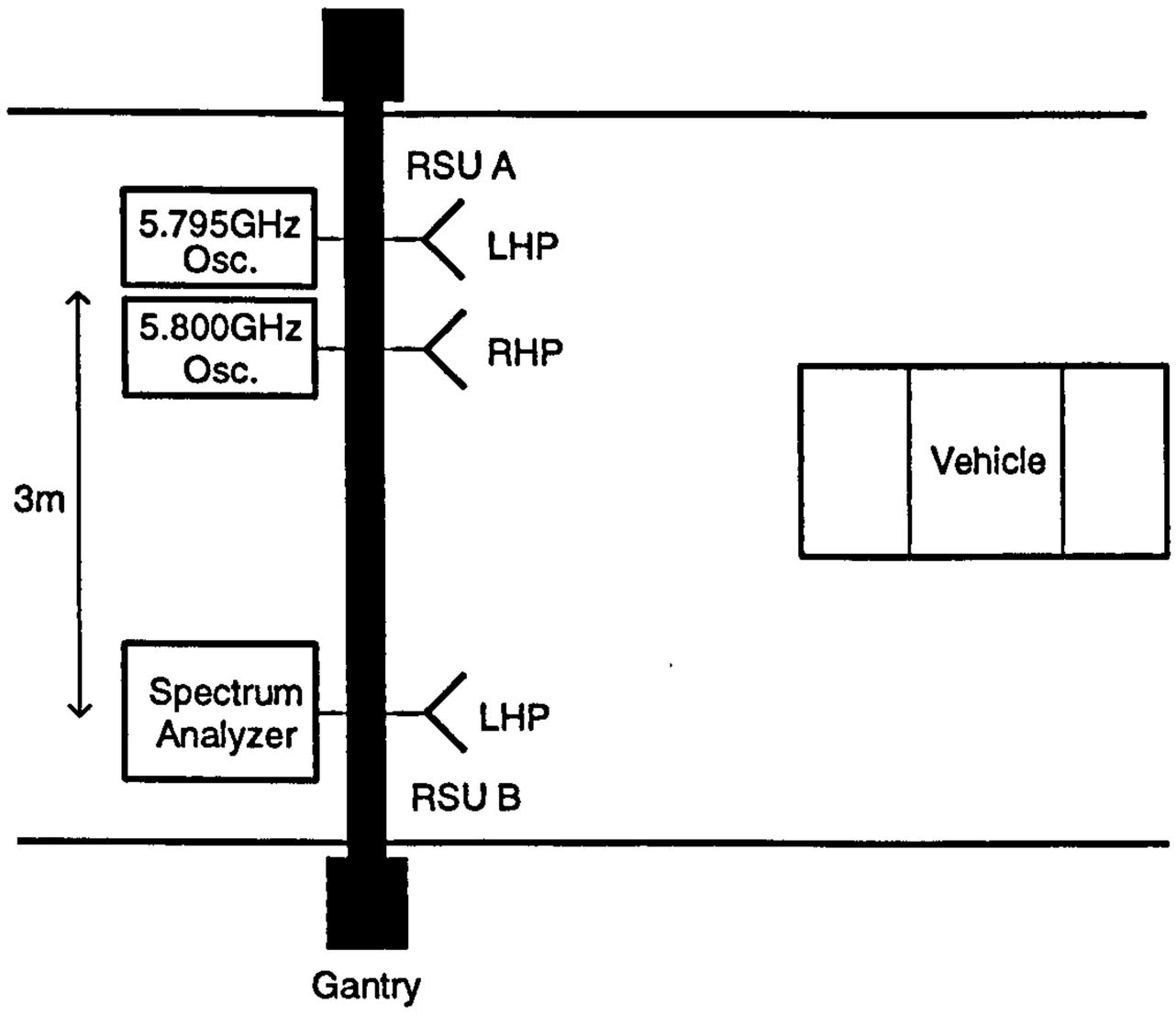

Figure 2.6. Configuration 1 of test measurements.

In order to be able to distinguish between the co- and cross-polar signals received by the RSU B, the RSU A is simulated by two antennas fed by signals with slightly different frequencies. One antenna is transmitting on left-hand polarisation, while the other transmits on right-hand polarisation. The received signal levels are displayed on the spectrum analyser. Referring to Figure 2.6, the cross-polar signal is shown at 5.800GHz and the co-polar one at 5.795GHz on the analyser. Different types of vehicles were moved in front of the antennas, and, for each type the spectrum analyser was set to record the maximum received level. The measurement was then repeated simulating the interference between RSU B and RSU C using configuration 2, which is shown in Figure 2.3.

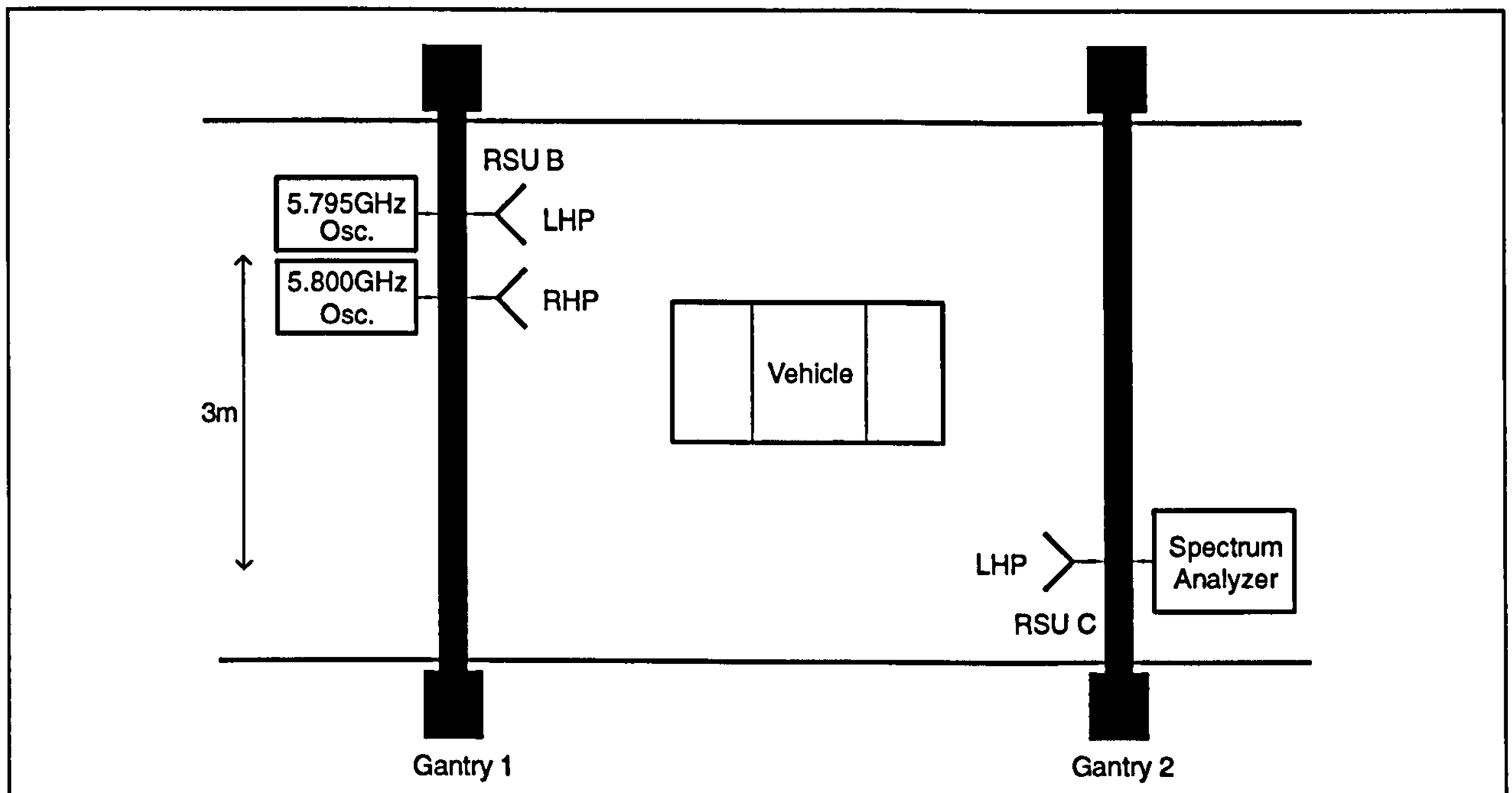

Figure 2.7. Configuration 2. of test measurements.

2.3.6 RESULTS OF MEASUREMENTS AND CONCLUSION

The recorded maximum power levels for the two configurations and for the various types of vehicles are summarised in Table 2.1.

Configuration 1.	**Background**	**Car**	**Van**	**Small Bus**
Co-Polar	-63	-55	-48	-50
Cross-Polar	-59	-49	-43	-47
Configuration 2.	**Background**	**Car**	**Van**	**Small Bus**
Co-Polar	-63	-50	-48	-52
Cross-Polar	-48	-43	-41	-46

Table 2.1. Received maximum power levels [dBm]

The measurement results are closest to the calculated values for the van. The probable reason for this is that the approximation used in the calculation with the reflecting mirror at 1.5m height, resembles best the van, which was of a similar height and a near rectangular shape.

However, the difference between the co- and cross-polar signal levels is smaller (5-7dB) than the cross-polar discrimination of the antenna (15dB). This means that the co-polar components are increased with multipath reflected signals.

It is surprising that the signals reflected by the bus are weaker than that by the van, which was smaller in size than the bus. This can be explained by the difference in the shape of the two vehicles. As it was mentioned earlier, the van had a near rectangular shape, while the bus was of a more stream-lined design, which probably scattered the reflected waves.

It can generally be concluded based on the practical results that the co-polar signals are 5-10dB weaker than the cross-polar ones, which suggest that polarisation option 2 should be used, which would reduce the interfering signal's level with 5-10dB. Based on this finding a prototype system has been developed using left-hand circular polarisation for both up- and down-links.

2.4 REALISATION OF THE COMMUNICATIONS SYSTEM

2.4.1 ROAD-SIDE UNIT

The block diagram of the RSU is shown in Figure 2.8. Due to the 3MHz channel spacing at 5.8GHz, and also to reduce phase noise a stable crystal controlled dielectric resonator oscillator (DRO) is used as the microwave source in the RSU. This is important when two systems' signals are interfering [Yacoubi 1994].

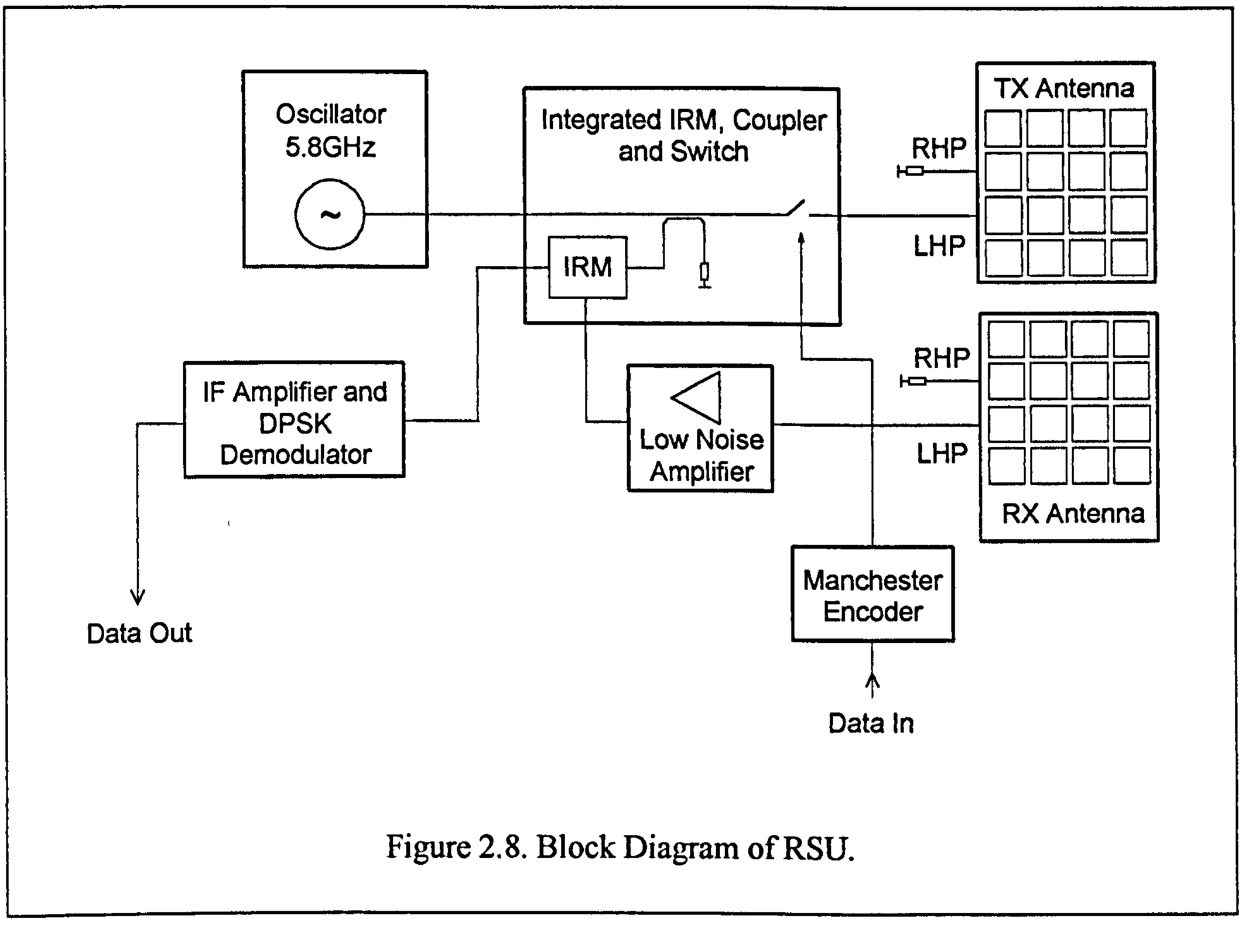

Figure 2.8. Block Diagram of RSU.

The RSU antennas are 4 X 4 microstrip arrays, which have a 16° wide main lobe. Two such antennas are required in the RSU since during up-link it needs both to transmit the unmodulated carrier while receiving simultaneously the reflected modulated signal.

A microwave switch is used in the road-side unit to ASK modulate the carrier by the Manchester encoded data when the system is in down-link mode. The microwave switch is continuously in closed position when in up-link mode so that the RSU transmits an unmodulated carrier.

The RX antenna receives the modulated carrier and the signal is amplified by a low-noise amplifier. The amplified up-link signal is fed into an image rejection mixer (IRM) where it is mixed with the local oscillator's signal supplied through a coupler. Since the position of the OBU is constantly changing, as does the phase of the incoming modulated carrier, a conventional mixer can not be used.

The mixer, switch and the coupler has been fabricated on a single piece of substrate as shown in Figure 2.9. A high permittivity material (Duroid 6010) is used to reduce spurious radiation and minimize the size of the circuit. The optimisation of the dimensions of circuit elements have been performed using the CAD software, Super-Compact from Compact Software Inc. .

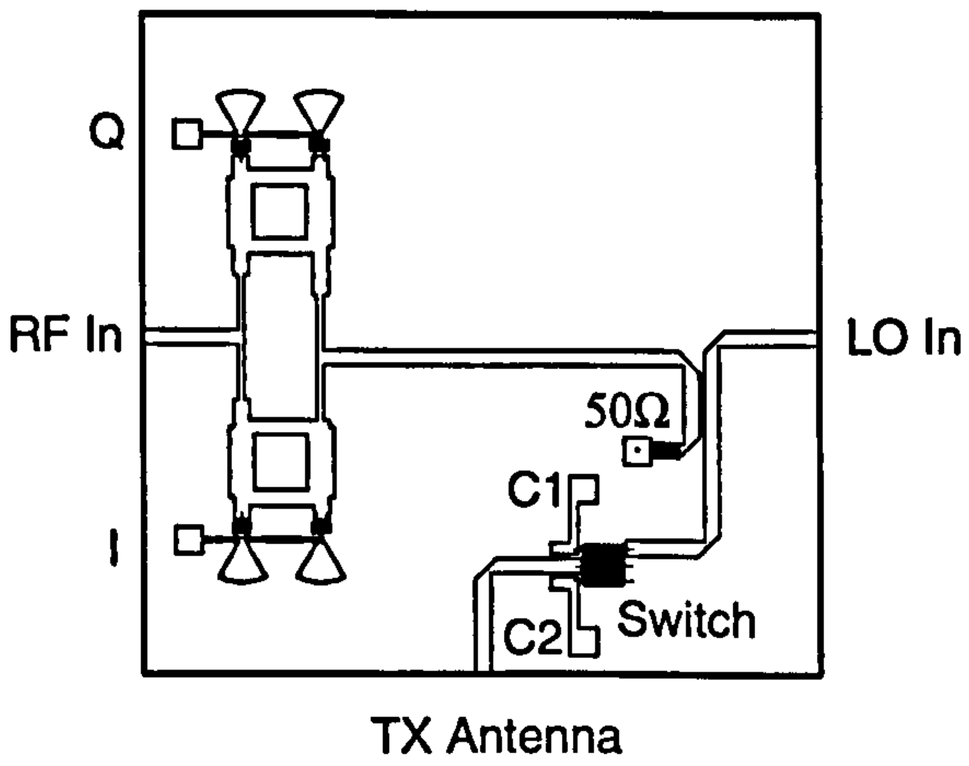

Figure 2.9. Layout of the image rejection mixer, 10dB coupler and microwave switch.

The IRM down-converts one of the carrier side-bands, recovering the modulated subcarrier with its frequency slightly changed by the Doppler-effect. In case of a vehicle approaching the RSU with a speed of 160km/h, the doppler-frequency is in the order of 2KHz, which can be neglected when comparing it to the 1MHz sub-carrier frequency. The DPSK modulated carrier is amplified and limited by the IF amplifier. The data is recovered in a coherent manner by a costas-loop.

2.4.2 ON-BOARD UNIT

The block diagram of the on-board unit is shown in Figure 2.10. The complexity of the microwave circuit of the on-board unit is kept at a minimum by the use of one microstrip antenna for transmission and reception and a single diode for detection and modulation.

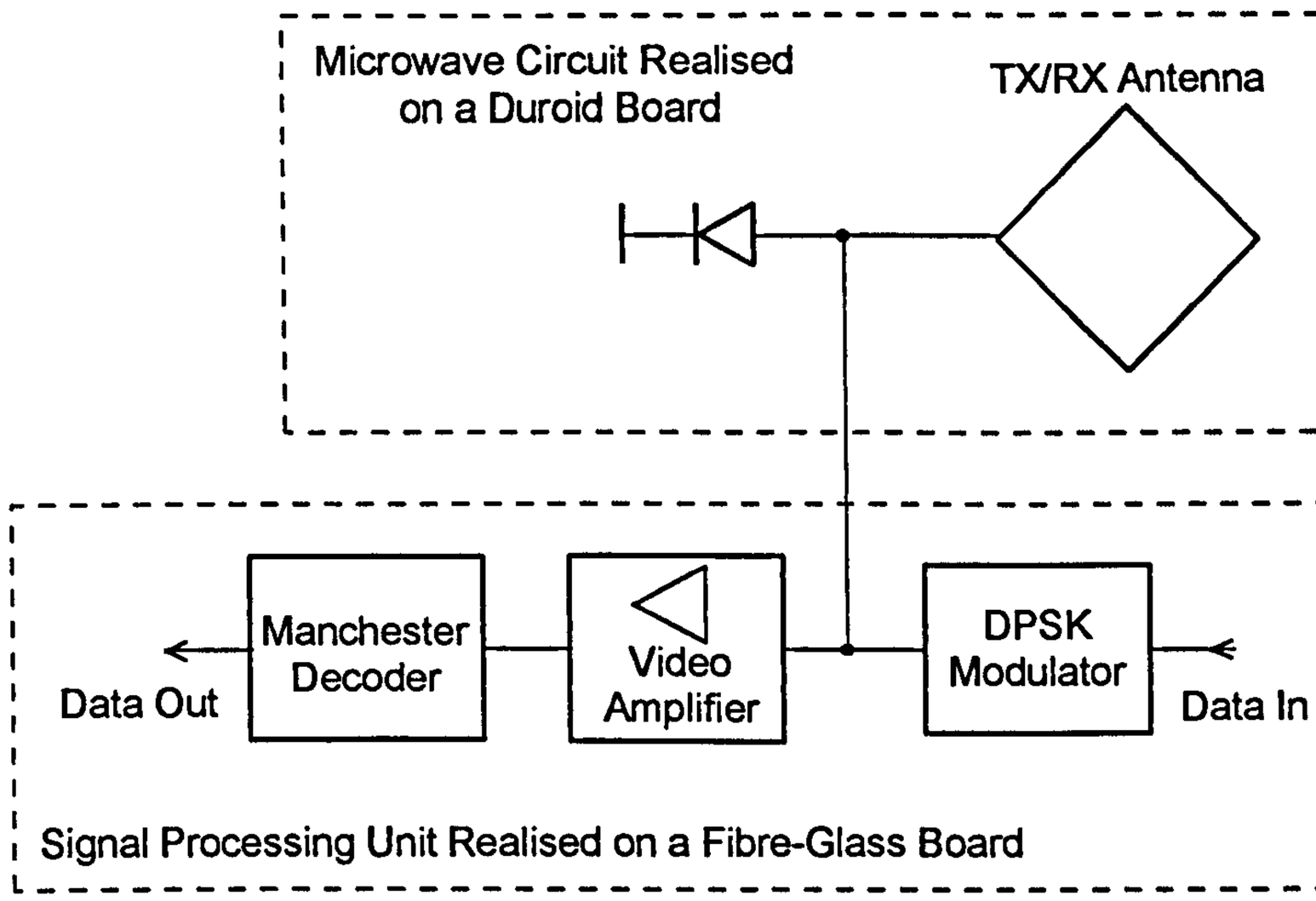

Figure 2.10. Block diagram of the on-board unit.

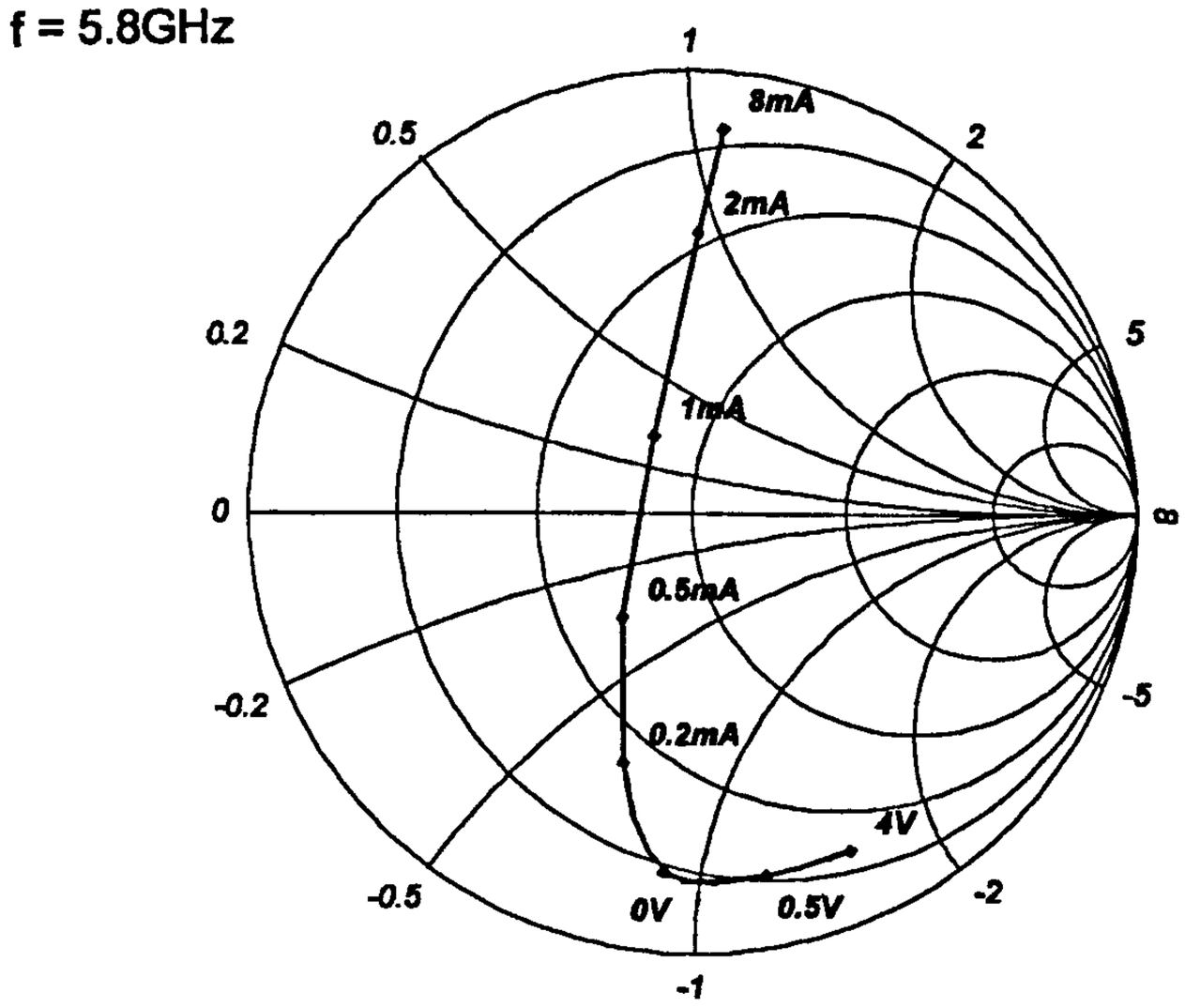

Figure 2.11. Impedance of HSMS8081 diode used in the on-board unit.

The type of the diode used in the on-board unit is HSMS8081 from Hewlett-Packard. In order to design the ASK detector and PSK modulator with this diode, its impedance for different bias conditions has been measured. The result of this measurement is shown in Figure 2.11.

In the general case a matching network is required for the diode when realising a reflective type phase shifter [Chan 1994]. However, it was found that for this particular diode the values of the reflection coefficient for 0mA and 3.7mA bias are of almost equal amplitude (-1.8dB) and have a phase difference of approximately 180°. This result suggests that the diode can be used as a PSK modulator without the need for a matching circuit. However, if no matching circuit is used the TSS of the diode will be reduced due to the mismatch at the antenna port. The value of TSS without using any matching network has been verified by measurements and it was found to be -49dBm. According to the link budget calculation (see Appendix A.) this value of TSS provides a down-link range of 15m, which is sufficient for ADS applications [Korolkiewicz 1994]. This allowed the microwave circuit of the on-board unit to be realised with a single diode used for ASK detection and PSK modulation minimizing its complexity as shown in Figure 2.10.

During the down-link mode the diode acts as an ASK detector. The received and detected down-link signal is amplified and limited by a high gain video amplifier. The Manchester encoded data is decoded and the clock signal is recovered in the Manchester decoder. During the up-link mode the antenna receives the unmodulated carrier and this signal is modulated by the reflective type phase shifter formed by the diode. The diode is biased at either 0mA or 3.7mA by the DPSK modulated sub-carrier signal and the resulting modulated carrier is re-transmitted by the microstrip antenna towards the RSU.

2.5 REQUIREMENT FOR A NEW OBU ANTENNA

The layout of the microwave circuit of the on-board unit which has been designed previously and is currently being used in the system is shown in Figure 2.12. It is implemented with a double feed patch antenna fed by a T-junction. The microwave circuit of the currently used on-board unit is implemented on a 0.79mm thick microwave substrate, namely RT Duroid 5870. In addition to the Duroid board, there is a fibre-glass printed circuit board in the on-board unit carrying the data processing, modulating and demodulating circuits as shown in Figure 2.10.

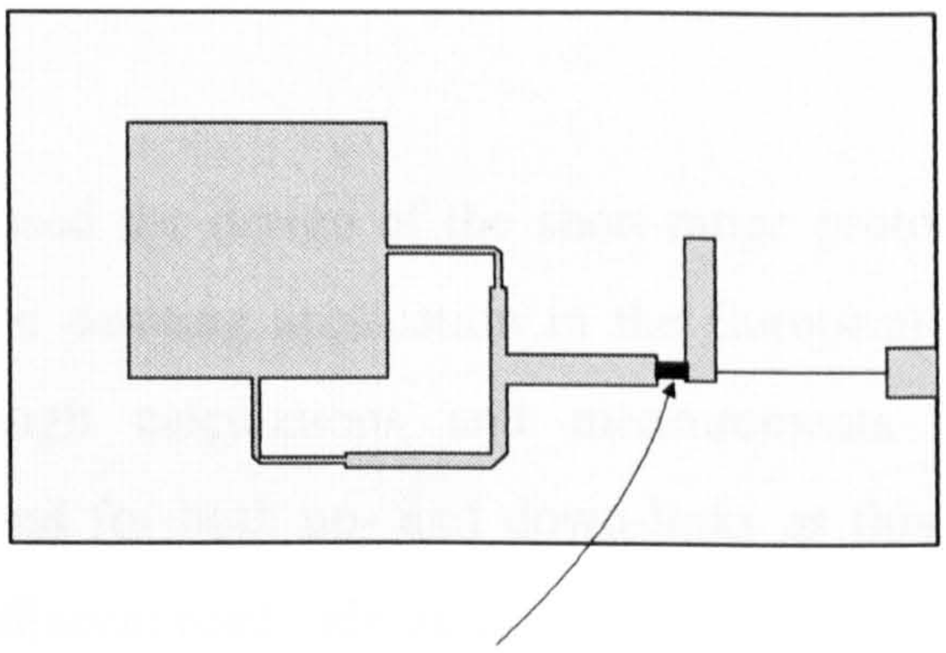

Figure 2.12. Layout of the current on-board unit with a double feed square patch antenna fed by a T-junction.

This double board arrangement of the on-board unit presents a number of problems associated with volume manufacturing of the on-board unit, such as:

- The fabrication of the antenna is expensive as the special microwave substrate has a high cost and the double feed antennas occupy a relatively large surface area. The material cost for the on-board unit microwave circuit shown in Figure 2.12 is approximately £4.

- The manufacturing of the on-board unit is complicated due to the connections required between the two boards used for the microwave circuit, and, for the signal processing unit.

Because of the above problems, it was decided that a new type of microstrip antenna is to be investigated and designed for use in the on-board unit. The requirement from this antenna is that it eliminates the above shortcomings, that is it should be compact in size and it should be possible to manufacture it inexpensively by placing it onto the fibreglass board carrying the data processing circuits. The structure of the antenna, with which this can be achieved is presented in the next chapter after a brief review of the different type of microstrip antennas.

2.6 CHAPTER SUMMARY

This chapter has discussed the design of the short-range prototype microwave system developed for automatic debiting application in the European ADEPT project. It has been determined through calculations and measurements that left-hand circular polarisation is to be used for both up- and down-links as this reduces the interfering signal levels between adjacent road-side units.

The layout of the road-side and on-board units has been presented and it was shown how a single diode can be used for both down-link ASK detection and up-link PSK modulation. The shortcomings associated with using a double feed patch on a separate special microwave substrate have been identified and it was decided that the development of a new OBU antenna is necessary. The important design parameters of microstrip antennas together with an analysis of the effect of manufacturing tolerance is presented in the following chapter. The specific type of the proposed microstrip antenna for use in the OBU is also identified.

CHAPTER 3.

CIRCULAR POLARISED MICROSTRIP ANTENNAS - BANDWIDTH AND TOLERANCE

3.1 INTRODUCTION

In this chapter a brief review of microstrip antenna technology focusing on the two types of circularly polarised patch antennas, the dual and single feed antennas, is first presented. A single feed antenna is preferred in the on-board unit as it does not need an external polarising network thereby allowing the reduction of the OBU's dimensions. However, single feed circularly polarised patch antennas typically have a narrow frequency bandwidth. Therefore, an analysis of the effect of manufacturing tolerance on the performance of a single feed CP antenna is carried out and shows that using a thick air substrate increases the bandwidth of single feed antennas to an acceptable level.

Hence, a single feed, cross-aperture coupled circularly polarised nearly square patch antenna with air substrate has been chosen as the new on-board unit antenna. The structure of this antenna is presented in this chapter. Finally, the available methods of modelling microstrip antennas are briefly reviewed.

An investigation demonstrating the excellent performance of the cross-aperture coupled patch antennawith air substrate has been published in the IEE Electronics Letters Vol. 32, No.7 (28 March 1996).

3.2 REVIEW OF CIRCULARLY POLARISED MICROSTRIP ANTENNAS

A number of different methods have been developed for generating circular polarisation with microstrip patch antennas. They can be categorised into two types by their feeding systems: dual-feed CP antenna with an external polariser, and, the single feed type without a polariser.

3.2.1. DUAL FEED CIRCULARLY POLARISED ANTENNAS

The dual-feed CP antennas are symmetrical in shape and rely on an external polariser which generates two input signals with equal amplitude and a 90° phase difference. The input signals are fed to two separate ports of the patch antenna and excite two orthogonal modes which generate the circular polarisation. The polariser can be realised by a T-junction with a $\lambda/4$ delay line (Figure 3.1a) or with a 3dB hybrid (Figure 3.1b).

For a dual feed CP patch one can also employ aperture coupling, as shown in Figure 3.1c and 3.1d. The advantage of the aperture coupling is twofold in that the antenna substrate and the feed substrate can be optimised independently, and, that the antenna can be impedance matched by the variation of the aperture length [Targonski and Pozar 1993]. The two main options of realising a circularly polarised dual feed aperture coupled microstrip antenna are to use two off-set slots, or, a cross-slot. With the off-set slot configuration a 3.5% bandwidth has been achieved [Adrian and Schaubert 1987], while the cross-aperture coupled antenna can exhibit bandwidths of up to 25% [Targonski and Pozar 1993].

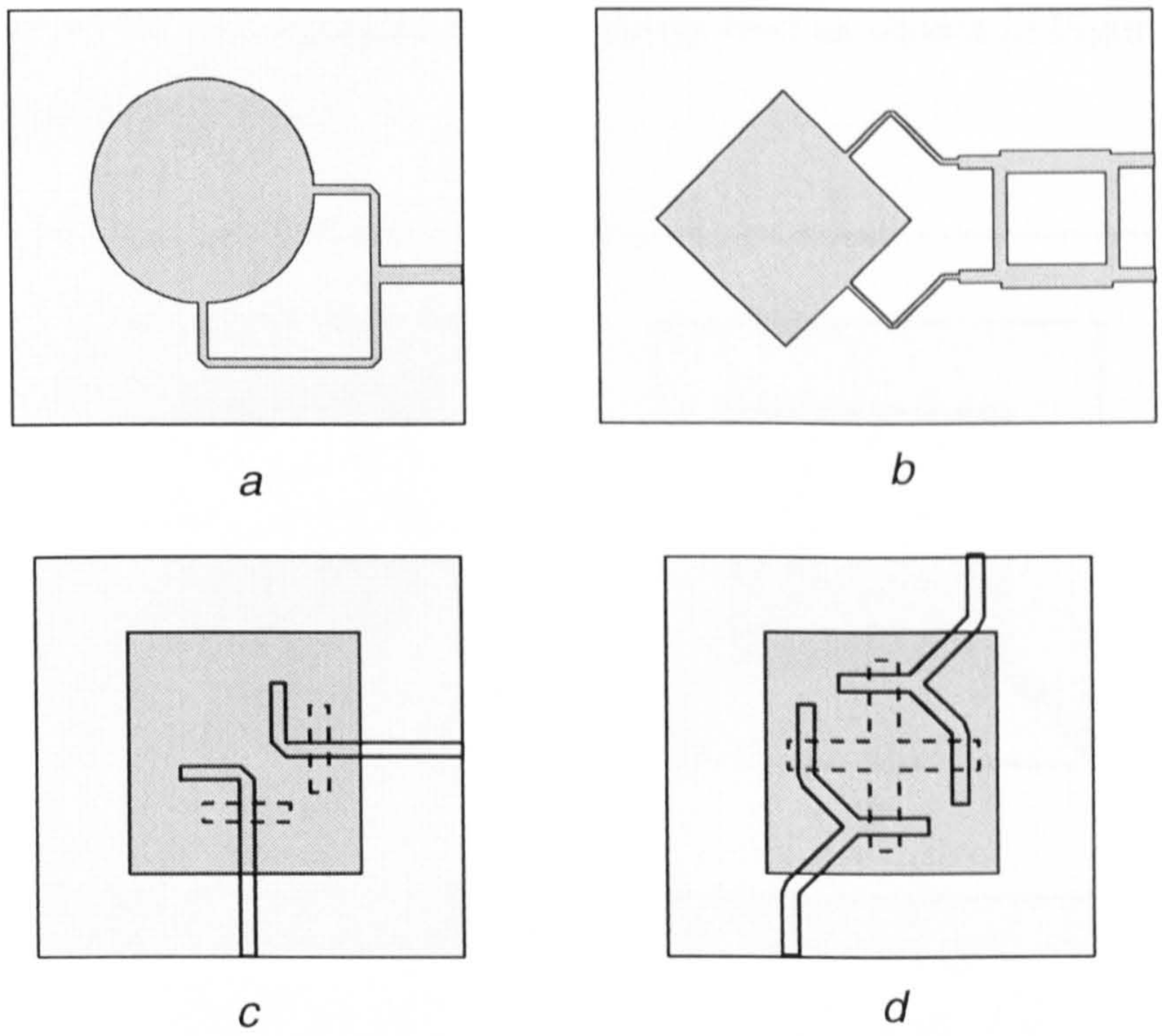

Figure 3.1. Dual-fed circularly-polarised patch antennas.

Although dual feed circularly polarised antennas such good performance, their main disadvantage is the increased board space required for the external polariser network. The increase in board space puts up the cost of the antenna.

3.2.2 SINGLE FEED CIRCULARLY POLARISED ANTENNAS

The principle of operation of single feed CP antennas is that two orthogonal modes are excited by means of a small perturbation of the antenna geometry. There are many possible configurations for single feed CP patches which differ in the shape of the patch and of the perturbation segment. Two basic types are the truncated corners patch and nearly square patch shown in Figures 3.2a and 3.2b, respectively. The bandwidth performance of single feed CP patches is typically in the range of 1-1.5% [Scharma and Gupta 1983; Palanisamy and Garg 1986].

One can also use an inclined slot to excite two modes in a nearly square patch antenna which can then employ an aperture coupled single feed as shown in Figure 3.2c [Aksun et al. 1989; Aksun et al. 1990].

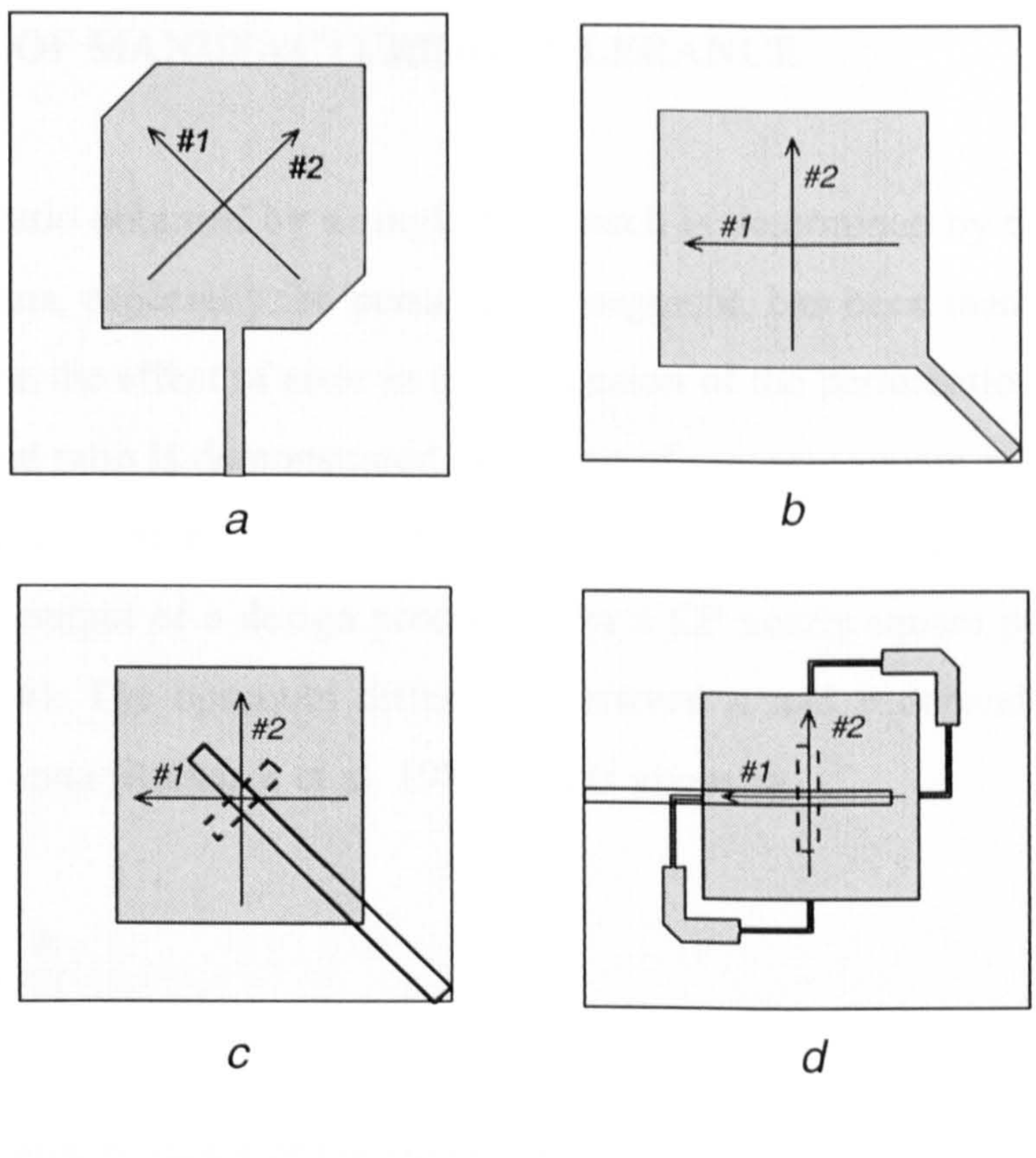

Figure 3.2. Single feed circularly-polarised microstrip patch antennas.

Another interesting technique which realises a single feed aperture coupled CP antenna is shown in Figure 3.2d. In this solution the aperture-excited mode of a linear polarised antenna is coupled to an orthogonal mode through two microstrip lines, which provide a 270° phase shift. The performance of this antenna is very similar to other single feed CP patches [Duffy and Pozar 1995].

Single feed circularly polarised antennas do not require any external polariser network, hence they can be implemented using less board space. However, they have a major disadvantage of small bandwidth performance, which demands high manufacturing accuracy.

3.2.3 EFFECT OF MANUFACTURING TOLERANCE

The best axial ratio obtained by a single feed patch is determined by the accuracy with which the antenna, especially the perturbation segment, has been manufactured. In the following section the effect of error in the dimension of the perturbation segment on the value of the axial ratio is demonstrated in respect of a nearly square patch antenna. The aim of the analysis is to relate the value of manufacturing tolerance to the error in the axial ratio. The output of a design procedure for a CP nearly square patch is its length (a) and width (b). The optimum difference between a and b depends on the quality factor of the antenna [Richards et al. 1981] and is given by

$$(a-b)_o = \frac{b}{Q} \tag{3.1}$$

where Q is the quality factor of the antenna and

$(a\text{-}b)_o$ is the optimum size of the perturbation segment

Using the narrow band network model, in which the resonant mode is modelled by a parallel RLC circuit, the input impedances of the two orthogonal modes at the operating frequency (f_0) can be written as

$$Z_{01} = \frac{R}{1+2jQ\frac{\Delta f}{f_1}} \qquad Z_{10} = \frac{R}{1-2jQ\frac{\Delta f}{f_2}} \tag{3.2}$$

where R is the resistance of the RLC equivalent circuit and

$$\Delta f = f_2 - f_1 \tag{3.3}$$

According to the simple transmission line model [Munson 1974], the resonant frequencies of the two modes, f_1 and f_2 can be calculated by

$$f_1 = q\frac{c}{2a\sqrt{\varepsilon_{eff}}} = q\frac{c}{2(b+(a-b))\sqrt{\varepsilon_{eff}}}$$

$$= q\frac{c}{2b\sqrt{\varepsilon_{eff}}}\cdot\frac{1}{1+\frac{a-b}{b}}$$

$$\cong q\frac{c}{2b\sqrt{\varepsilon_{eff}}}\cdot\left(1-\frac{a-b}{b}\right) \tag{3.4}$$

$$f_2 = q\frac{c}{2b\sqrt{\varepsilon_{eff}}} \tag{3.5}$$

where q is the fringing factor

c is the speed of light in free space and

ε_{eff} is the effective permittivity of the antenna.

As f_1 and f_2 are close to each other then approximately

$$\frac{\Delta f}{f_1} \approx \frac{\Delta f}{f_2} \approx \frac{a-b}{b} \tag{3.6}$$

Substituting (3.1) and (3.6) into equation (3.2) the impedances of the modes are given by

$$Z_{01} = \frac{R}{1+j\frac{a-b}{(a-b)_o}} \qquad Z_{10} = \frac{R}{1-j\frac{a-b}{(a-b)_o}} \tag{3.7}$$

The value of the axial ratio can be calculated by determining the phase and amplitude errors of the two modes as given by

$$\phi_e = \arg\left(\frac{Z_{01}}{Z_{10}}\right) \tag{3.8}$$

$$A_e = \frac{|Z_{01}|}{|Z_{10}|} \tag{3.9}$$

The axial ratio (AR) can be then calculated by the formula given in [Balanis 1982]

$$AR = \sqrt{\frac{1+A_e^2+\left[1+A_e^4+2A_e^2\cos(2\phi_e)\right]^{1/2}}{1+A_e^2-\left[1+A_e^4+2A_e^2\cos(2\phi_e)\right]^{1/2}}} \tag{3.10}$$

Numerical evaluation of (3.10) shows that the axial ratio is degraded to 3dB when the actual difference between a and b is 30% different from the desired value. This means that calculating for the worst case, when, for example, dimension a is slightly larger and b is slightly smaller than the desired values, the acceptable tolerance limit belonging to 3dB axial ratio for a nearly square microstrip antenna is 15% of the optimum difference between the dimensions of the two edges of the rectangle. The dimensions of a number of single feed CP antennas are presented in the next section, so that an absolute value for the tolerance requirement is obtained for a number of different substrates.

3.2.4 DEPENDENCE OF TOLERANCE REQUIREMENTS ON SUBSTRATE PROPERTIES

It is generally accepted that using a thick, low permittivity substrate increases the bandwidth of a microstrip antenna [Schaubert et al. 1989]. However, there is no data available in the literature on how the tolerance required for a circularly polarised antenna depends on the thickness and the relative permittivity of the substrate.

Based on the value of the required relative tolerance discussed in the previous section, the absolute values of allowed inaccuracy in the patch dimensions are given in this section for a number of nearly square circularly polarised patch antennas. The antennas have been designed by the application of a full wave simulation package (Ensemble Design from Boulder Microwave Technologies) for two different frequencies and using several different substrate materials. The frequencies chosen were 5.8GHz and 2.45GHz as the majority of the microwave systems used for traffic applications operate at these frequencies. The substrate materials considered were, air with $\varepsilon_r = 1$, Duroid 5870 with $\varepsilon_r = 2.33$ and fibre glass printed circuit board with $\varepsilon_r = 4.6$. The optimised dimensions of the patch antennas are shown in Table 3.1.

ε_r	d_a [mm]	$f0$ [GHz]	a [mm]	b [mm]	3dB axial ratio bandwidth	required tolerance [μm]
1	0.79	5.8	23.96	24.64	0.95	102
1	1.575	5.8	22.53	23.81	1.72	192
1	3.15	5.8	20.30	22.90	3.7	390
2.33	0.79	5.8	16.11	16.62	1.07	76
2.33	1.575	5.8	15.29	16.30	1.9	151
2.33	3.15	5.8	13.74	15.75	3.8	301
4.6	0.79	5.8	11.75	12.10	0.9	52
4.6	1.575	5.8	11.12	11.75	1.55	94
4.6	3.15	5.8	9.65	11.25	3.6	240
1	1.575	2.45	58.18	59.50	0.75	198
1	3.15	2.45	55.71	58.23	1.47	378
1	7.1	2.45	49.62	55.70	3.46	912
2.33	1.575	2.45	39.00	39.85	0.67	127
2.33	3.15	2.45	37.88	39.55	1.37	250
2.33	7.1	2.45	36.92	41.24	3.08	648
4.6	1.575	2.45	28.36	28.72	0.42	54
4.6	3.15	2.45	27.82	28.48	1.02	99
4.6	7.1	2.45	25.37	28.12	2.89	412

Table 1.1. Parameters of the simulated single feed CP antennas.
ε_r relative permittivity of antenna substrate,
d_a thickness of antenna substrate,
f_0 frequency of operation,
a, b dimensions of the nearly square patch antenna.

Based on the tolerance data in Table 3.1, it can be stated that at both frequencies for a given substrate thickness, the larger the relative permittivity, the tighter is the tolerance required. For a given relative permittivity, it is beneficial to use a thicker substrate as this allows the tolerance requirements to be relaxed. What is interesting to note is that the realisation of an antenna for the higher frequency requires less precision than for the lower frequency on the same substrate. This is probably due to the increased radiation at higher frequencies, which increases the overall losses, and, hence reduces the quality factor of the antenna.

The analysis presented in Section 3.2.3 and the data given in Section 3.2.4 demonstrates that it is possible to achive large enough bandwidth with a single feed circularly polarised antenna, so that the tight manufacturing tolerance can be relaxed. This result enables the application of a single feed type antenna in the on-board unit, as they have the advantage of being compact in size.

In order to relax the manufacturing tolerance requirements as much as possible and taking into account the high cost of microwave substrate materials such as the Duroid 5870, air has been chosen as substrate material for the on-board unit antenna which was designed and implemented. It can be seen from the table, that, for antenna operating at 5.8GHz depending on the thickness of air substrate, the required tolerance from the manufacturing process is approximately in between 0.2-0.4mm, a range which can easily be achieved, as the usual tolerance of an etching process is approximately 0.1mm.

3.2.5 MICROSTRIP ANTENNA STRUCTURE CHOSEN FOR INVESTIGATION AND IMPLEMENTATION IN THE ON-BOARD UNIT

A new structure has been chosen as the on-board unit antenna, which is a single feed, cross-aperture coupled, nearly square patch shown in Figure 3.3.

As this antenna is of a single feed type, it has the advantage of being small in size, which is an important factor, as the preferred location of the on-board unit is on the windscreen of the vehicle. Aperture coupling facilitates the use of different substrate materials for the feed network and for the antenna. It also allows the matching of the impedance of the antenna to that of the feed by variation of the aperture length. This eliminates the need for any external matching network which would increase the size of the antenna.

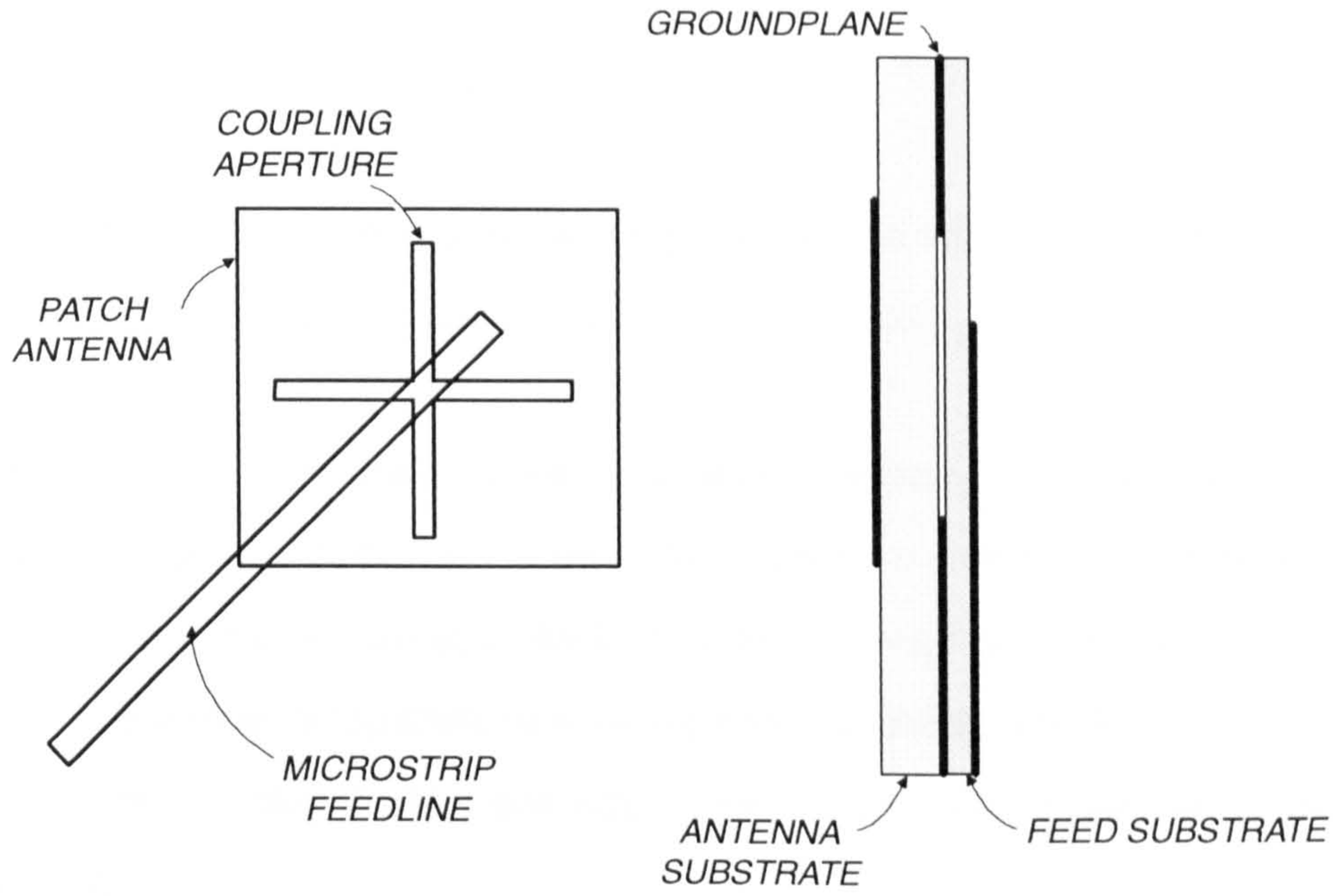

Figure 3.3. Cross-aperture coupled single feed circularly polarised patch antenna.

As shown in the previous section, using a thick air substrate would have a beneficial effect on both the cost of the antenna and on the manufacturing process as the tolerance requirement could be relaxed. Therefore a variation of the cross-aperture coupled antenna has been implemented in the on-board unit as shown in Figure 3.4.

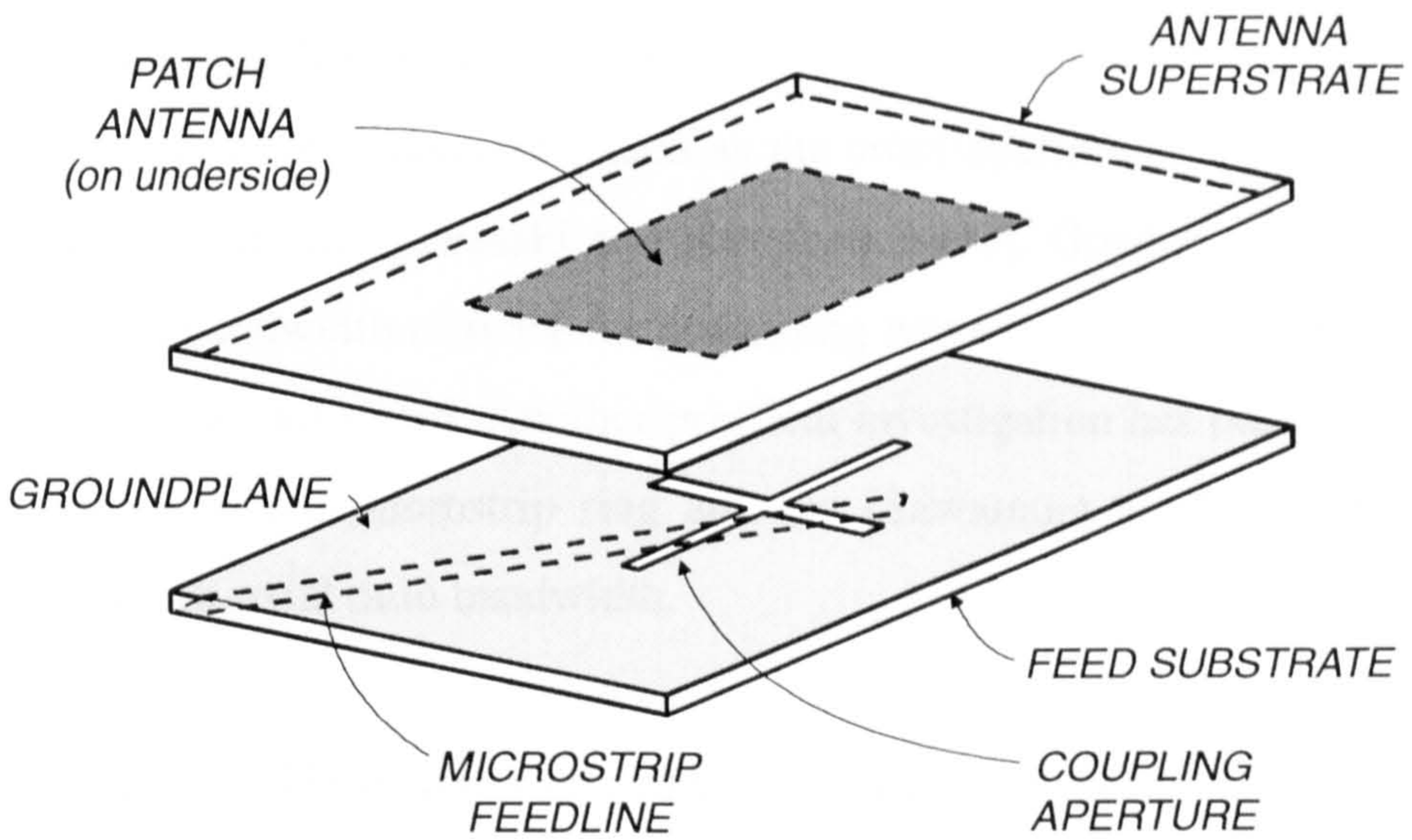

Figure 3.4. Cross-aperture coupled antenna with air substrate.

The antenna shown in Figure 3.4 has a similar structure to the so called Strip-Slot-Foam-Inverted Patch (SSFIP) antennas. This technique combines the benefits of the aperture feed with that of using a thick, low permittivity antenna substrate [Zürcher 1988]. The superstrate is required only to support the patch, which is usually chosen to be relatively thin so that it does not significantly affect the properties of the antenna [Zürcher 1995].

By using a thick air substrate in the cross-aperture coupled patch the main disadvantage of low axial ratio bandwidth (i.e. tight tolerance requirement for the manufacturing) is eliminated. Hence, a compact on-board unit antenna, manufacturable at a low cost, can be obtained.

The improvement in bandwidth using this new structure has been demonstrated by fabricating and measuring the axial ratio performance of a cross-aperture coupled antenna with air substrate operating at 2.45GHz. The results show a 2.5% axial ratio bandwidth, which is approximately double that achived with other structures [Sharma and Gupta 1983; Palanisamy and Garg 1986].

The cross-aperture coupled nearly square patch antenna has not to date been investigated neither practically nor theoretically in the literature. Only practical investigations have been performed on similar structures, such as the cross-aperture coupled circular patch with non equal slot lengths [Iwasaki and Kawabata 1991]. Good impedance matching was reported in a bandwidth of 6.5% for a standing wave ratio of 2, but, the bandwidth of the axial ratio was not stated. Another practical investigation has been carried out on a cross-aperture coupled microstrip ring antenna [Sawamura et al. 1995] showing a 1.5% fractional 3dB axial ratio bandwidth.

As there was no available theoretical model in the literature for the structures shown in Figure 3.3 and 3.4, two analytic methods have been developed in this thesis to predict the input impedance and axial ratio performance. The transmission line and the cavity modelling methods are employed in this thesis for these antennas.

3.3 MODELLING TECHNIQUES OF MICROSTRIP ANTENNAS

There are a number of different methods of analysis for microstrip antennas, which require different levels of computational effort and provide different degrees of accuracy.

3.3.1. TRANSMISSION LINE METHOD

The transmission line model is based on the primary assumption that the patch antenna can be regarded as a wide microstrip line. In the simple transmission line model [Munson 1974] the radiation from the antenna is modelled by two parallel slots radiating into half space above the ground plane. An improved transmission line model provides better accuracy by taking into account the radiation also from the side slots and by providing more accurate formulas for the parameters of the equivalent microstrip line [Derneryd 1978; Pues and Van de Capelle 1984].

Lately, the transmission line analysis has been extended in order to model linear polarised aperture coupled antennas [Himdi et al. 1989a], dual frequency linear polarised aperture coupled antennas [Yazidi et al. 1993a], aperture coupled antennas with non-linear slots [Yazidi et al. 1992] and slot antennas [Himdi and Daniel 1992]. In this thesis the transmission line method will be extended in order to model the circularly polarised cross-aperture coupled patch antenna.

3.3.2 CAVITY METHOD

The cavity model is based on the assumption that the thickness of the substrate is much less than the wavelength (i.e. $t << \lambda$) so that the electric field has only a single component perpendicular to the ground plane, and, the magnetic field has only transverse components in the region bounded by the patch and the ground plane. As a result of this, the microstrip antenna can be considered as a resonant cavity with the patch element and the ground plane represented by electric walls and the perimeter of the patch as a magnetic wall.

The method of solution uses the expansion of the fields under the patch in terms of the resonant modes [Lo et al. 1979]. The radiation of the patch is taken into account by either the introduction of an effective loss tangent for the filling material of the cavity [Richards et al. 1981], or, by an impedance boundary condition at the radiating edges [Carver 1979].

The cavity model provides better accuracy as compared to the transmission line method [Daniel et al. 1993] with only a moderate increase in processing time. It has lately been applied to linear polarised aperture coupled patch antennas [Himdi et al. 1989b] and to aperture coupled circular microstrip antennas [Yazidi et al. 1993b]. It has been chosen as the second method to be applied to the investigation of the circularly polarised cross-aperture coupled patch antenna in this thesis.

3.3.3 FULL WAVE METHOD

The rigorous analysis and solution of the field equations for a given structure is referred to as full-wave analysis method [Pozar and Voda 1987; Scott 1989] and this usually provides the most accurate results as compared to other methods. However, this technique generally requires a very considerable increase in computational resources. The solution of the field equations is performed through the determination of Green's functions which allow space wave radiation, surface wave modes, dielectric losses and coupling to external elements to be included in the analysis. The unknown currents on the feed and antenna elements are expanded in a set of basis functions and a set of linear algebraic equations is then produced which are solved for the unknown mode coefficients of the basis functions.

The full wave method is used in this thesis indirectly through the application of a commercially available software (Ensemble Design from Boulder Microwave Technologies) which is based on this modelling technique. The calculation of input impedance and axial ratio performance of a multi-layer structure such as the cross-aperture coupled patch for one frequency point, however, takes approximately one minute on a personal computer (486 type with 33MHz clock speed and 8MByte RAM) as compared to 1-10 seconds when using the transmission line or cavity models.

3.4 CHAPTER SUMMARY

A number of dual and single feed circularly polarised microstrip patch antennas have been presented in this chapter. It has been shown that single feed CP patches can be built using less board space but that they are able to produce good circular polarisation only in a narrow frequency band. It was then shown by analysis and simulation that this drawback can be reduced to an acceptable level by the application of a thick air substrate.

The structure of a cross-aperture coupled single feed patch antenna with air substrate has been presented. Fabricating an antenna of this type, an axial ratio bandwidth of 2.5% has been achieved, which is in excess of what has been obtained by other single feed patch antennas. Therefore the cross-aperture coupled circularly polarised antenna has been selected for theoretical investigation and for implementation in the on-board unit.

The three main modelling techniques have been briefly reviewed, two of which are developed for the cross-aperture coupled antenna in this thesis, namely the transmission line and the cavity models, which usually combine accurate results with numerical efficiency. The third technique of full wave modelling is used in this thesis through a commercially available software package as a reference.

CHAPTER 4.

TRANSMISSION LINE ANALYSIS OF THE CROSS-APERTURE COUPLED CIRCULAR POLARISED MICROSTRIP ANTENNA

4.1 INTRODUCTION

In this chapter an original analysis of a cross-aperture coupled circularly polarised antenna (see Figure 4.1) is presented based on the transmission line method. A theoretical model of the transition between a cross-shaped aperture and a microstrip line is first developed and verified by the application of a full wave computer simulation package. The result of this work shows that the transition between a cross-aperture and a microstrip line can be modelled by two ideal transformers connected in series, which correspond to the two slots forming the cross-aperture. This enables the analysis of the circularly polarised patch, based on the transmission line method, to be implemented by modelling the antenna in two orthogonal directions independently.

The radiation admittance of the antenna is obtained by considering the edges of the patch as slots radiating into half-space. Then, using the transmission line theory, the impedance of the patch is referenced to the apertures. Based on the investigation regarding the cross-aperture, these impedance values are then transferred to the feeding microstrip line providing the input impedance of the structure. The analysis also facilitates the determination of an equivalent circuit, which is, in turn, used to derive a formula for the axial ratio of the antenna as a function of the frequency.

Based upon the work presented in this chapter, a paper has been published in the IEE Electronics Letters (Vol.32 No22., 24 Nov. 1996).

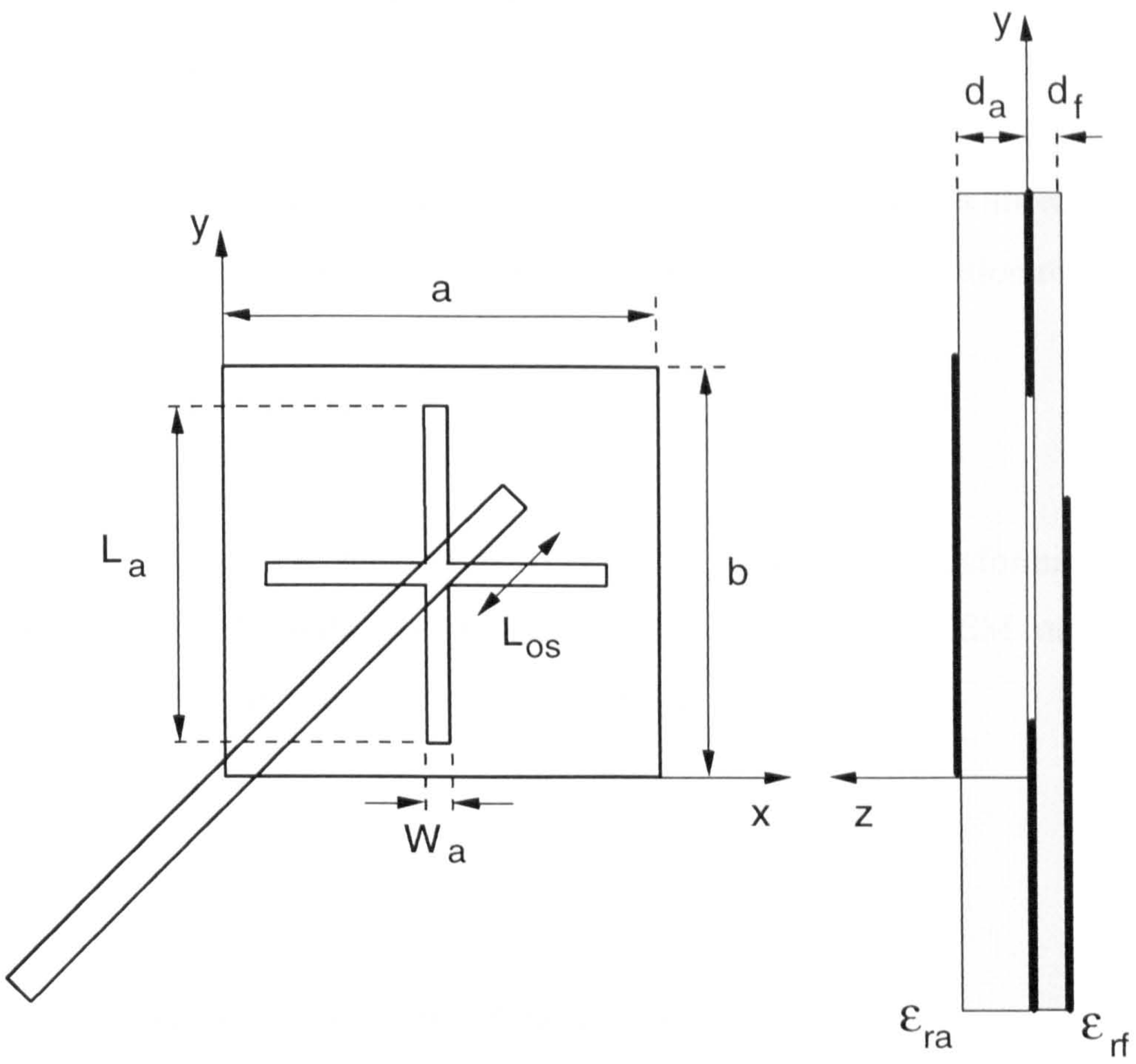

Figure 4.1. Design parameters of the cross-aperture coupled microstrip antenna.

4.2 CROSS-APERTURE IN THE GROUND PLANE OF A MICROSTRIP LINE

Several authors have investigated slot discontinuities in the ground plane of a microstrip line by using the spectral domain technique [Antar et al. 1992; Bhattacharyya et al. 1992], and, also the multiport reciprocity analysis [Das 1993]. However, there is no information available in the literature on how a cross-shaped aperture structure could be modelled accurately and with numerical efficiency.

In this section an original theoretical analysis of the cross-aperture to microstrip line transition is developed. An aperture inclined with respect to the microstrip line is first modelled, and, then it is shown that the cross-shaped aperture can be considered as the superposition of two inclined slots at an angle of +45° and -45° with respect to the microstrip line. This result is supported by full wave computer simulation results.

4.2.1 INCLINED APERTURE

The turns ratio (n) of the microstrip to aperture impedance transformation can be calculated from the discontinuity in the modal voltage (quasi TEM mode) on the microstrip line and is given by [Himdi et al. 1989b]

$$n = \frac{\Delta v}{V_0} \tag{4.1}$$

where, V_0 is the voltage at the centre of the aperture and

Δv is the discontinuity in the modal voltage on the microstrip line.

The discontinuity voltage on the microstrip line is given by

$$\Delta v = \iint_{slot} \mathbf{E}_a \times (-\mathbf{z})\,\mathbf{h}_m \, ds \tag{4.2}$$

where, $\mathbf{E_a}$ is the electric field in the aperture and

$\mathbf{h_m}$ is the normalized magnetic field on the microstrip line.

The electric field distribution in the aperture is taken to be in the form of a single piece-wise sinusoidal (PWS) function [Sullivan and Schaubert 1986], which for analytic convenience is given in the u-v co-ordinate system (see Figure 4.2) by

$$\mathbf{E_a} = \frac{V_0}{W_a} \frac{\sin\left[k_a\left(\frac{L_a}{2} - |u|\right)\right]}{\sin\left(k_a \frac{L_a}{2}\right)} \cdot \mathbf{v}; \qquad \frac{-L_a}{2} \le u \le \frac{L_a}{2}, \quad \frac{-W_a}{2} \le v \le \frac{W_a}{2}$$

$$= 0; \qquad \text{otherwise} \qquad (4.3)$$

where, V_0 is the voltage at the middle of the aperture parallel to the y axis and k_a is the wave number of the aperture determined using Cohn's method [Cohn 1969; Himdi and Daniel 1991] (see Appendix B.).

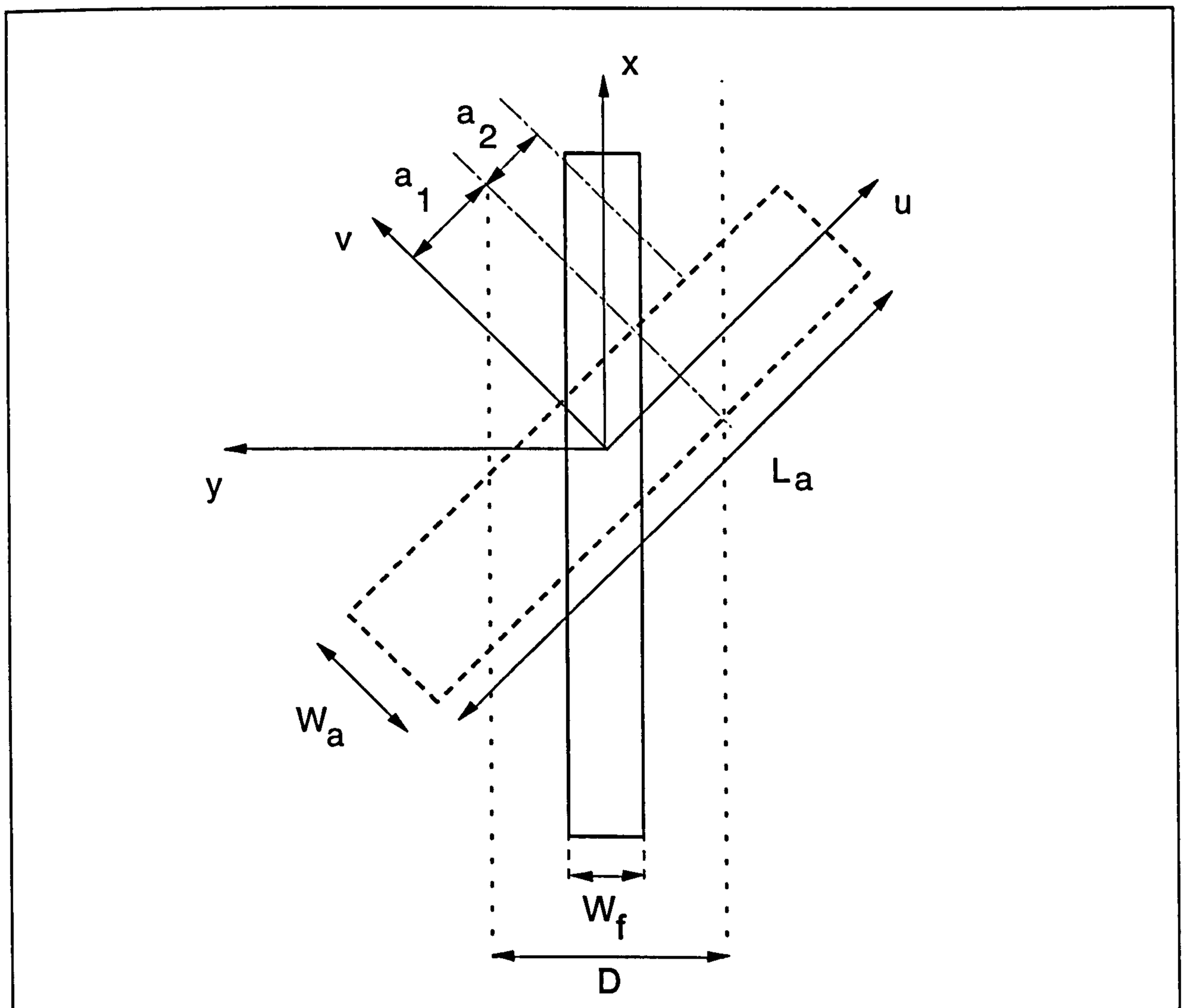

Figure 4.2. Inclined aperture to microstrip line transition.

The normalized magnetic field of the microstrip line is assumed to have a uniform distribution [Rao et al. 1981] as expressed by

$$\mathbf{h}_m = \frac{1}{\sqrt{Dh}} \cdot \mathbf{y} \qquad \frac{-D}{2} \le y \le \frac{D}{2}$$

$$= 0\ ; \qquad \text{otherwise} \qquad (4.4)$$

where, h is the thickness of the substrate and

D is the width of the parallel plate equivalent of the microstrip line [Rao et al. 1981], given by

$$D = \frac{120\pi \cdot h}{Z_{cf}\sqrt{\varepsilon_{eff}}} \qquad (4.5)$$

where Z_{cf} is the characteristic impedance of the microstrip line and

ε_{eff} is the effective permittivity of the microstrip line, which are calculated as given in [Woermbke 1982].

With the above field distributions the discontinuity voltage given by (4.2) can be written in the following form:

$$\Delta v = \frac{V_0 \cos\theta_s}{W_a\sqrt{Dh}\sin\left(k_a\frac{L_a}{2}\right)}\iint_{slot}\sin\left[k_a\left(\frac{L_a}{2}-|u|\right)\right]dudv \qquad (4.6)$$

The evaluation of (4.6) is lengthy due to the geometry of the structure, and is included in Appendix C. The final result is given here, as follows

$$\Delta v = AB\left(I_1 + I_2\right)$$

$$A=\frac{V_{0u}}{W_a\sqrt{2Dh}\sin\left(k_a\frac{L_a}{2}\right)}$$

$$B=\begin{cases}1 & \sqrt{2}D\le W_a\\ \dfrac{\sqrt{2}D}{W_a} & \sqrt{2}D<W_a\end{cases}$$

$$I_1=\frac{2W_a}{k_a}\left[-\cos\left[k_a\left(\frac{L_a}{2}-u\right)\right]\right]_0^{U_1}$$

$$U_1=\begin{cases}a_1 & \mathrm{L_a}<a_1\\ L_a & L_a\ge a_1\end{cases}$$

$$I_2=\frac{W_a}{k_a}\left[\frac{U_2-a_1-a_2}{a_2}\cos\left[k_a\left(\frac{L_a}{2}-U_2\right)\right]+\cos\left[k_a\left(\frac{L_a}{2}-a_1\right)\right]\right]$$

$$+\frac{W_a}{k_a^2a_2}\left[\sin\left[k_a\left(\frac{L_a}{2}-a_1\right)\right]-\sin\left[k_a\left(\frac{L_a}{2}-U_2\right)\right]\right]$$

$$U_2=\begin{cases}a_1 & \mathrm{L_a}<a_1\\ L_a & a_1\le L_a<a_2\\ a_2 & L_a\ge a_2\end{cases}$$

$$a_1=\left|\frac{D}{\sqrt{2}}-\frac{W_a}{2}\right| \qquad a_2=\begin{cases}a_1+W_a & \sqrt{2}D\ge W_a\\ a_1+D\sqrt{2} & \sqrt{2}D<W_a\end{cases} \qquad \text{(C.10)}$$

The value of the turns ratio can be calculated by substituting the discontinuity voltage (Δv) given by (4.7) into (4.1). The results given by this model are verified in section 4.2.3.

4.2.2 CROSS-APERTURE

The discontinuity voltage on the microstrip line with a cross-shaped aperture in its ground plane is given by

$$\Delta v = \iint_{slot} \mathbf{E}_{a,cr} \times (-\mathbf{z})\,\mathbf{h}_m \, ds \tag{4.8}$$

where the electric field $\mathbf{E_{a,cr}}$, assuming a single piecewise sinusoidal distribution in each of the two orthogonal apertures can be written as

$$\mathbf{E}_{a,cr} = \mathbf{E}_{au} + \mathbf{E}_{av} \tag{4.9}$$

where $\mathbf{E_{au}}$ is the electric field in the aperture parallel to the v axis as shown in Figure 4.3a, which as given by

$$\mathbf{E}_{au} = \frac{-V_{0u}}{W_a} \frac{\sin\left[k_a\left(\frac{L_a}{2} - |v|\right)\right]}{\sin\left(k_a \frac{L_a}{2}\right)} \cdot \mathbf{u} \qquad \begin{matrix} \frac{-W_a}{2} \le u \le \frac{W_a}{2} \\ \frac{-L_a}{2} \le v \le \frac{L_a}{2} \end{matrix} \tag{4.10a}$$

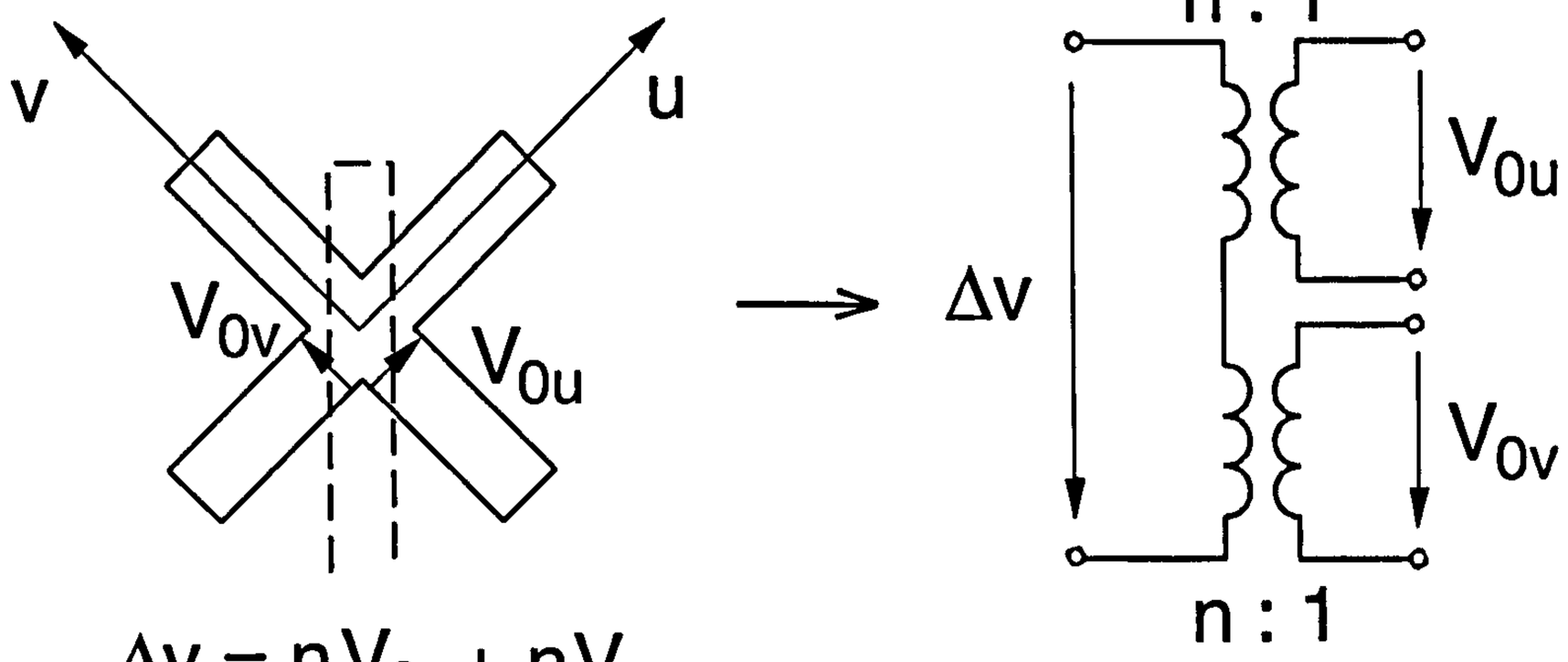

Figure 4.3. Equivalent circuit of the cross-aperture to microstrip line transition.

$\mathbf{E_{av}}$ is the electric field in the aperture parallel to the *u* axis, as given by

$$\mathbf{E}_{\mathbf{av}} = \frac{-V_{0v}}{W_a} \frac{\sin\left[k_a\left(\frac{L_a}{2} - |u|\right)\right]}{\sin\left(k_a \frac{L_a}{2}\right)} \cdot \mathbf{v} \qquad \begin{matrix} \frac{-L_a}{2} \le u \le \frac{L_a}{2} \\ \\ \frac{-W_a}{2} \le v \le \frac{W_a}{2} \end{matrix} \tag{4.10b}$$

The integral in equation (4.8) is then given by

$$\Delta v = \iint_{S_1} \mathbf{E}_{\mathbf{au}} \times (-\mathbf{z}) \mathbf{h}_{\mathbf{m}}\, ds + \iint_{S_2} \mathbf{E}_{\mathbf{av}} \times (-\mathbf{z}) \mathbf{h}_{\mathbf{m}}\, ds \tag{4.11}$$

where, S_1 is the area of the slot parallel to the v axis and

S_2 is the area of the slot parallel to the u axis.

From (4.7) and from the symmetry of the cross-aperture with respect to the microstrip line, it follows that

$$\iint_{S_1} \mathbf{E}_{au} \times (-\mathbf{z}) \mathbf{h}_m \, ds = V_{0u} \cdot n \tag{4.12}$$

$$\iint_{S_2} \mathbf{E}_{av} \times (-\mathbf{z}) \mathbf{h}_m \, ds = V_{0v} \cdot n \tag{4.13}$$

where n is the turns ratio of an aperture to microstrip line transition with the aperture being at 45° with respect to the microstrip line calculated from (4.7).

Therefore equation (4.11) can be written in the form

$$\Delta v = nV_{0u} + nV_{0v} = n\left(V_{0u} + V_{0v}\right) \tag{4.14}$$

The significance of equation (4.14) is that the cross-aperture in the ground plane of a microstrip line can be regarded as the series connection of two apertures, each at 45° with respect to the microstrip line. Therefore, the transition between a cross-aperture and a microstrip line can be substituted by the series connection of two ideal transformers as shown in Figure 4.3b.

4.2.3 VERIFICATION BY COMPUTER SIMULATION

The value of the turns ratio for an inclined slot and the assumption that the cross slot can be modelled by the series connection of two inclined slots have been verified using a computer simulation package (Ensemble V4.0, Boulder Microwave Technologies) which is based on the accurate modelling technique of full wave simulation.

The layouts of the models for one set of simulations are shown in Figure 4.4.

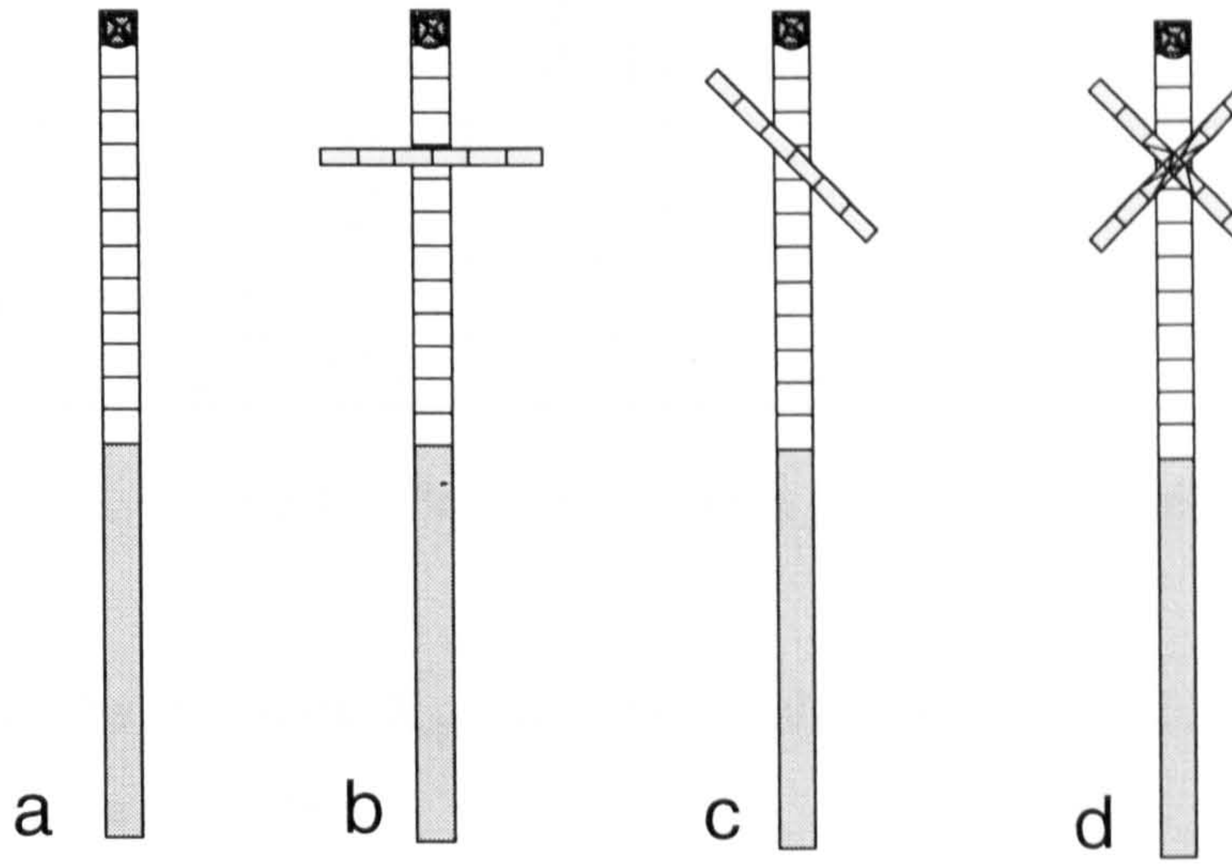

Figure 4.4. Layouts used for modelling the inclined, and, the cross-shaped apertures.

The model shown in Figure 4.4a consists of a microstrip line with a characteristic impedance of 50Ω, which terminates in a probe load of also 50Ω. This model was used to obtain the initial reference input impedance. The layouts shown in Figures 4.4b, c, and d, were used to obtain the impedance, as seen by the microstrip line, of a rectangular, an inclined, and, a cross-slot, respectively.

The distance of the slots measured from the feed point has been chosen to be exactly half of the guided wavelength. This ensures that the input impedance of the model equals the series impedance due to the aperture plus the characteristic impedance of 50Ω. Four such sets of simulations were performed with the parameters shown in Table 4.1.

No.	ε_r	d_f [mm]	f [GHz]	W_f [mm]	L_{ap} [mm]	W_{ap} [mm]
1	2.33	1.575	3	4.6	18.4	1
2	2.33	1.575	3	4.6	27.6	2
3	10.2	0.79	6	0.74	4.44	0.5
4	10.2	0.79	6	0.74	6.66	1

Table 4.1. Parameters of the simulation models.

The impedance of the apertures (X_{ap}) have been calculated by considering them as short circuited slot lines, as given by

$$X_{ap} = \frac{Z_{ca}}{2j} \cdot \tan\left(k_a \frac{L_a}{2}\right) \tag{4.15}$$

where, Z_{ca} and k_a are the characteristic impedance and the wave number of the aperture respectively, being determined by Cohns method, taking into account the influence of the patch antenna [Cohn 1969; Himdi and Daniel 1991]. In the calculation, the real part of the admittance, due to radiation, has been neglected, because of the small length of the simulated apertures. The turns ratio, as given by the simulation can be calculated from

$$n_{sim} = \sqrt{\frac{X_{m,sim}}{X_{ap}}} \tag{4.16}$$

with $X_{m,sim}$ being the simulated series impedance coupled to the microstrip line. The results of the simulations together with the values of turns ratios obtained by simulation (n_{sim}) and by calculation (n_{calc}) using (4.7) and (4.1) are shown in Table 4.2.

No.	X_{ap}	X_m θ=0°	X_m θ=45°	X_m cross	n_{sim} / n_{calc} θ=0°	n_{sim} / n_{calc} θ=45°
1	10.8Ω	34.5Ω	27.5 Ω	52.5 Ω	1.78 / 1.81	1.60 / 1.64
2	23.3Ω	92.5 Ω	78.5 Ω	132.5 Ω	1.99 / 2.02	1.83 / 1.85
3	9.6 Ω	16 Ω	11.8 Ω	23 Ω	1.29 / 1.28	1.11 / 1.08
4	21.4Ω	42.5 Ω	32.8 Ω	60.5 Ω	1.41 / 1.45	1.23 / 1.26

Table 4.2. Simulation results for perpendicular, inclined (45°), and cross-shaped slots.

It can be seen from Table 4.2. that there is a good match between the turns ratios calculated from (4.1) and that obtained from the simulation. The computer simulation also confirms that the cross-shaped aperture in the ground plane of a microstrip line can be regarded as the series connection of two slots, each at an angle of 45° with respect to the microstrip feed line. This is an important fundamental result which is used in the transmission line equivalent circuit of the circularly polarised patch antenna in the next section.

4.3 TRANSMISSION LINE ANALYSIS OF THE CROSS-APERTURE COUPLED PATCH

The operation of the circularly polarised patch antenna shown in Figure 4.1 is based on the two orthogonal apertures exciting the patch independently in the *x* and *y* directions. Therefore, the transmission line model is applied to the CP antenna, by modelling the patch in the *x* and *y* directions separately. This way two admittance values are obtained for the patch at the two apertures, which are combined together at the cross-aperture and transferred to the microstrip line.

4.3.1 RADIATION ADMITTANCE

The equivalent slot model has been described by Van de Capelle [Van de Capelle 1989] for a microstrip line or a probe fed linearly polarised antenna. This method is applied to the circularly polarised, aperture coupled antenna here, in order to obtain the self admittance, and, the mutual admittance of the radiating edges of the patch. Figure 4.5 shows how the CP patch is regarded as the superposition of two pairs of radiating slots.

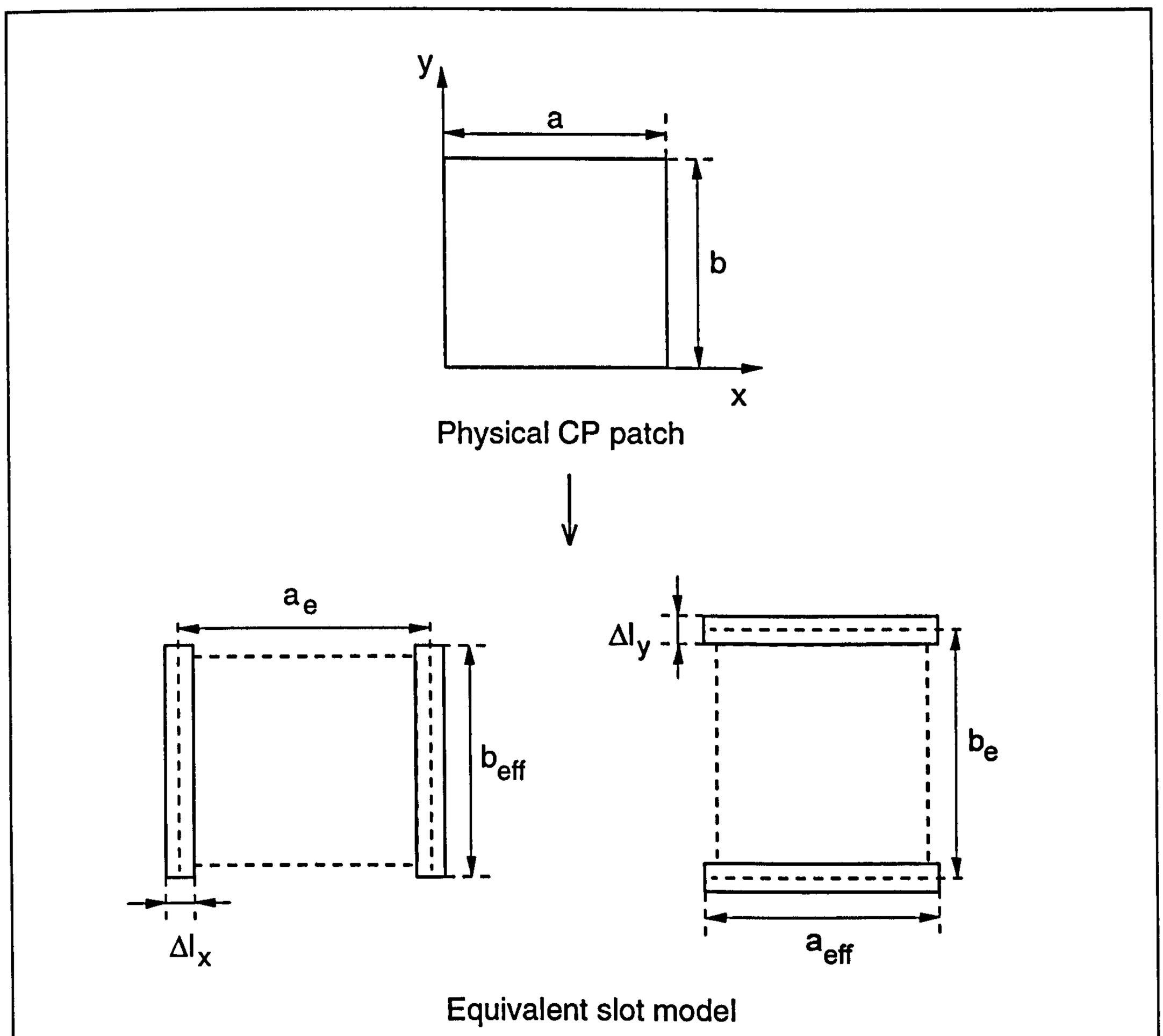

Figure 4.5. Application of the equivalent slot model for the CP patch.

As a first step the radiation admittance ($Y_{sx} = G_{sx} + jB_{sx}$) of the edges of the patch at $x = 0$ and $x = a$ are calculated. The slots have a width of Δl_x, which is the equivalent open-end extension of the patch antenna at edges $x = 0$ and $x = a$ accounting for the effect of the fringing fields. The expressions to calculate Δl_x is given in the Appendix D together with that for b_{eff}, which is the length of the equivalent slots. The centre-distance of the two slots are given by

$$a_e = a + \Delta l_x \tag{4.17}$$

The expression for the susceptance of the radiating edges at $x = 0$ and $x = a$ is based on the transmission line theory as given by

$$B_{sx} = Y_{cx} \tan(\beta_x \cdot \Delta l_x) \tag{4.18}$$

where Y_{cx}, β_x, are, respectively, the characteristic admittance and the phase constant of the patch antenna for wave propagation in the x direction (see Section 4.3.3).

The radiation conductance of the edges at $x = 0$ and $x = a$ is obtained by assuming a uniform electrical field distribution in the slots and calculating the total power radiated into half-space. The expression for the self-conductance is given by

$$G_{sx} = \frac{1}{Z_0 \cdot \pi}\left\{\left[w \cdot \mathrm{Si}(w) + \frac{\sin(w)}{w} + \cos(w) - 2\right] \times \left(1 - \frac{s^2}{24}\right) + \frac{s^2}{12}\left(\frac{1}{3} + \frac{\cos(w)}{w^2} - \frac{\sin(w)}{w^3}\right)\right\} \tag{4.19}$$

where, w is the normalised slot-length, and s is the normalised slot width, which are given by

$$w = kb_{eff} \tag{4.20}$$

$$s = k\Delta l_x \tag{4.21}$$

The function $Si(x)$ is defined as

$$\mathrm{Si}(x) = \int_0^x \frac{\sin(u)}{u} du \tag{4.22}$$

When determining the self-admittance ($Y_{sy} = G_{sy} + jB_{sy}$) of the patch in the y direction, the self-susceptance (B_{sy}) of the edges of the patch at $y = 0$ and $y = b$ is calculated as

$$B_{sy} = Y_{cy} \tan(\beta_y \cdot \Delta l_y) \tag{4.23}$$

where Y_{cy}, β_y, are, respectively, the characteristic admittance and the phase constant of the patch antenna for wave propagation in the y direction. The radiation conductance (G_{sy}) of the edges at $y = 0$ and $y = b$ is calculated using (4.19) with the following parameters

$$w = ka_{eff} \tag{4.24}$$

$$s = k\Delta l_y \tag{4.25}$$

(see Appendix D for expressions for a_{eff} and Δl_y).

4.3.2 MUTUAL COUPLING

There will be also mutual coupling between the two radiating edges at $x = 0$ and $x = a$, which is characterised by the mutual admittance ($Y_{mx} = G_{mx} + jB_{mx}$). The mutual conductance of the two radiating slots is calculated by assuming that the ratio of the self-conductance and mutual conductance is the same for slots of infinite and finite length. This assumption has been verified by Pues and Van de Capelle [Pues and Van de Capelle 1984] and proved to be adequate. Therefore, the mutual conductance between the edges at $x = 0$ and $x = a$, can be calculated as given by

$$G_{mx} = F_{gx} G_{sx} \tag{4.26}$$

where F_{gx} is the ratio of the mutual and self conductance of two slots of infinite length, having widths of Δl_x and distance of a_{eff} from each other. The value of F_{gx} is given by

$$F_{gx} = J_0(l) + J_2(l) \cdot \frac{s^2}{24 - s^2} \tag{4.27}$$

with

$$s = k\Delta l_x \tag{4.28}$$

$$l = k a_e \tag{4.29}$$

and where $J_0(x)$ and $J_2(x)$ are the zero and second order Bessel-functions, respectively.

The mutual susceptance of the edges at $x = 0$ and $x = a$ is given by

$$B_{mx} = F_{bx} K_{bx} B_{sx} \tag{4.30}$$

where F_{bx} is the ratio of the mutual and self susceptances of two infinite slot lines having with of Δl_x and distance of a_{eff} between each other. K_{bx} is a correction factor, since in the present case, the assumption that the ratios of mutual and self susceptances for slots of infinite and finite length are the same, does not provide sufficient accuracy. The value of F_{bx} can be calculated as given by

$$F_{bx} = \frac{\pi}{2} \cdot \frac{Y_0(l) + Y_2(l) \cdot \dfrac{s^2}{24 - s^2}}{\ln\left(\dfrac{s}{2}\right) + C_e - \dfrac{3}{2} + \dfrac{s^2}{12 \cdot \left(24 - s^2\right)}} \tag{4.31}$$

The value of the correction factor is a function of the slot length [Van de Capelle 1989] as given by

$$K_{bx} = 1 - \exp\left(-0.21w\right) \tag{4.32}$$

where

$$w = kb_{eff} \tag{4.33}$$

The mutual conductance and susceptance of the edges at $y = 0$ and $y = b$ is calculated by substituting

$$w = ka_{eff} \tag{4.34}$$

$$s = k\Delta l_y \tag{4.35}$$

$$l = kb_e \tag{4.36}$$

into (4.26) and (4.30), respectively.

4.3.3 LINE PARAMETERS

In order to reference the radiation admittance of the edges to the feeding aperture, the determination of the line parameters of the transmission line representing the antenna is required, which consist of the characteristic impedance and the propagation constant. As in the circular polarised antenna there are waves propagating in both the x and y directions, two sets of these parameters need to be determined. The characteristic impedance and the propagation constant of the transmission line representing the antenna in the x direction are given by [Van de Capelle 1989]

$$Z_{cx} = \frac{1}{Y_{cx}} = \frac{Z_0}{\sqrt{\varepsilon_{effx}}} \cdot \frac{d_a}{b_e} \tag{4.37}$$

$$\gamma_x = \alpha_x + j\beta_x = \alpha_x + j2\pi \cdot f\sqrt{\mu_0\varepsilon_0} \cdot \sqrt{\varepsilon_{effx}} \tag{4.38}$$

where, α_x is the attenuation constant incorporating the effect of dielectric, substrate and conductor losses and ε_{effx} is the effective permittivity, which is frequency dependent. The expressions for α_x and ε_{effx} are given in Appendix D. For wave propagation in the y direction, the line parameters (α_y and ε_{effy}) are calculated by substituting α_y and ε_{effy} into equations (4.37) and (4.38).

4.3.4 ADMITTANCE OF THE ANTENNA AT THE APERTURES

Once the radiation and mutual admittance of the edges and the line parameters are known, the transmission line theory is applied to determine the admittance of the patch at the apertures. First the admittance at the aperture parallel to the y axis is determined by considering the patch antenna in the x direction as a three port transmission line network as shown in Figure 4.6.

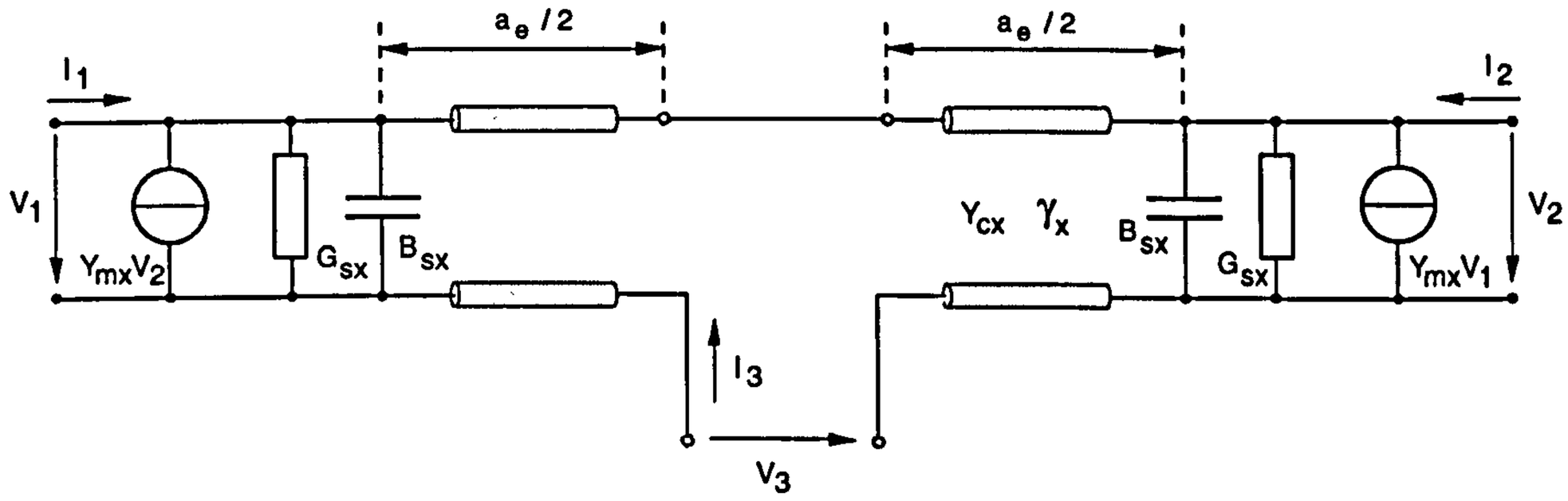

Figure 4.6. Equivalent circuit of the patch for the x direction.

The admittance of the patch at the aperture is calculated from the admittance matrix of the network. The m,n-th element of the matrix is given by

$$Y_{px,mn} = \left.\frac{I_m}{V_n}\right| \qquad V_{m'} = 0 \quad m' \neq m \tag{4.39}$$

Therefore, by the application of the transmission line theory [Helszajn 1992], the admittance matrix of the patch for wave propagation in the x direction is given by (see Appendix E.)

$$Y_{px} = \begin{bmatrix} Y_{sx} + Y_{cx}\coth(\gamma_x a_e) & -Y_{mx} - \dfrac{Y_{cx}}{\sinh(\gamma_x a_e)} & \dfrac{Y_{cx}}{2\sinh\left(\gamma_x \dfrac{a_e}{2}\right)} \\ -Y_{mx} - \dfrac{Y_{cx}}{\sinh(\gamma_x a_e)} & Y_{sx} + Y_{cx}\coth(\gamma_x a_e) & \dfrac{-Y_{cx}}{2\sinh\left(\gamma_x \dfrac{a_e}{2}\right)} \\ \dfrac{Y_{cx}}{2\sinh\left(\gamma_x \dfrac{a_e}{2}\right)} & \dfrac{-Y_{cx}}{2\sinh\left(\gamma_x \dfrac{a_e}{2}\right)} & \dfrac{Y_{cx}}{2}\coth\left(\gamma_x \dfrac{a_e}{2}\right) \end{bmatrix} \tag{4.40}$$

From this, the input admittance at port 3 can be expressed by assuming zero currents at ports 1 and 2 ($I_{x,1} = I_{x,2} = 0$), as given by

$$\frac{I_3}{V_3} = \frac{\left|\left[Y_{px}\right]\right|}{Y^{c}_{px,33}} \tag{4.41}$$

where $\left|\left[Y_{px}\right]\right|$ is the determinant of the matrix $\left[Y_{px}\right]$ and

$Y^{c}_{px,33}$ is the cofactor of element $Y_{px,33}$

Hence the patch admittance at the aperture parallel to the y axis is given by (see Appendix E.)

$$Y_{PX} = 1 - \frac{Y_{cx}}{\sinh\left(\gamma_x \frac{a_e}{2}\right)\cosh\left(\gamma_x \frac{a_e}{2}\right)\left[Y_{sx} + Y_{cx}\coth\left(\gamma_x a_e\right) + Y_{mx} + \frac{Y_{cx}}{\sinh\left(\gamma_x a_e\right)}\right]} \tag{4.42}$$

Following a similar procedure, the admittance matrix of the patch in the y direction is determined, which is given by

$$Y_{py} = \begin{bmatrix} Y_{sy} + Y_{cy}\coth\left(\gamma_y b_e\right) & -Y_{my} - \dfrac{Y_{cy}}{\sinh\left(\gamma_y b_e\right)} & \dfrac{Y_{cy}}{2\sinh\left(\gamma_y \dfrac{b_e}{2}\right)} \\ -Y_{my} - \dfrac{Y_{cy}}{\sinh\left(\gamma_y b_e\right)} & Y_{sy} + Y_{cy}\coth\left(\gamma_y b_e\right) & \dfrac{-Y_{cy}}{2\sinh\left(\gamma_y \dfrac{b_e}{2}\right)} \\ \dfrac{Y_{cy}}{2\sinh\left(\gamma_y \dfrac{b_e}{2}\right)} & \dfrac{-Y_{cy}}{2\sinh\left(\gamma_y \dfrac{b_e}{2}\right)} & \dfrac{Y_{cy}}{2}\coth\left(\gamma_y \dfrac{b_e}{2}\right) \end{bmatrix} \tag{4.43}$$

and from this, the admittance of the antenna at the aperture parallel to the x axis is calculated as given by

$$Y_{PY} = \frac{\left|\left[Y_{py}\right]\right|}{Y^{c}_{py,33}} \tag{4.44}$$

where $\left|\left[Y_{py}\right]\right|$ is the determinant of the matrix $\left[Y_{py}\right]$ and

$Y^{c}_{py,33}$ is the cofactor of element $Y_{py,33}$

Hence the patch admittance at the aperture parallel to the y axis is given by (see Appendix E.)

$$Y_{PY} = 1 - \frac{Y_{cy}}{\sinh\left(\gamma_y \dfrac{b_e}{2}\right)\cosh\left(\gamma_y \dfrac{b_e}{2}\right)\left[Y_{sy} + Y_{cy}\coth\left(\gamma_y b_e\right) + Y_{my} + \dfrac{Y_{cy}}{\sinh\left(\gamma_y b_e\right)}\right]} \tag{4.45}$$

4.3.5 INPUT IMPEDANCE AND EQUIVALENT CIRCUIT

The individual self-admittance (Y_{ap}) of the two orthogonal slots are taken into account by considering them as short circuited slot lines. Therefore

$$Y_{ap} = -\frac{2j}{Z_{ca}} \cdot \cot\left(k_a \frac{L_a}{2}\right) \tag{4.46}$$

The values of the total admittance at the two apertures are

$$Y_{ta} = n_{1a}^2 Y_{PX} + Y_{ap} \qquad \text{and} \qquad Y_{tb} = n_{1b}^2 Y_{PY} + Y_{ap} \tag{4.47}$$

where, n_{1a} and n_{1b} are the turns ratios of the patch-to-slot impedance transformers, which are obtained by assuming that, due to the size of the antenna, there is a uniform current distribution in the ground plane under the patch. The turns ratios are then the ratios of the fraction of current flowing through the apertures over the total current in the patch [Himdi et al. 1989a], and are given by

$$n_{1a} = \frac{L_a}{a} \qquad \text{and} \qquad n_{1b} = \frac{L_a}{b} \tag{4.48}$$

Since it has been established that the cross-slot can be regarded as two orthogonal slots in series connection, the input impedance of the CP antenna on the microstrip feed line under the centre of the aperture is given by

$$Z_{in} = n_{2(45)}^2 \cdot \left(\frac{1}{Y_{ta}} + \frac{1}{Y_{tb}}\right) - jZ_{cf} \cdot \cot\left(k_f L_{os}\right) \tag{4.49}$$

where, Z_{cf} is the characteristic impedance of the microstrip feed line,

k_f is the wave number of the microstrip feed line, and

$n_{2(45)}$ is the turns ratio of the 45° slot line-to-microstrip transition.

The result of the investigation of the cross-aperture and the calculation regarding the circular polarised antenna can be summarised in an equivalent circuit as shown in Figure 4.6.

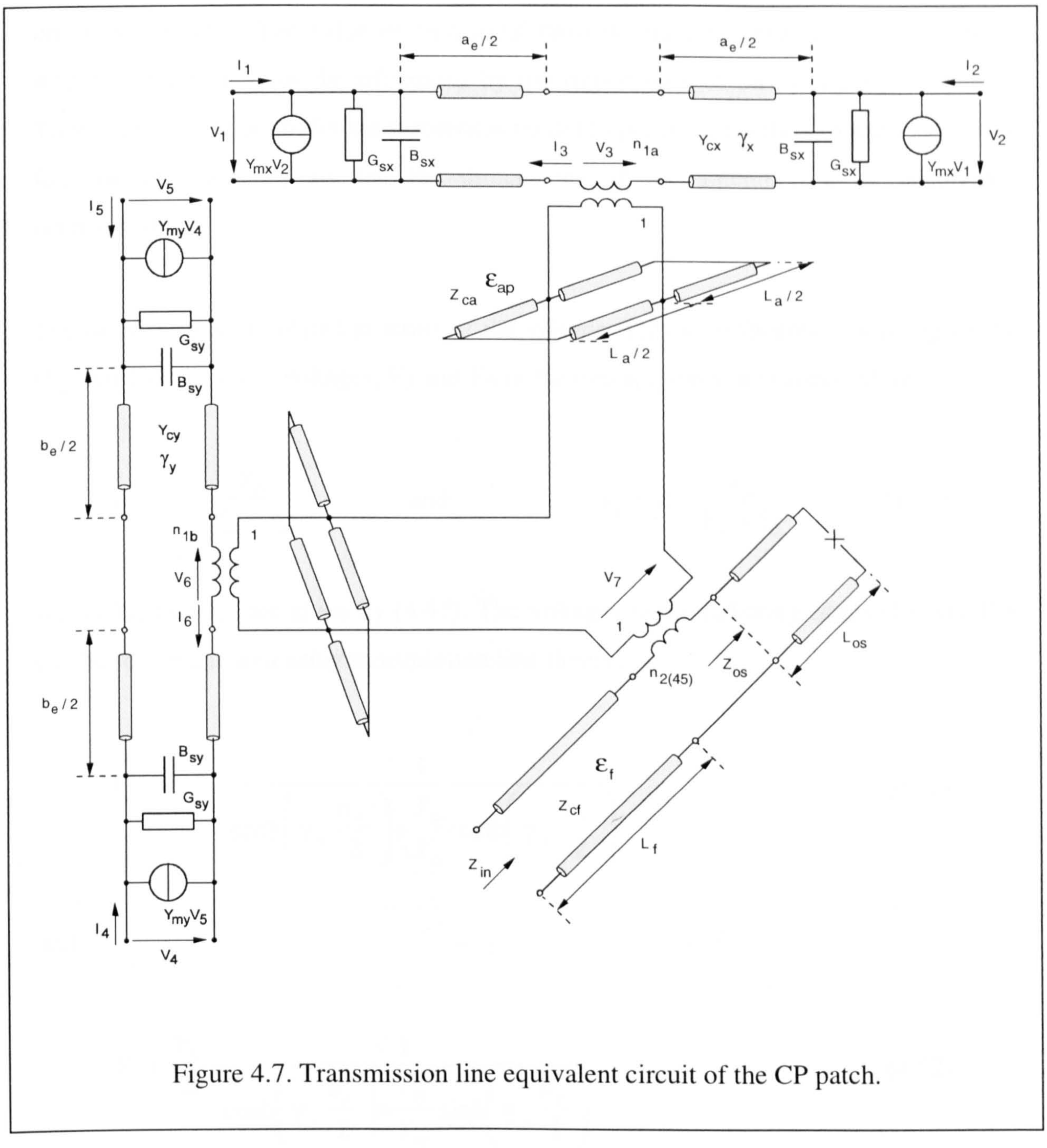

Figure 4.7. Transmission line equivalent circuit of the CP patch.

4.4 CALCULATION OF THE AXIAL RATIO

Single feed circular polarised patches typically provide good axial ratio performance in a limited frequency band only, contained between the resonant frequencies of the two orthogonal modes. The value of best axial ratio within this band and the frequency where it occurs is strongly influenced by the dimensions of the nearly square patch. Therefore it is important for the theoretical model to predict the values of axial ratio as a function of frequency so that the dimensions of the antenna can be accurately determined.

The axial ratio is calculated in terms of the voltages for two orthogonal radiating edges (V_2 and V_5). First, the voltages, V_3 and V_6 in the two apertures are expressed as

$$V_3 = V_7 \cdot \frac{Y_{tb}}{Y_{ta} + Y_{tb}} \qquad \text{and} \qquad V_6 = V_7 \cdot \frac{Y_{ta}}{Y_{ta} + Y_{tb}} \tag{4.50}$$

where Y_{ta} and Y_{tb} are given by (4.47). The voltages at the radiating edges (V_2 and V_5) can be then expressed using transmission line theory:

$$V_2 = \frac{V_3}{2} \cdot \frac{1}{\cosh\left(\gamma_x \frac{a_e}{2}\right) + \frac{Y_{sx}}{Y_{cx}} \sinh\left(\gamma_x \frac{a_e}{2}\right)} \tag{4.51}$$

and

$$V_5 = \frac{V_6}{2} \cdot \frac{1}{\cosh\left(\gamma_y \frac{b_e}{2}\right) + \frac{Y_{sy}}{Y_{cy}} \sinh\left(\gamma_y \frac{b_e}{2}\right)} \tag{4.52}$$

As the radiated electric field is generated by the voltage on the patch at the edges, the phase difference between the x and y components of the electric field in the boresight (phase error, ϕ_e) is the same as the phase difference between V_2 and V_5 , namely

$$\phi_e = \arg(V_5) - \arg(V_2) \tag{4.53}$$

The x and y directed electric field components in the far field are directly proportional to the voltages V_2 and V_5 respectively, therefore the amplitude error (A_e) is given by:

$$A_e = \frac{|V_5|}{|V_2|} \tag{4.54}$$

The axial ratio (AR) can be then calculated from the amplitude and phase error as given by [Balanis 1982]

$$AR = \sqrt{\frac{1 + A_e^2 + \left[1 + A_e^4 + 2A_e^2 \cos(2\phi_e)\right]^{1/2}}{1 + A_e^2 - \left[1 + A_e^4 + 2A_e^2 \cos(2\phi_e)\right]^{1/2}}} \tag{4.55}$$

Equations (4.50) through (4.55) provide a numerical means of determining the axial ratio of the cross-aperture coupled patch antenna at a certain frequency when the design parameters shown in Figure 4.1 are known. The accuracy of the predicted axial ratio is examined in Chapter six.

4.5 CHAPTER SUMMARY

In this chapter an original analysis of a cross-aperture coupled circularly polarised antenna based on the transmission line method has been presented. In order to apply the transmission line method, the transition between a cross-shaped aperture and a microstrip line has been investigated and it was found that the cross-aperture can be regarded as the series connection of two orthogonal slots, which excite the patch in the x and y directions independently.

This allowed the representation of the patch, in the direction of its two orthogonal modes, by transmission line networks. The input impedance and the axial ratio of the cross-aperture coupled circular polarised antenna, based on the transmission line theory, have been derived.

The next chapter presents the cavity model analysis of the cross-aperture coupled antenna, which is usually a more accurate technique, but it requires more computation. The results of the two methods of analysis are compared to each other and to measurement and full wave computer simulation results in Chapter six.

CHAPTER 5.

CAVITY MODEL OF THE CROSS-APERTURE COUPLED CP MICROSTRIP ANTENNA

5.1 INTRODUCTION

This chapter presents an original analysis of a cross-aperture coupled CP microstrip antenna, shown in Figure 5.1, by the application of the cavity method. Initially, the electric field in each of the two orthogonal apertures are replaced by equivalent magnetic currents, which are uniformly distributed in the volume of the patch above the slot. In this way the apertures can be closed off and the ground plane modelled with the slots removed. This, together with the assignment of four magnetic walls at the edges of the patch allows the antenna to be modelled in terms of a cavity resonator. Then the magnetic current excitation and the boundary conditions enable the coefficients of all the possible field modes under the patch to be obtained using the Maxwell's equations.

After the components of the magnetic and electric fields are known in the volume of the patch, an equivalent circuit based on the resonant cavity method is given and the input impedance and the axial ratio of the cross-aperture coupled antenna are calculated.

5.2 FIELD DISTRIBUTION

When applying the cavity method to the cross-aperture coupled circularly polarised antenna, a number of assumptions are made as follows:

- Due to the small d_a/λ_0 ratio (less than 0.1), the electric field in the volume of the antenna has a z component only.

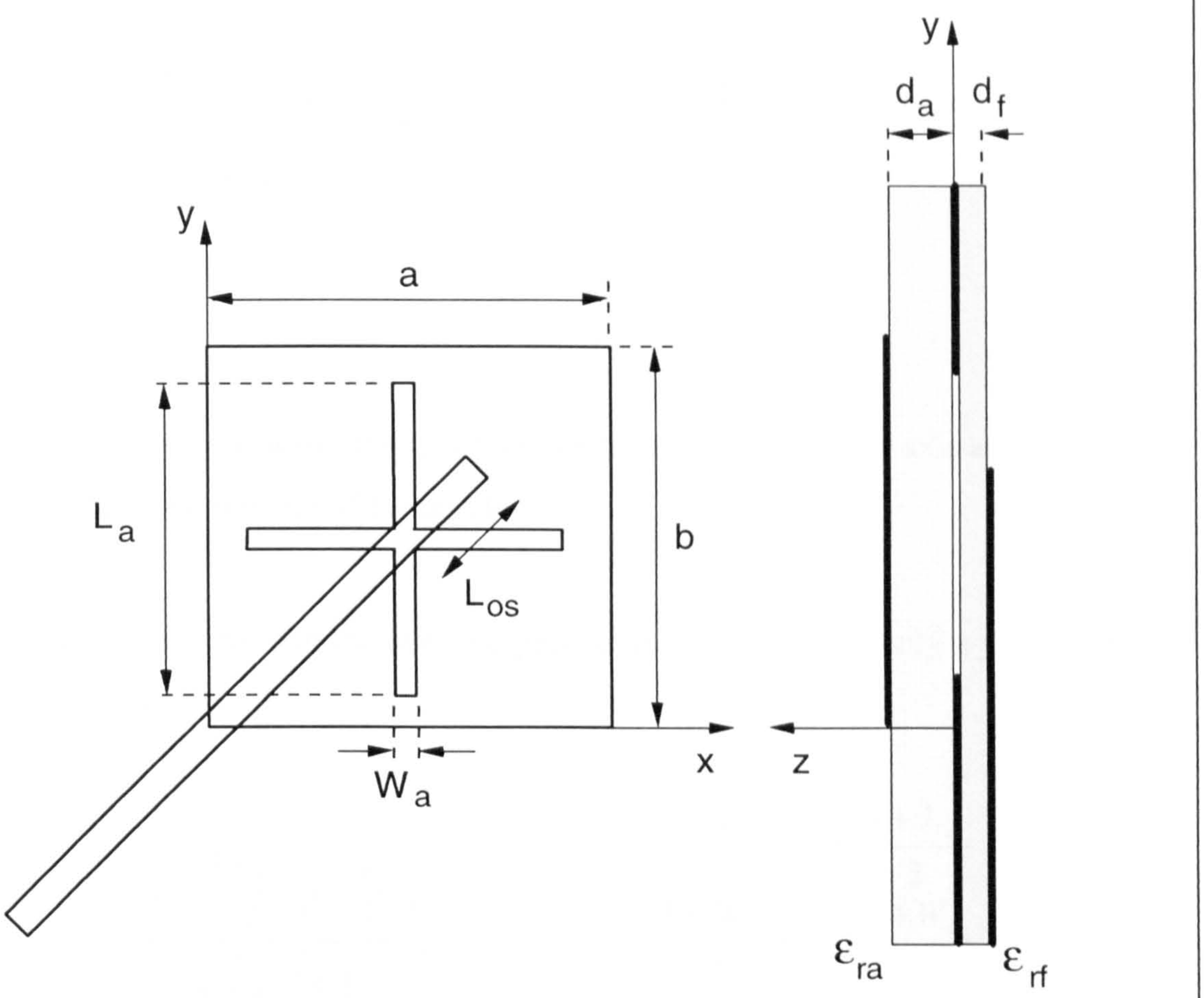

Figure 5.1. Design parameters of the cross-aperture coupled microstrip antenna.

- Four magnetic walls are assumed at the edges of the patch as boundary conditions.

- A uniform magnetic current excitation is introduced above the slot, which replaces the electric field in the aperture.

- The perturbation due to the local field of the aperture is taken into account by the self-admittance of short circuited slot lines.

The electric field distribution in each of the two orthogonal apertures is assumed to be in the form of a single piece-wise sinusoidal mode [Sullivan and Schaubert 1986]. The electric field in the aperture parallel to the y axis has only an x directed component (E_{ax}) which is given by

$$E_{ax} = \frac{V_{0y}}{W_a} \frac{\sin\left[k_a\left(\frac{L_a}{2} - \left|y - \frac{b}{2}\right|\right)\right]}{\sin\left(k_a \frac{L_a}{2}\right)}; \qquad \begin{array}{c} \frac{a - W_a}{2} \le x \le \frac{a + W_a}{2} \\ \frac{b - L_a}{2} \le y \le \frac{b + L_a}{2} \\ z = 0 \end{array}$$

$$= 0\ ; \qquad \text{otherwise} \qquad (5.1a)$$

where, V_{0y} is the voltage at the middle of the aperture parallel to the y axis and

k_a is the wave number of the aperture.

Similarly, the electric field in the aperture parallel to the x axis has only a y component (E_{ay}) which is given by

$$E_{ay} = \frac{V_{0x}}{W_a} \frac{\sin\left[k_a\left(\frac{L_a}{2} - \left|x - \frac{a}{2}\right|\right)\right]}{\sin\left(k_a \frac{L_a}{2}\right)}; \qquad \begin{array}{c} \frac{a - L_a}{2} \le x \le \frac{a + L_a}{2} \\ \frac{b - W_a}{2} \le y \le \frac{b + W_a}{2} \\ z = 0 \end{array}$$

$$= 0\ ; \qquad \text{otherwise} \qquad (5.1b)$$

where, V_{0x} is the voltage at the middle of the aperture parallel to the x axis.

The electric field in the apertures can be written as

$$\mathbf{E_a} = E_{ax} \cdot \mathbf{x} + E_{ay} \cdot \mathbf{y} \qquad (5.2)$$

By applying the equivalence principle [Balanis 1989], the electric fields in the apertures are replaced by magnetic currents. The value of the equivalent magnetic current is given by

$$\mathbf{M_a} = 2 \cdot \mathbf{E_a} \times \mathbf{z} \qquad (5.3)$$

Thus, from (5.2), (5.3) the x and y components of the equivalent magnetic current are

$$M_{ax} = -2E_{ay} \tag{5.4a}$$

$$M_{ay} = 2E_{ax} \tag{5.4b}$$

The equivalent magnetic current excitation is assumed to be uniformly distributed in the volume above the slot as shown in Figure 5.2 [Himdi 1989b].

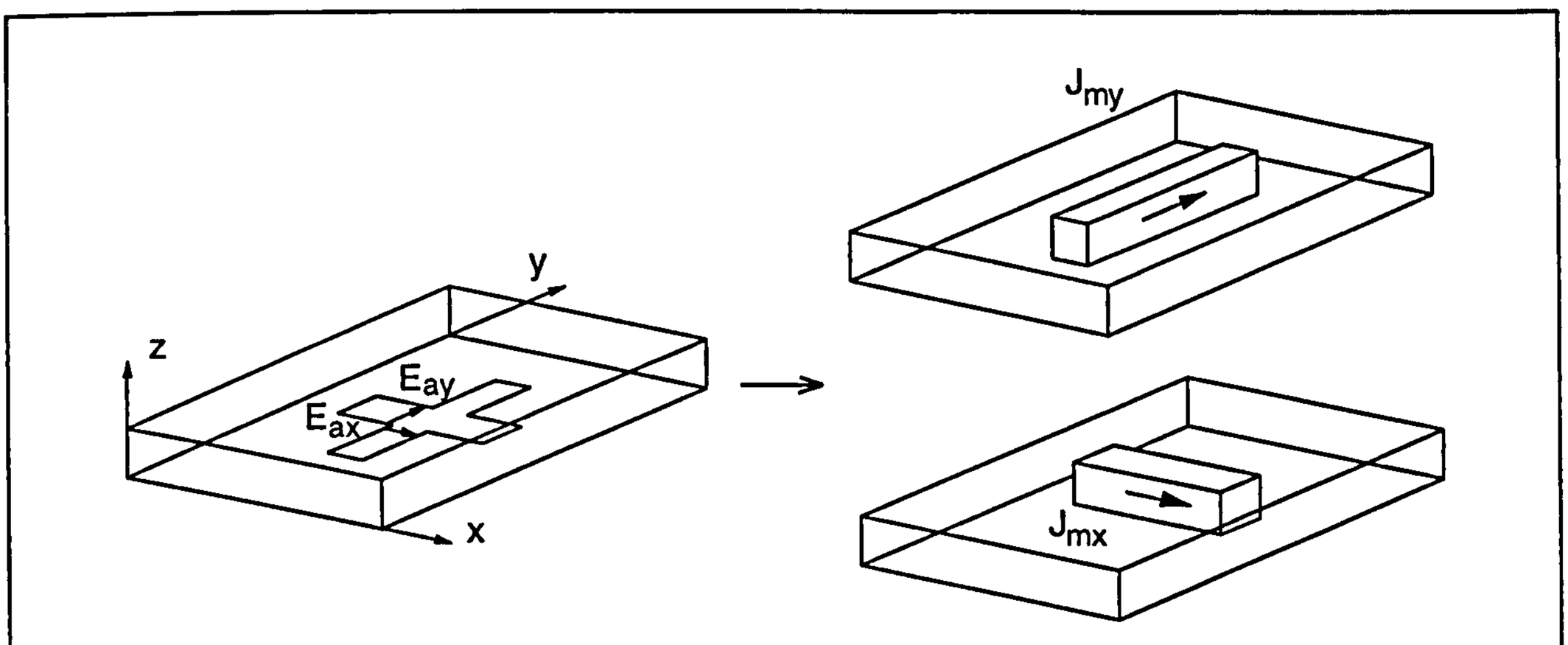

Figure 5.2. Equivalent magnetic currents replacing the electric fields in the apertures.

The three-dimensional current density due to the two orthogonal apertures are therefore given by

$$J_{mx} = \frac{-2V_{0x}}{d_a W_a} \frac{\sin\left[k_a\left(\frac{L_a}{2} - \left|x - \frac{a}{2}\right|\right)\right]}{\sin\left(k_a \frac{L_a}{2}\right)}; \qquad \begin{matrix} \frac{a-L_a}{2} \le x \le \frac{a+L_a}{2} \\ \frac{b-W_a}{2} \le y \le \frac{b+W_a}{2} \\ 0 \le z \le d_a \end{matrix}$$

$$= 0\ ; \qquad \text{otherwise} \tag{5.5a}$$

and

$$J_{my} = \frac{2V_{0y}}{d_a W_a} \frac{\sin\left[k_a\left(\frac{L_a}{2} - \left|y - \frac{b}{2}\right|\right)\right]}{\sin\left(k_a \frac{L_a}{2}\right)}; \qquad \begin{matrix} \frac{a - W_a}{2} \le x \le \frac{a + W_a}{2} \\ \frac{b - L_a}{2} \le y \le \frac{b + L_a}{2} \\ 0 \le z \le d_a \end{matrix}$$

$$= 0\ ; \qquad \text{otherwise} \qquad (5.5b)$$

The total magnetic current due to the cross-aperture is then given by

$$\mathbf{J}_{\mathrm{m}} = J_{mx} \cdot \mathbf{x} + J_{my} \cdot \mathbf{y} \qquad (5.6)$$

The field inside the cavity is determined by solving Maxwell's equations, which are given in time harmonic form (phasor form) by

$$\nabla \times \mathbf{E} = -j\omega\mu_0 \mathbf{H} - \mathbf{J}_{\mathrm{m}} \qquad (5.7)$$

$$\nabla \times \mathbf{H} = j\omega\varepsilon \mathbf{E} \qquad (5.8)$$

From (5.7) and (5.8) one obtains the wave equation for the magnetic field in the form

$$\nabla \times \nabla \times \mathbf{H} - k^2 \mathbf{H} = -j\omega\mu_0 \mathbf{J}_{\mathrm{m}} \qquad (5.9)$$

From the assumptions made at the beginning of the chapter, and in particular, that the magnetic field has only x and y components, the above vector equation can be separated into the following two scalar differential equations:

$$\frac{d^2 H_y}{dxdy} - \frac{d^2 H_x}{dy^2} - k^2 H_x = -j\omega\mu_0 J_{mx} \qquad (5.10a)$$

$$\frac{d^2 H_x}{dxdy} - \frac{d^2 H_y}{dy^2} - k^2 H_y = -j\omega\mu_0 J_{my} \qquad (5.10b)$$

The solution of the above two non-homogeneous differential-equations can be written in the form of

$$H_x = \sum_m \sum_n B_{x,mn} \Psi_{x,mn} \tag{5.11a}$$

$$H_y = \sum_m \sum_n B_{y,mn} \Psi_{y,mn} \tag{5.11b}$$

where, $B_{x,mn}$ and $B_{y,mn}$ are the unknown mode coefficients and $\Psi_{x,mn}$ and $\Psi_{y,mn}$ are the eigenfunctions of equation (5.9) and its associated boundary conditions. The eigenfunctions must satisfy the associated homogenous equations

$$\frac{d^2\Psi_{x,mn}}{dxdy} - \frac{d^2\Psi_{y,mn}}{dy^2} - k_{mn}\Psi_{x,mn} = 0 \tag{5.12a}$$

$$\frac{d^2\Psi_{y,mn}}{dxdy} - \frac{d^2\Psi_{x,mn}}{dy^2} - k_{mn}\Psi_{y,mn} = 0 \tag{5.12b}$$

where k_{mn} are the associated eigenvalues given by

$$k_{mn} = \sqrt{k_m^2 + k_n^2} \tag{5.13}$$

The four magnetic wall boundary conditions require that

$$\begin{aligned} \Psi_{x,mn} &= 0 \qquad \text{at } y = 0 \text{ and at } y = b \text{ and} \\ \Psi_{y,mn} &= 0 \qquad \text{at } x = 0 \text{ and at } x = a \end{aligned} \tag{5.14}$$

and hence the eigenfunctions are of the form

$$\Psi_{x,mn} = A_{mn} \cdot k_n \cdot \cos(k_m x)\sin(k_n y) \tag{5.15a}$$

$$\Psi_{y,mn} = A_{mn} \cdot k_m \cdot \sin(k_m x)\cos(k_n y) \tag{5.15b}$$

with

$$A_{mn} = \sqrt{\frac{\chi_m \chi_n}{ab}} \qquad \text{where} \qquad \chi_p = \begin{cases} 1 \text{ if } p = 0 \\ \\ 2 \text{ if } p \neq 0 \end{cases} \tag{5.16}$$

and

$$k_m = \frac{m \cdot \pi}{a} \qquad k_n = \frac{n \cdot \pi}{b} \tag{5.17}$$

The mode coefficients ($B_{x,mn}$ and $B_{y,mn}$) can be found by substituting the solution for H_x and H_y from (5.11a) and (5.11b) into the original differential equations (5.10a) and (5.10b) which gives

$$\sum_m \sum_n B_{x,mn}\left(k_{mn}^2 - k^2\right)\Psi_{x,mn} = -j\omega\varepsilon J_{mx} \tag{5.18a}$$

$$\sum_m \sum_n B_{y,mn}\left(k_{mn}^2 - k^2\right)\Psi_{y,mn} = -j\omega\varepsilon J_{my} \tag{5.18b}$$

By multiplying (5.18a) with the modal function of mode m', n' ($\Psi_{x,m'n'}$) and (5.18b) with ($\Psi_{y,m'n'}$) and integrating the equations over the volume of the patch, one obtains

$$\sum_m \sum_n B_{x,mn}\left(k_{mn}^2 - k^2\right)\int_0^a\int_0^b \Psi_{x,mn}\Psi_{x,m'n'}\,dxdy = -j\omega\varepsilon\int_0^a\int_0^b J_{mx}\Psi_{x,m'n'}\,dxdy \tag{5.19a}$$

$$\sum_m \sum_n B_{y,mn}\left(k_{mn}^2 - k^2\right)\int_0^a\int_0^b \Psi_{y,mn}\Psi_{y,m'n'}\,dxdy = -j\omega\varepsilon\int_0^a\int_0^b J_{my}\Psi_{y,m'n'}\,dxdy \tag{5.19b}$$

Due to the orthogonal properties of $\Psi_{x,mn}$ and $\Psi_{y,mn}$ the value of the integrals on the left side are

$$\int_0^a\int_0^b \Psi_{x,mn}\Psi_{x,m'n'}\,dxdy = \begin{cases} k_n^2 & \text{if } m = m\text{'} \text{ and } n = n\text{'} \\ 0 & \text{otherwise} \end{cases} \tag{5.20a}$$

$$\int_0^a\int_0^b \Psi_{y,mn}\Psi_{y,m'n'}\,dxdy = \begin{cases} k_m^2 & \text{if } m = m\text{'} \text{ and } n = n\text{'} \\ 0 & \text{otherwise} \end{cases} \tag{5.20b}$$

Therefore equations (5.19a) and (5.19b) can be simplified to

$$B_{x,mn}\left(k_{mn}^2-k^2\right)\cdot k_n^2=-j\omega\varepsilon\int_0^a\int_0^b J_{mx}\Psi_{x,mn}dxdy \tag{5.21a}$$

$$B_{y,mn}\left(k_{mn}^2-k^2\right)\cdot k_m^2=-j\omega\varepsilon\int_0^a\int_0^b J_{my}\Psi_{y,mn}dxdy \tag{5.21b}$$

from which the mode coefficients can be expressed as

$$B_{x,mn}=\frac{j\omega\varepsilon}{\left(k^2-k_{mn}^2\right)\cdot k_n^2}\int_0^a\int_0^b J_{mx}\Psi_{x,mn}dxdy \tag{5.22a}$$

$$B_{y,mn}=\frac{j\omega\varepsilon}{\left(k^2-k_{mn}^2\right)\cdot k_m^2}\int_0^a\int_0^b J_{my}\Psi_{y,mn}dxdy \tag{5.22b}$$

After evaluating the integrals (see Appendix F) in the above equations, the values of the mode coefficients are

$$B_{x,mn}=\frac{-j\omega\varepsilon\cdot A_{mn}V_{0x}}{d_a k_n\cdot\left(k^2-k_{mn}^2\right)}\cdot\frac{4\mathrm{sinc}\left(k_n\frac{W_a}{2}\right)\sin\left(\frac{n\pi}{2}\right)\cos\left(\frac{m\pi}{2}\right)}{\sin\left(k_a\frac{L_a}{2}\right)}\cdot\frac{k_a\left[\cos\left(k_m\frac{L_a}{2}\right)-\cos\left(k_a\frac{L_a}{2}\right)\right]}{k_a^2-k_m^2} \tag{5.23a}$$

$$B_{y,mn}=\frac{j\omega\varepsilon\cdot A_{mn}V_{0y}}{d_a k_m\cdot\left(k^2-k_{mn}^2\right)}\cdot\frac{4\mathrm{sinc}\left(k_m\frac{W_a}{2}\right)\sin\left(\frac{m\pi}{2}\right)\cos\left(\frac{n\pi}{2}\right)}{\sin\left(k_a\frac{L_a}{2}\right)}\cdot\frac{k_a\left[\cos\left(k_n\frac{L_a}{2}\right)-\cos\left(k_a\frac{L_a}{2}\right)\right]}{k_a^2-k_n^2} \tag{5.23b}$$

With the known mode coefficients the components of the magnetic field in the volume of the patch is given as

$$H_x=\sum_m\sum_n A_{mn}B_{x,mn}k_n\cos\left(k_m x\right)\sin\left(k_n y\right) \tag{5.24a}$$

$$H_y=\sum_m\sum_n A_{mn}B_{y,mn}k_m\sin\left(k_m x\right)\cos\left(k_n y\right) \tag{5.24b}$$

The z directed electric field is determined from Maxwell's equation (5.8) which can be written in the form

$$E_{z(x,y)} = \frac{1}{j\omega\epsilon}\left[\frac{dH_y}{dx} - \frac{dH_x}{dy}\right] \tag{5.25}$$

Therefore

$$E_{z(x,y)} = \frac{1}{j\omega\varepsilon}\sum_m\sum_n A_{mn}C_{mn}\cos(k_m x)\cos(k_n y) \tag{5.26}$$

where

$$C_{mn} = B_{x,mn}k_m^2 - B_{y,mn}k_n^2 \tag{5.27}$$

Hence, the electromagnetic field in the volume of the patch is determined and is given by equations (5.24a), (5.24b) and (5.26).

5.3 TAKING THE LOSSES INTO ACCOUNT

The losses are accounted for by replacing k by an effective wave number as given by

$$k_{eff}^2 = k_0^2\varepsilon_r\left(1 - j\delta_{eff}\right) \tag{5.28}$$

where δ_{eff} is the effective loss tangent including the radiation, copper and dielectric losses [Richards et al. 1981]. A formula for the calculation of δ_{eff}, which has recently appeared in the literature [Thouroude et al. 1990] has been used in the analysis and is given by

$$\delta_{eff} = \delta + \frac{\Delta}{d_a} + \frac{d_a A\pi^4}{\omega_r\varepsilon_0\varepsilon_{ra}r^2}\cdot\frac{1}{11520}\cdot\left[(1-B)\left(1 - \frac{A}{15} + \frac{A^2}{420}\right) + \frac{B^2}{5}\left(2 - \frac{A}{7} + \frac{A^2}{189}\right)\right] \tag{5.29}$$

where, δ is the loss tangent of the substrate,

Δ is the skin depth and

$$A=\left(\frac{2r}{\lambda_0}\right)^2 \qquad B=\left(\frac{\pi\cdot r}{\lambda_0}\right) \qquad r=\frac{a+b}{2} \tag{5.30}$$

and

$$\omega_r=\frac{c}{2(r+2\Delta l)\sqrt{\varepsilon_{el}}} \qquad \varepsilon_{el}=\frac{1}{2}\left[\varepsilon_{ra}+1+(\varepsilon_{ra}-1)\left(1+\frac{12d_a}{r}\right)^{-\frac{1}{2}}\right] \tag{5.31}$$

and

$$\Delta l=\frac{d_a}{2\cdot\pi}\cdot\frac{\frac{r}{d_a}+0.366}{\frac{r}{d_a}+0.556}\cdot\left[0.28+\frac{\varepsilon_{ra}+1}{\varepsilon_{ra}}\left(0.274+\log\left(\frac{r}{d_a}+0.366\right)\right)\right] \tag{5.32}$$

In the above expressions, it was assumed that the values of δ_{eff} are close to each other for wave propagation in the x and the y direction, since the values a and b are close. Hence, an average loss tangent was calculated by the introduction of r in (5.30).

5.4 INPUT IMPEDANCE

The admittance of the patch at the two orthogonal apertures can be calculated using the energy conservation theorem [Balanis 1989] which states that for a volume of V enclosed by a surface of S

$$\iint_S \mathbf{E}\times\mathbf{H}^* ds+\iiint_V\left(\mathbf{E}\mathbf{J}_e^*+\mathbf{H}\mathbf{J}_m^*\right)dv=0 \tag{5.33}$$

By applying the above formula to the antenna cavity, one obtains the following expression for the patch admittances as seen by the two orthogonal apertures

$$Y_{x,ant} = \frac{\iiint_V H_x J_{mx}^* dv}{|V_{0x}|^2} \tag{5.34a}$$

$$Y_{y,ant} = \frac{\iiint_V H_y J_{my}^* dv}{|V_{0y}|^2} \tag{5.34b}$$

Substituting the expressions for the magnetic field (5.24a), (5.24b) and the magnetic current (5.5a), (5.5b) and performing the integration (see Appendix G), the following analytical formulas are obtained for the admittance values of the antenna at the apertures

$$Y_{x,ant} = \sum_m \sum_n \frac{16 \cdot j\omega\varepsilon \cdot A_{mn}^2}{d_a\left((k^*)^2 - k_{mn}^2\right)} \cdot \left\{ \frac{\operatorname{sinc}\left(k_n \frac{W_a}{2}\right) \sin\left(\frac{n\pi}{2}\right) \cos\left(\frac{m\pi}{2}\right)}{\sin\left(k_a \frac{L_a}{2}\right)} \cdot \frac{k_a\left[\cos\left(k_m \frac{L_a}{2}\right) - \cos\left(k_a \frac{L_a}{2}\right)\right]}{k_a^2 - k_m^2} \right\}^2 \tag{5.35a}$$

$$Y_{y,ant} = \sum_m \sum_n \frac{16 \cdot j\omega\varepsilon \cdot A_{mn}^2}{d_a\left((k^*)^2 - k_{mn}^2\right)} \cdot \left\{ \frac{\operatorname{sinc}\left(k_m \frac{W_a}{2}\right) \sin\left(\frac{m\pi}{2}\right) \cos\left(\frac{n\pi}{2}\right)}{\sin\left(k_a \frac{L_a}{2}\right)} \cdot \frac{k_a\left[\cos\left(k_n \frac{L_a}{2}\right) - \cos\left(k_a \frac{L_a}{2}\right)\right]}{k_a^2 - k_n^2} \right\}^2 \tag{5.35b}$$

The self-admittance of the aperture is calculated by considering it as two short circuited slot lines of length $L_a/2$, and, is thus given by

$$Y_{ap} = -\frac{2j}{Z_{ca}} \cot\left(k_a \frac{L_a}{2}\right) \tag{5.36}$$

Finally, the input impedance of the antenna is given by the following expression

$$Z_{in} = \frac{n_{2(45)}^2}{Y_{x,ant} + Y_{ap}} + \frac{n_{2(45)}^2}{Y_{y,ant} + Y_{ap}} - jZ_f \cot\left(k_f L_{os}\right) \tag{5.37}$$

where $n_{2(45)}$ is the turns ratio of the microstrip to aperture impedance transformation, for the two orthogonal apertures, each at 45° with respect to the microstrip line.

5.5 EQUIVALENT CIRCUIT

Using the analytical expressions for the patch admittance at the apertures, (5.35a) and (5.35b), it is possible to draw an equivalent circuit of the cross-aperture coupled CP antenna based on the cavity method. Equations (5.35a) and (5.35b) can be written in the form of

$$Y_{x,ant} = \sum_m \sum_n \frac{16 \cdot j\omega\varepsilon \cdot A_{mn}^2}{d_a\left[\omega^2 - \omega_{mn}^2\left(1 + j\delta_{eff}\frac{\omega^2}{\omega_{mn}^2}\right)\right]} \cdot \left\{\frac{\operatorname{sinc}\left(k_n\frac{W_a}{2}\right)\sin\left(\frac{n\pi}{2}\right)\cos\left(\frac{m\pi}{2}\right)}{\sin\left(k_a\frac{L_a}{2}\right)} \cdot \frac{k_a\left[\cos\left(k_m\frac{L_a}{2}\right) - \cos\left(k_a\frac{L_a}{2}\right)\right]}{k_a^2 - k_m^2}\right\}^2 \quad (5.38a)$$

$$Y_{y,ant} = \sum_m \sum_n \frac{16 \cdot j\omega\varepsilon \cdot A_{mn}^2}{d_a\left[\omega^2 - \omega_{mn}^2\left(1 + j\delta_{eff}\frac{\omega^2}{\omega_{mn}^2}\right)\right]} \cdot \left\{\frac{\operatorname{sinc}\left(k_m\frac{W_a}{2}\right)\sin\left(\frac{m\pi}{2}\right)\cos\left(\frac{n\pi}{2}\right)}{\sin\left(k_a\frac{L_a}{2}\right)} \cdot \frac{k_a\left[\cos\left(k_n\frac{L_a}{2}\right) - \cos\left(k_a\frac{L_a}{2}\right)\right]}{k_a^2 - k_n^2}\right\}^2 \quad (5.38b)$$

Each of these formulas correspond to the expression of the admittance of m x n series RLC circuits, which are connected in parallel. The equivalent circuit of the patch admittance, as seen by the slot parallel to the y axis, has the following element values

$$L_{x,mn} = \frac{d_a}{16\varepsilon c^2 A_{mn}^2} \cdot \left\{ \frac{\operatorname{sinc}\left(k_n \frac{W_a}{2}\right) \sin\left(\frac{n\pi}{2}\right) \cos\left(\frac{m\pi}{2}\right)}{\sin\left(k_a \frac{L_a}{2}\right)} \cdot \frac{k_a\left[\cos\left(k_m \frac{L_a}{2}\right) - \cos\left(k_a \frac{L_a}{2}\right)\right]}{k_a^2 - k_m^2} \right\}^{-2}$$

$$C_{x,mn} = L_{x,mn}^{-1} \frac{\varepsilon_{ra} k_{mn}^2}{c^2} \qquad R_{x,mn} = L_{x,mn} k_{mn} c \delta_{eff} \tag{5.39a}$$

Similarly, the equivalent circuit of the patch, as seen by the slot parallel to the x axis, has element values of

$$L_{y,mn} = \frac{d_a}{16\varepsilon c^2 A_{mn}^2} \cdot \left\{ \frac{\operatorname{sinc}\left(k_m \frac{W_a}{2}\right) \sin\left(\frac{m\pi}{2}\right) \cos\left(\frac{n\pi}{2}\right)}{\sin\left(k_a \frac{L_a}{2}\right)} \cdot \frac{k_a\left[\cos\left(k_n \frac{L_a}{2}\right) - \cos\left(k_a \frac{L_a}{2}\right)\right]}{k_a^2 - k_n^2} \right\}^{-2}$$

$$C_{y,mn} = L_{y,mn}^{-1} \frac{\varepsilon_{ra} k_{mn}^2}{c^2} \qquad R_{y,mn} = L_{y,mn} k_{mn} c \delta_{eff} \tag{5.39b}$$

With these component values, the equivalent circuit of the cross-aperture coupled CP patch can be drawn, as shown in Figure 5.3.

5.6 AXIAL RATIO

For the calculation of the axial ratio, the far field components of the antenna are first determined in the boresight. This is performed by replacing the electric field at the edges of the patch by equivalent magnetic currents as given by [Carver 1981]

$$\mathbf{M} = 2 d_a \cdot E_{z(x,y)} \cdot \mathbf{z} \times \mathbf{n} \tag{5.40}$$

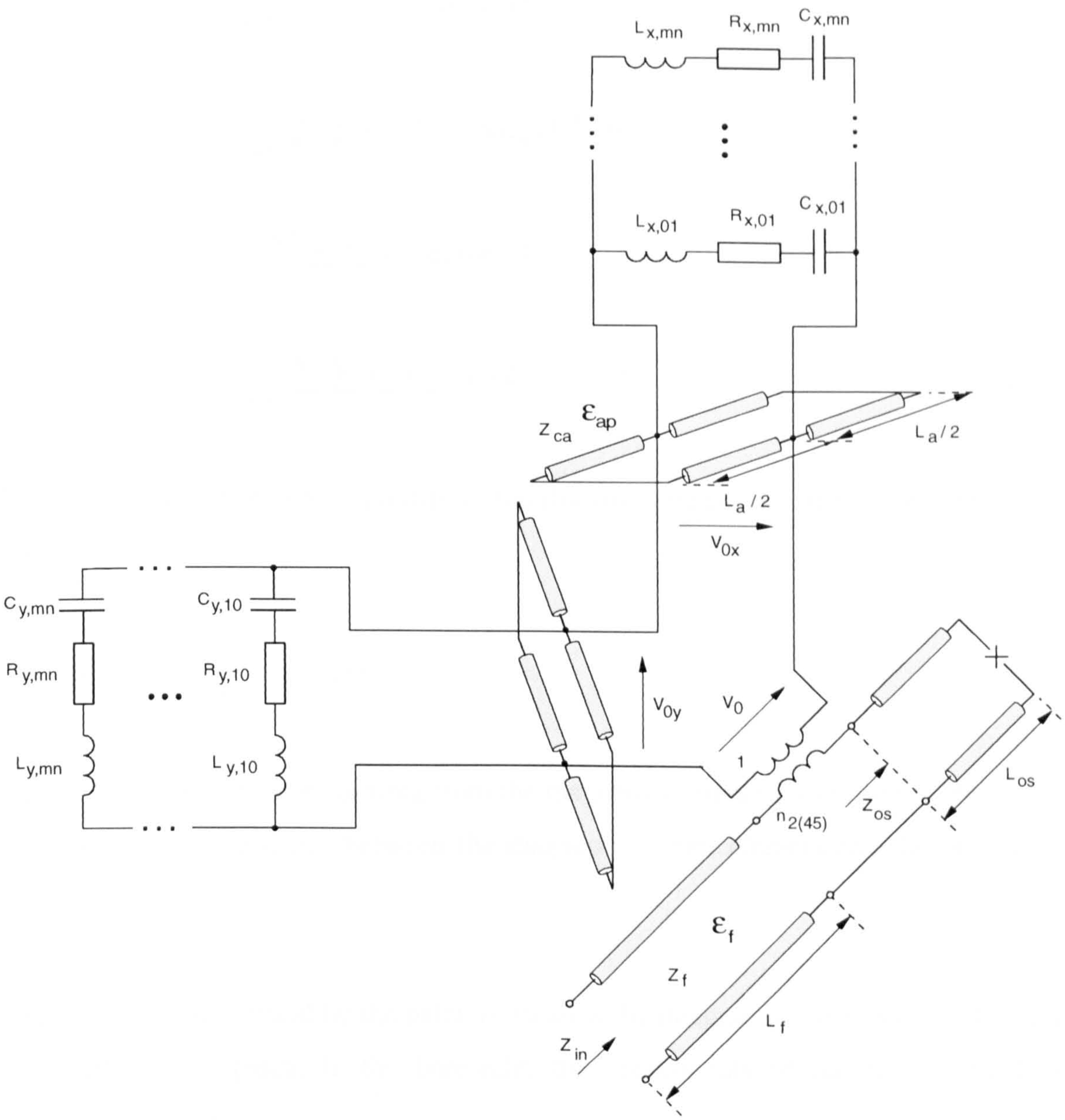

Figure 5.3. Equivalent circuit based on the cavity model.

where **n** is the unit vector outer normal to the magnetic wall at the edges of the patch. Substituting the expression of the electric field from (5.26) one obtains the following values of magnetic currents at the four edges of the patch:

$$M_{x(x,y=0)} = \frac{d_a}{j\omega\varepsilon}\sum_m\sum_n A_{mn}C_{mn}\cos(k_m x) \tag{5.41a}$$

$$M_{x(x,y=b)} = -\frac{d_a}{j\omega\varepsilon}\sum_m\sum_n A_{mn}C_{mn}\cos(k_m x)\cdot(-1)^n \tag{5.41b}$$

$$M_{y(x=0,y)} = \frac{d_a}{j\omega\varepsilon}\sum_m\sum_n A_{mn}C_{mn}\cos(k_n y) \tag{5.41c}$$

$$M_{y(x=a,y)} = -\frac{d_a}{j\omega\varepsilon}\sum_m\sum_n A_{mn}C_{mn}\cos(k_n y)\cdot(-1)^m \tag{5.41d}$$

The electric field $\mathbf{E}(\mathbf{r})$ due to an infinitesimally small magnetic current element ($d\mathbf{M}$) is obtained as

$$\mathbf{E}(\mathbf{r}) = \frac{jk_0 e^{-jk_0 r}}{4\pi r}\cdot\mathbf{r}\times d\mathbf{M} \tag{5.42}$$

where, $\mathbf{r}$ is the unit vector pointing from the magnetic current element to the observation point and r is the distance between the magnetic current element and the observation point.

The electric field radiated by the patch is obtained by integrating expression (5.42) along the edges of the patch. In the boresight, the components of the electric field are, therefore, given by

$$E_x = \frac{d_a k_0 e^{-jk_0 r}}{4\pi\omega\varepsilon r}\cdot\int_0^b\left(\sum_m\sum_n A_{mn}C_{mn}\cos(k_n y)\cdot(-1)^m - \sum_m\sum_n A_{mn}C_{mn}\cos(k_n y)\right)dy \tag{5.43a}$$

$$E_y = \frac{d_a k_0 e^{-jk_0 r}}{4\pi\omega\varepsilon r}\cdot\int_0^a\left(\sum_m\sum_n A_{mn}C_{mn}\cos(k_m x) - \sum_m\sum_n A_{mn}C_{mn}\cos(k_m x)\cdot(-1)^n\right)dx \tag{5.43b}$$

which can be written as

$$E_x = \frac{d_a k_0 e^{-jk_0 r}}{4\pi\omega\varepsilon r}\cdot\sum_m\sum_n A_{mn}C_{mn}\cdot[(-1)^m - 1]\cdot\int_0^b\cos(k_n y)dy \tag{5.44a}$$

$$E_y = \frac{d_a k_0 e^{-jk_0 r}}{4\pi\omega\varepsilon r} \cdot \sum_m \sum_n A_{mn} C_{mn} \cdot \left[1-(-1)^n\right] \cdot \int_0^a \cos(k_m x) dx \tag{5.44b}$$

Since

$$\int_0^b \cos(k_n y) dy = \begin{cases} 1 & \text{if} \quad n = 0 \\ \\ 0 & \text{otherwise} \end{cases} \tag{5.45a}$$

$$\int_0^a \cos(k_m x) dx = \begin{cases} 1 & \text{if} \quad m = 0 \\ \\ 0 & \text{otherwise} \end{cases} \tag{5.45b}$$

equations (5.44a) and (5.44b) can be simplified as

$$E_x = \frac{d_a k_0 e^{-jk_0 r}}{4\pi\omega\varepsilon r} \cdot \sum_m A_{m0} C_{m0} \cdot \left[(-1)^m - 1\right] \tag{5.46a}$$

$$E_y = \frac{d_a k_0 e^{-jk_0 r}}{4\pi\omega\varepsilon r} \cdot \sum_n A_{0n} C_{0n} \cdot \left[1-(-1)^n\right] \tag{5.46b}$$

From (5.23a),(5.23b) and (5.27)

$$C_{m0} = \begin{cases} -B_{y,m0} & \text{if } m \text{ odd} \\ \\ 0 & \text{if } m \text{ even} \end{cases} \tag{5.47a}$$

$$C_{0n} = \begin{cases} B_{x,0n} & \text{if } n \text{ odd} \\ \\ 0 & \text{if } n \text{ even} \end{cases} \tag{5.47b}$$

and therefore

$$E_x = \frac{d_a k_0 e^{-jk_0 r}}{2\pi\omega\varepsilon r} \cdot \sum_m A_{m0} B_{y,m0} \tag{5.48a}$$

$$E_y = \frac{d_a k_0 e^{-jk_0 r}}{4\pi\omega\varepsilon r} \cdot \sum_n A_{0n} B_{x,0n} \tag{5.48b}$$

The expressions for $B_{x,0n}$ and $B_{y,m0}$ can be written in the following form:

$$B_{x,0n} = V_{0x} \cdot B'_{x,0n} \tag{5.49a}$$

$$B_{y,m0} = V_{0y} \cdot B'_{y,m0} \tag{5.49b}$$

where

$$B'_{x,0n} = \frac{j\omega\varepsilon \cdot A_{0n}}{d_a k_n \cdot \left(k^2 - k_n^2\right)} \cdot \frac{4\mathrm{sinc}\left(k_n \frac{W_a}{2}\right)\sin\left(\frac{n\pi}{2}\right)}{\sin\left(k_a \frac{L_a}{2}\right)} \cdot \frac{k_a\left[1-\cos\left(k_a \frac{L_a}{2}\right)\right]}{k_a^2} \tag{5.50a}$$

$$B'_{y,m0} = \frac{j\omega\varepsilon \cdot A_{m0}}{d_a k_m \cdot \left(k^2 - k_m^2\right)} \cdot \frac{4\mathrm{sinc}\left(k_m \frac{W_a}{2}\right)\sin\left(\frac{m\pi}{2}\right)}{\sin\left(k_a \frac{L_a}{2}\right)} \cdot \frac{k_a\left[1-\cos\left(k_a \frac{L_a}{2}\right)\right]}{k_a^2} \tag{5.50b}$$

From the equivalent circuit, the voltages V_{0x} and V_{0y} can be expressed as

$$V_{0x} = V_0 \cdot \frac{\left(Y_{x,ant} + Y_{ap}\right)^{-1}}{\left(Y_{x,ant} + Y_{ap}\right)^{-1} + \left(Y_{y,ant} + Y_{ap}\right)^{-1}} \tag{5.51a}$$

$$V_{0y} = V_0 \cdot \frac{\left(Y_{y,ant} + Y_{ap}\right)^{-1}}{\left(Y_{x,ant} + Y_{ap}\right)^{-1} + \left(Y_{y,ant} + Y_{ap}\right)^{-1}} \tag{5.51b}$$

Substituting the above into the expressions for the electric field components in the boresight, one obtains

$$E_x = \frac{V_0 d_a k_0 e^{-jk_0 r}}{2\pi\omega\varepsilon r} \cdot \frac{\left(Y_{x,ant} + Y_{ap}\right)^{-1}}{\left(Y_{x,ant} + Y_{ap}\right)^{-1} + \left(Y_{y,ant} + Y_{ap}\right)^{-1}} \cdot \sum_m A_{m0} B'_{y,m0} \tag{5.52a}$$

$$E_y = \frac{V_{0y} d_a k_0 e^{-jk_0 r}}{4\pi\omega\varepsilon r} \cdot \frac{\left(Y_{y,ant} + Y_{ap}\right)^{-1}}{\left(Y_{x,ant} + Y_{ap}\right)^{-1} + \left(Y_{y,ant} + Y_{ap}\right)^{-1}} \cdot \sum_n A_{0n} B'_{x,0n} \tag{5.52b}$$

Now, the amplitude error (A_e) and phase error (ϕ_e) required for the calculation of the axial ratio can be expressed as

$$A_e = \frac{|E_x|}{|E_y|} = \frac{|Y_{y,ant} + Y_{ap}|}{|Y_{x,ant} + Y_{ap}|} \cdot \frac{\left|\sum_m A_{m0} B'_{y,m0}\right|}{\left|\sum_n A_{0n} B'_{x,0n}\right|} \tag{5.53}$$

$$\phi_e = \angle\left(\frac{E_x}{E_y}\right) = \angle\left(\frac{Y_{y,ant} + Y_{ap}}{Y_{x,ant} + Y_{ap}} \cdot \frac{\sum_m A_{m0} B'_{y,m0}}{\sum_n A_{0n} B'_{x,0n}}\right) \tag{5.54}$$

From which finally, the value of axial ratio is calculated as given by [Balanis 1982]

$$AR = \sqrt{\frac{1 + A_e^2 + \left[1 + A_e^4 + 2A_e^2 \cos(2\phi_e)\right]^{1/2}}{1 + A_e^2 - \left[1 + A_e^4 + 2A_e^2 \cos(2\phi_e)\right]^{1/2}}} \tag{5.55}$$

Equations (5.53) through (5.55) provide a numerical means of determining the axial ratio of the cross-aperture coupled patch antenna at a certain frequency when the design parameters shown in Figure 4.1 are known based on the resonant cavity model. The accuracy of the predicted axial ratio by these expressions is examined in Chapter six.

5.7 CHAPTER SUMMARY

In this chapter the analysis of the cross-aperture coupled circularly polarised microstrip antenna has been presented in terms of the cavity resonator model. The electric field in the two orthogonal apertures have been replaced by equivalent magnetic currents, which were assumed to be uniformly distributed in the volume of the patch above the slot. This and the assumption of magnetic walls at the edges of the patch as boundary conditions allowed the determination of the magnetic and electric fields under the patch antenna. This in turn facilitated the derivation of expressions for the input impedance and the determination of an equivalent circuit based on the resonant cavity method. Finally, expressions have been derived in order to calculate the axial ratio as functions of the frequency.

The next chapter presents the results of this cavity model together with that of the transmission line model, which was described in the previous chapter. Numerical results obtained from each of the two models are compared with values obtained from measurements and from full wave computer simulation.

CHAPTER 6.

EVALUATION AND EXPLOITATION OF THE THEORETICAL MODELS

6.1 INTRODUCTION

Initially in this chapter the theoretical input impedance and axial ratio results obtained from the transmission line method, and, the cavity model, are compared to measurement and full wave computer simulation results for two cross-aperture coupled antennas.

Then the different design parameters of the antenna, such as the aperture length, aperture width, thickness of antenna substrate, etc. are varied and the input impedance is calculated by the application of both the transmission line and cavity models. Computer simulation is also performed using these different parameters. The results obtained for the various design parameters allow the observation of their effect on the input impedance of the antenna, giving a physical insight into the electromagnetic operation of the structure. The results are then compared to each other which facilitates the evaluation of the developed theoretical models for a large number of different parameter values, and, also reveals their limitations.

Finally, the effect of antenna substrate thickness is investigated on both the input impedance and axial ratio performance. It is shown that increasing antenna substrate thickness improves the fractional axial ratio bandwidth of the cross-aperture coupled antenna. However, the impedance matching of the antenna will be degraded when increasing the antenna thickness beyond a certain value. Hence, when designing a cross-aperture coupled circularly polarised antenna, a compromise between the bandwidth and impedance matching must be found.

6.2 COMPARISON OF THEORETICAL, SIMULATION AND MEASUREMENT RESULTS

A cross-aperture coupled antenna with its dimensions is shown in Figure 6.1. The input impedance of this antenna has been calculated over a frequency range of 2.25-2.7GHz by both the transmission line and the resonant cavity methods and is shown in Figure 6.2. The antenna has been fabricated and its input impedance was measured using a Wiltron 360 Network Analyser. The practically obtained input impedance is also shown in Figure 6.2 over the same frequency range.

It can be seen from Figure 6.2 that both the transmission line and the resonant cavity methods are able to predict the input impedance of the cross-aperture coupled antenna with good accuracy. They provide the impedance loci with the double resonant loop corresponding to the two orthogonal modes which is typical to single feed circularly polarised antennas.

Regarding the prediction of the resonant frequency of the antenna, which is defined as the frequency where the imaginary part of the impedance is zero, the transmission line model is more accurate for this specific antenna. The cavity model gave a resonant frequency, which is approximately 1% below the measured value.

The same antenna has also been simulated using the full wave simulation package, Ensemble from Boulder Microwave Technologies Inc. The accuracy of this software package has been verified by the manufacturer for a large number of structures and it was found that it lied within the limits expected from the tolerances in the physical parameters [Boulder 1995]. The layout of the model used in the simulation with the segmentation grid is shown in Figure 6.3. The input impedance of the antenna obtained from the computer simulation is shown in Figure 6.4 together with the measured values demonstrating the high level of accuracy of this simulation package.

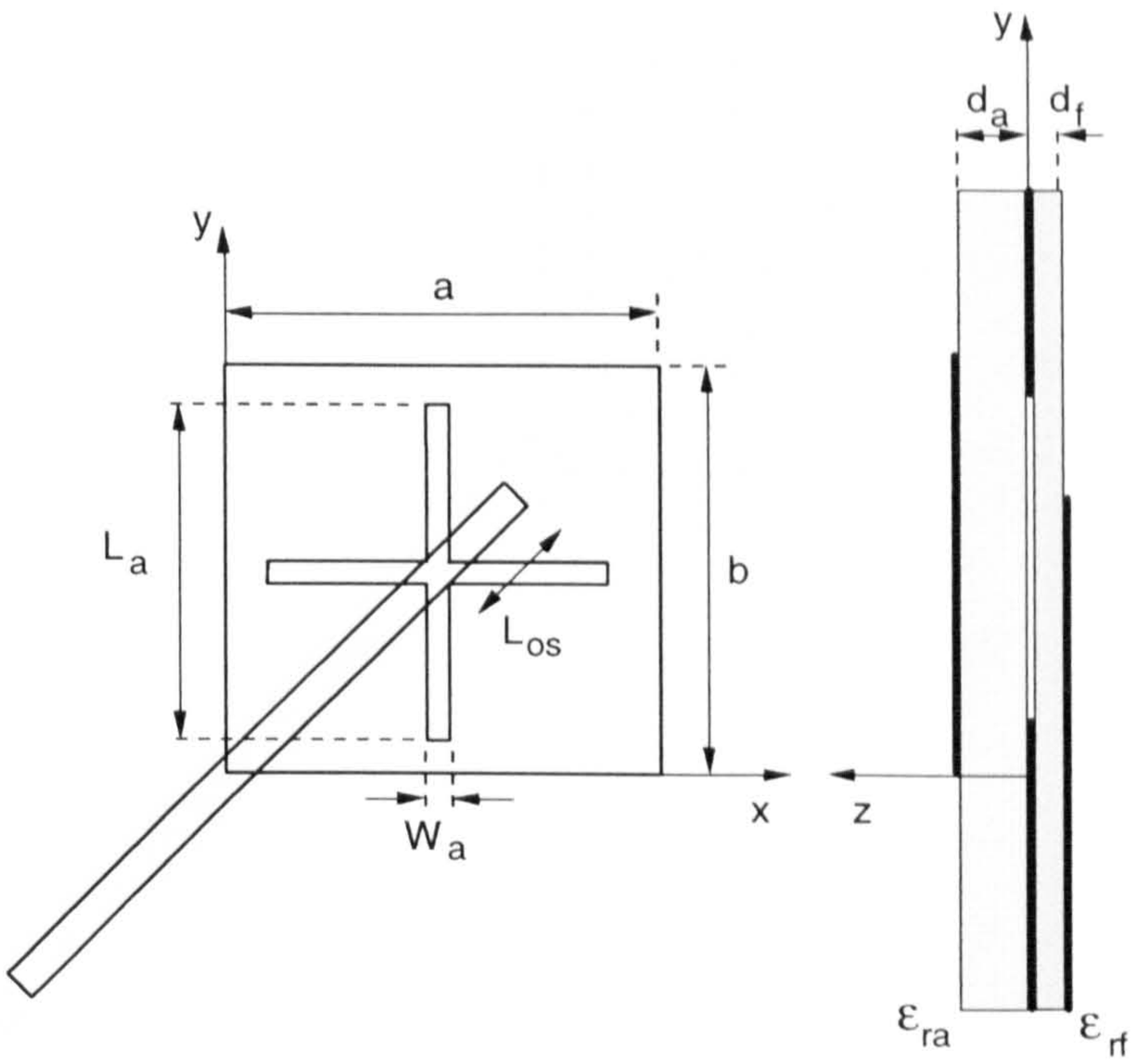

Figure 6.1. Design parameters of the cross-aperture coupled antenna.

a = 33.9mm, b = 36.1mm, L_{OS} = 10mm, W_a = 2mm, L_a = 18mm,

ε_{ra} = 2.33, ε_{rf} = 2.33, d_a = 3.15mm, df = 1.575mm.

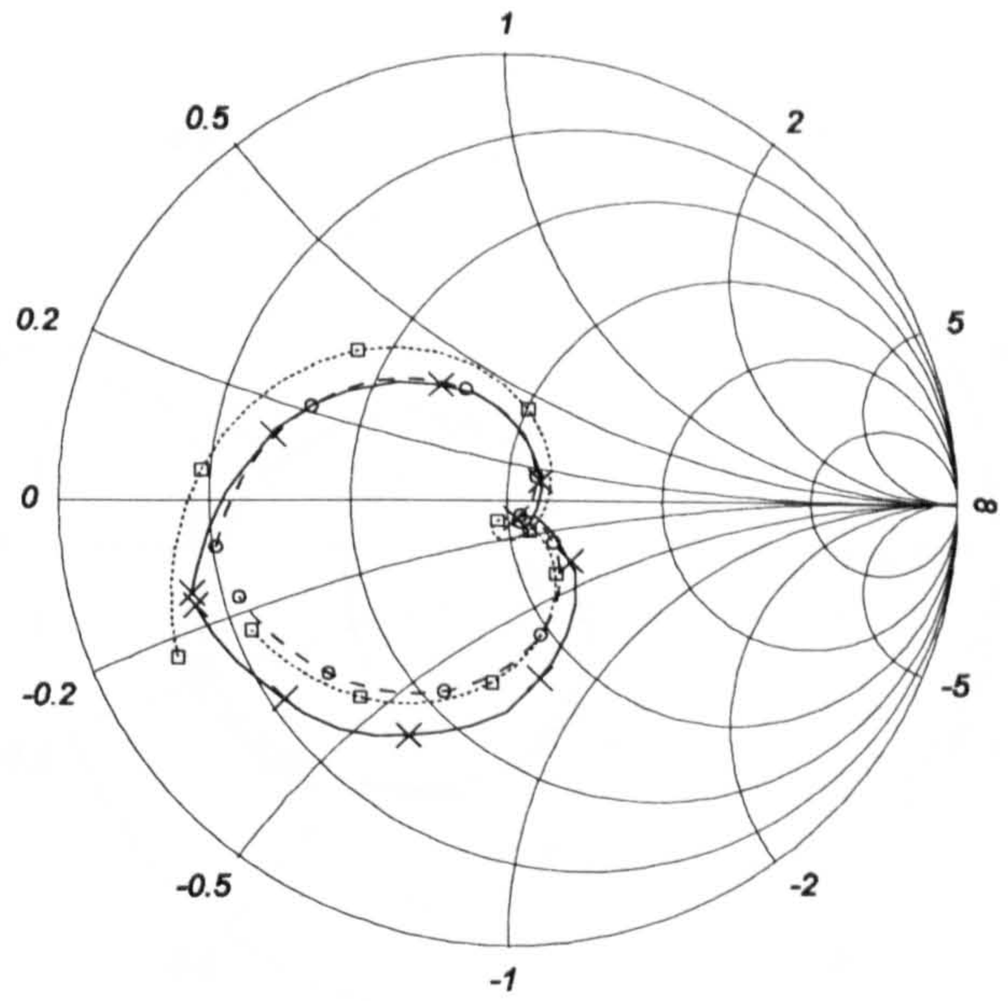

Figure 6.2. Input impedance of the cross-aperture coupled antenna of Figure 6.1.

Frequency range: **2.25 - 2.7 GHz;** Step: **50MHz;**

measured results, transmission line method, cavity model.

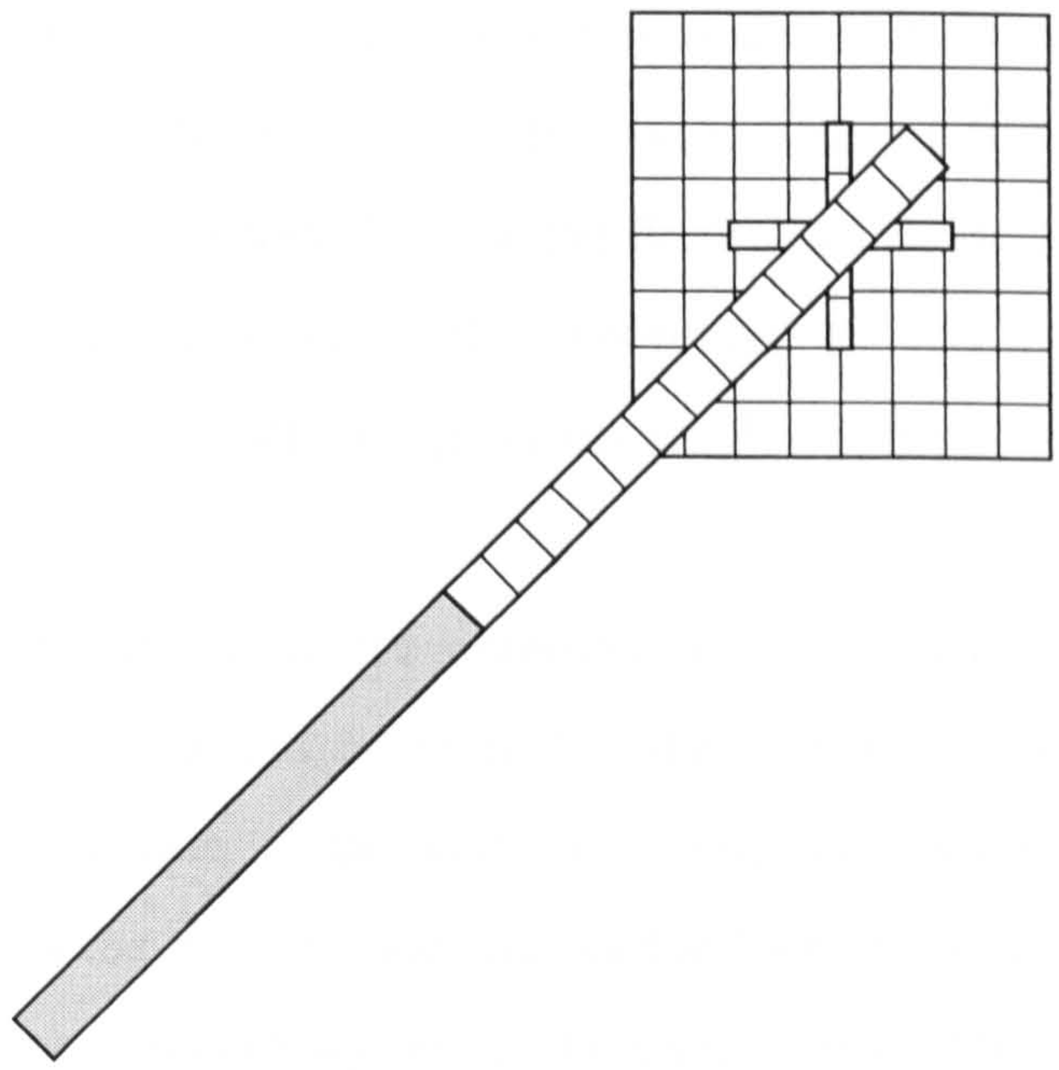

Figure 6.3. Full wave computer simulation model of cross-aperture coupled antenna shown in Figure 6.1.

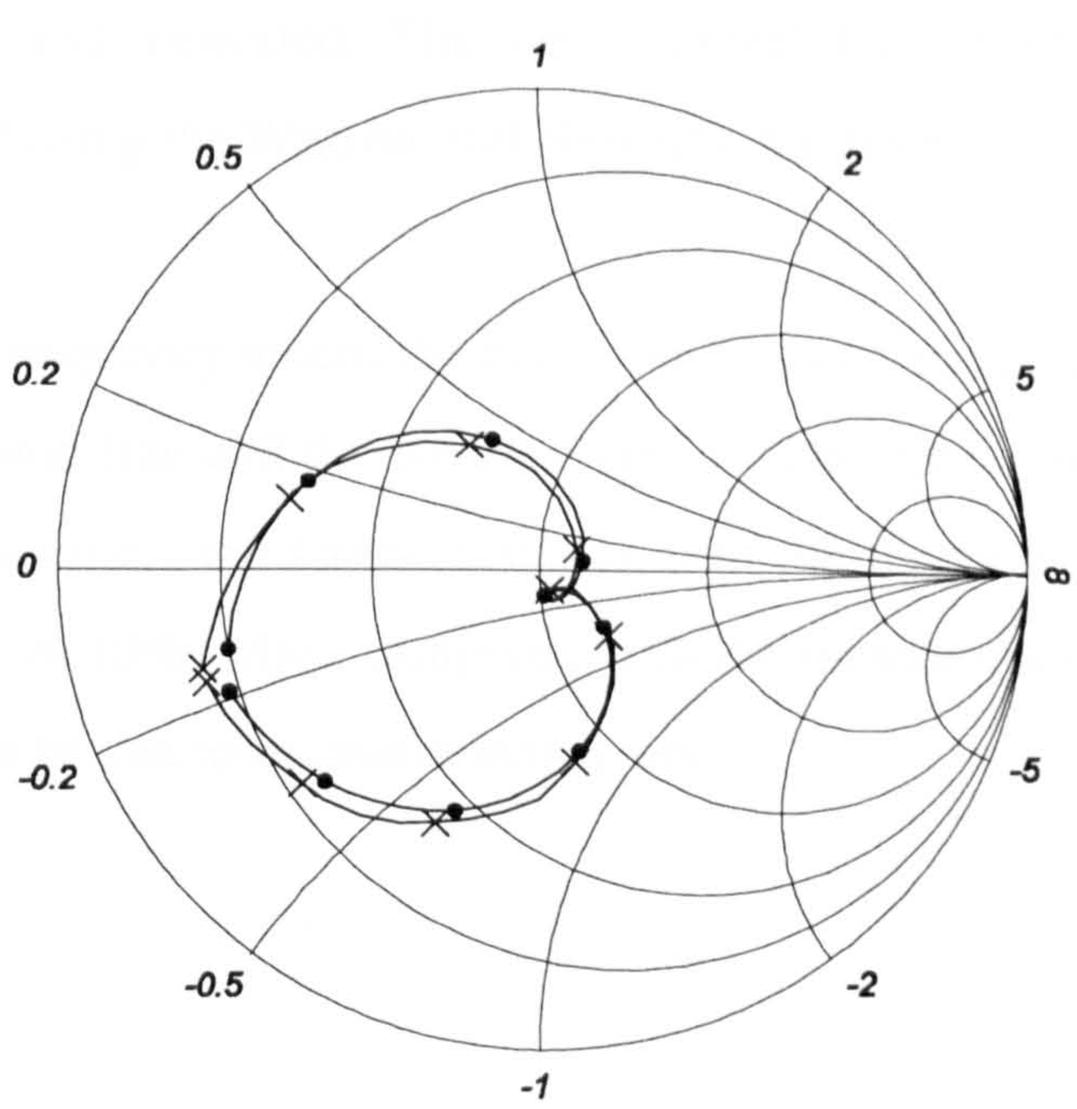

Figure 6.4. Input impedance of cross-aperture coupled antenna shown in Figure 6.1.

Frequency range: **2.25 - 2.7 GHz;** Step: **50MHz;**

full wave simulation, measured results

Another cross-aperture coupled antenna has been fabricated using air as antenna substrate and a radome to support the patch as shown in Figure 6.5. Its input impedance was measured in a range of 2.2-2.75GHz and it is shown in Figure 6.6 together with the input impedance locis obtained using the theoretical models. The effect of the radome has been taken into account in the theoretical models by replacing the substrate-superstrate double layer with an equivalent single substrate layer (see Appendix H).

Comparing the input impedance obtained from the theoretical models and from the computer simulation, it can be seen that the full wave method is the most accurate regarding the prediction of the value of input impedance over the tested frequency range. Again it is the transmission line method which predicted the resonant frequency of the antenna more accurately, while the cavity method had an error of approximately 2%. The cavity method also shows larger error in the prediction of input impedance at frequencies well below the resonant frequency.

The axial ratio of the two antennas shown in Figures 6.1 and 6.5 have also been calculated, simulated and measured. The measurement have been carried out in an anechoic chamber and using the Wiltron 360 Network Analyser.

The prediction of the frequency where the best axial ratio occurs is approximately 1.2% for both the transmission line and the cavity methods. The prediction of the axial ratio bandwidth was less accurate, the largest error of both the transmission line and cavity models is in the range of 10%, when compared with the measurement results. However, part of this error could be due to measurement errors.

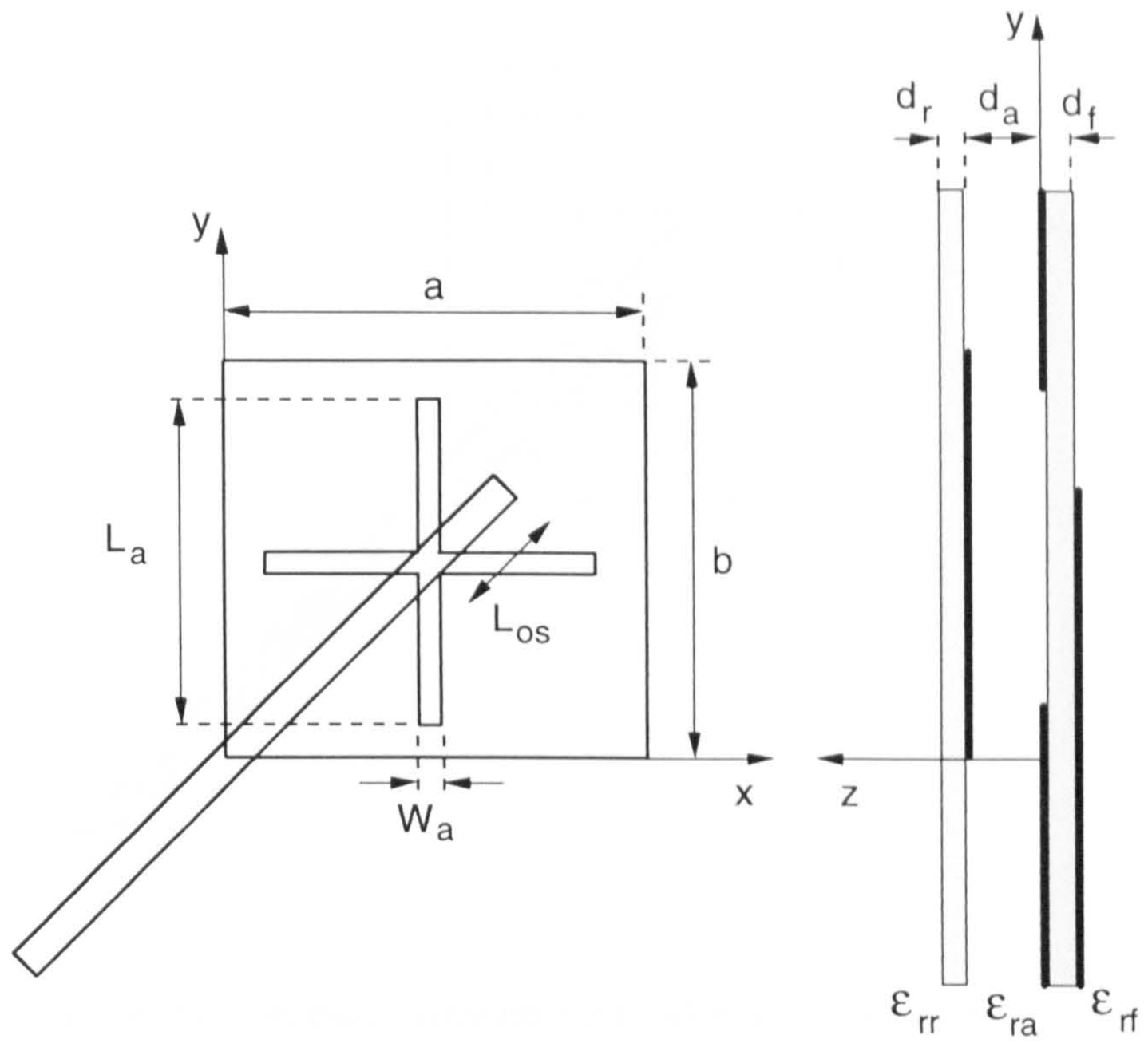

Figure 6.5. Cross-aperture coupled antenna with air substrate.

a = 45.5mm, b = 48.6mm, L_{os} = 9.8mm, W_a = 1.5mm, L_a = 23.7mm,

ε_{ra} = 1, ε_{rf} = 2.33, ε_{rr} = 2.33, d_a = 4.5mm, d_f = 1.575mm, d_r = 1.575mm.

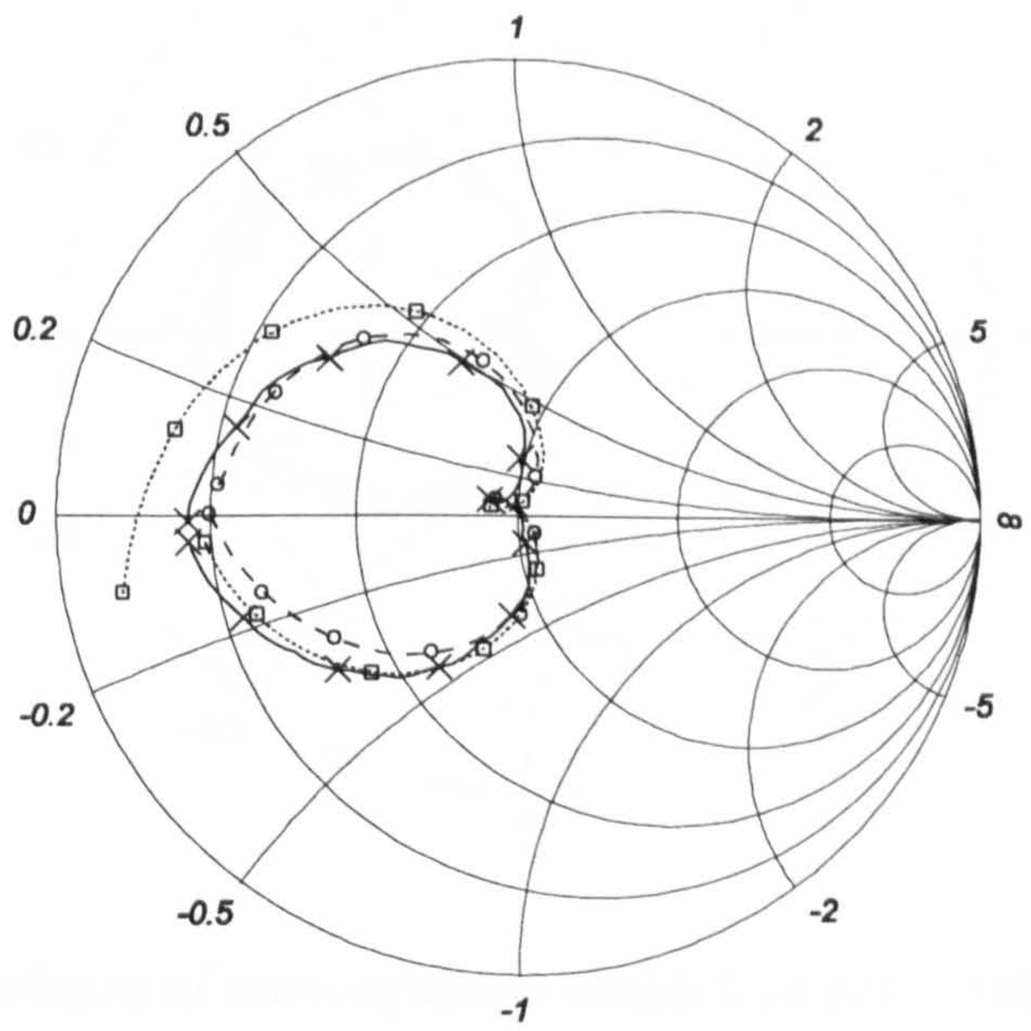

Figure 6.6. Input impedance of cross-aperture coupled antenna with air substrate shown in Figure 6.5; Frequency range: **2.2 - 2.75 GHz;** Step: **50MHz;**

measured results, **transmission line method**, **cavity model.**

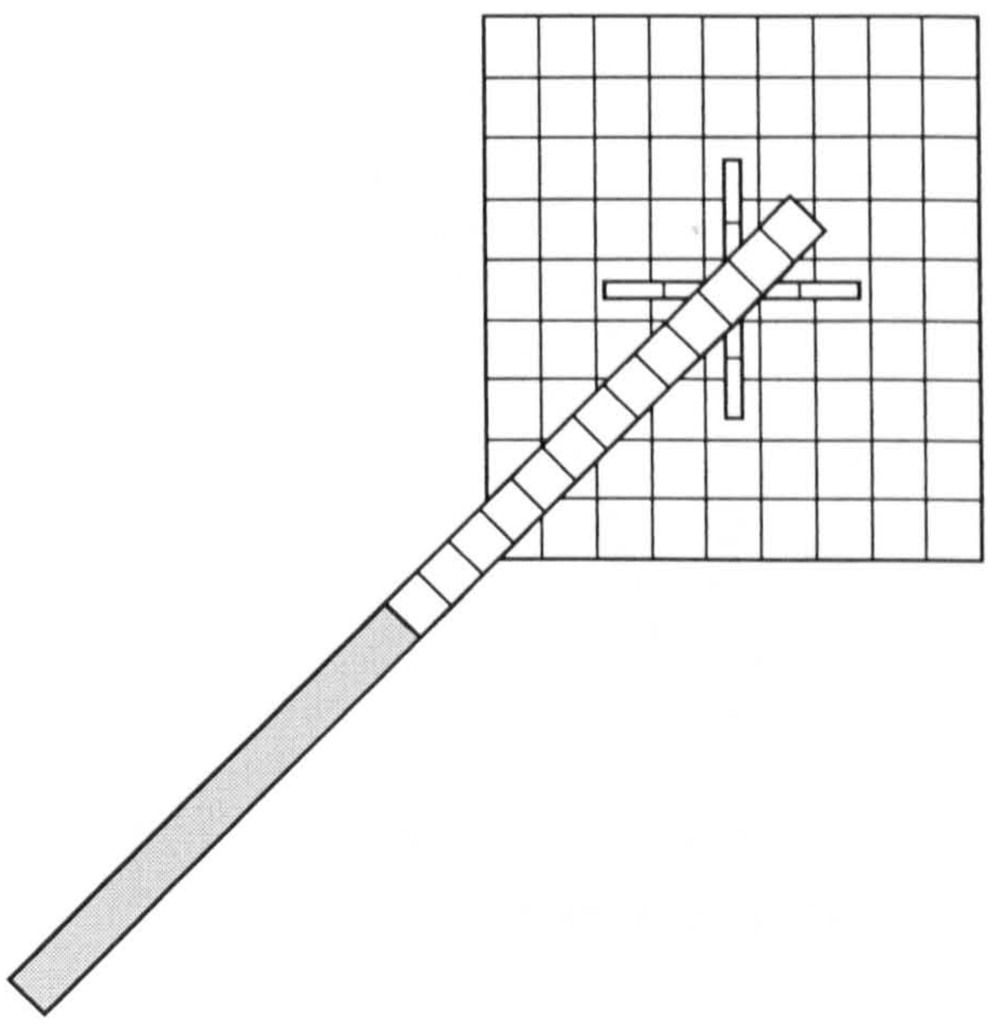

Figure 6.7. Full wave computer simulation model of cross-aperture coupled antenna with air substrate shown in Figure 6.5.

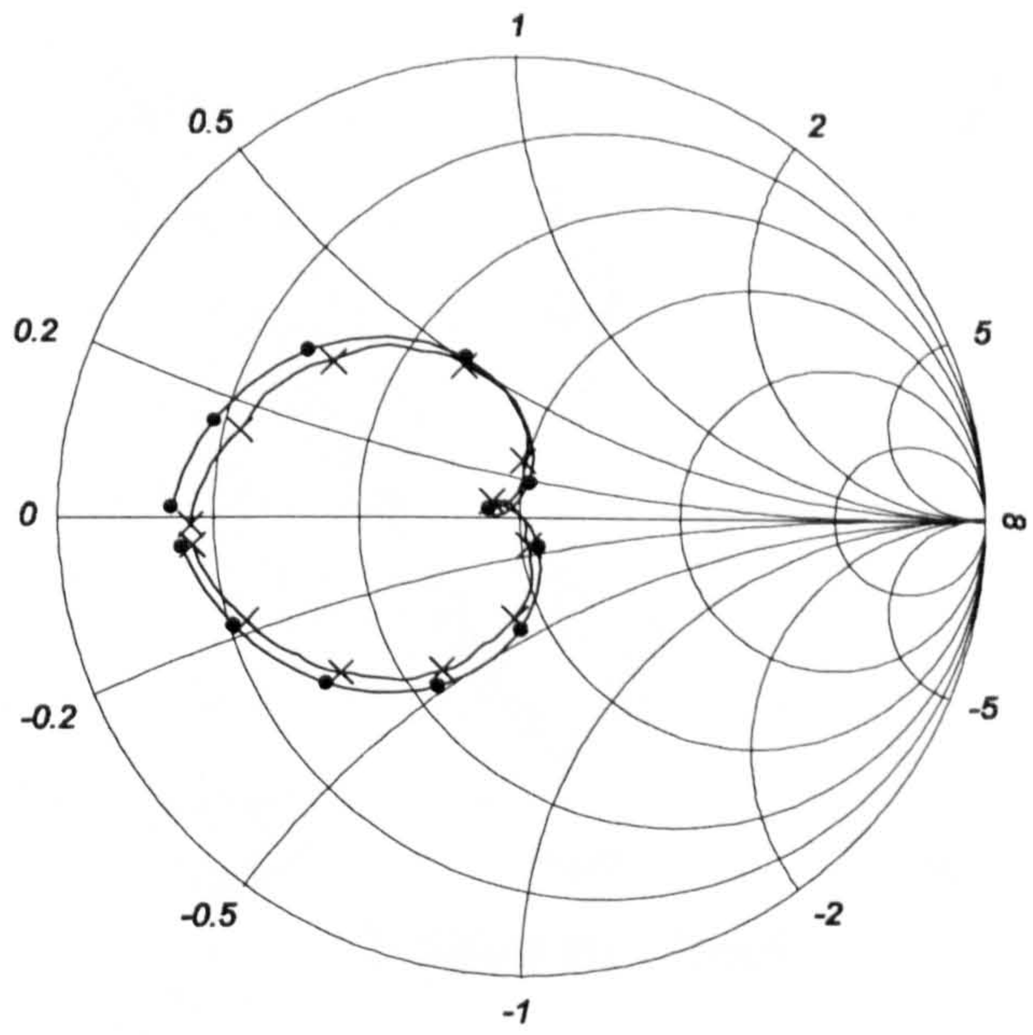

Figure 6.8. Input impedance of cross-aperture coupled antenna with air substrate shown in Figure 6.5. Frequency range: **2.2 - 2.75 GHz;** Step: **50MHz;**

measured results, full wave simulation.

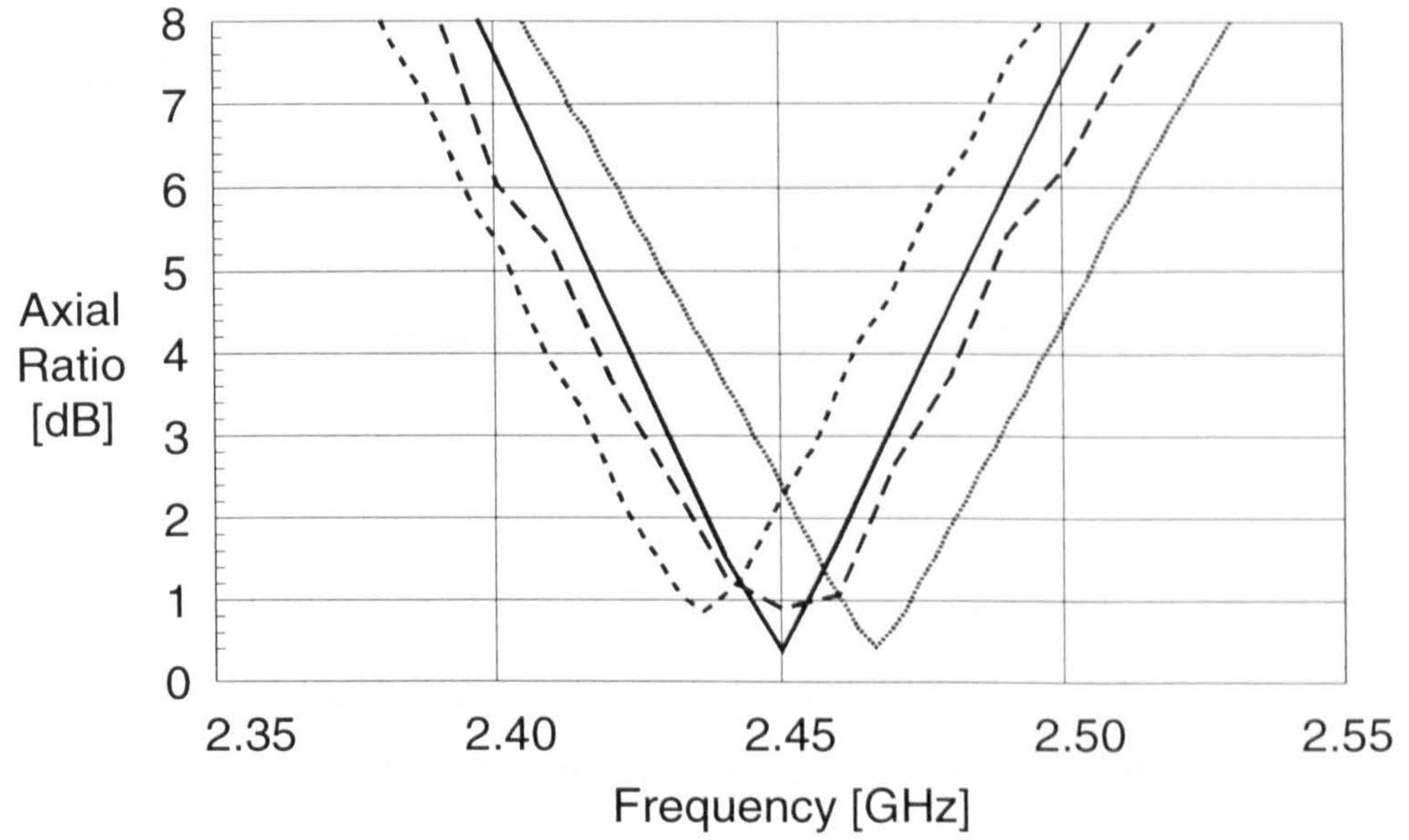

Figure 6.9. Axial ratio of cross-aperture coupled antenna shown in Figure 6.1.

– – – – measured results, ——— full wave simulation,

– – – – – – transmission line method, ····· cavity model.

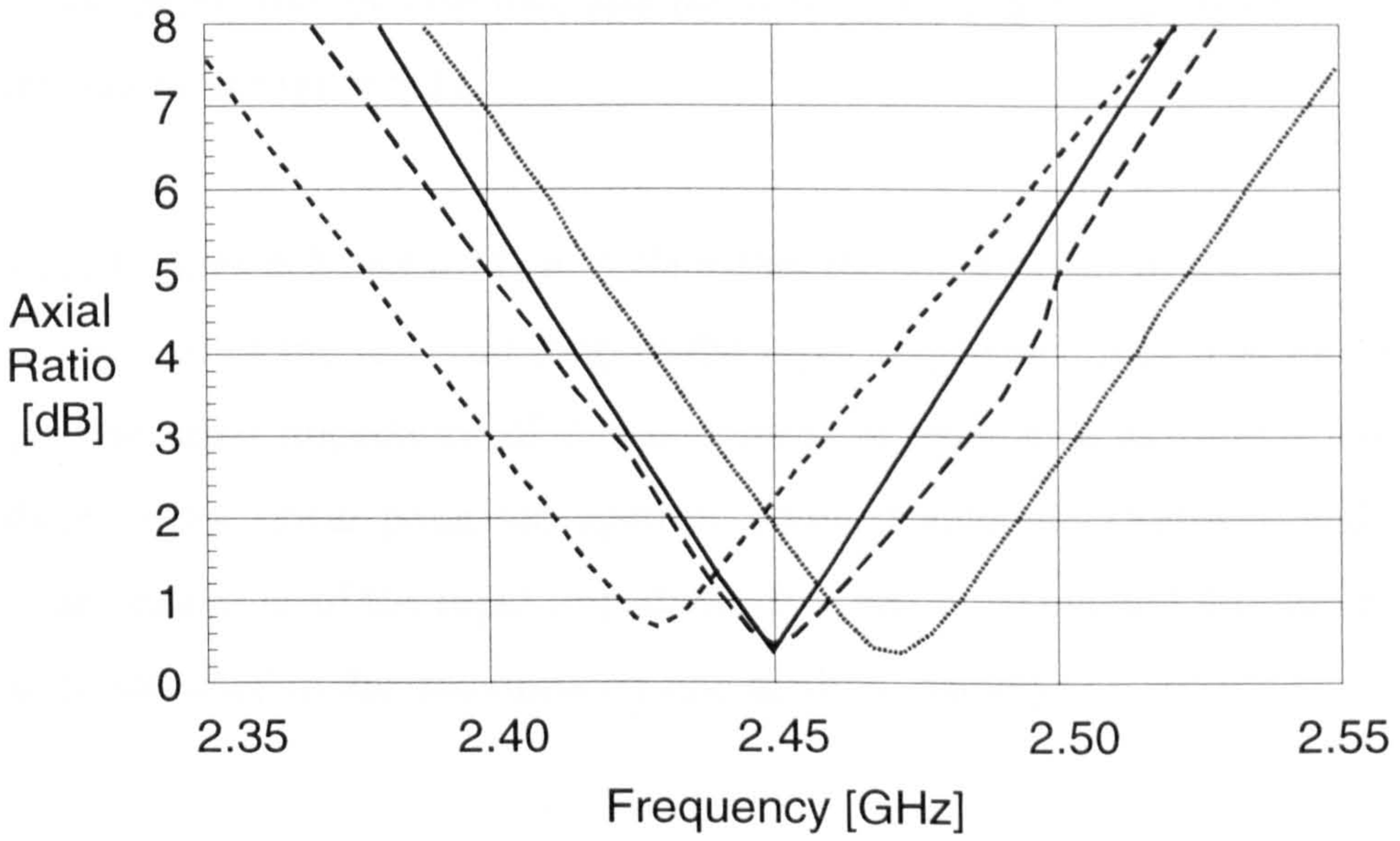

Figure 6.10. Axial ratio of cross-aperture coupled antenna shown in Figure 6.5.

– – – – measured results, ——— full wave simulation,

– – – – – – transmission line method, ····· cavity model.

6.3 EFFECT OF DESIGN PARAMETERS ON THE INPUT IMPEDANCE

In this section, the dimensions given in Figure 6.1 are taken as default values. In the following figures, only those parameter values which differ from these defaults are shown.

In each of the following sections, a selected design parameter is set to two different values for which the input impedance locis are calculated. Together with the impedance loci of the antenna with the default dimensions shown in Figure 6.2, this gives three different cases for each design parameter.

6.3.1 APERTURE LENGTH

The input impedance of two cross-aperture coupled antennas with two different aperture lengths, one being shorter (14mm), and the other one longer, (22mm) than the default value are shown in Figure 6.11.

Comparing Figures 6.2 and 6.11, it is clear that the main effect of the varying aperture length is the size of the resonant loop in the input impedance loci. The longer the slot, the larger the input impedance of the antenna is at resonance as similar tendency has been observed for linear polarised aperture coupled antennas [Sullivan and Schaubert 1986]. The behaviour of the input impedance loci can be explained through expressions (4.46) to (4.48) used in the transmission line method, namely:

$$Z_{in} = n_{2(45)}^2 \cdot \left(\frac{1}{Y_{ta}} + \frac{1}{Y_{tb}} \right) - jZ_{cf} \cdot \cot\left(k_f L_{os}\right) \tag{6.1}$$

$$Y_{ta} = n_{1a}^2 Y_{PX} + Y_{ap} \qquad \text{and} \qquad Y_{tb} = n_{1b}^2 Y_{PY} + Y_{ap} \tag{6.2}$$

L_a = 22mm

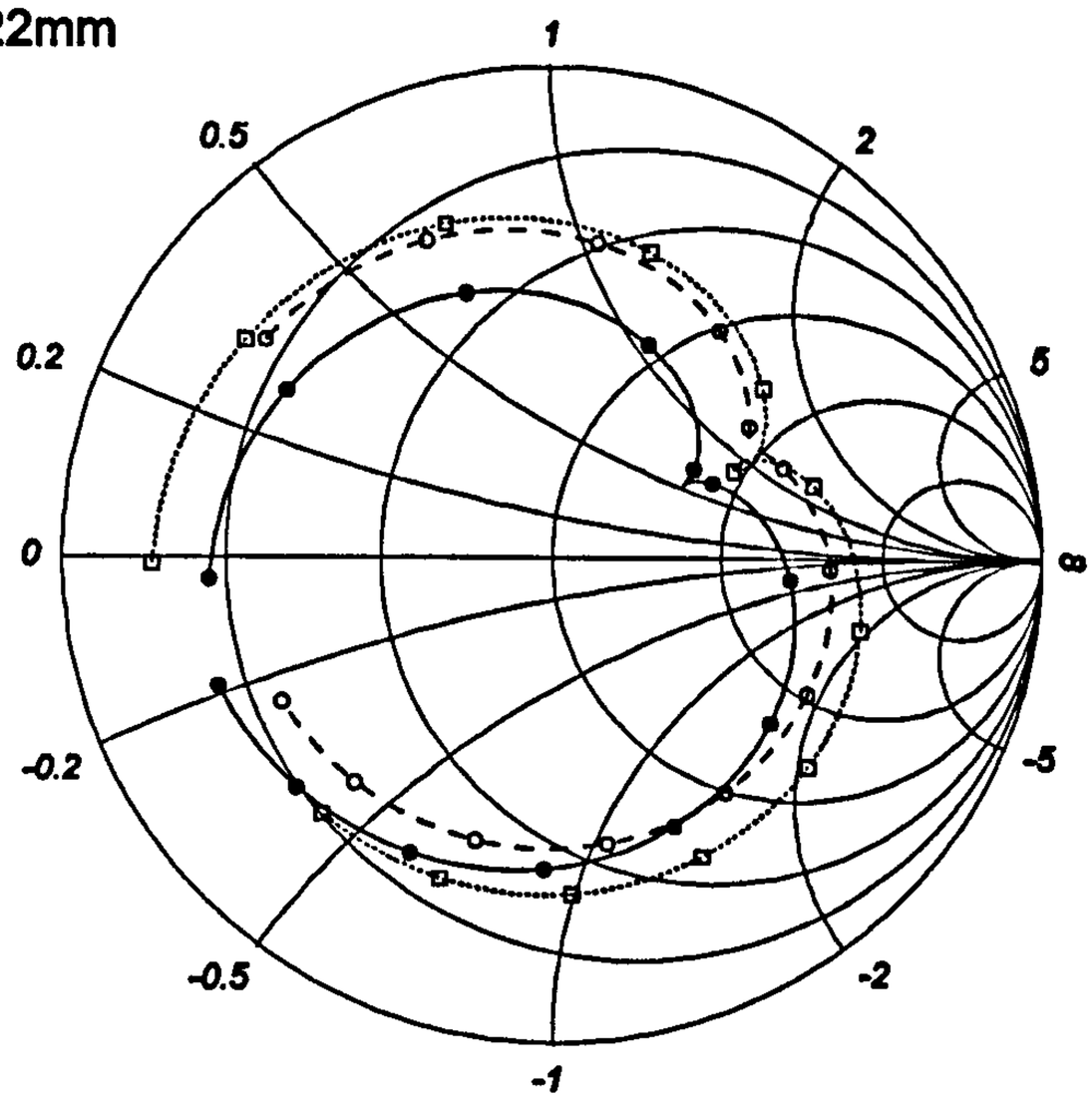

Frequency range: **2.10 - 2.70 GHz**; Step: **50MHz.**

L_a = 14mm

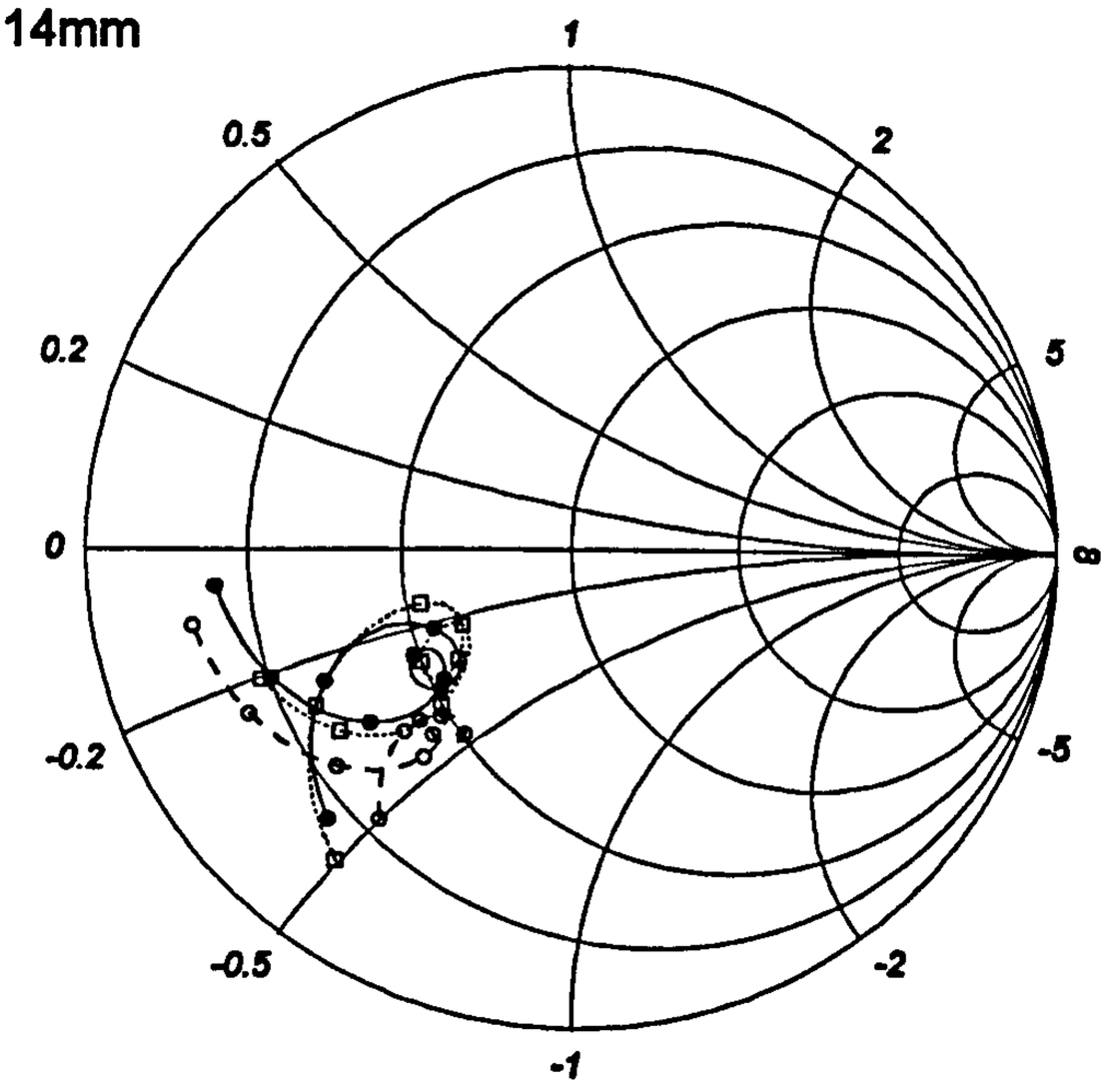

Frequency range: **2.35 - 2.75 GHz;** Step: **50MHz.**

Figure 6.11. Parameter: Aperture length.

full wave simulation, transmission line method, cavity model

$$n_{1a} = \frac{L_a}{a} \qquad \text{and} \qquad n_{1b} = \frac{L_a}{b} \tag{6.3}$$

Although for different values of aperture length, both antenna to slot (n_1) and slot to microstrip line (n_2) turns ratios vary, the effect of change in n_1 is stronger. When the length of the aperture is increased from 14mm to 22mm, the value of n_1 increases by a factor of 1.5, while that for n_2 it is only 1.08. From equations (6.2) and (6.3) it can be seen that the admittance of the patch being coupled to the feed line is directly proportional to the square of the aperture length. This is demonstrated in Figure 6.12, which shows the real and imaginary parts of the total admittances (due to the patch and the slot) of the two orthogonal modes at the aperture, for the two different aperture lengths.

It can be seen from Figures 6.12 that the resonant frequency of the patch antenna is unchanged, but the value of the real part of the admittance is greater when the aperture is longer.

Beside the change in the turns ratios, the self-admittance of the aperture also varies with its length. The admittance of the aperture has been calculated in both the transmission line and cavity models using the expression

$$Y_{ap} = -\frac{2j}{Z_{ca}} \cdot \cot\left(k_a \frac{L_a}{2}\right) \tag{6.4}$$

The argument of the cotangent is smaller than π in a practical case when the aperture length is smaller than half a wavelength. This means that when a longer aperture is used the susceptance of the aperture self-admittance is smaller in absolute value. The effect of this on the total impedance ($1/Y_{ta}$ and $1/Y_{tb}$) is shown in Figure 6.13.

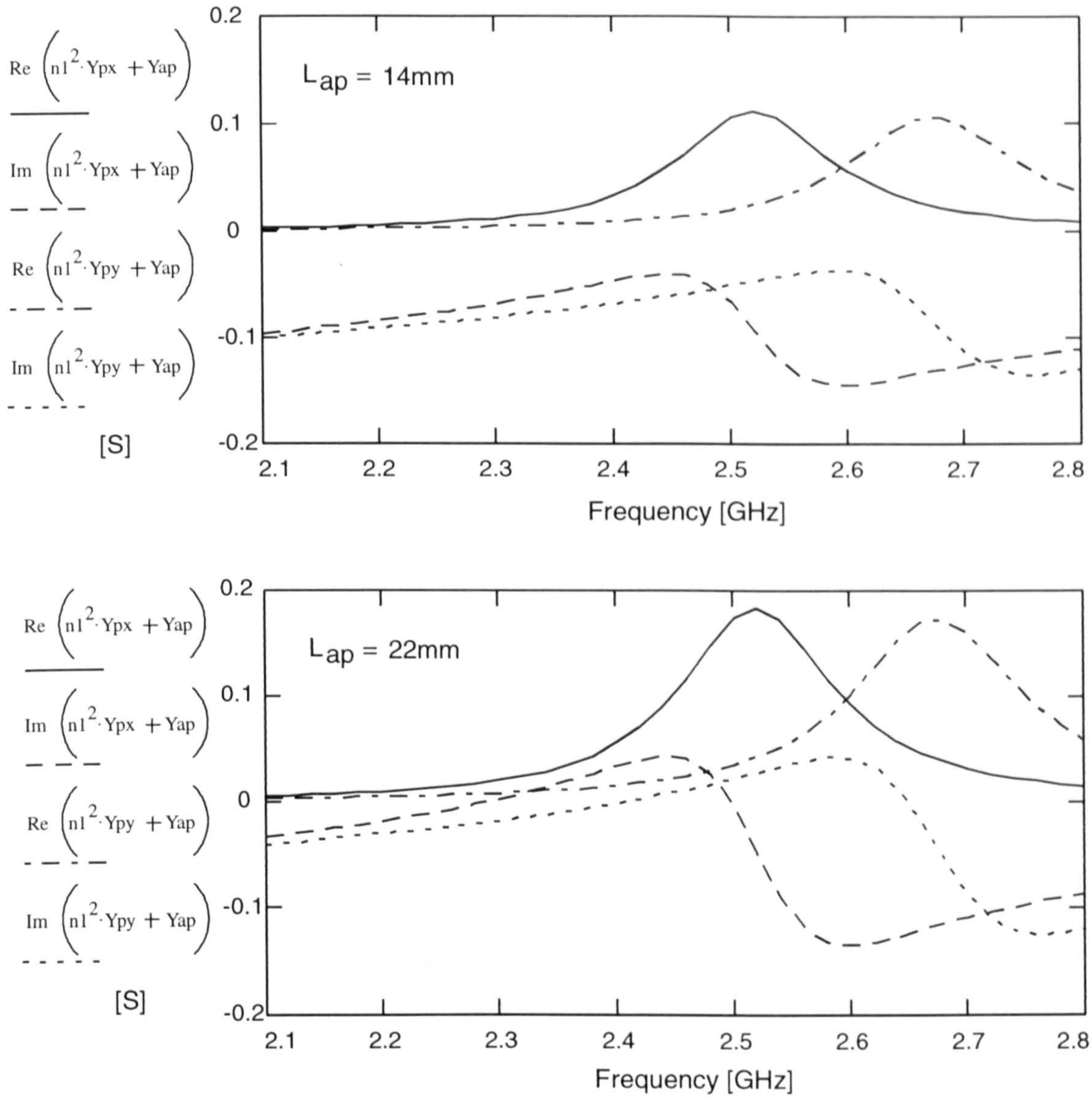

Figure 6.12. Total admittance at the aperture.

It can be seen from Figures 6.13 that when a larger aperture is used, the resistance belonging to the resonance is greater due to the larger aperture susceptance. This is shown on the Smith-chart in Figure 6.13 as a larger resonant loop. It can also be noted that although the frequency of the patch self-resonance is independent of the aperture length (see Figure 6.12), the resulting resonant frequency, which is defined as the frequency where the imaginary part of the input impedance is zero, is lower when using a longer coupling slot. This is also due to the changing self-susceptance of the aperture.

The variation of resonant impedance with the slot length can be used to match the input impedance of the antenna to that of the feed line, eliminating the need for an external matching network, which would increase the board space required for the antenna.

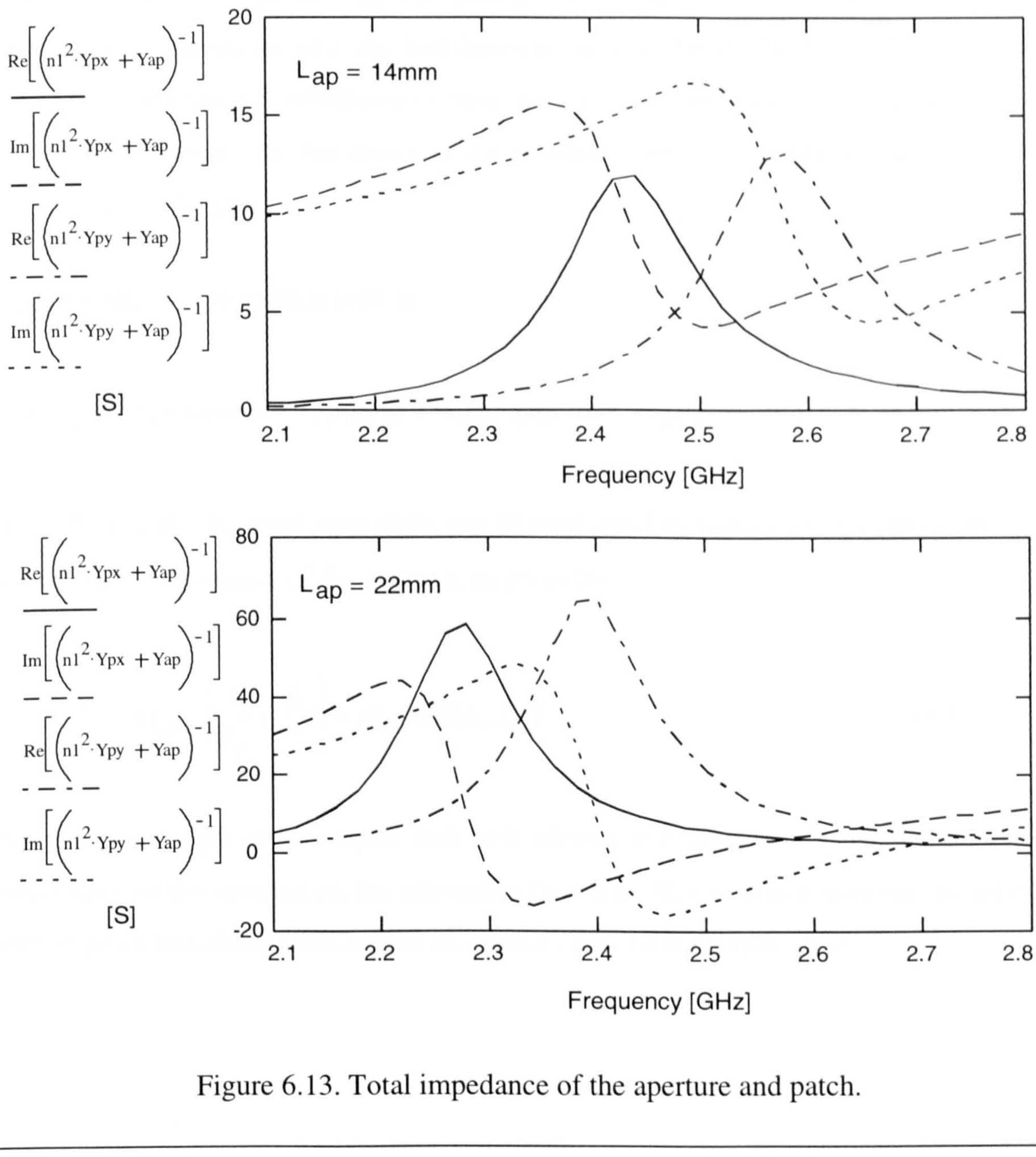

Figure 6.13. Total impedance of the aperture and patch.

6.3.2 APERTURE WIDTH

The input impedance for aperture widths of 1mm and 4mm are shown in Figure 6.14 from which it can be seen that there is a direct relationship between the magnitude of real impedance at the resonance and the aperture width.

This can also be explained by the change in the aperture self-susceptance, as the characteristic impedance of a slot line depends on its width [Cohn 1969]. Larger widths cause the characteristic impedance to raise, which in turn reduces the self susceptance of the aperture. Hence, the resistance at the resonance will be greater, as in the case of larger aperture length.

6.3.3 LENGTH OF OPEN STUB

The input impedance for 15mm and 5mm open stub lengths are shown in Figure 6.15.

The effect of the different open stubs can be explained considering the formula obtained for the input impedance of the antenna, as given by

$$Z_{in} = n_{2(45)}^2 \cdot \left(\frac{1}{Y_{ta}} + \frac{1}{Y_{tb}} \right) - jZ_{cf} \cdot \cot\left(k_f L_{os}\right) \tag{6.5}$$

Varying the length of the open stub will change the reactance added to the series impedance of the antenna on the microstrip feed line. Hence, this causes the impedance loci to be shifted along the constant resonance curve of the Smith-chart.

W_a = 1mm

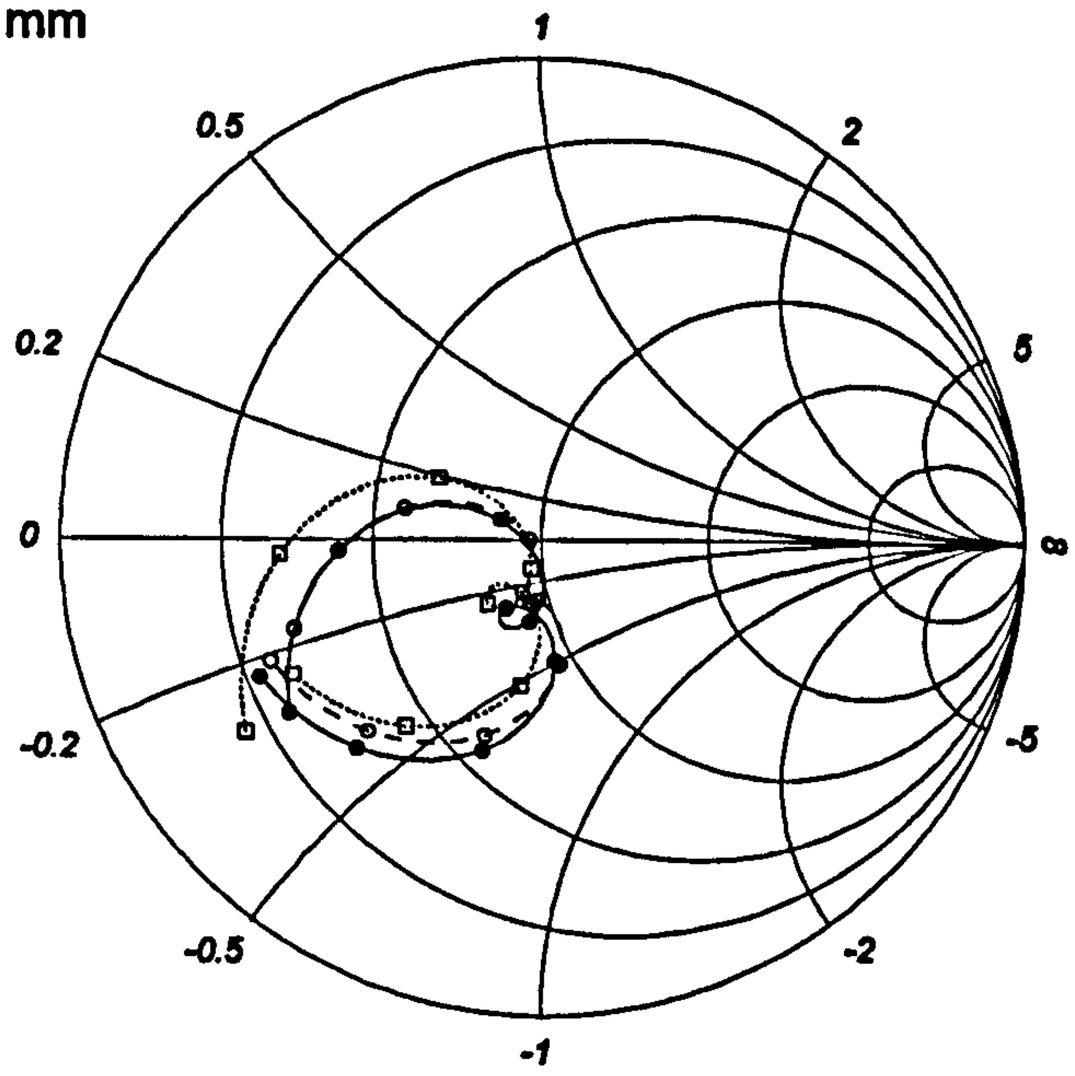

Frequency range: **2.30 - 2.70 GHz**; Step: **50MHz.**

W_a = 4mm

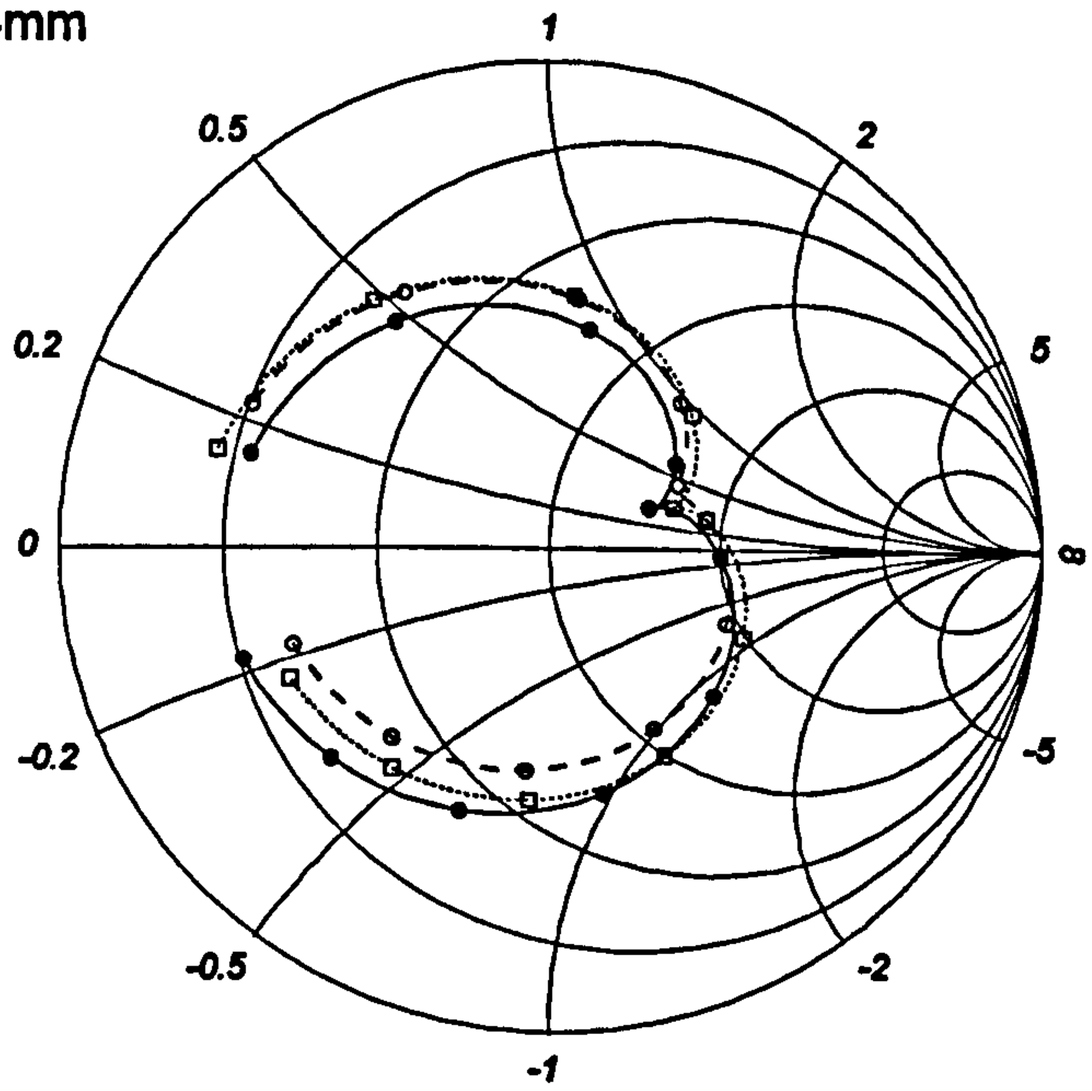

Frequency range: **2.20 - 2.70 GHz**; Step: **50MHz.**

Figure 6.14. Parameter: Aperture width.

full wave simulation, transmission line method, cavity model

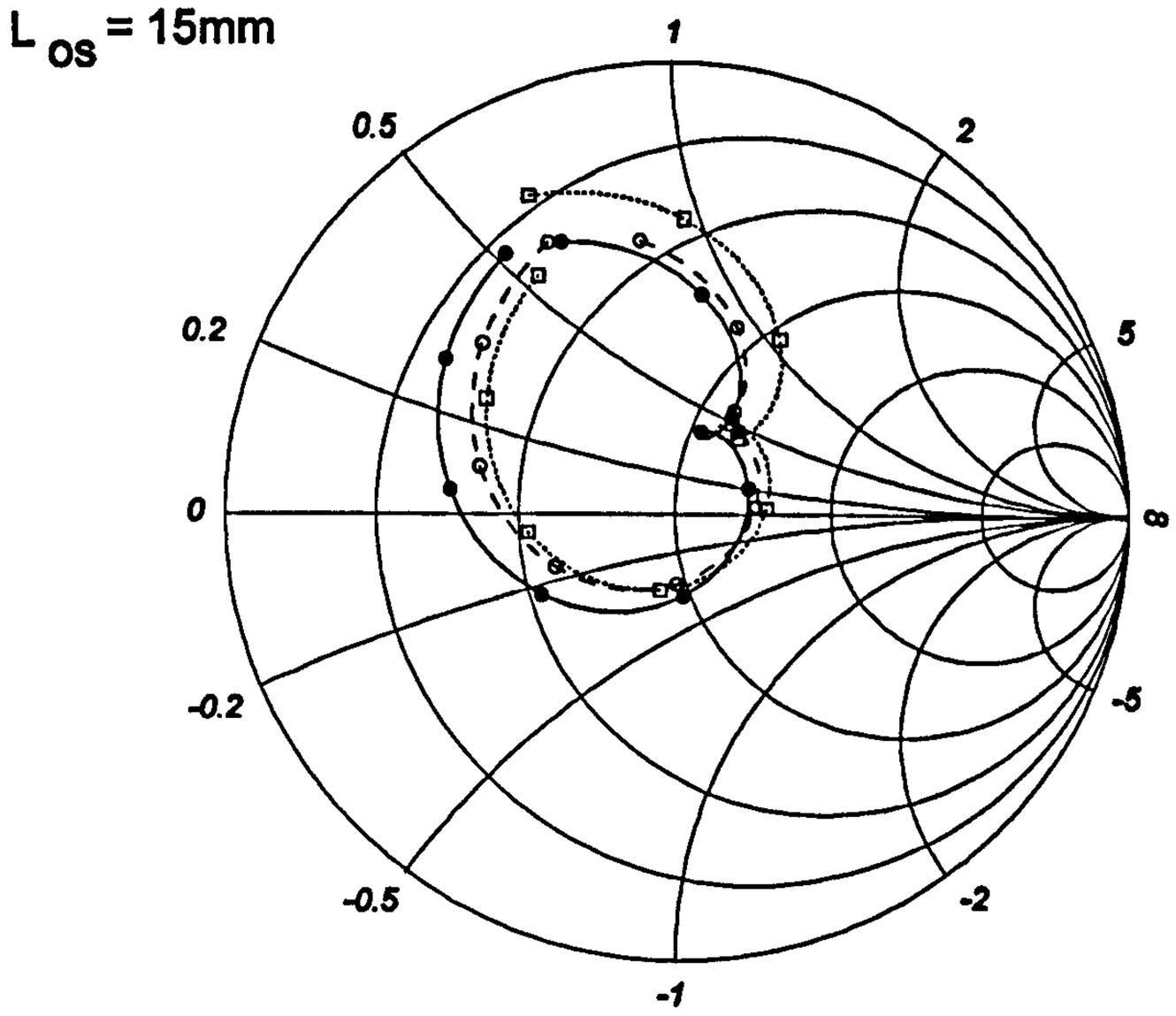

Frequency range: **2.30 - 2.75 GHz**; Step: **50MHz.**

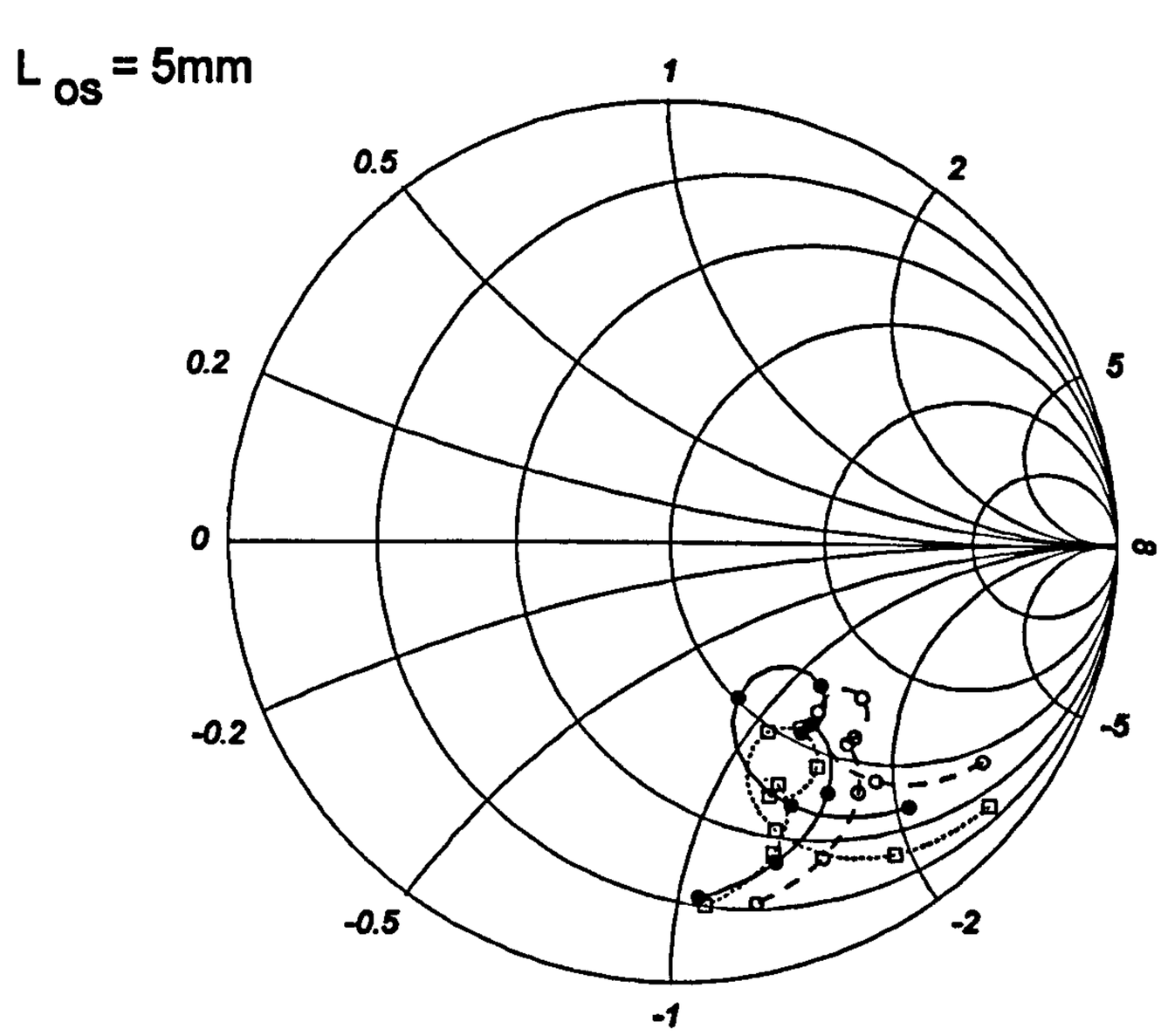

Frequency range: **2.25 - 2.65 GHz;** Step: **50MHz;**

Figure 6.15. Parameter: Length of open stub.

full wave simulation, transmission line method, cavity model

6.3.4 RELATIVE PERMITTIVITY OF FEED SUBSTRATE

Although, the permittivity of the feed substrate can not usually be selected freely when designing an aperture coupled antenna, in order to verify the accuracy of the models, two values of this parameter have been tested. The impedance results are shown in Figure 6.16.

In this case, the feed substrate permittivity has been changed and this modifies the characteristic impedance of the microstrip feed line. Therefore, the width of the feed line has been reduced accordingly, when using a feed substrate with higher permittivity, keeping the feed impedance at 50Ω.

Changing the width of the feed line causes the aperture to feed line turns ratio to change, which reduces to a value of approximately 1.5 from 1.8 when using a substrate with ε_r of 10.2 instead of 2.33. The characteristic impedance of the slot also reduces to 18Ω from 35Ω, but the effective permittivity of the aperture increases from 2.2 to 6.5. The resulting effect of these changes is that the susceptance of the aperture reduces, which is not compensated fully by the increasing n_2, and therefore the resonant impedance slightly increases.

$\varepsilon_{rf} = 6$

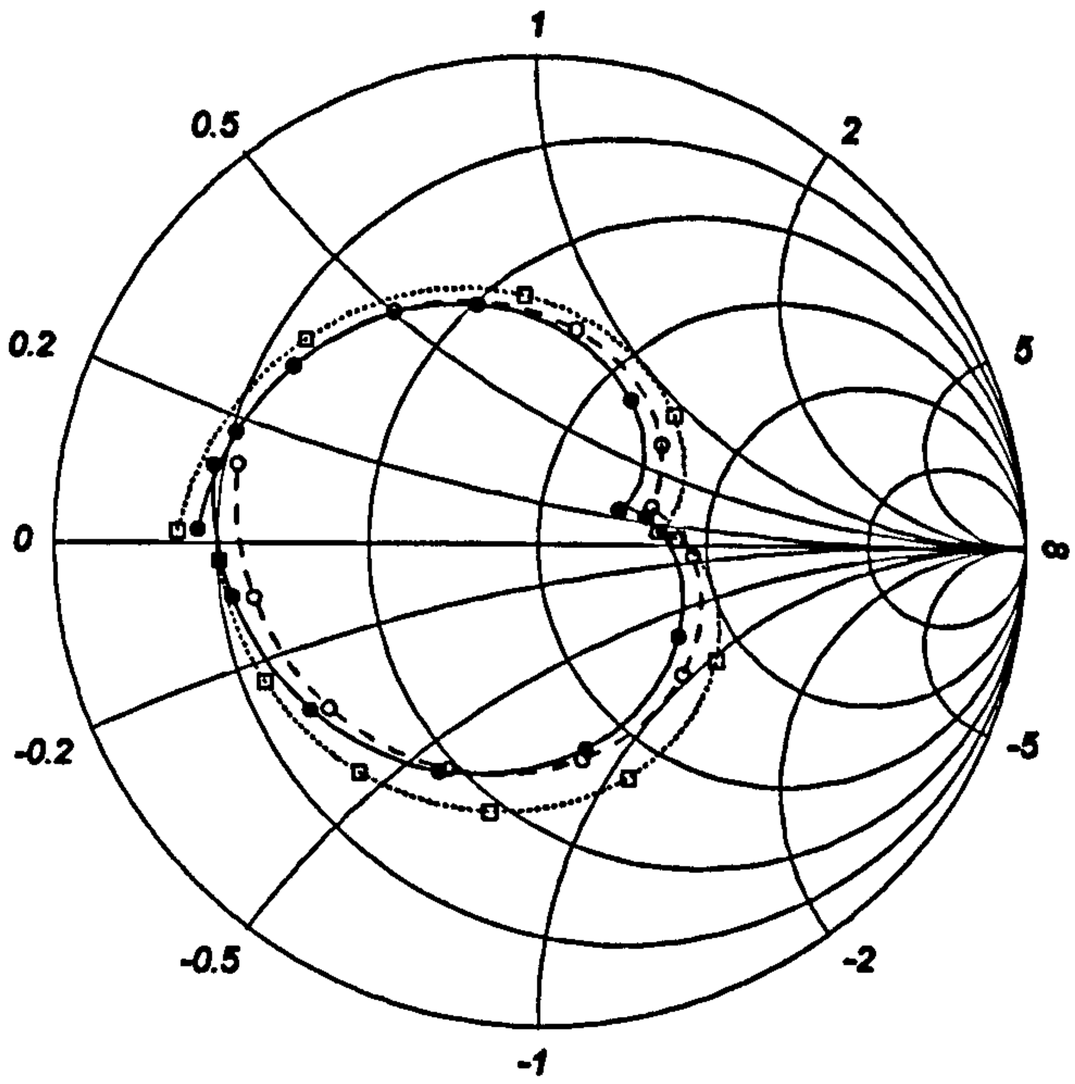

Frequency range: **2.20 - 2.75 GHz;** Step: **50MHz.**

$\varepsilon_{rf} = 10.2$

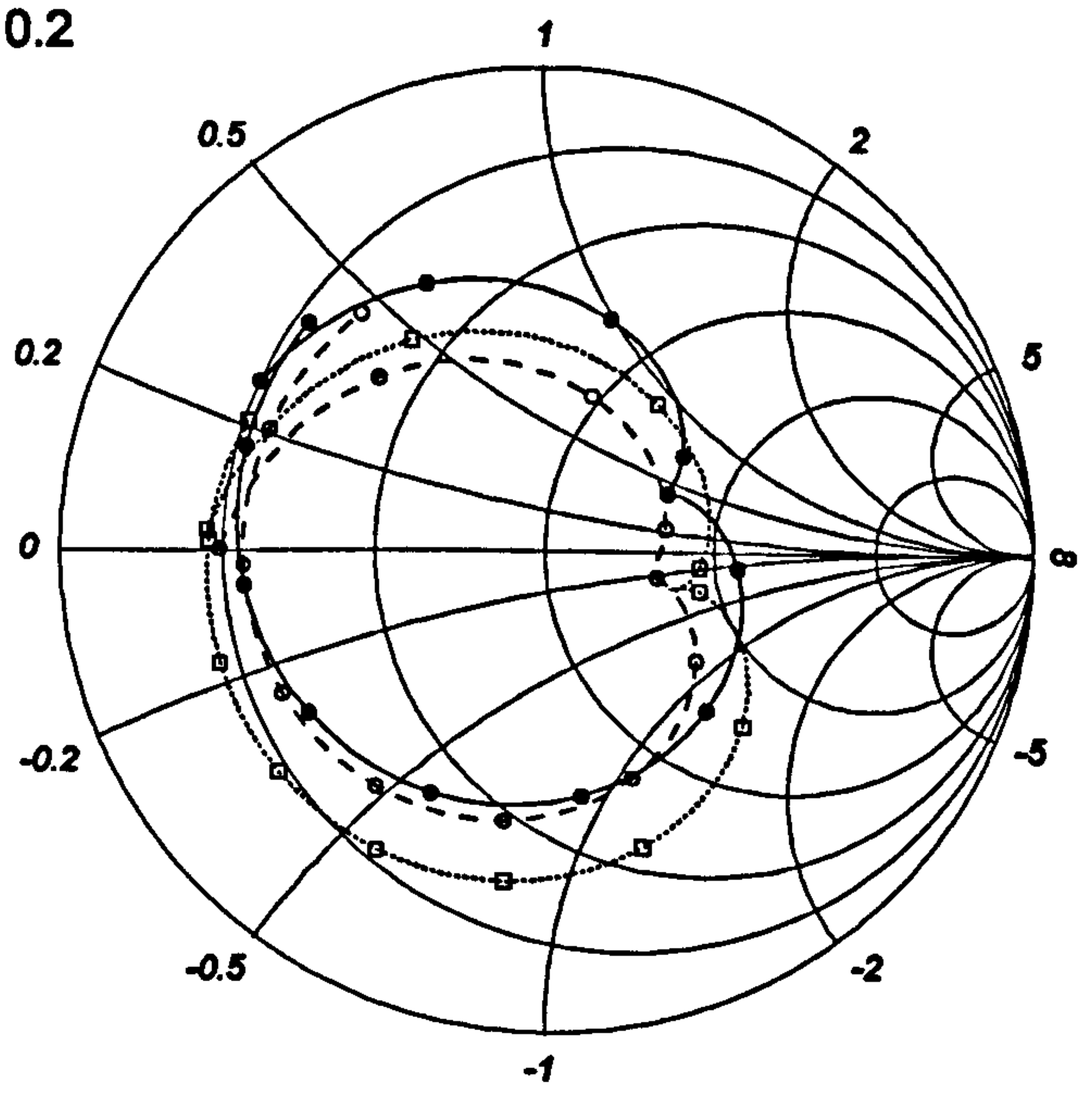

Frequency range: **2.20 - 2.80 GHz;** Step: **50MHz.**

Figure 6.16. Parameter: Permittivity of feed substrate.

full wave simulation, transmission line method, cavity model

6.3.5 THICKNESS OF FEED SUBSTRATE

The input impedance of the cross-aperture coupled antenna has been calculated for two values of feed thickness, namely 0.8mm and 3.15mm. In practice a thick feed substrate would not be employed as this increases the spurious radiation from the feed network, but here it is only used to verify the theoretical models. The input impedance for the two values of feed substrate thicknesses are shown in Figure 6.17.

The main effect of the different feed substrate thickness is the change of aperture to microstrip line turns ratio (n_2). For the 0.8mm thick substrate, the value of turns ratio is 2.1, while for the 3.15mm thick substrate it is 1.3, which explains, through equation (6.5) the variation of the size of the resonant loop.

6.4 EFFECT OF ANTENNA SUBSTRATE THICKNESS

The effect of antenna substrate thickness has been examined in a slightly different manner to that of the other parameters. This is because the antenna substrate thickness is the main parameter determining one of the most important performance characteristics, the fractional axial ratio bandwidth of the antenna. In order to see how the antenna thickness influences the bandwidth, for each value of thickness, the aperture length and the dimensions of the nearly square patch have been re-adjusted to optimise the axial ratio.

6.4.1 INPUT IMPEDANCE

In addition to Figure 6.2, which shows the input impedance of a cross-aperture coupled antenna with thickness of 3.15mm, the impedance of three other antennas, with values of substrate thickness of 4.7mm, 6.3mm and 7.1mm are shown in Figure 6.18, 6.19 and 6.20, respectively.

d_f = 0.8mm

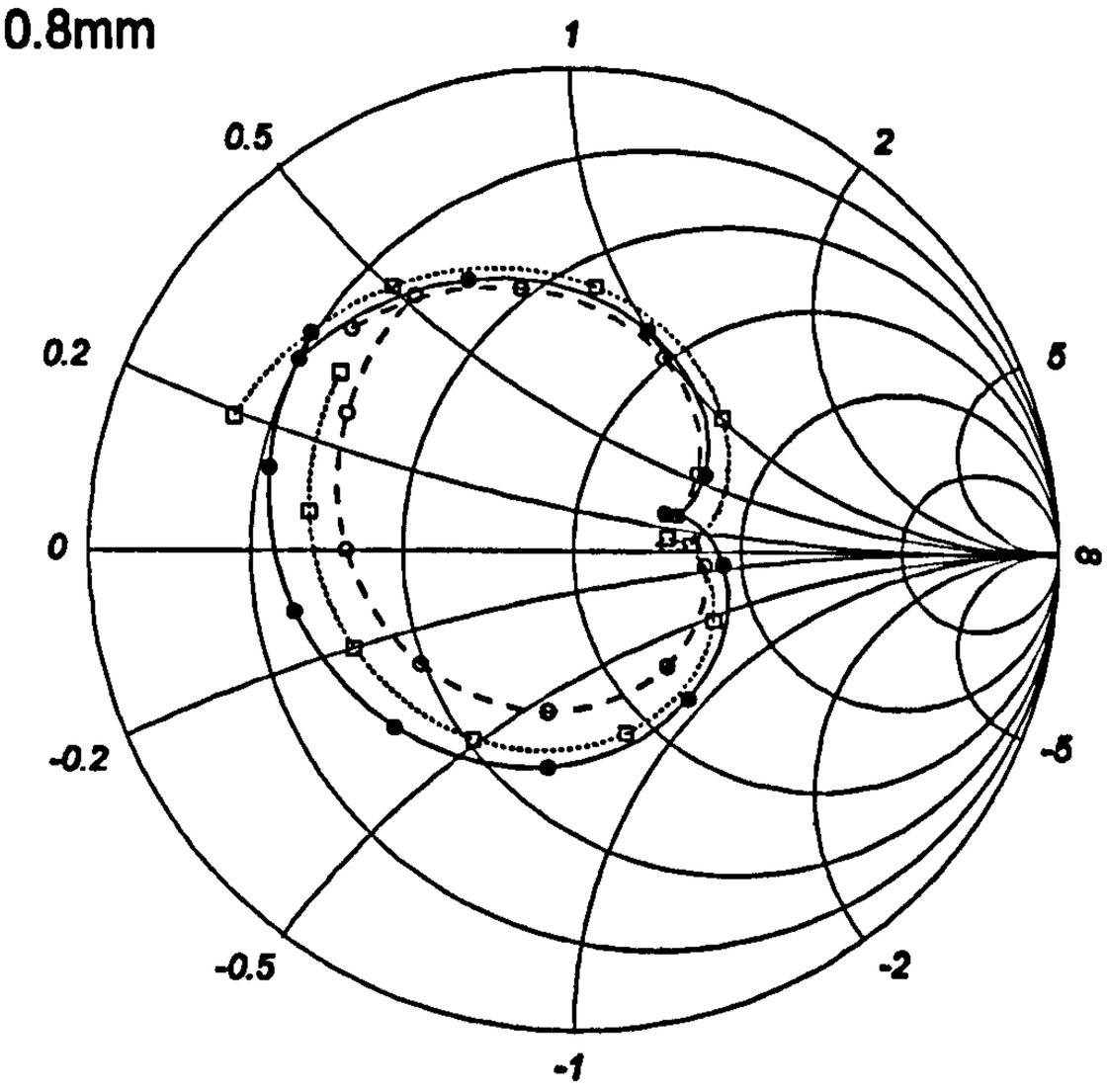

Frequency range: **2.25 - 2.80 GHz;** Step: **50MHz.**

d_f = 3.1mm

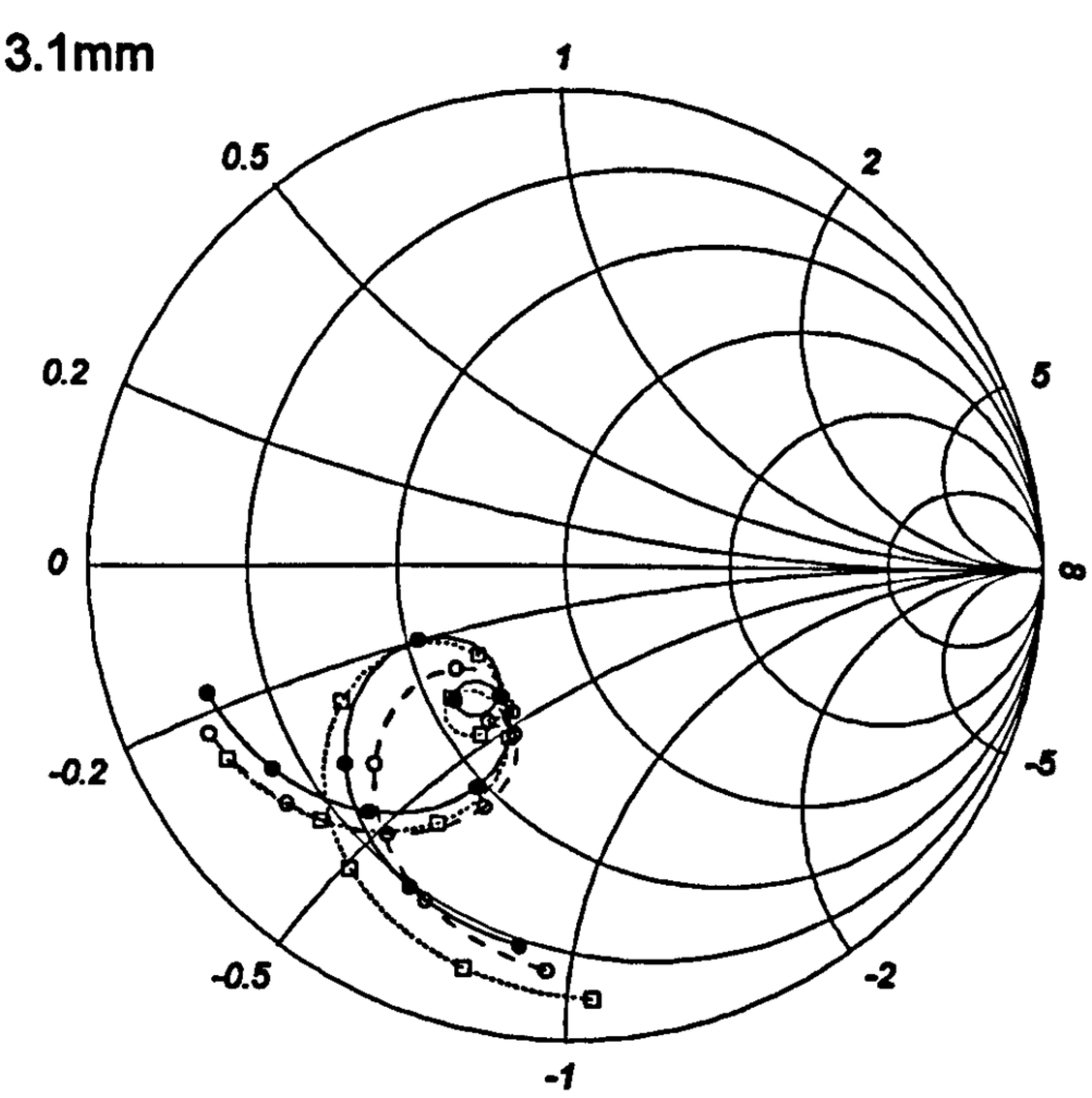

Frequency range: **2.20 - 2.70 GHz;** Step: **50MHz.**

Figure 6.17. Parameter: Thickness of feed substrate.

full wave simulation, transmission line method, cavity model

An important change in the feed loci can be observed when increasing the thickness of the antenna substrate. The quality factor of the antenna reduces due to the increased radiation from the thicker antenna, and therefore, the two resonant frequencies of the orthogonal modes must be further separated to keep the optimal condition for circular polarisation.

This is done by increasing the difference between the two dimensions of the nearly square patch, *a* and *b*. This difference for the 3.15mm thick antenna is 2.2mm, while being 6.6mm for the 7.1mm thick one. The reducing quality factor also reduces the amplitude of the resonance, causing the single impedance loop with the cusp to separate into two smaller loops as shown in Figure 6.20.

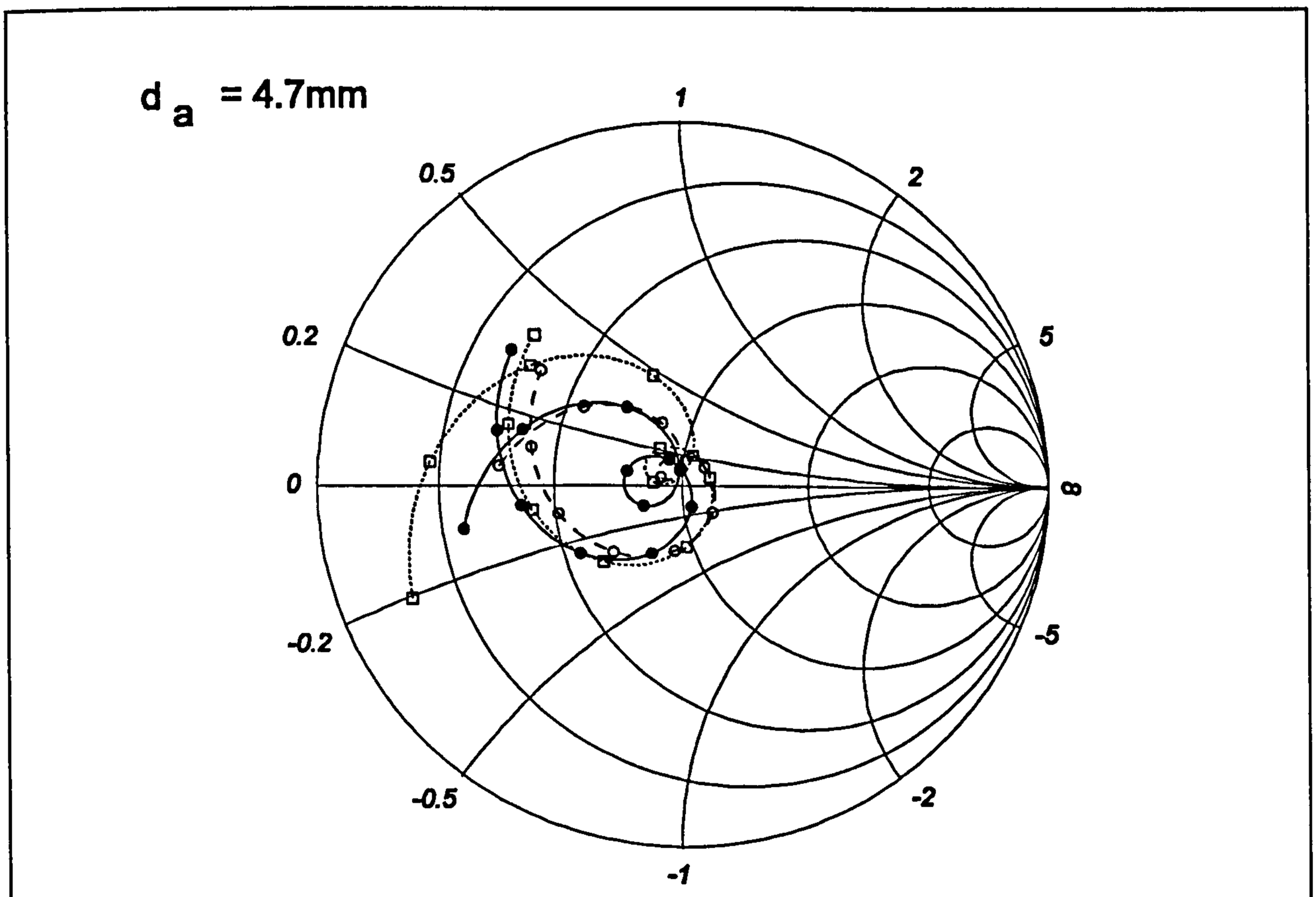

Frequency range: **2.20 - 2.80 GHz;** Step: **50MHz.**

Figure 6.18. Parameter: Antenna thickness.

full wave simulation, transmission line method, cavity model

Secondary parameters changed: a = 32.2mm, b = 36.0mm, L_a = 20mm.

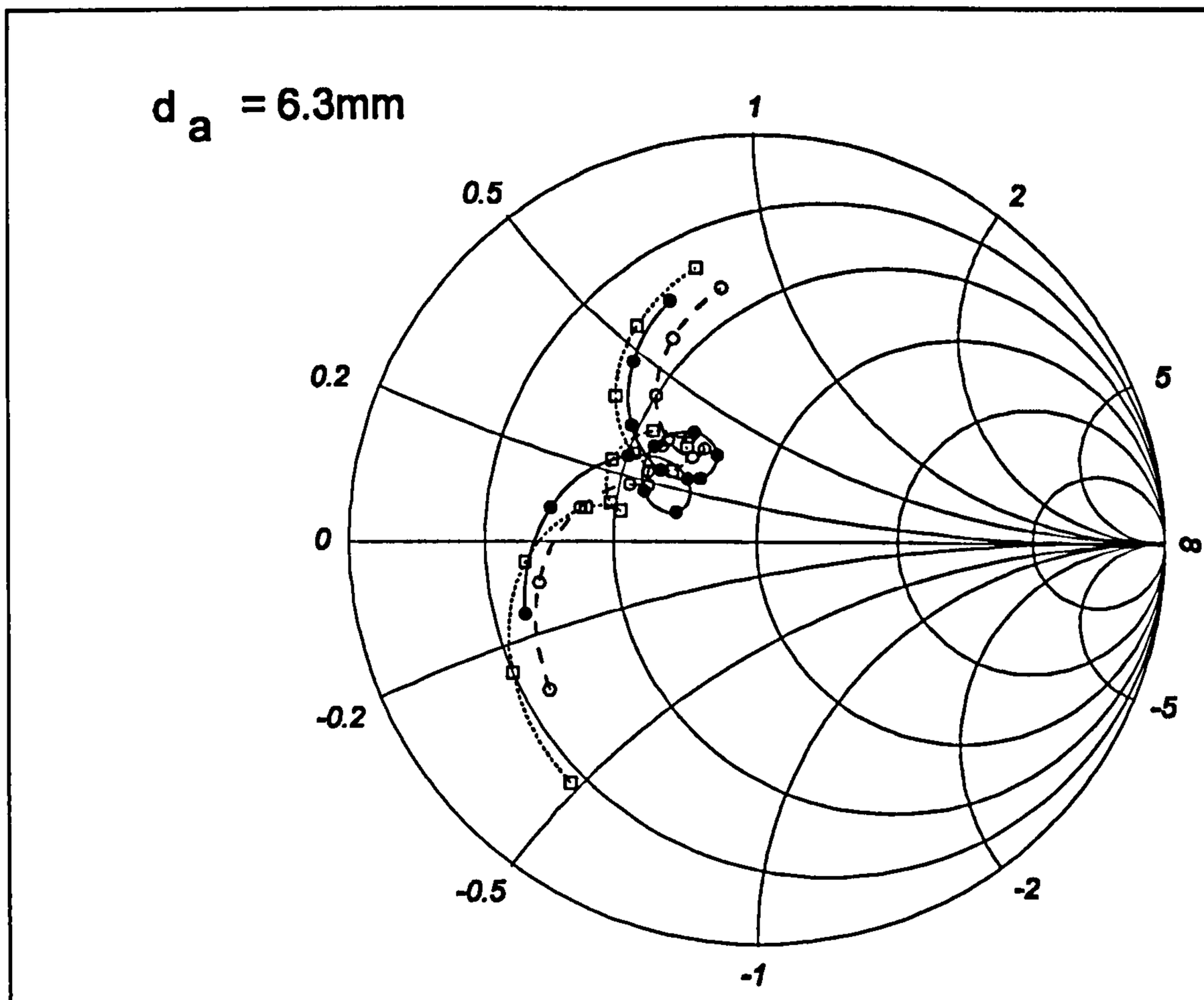

Frequency range: **2.15 - 2.80 GHz;** Step: **50MHz.**

Figure 6.19. Parameter: Antenna thickness.

full wave simulation, transmission line method, cavity model

Secondary parameters changed: a = 31mm, b = 36.0mm, L_a = 21mm.

As the antenna thickness increases, the feed loci gradually moves away from the centre of the Smith-chart, which represents the matched condition. This is due to the lowering of the quality factor and it was not possible to compensate for this by varying any of the other design parameters.

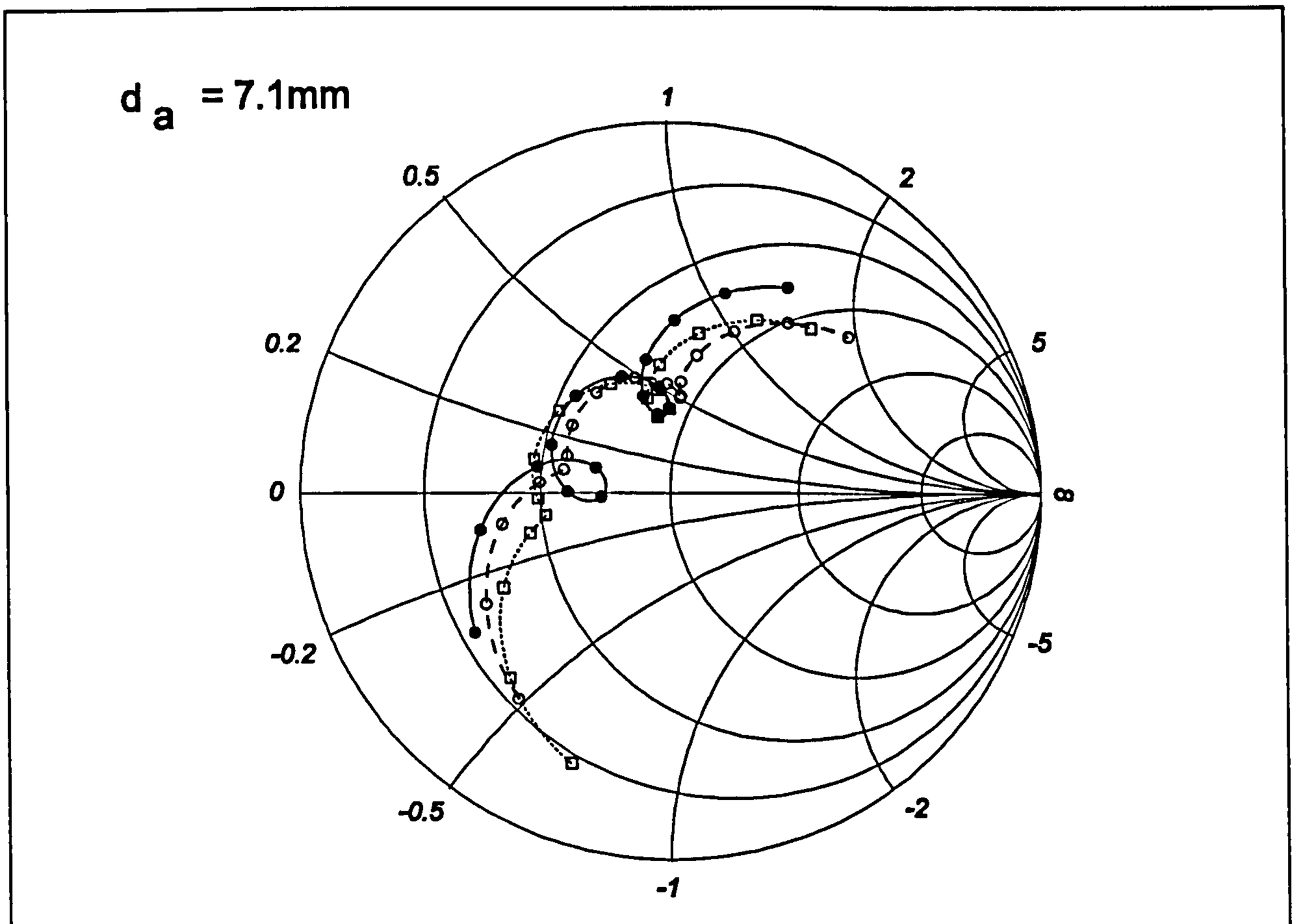

Frequency range: **2.10 - 2.90 GH;** Step: **50MHz.**

Figure 6.20. Parameter: Antenna thickness.

full wave simulation, transmission line method, cavity model

Secondary parameters changed: a = 29.5mm, b = 36.1mm, L_a = 22mm.

6.4.2 AXIAL RATIO

The theoretically predicted and simulated axial ratio values versus frequency are shown in Figures 6.9, 6.21, 6.22 and 6.23 for four antennas with antenna thicknesses of 3.15mm, 4.7mm, 6.3mm and 7.1mm, respectively.

It can be seen that there is a direct relationship between antenna thickness and fractional axial ratio bandwidth. The 3dB fractional axial ratio bandwidth for the 3.15mm thick antenna is 1.6%, while being 3.8% for the 7.1mm thick one. Hence, in respect of the axial ratio bandwidth, one should use a substrate as thick as possible.

The values of axial ratio bandwidth are slightly better in the case of the cross-aperture coupled antenna than that of the corner fed nearly square patch antenna realised on the same substrate. This can be seen from Table 3.1, which gives 1.37% bandwidth for a 3.15mm thick microstrip line fed nearly square patch and 3.08% for a 7.1mm thick one. This is due to the additional susceptance of the aperture, which varies only slightly with the frequency.

As a result of this investigation carried out on how the antenna substrate thickness influences the bandwidth of the cross-aperture coupled antenna, an important relationship has been observed between the bandwidth of the antenna and the value of the standing wave ratio. The standing wave ratio and the axial ratio for the different antenna substrate thicknesses are shown in Figure 6.24.

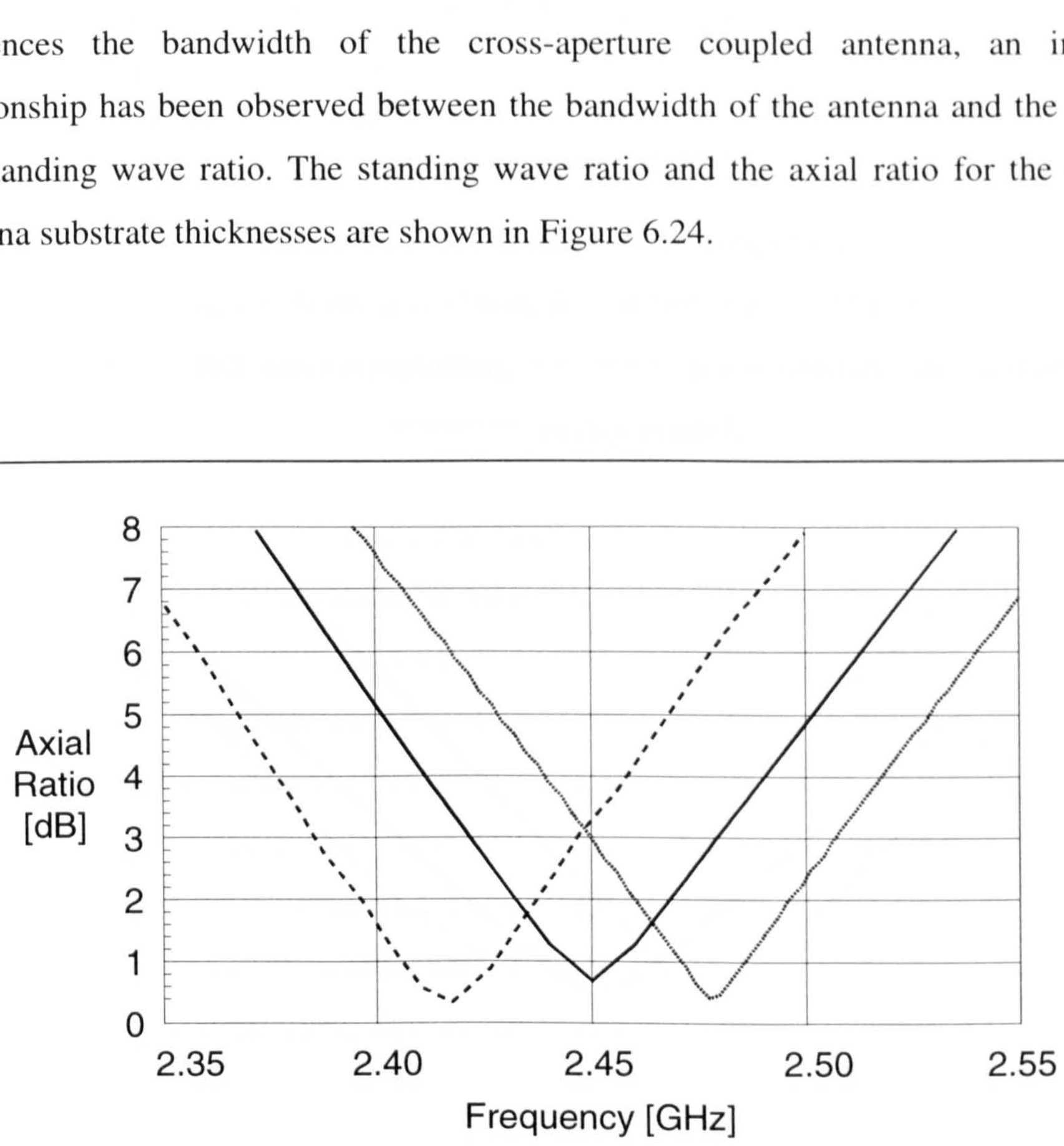

Figure 6.21. Axial ratio versus frequency.

d_a = 4.7mm, a = 32.2mm, b = 36.0mm, L_a = 20mm.

——— full wave simulation, - - - - - - transmission line method,

..... cavity model.

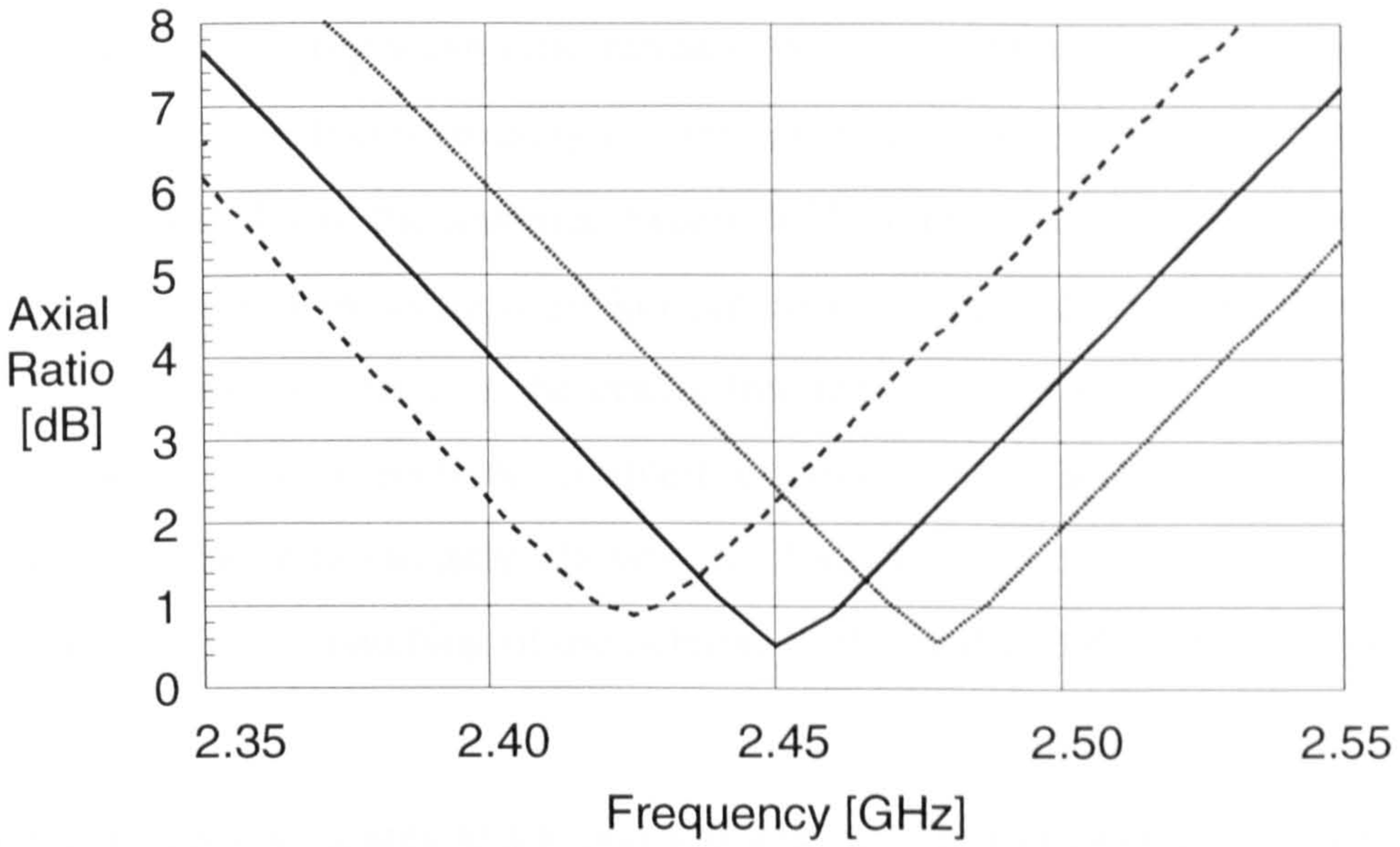

Figure 6.22. Axial ratio versus frequency.

d_a = 6.3mm, a = 31mm, b = 36.0mm, L_a = 21mm.

——— full wave simulation, - - - - - - transmission line method,

..... cavity model.

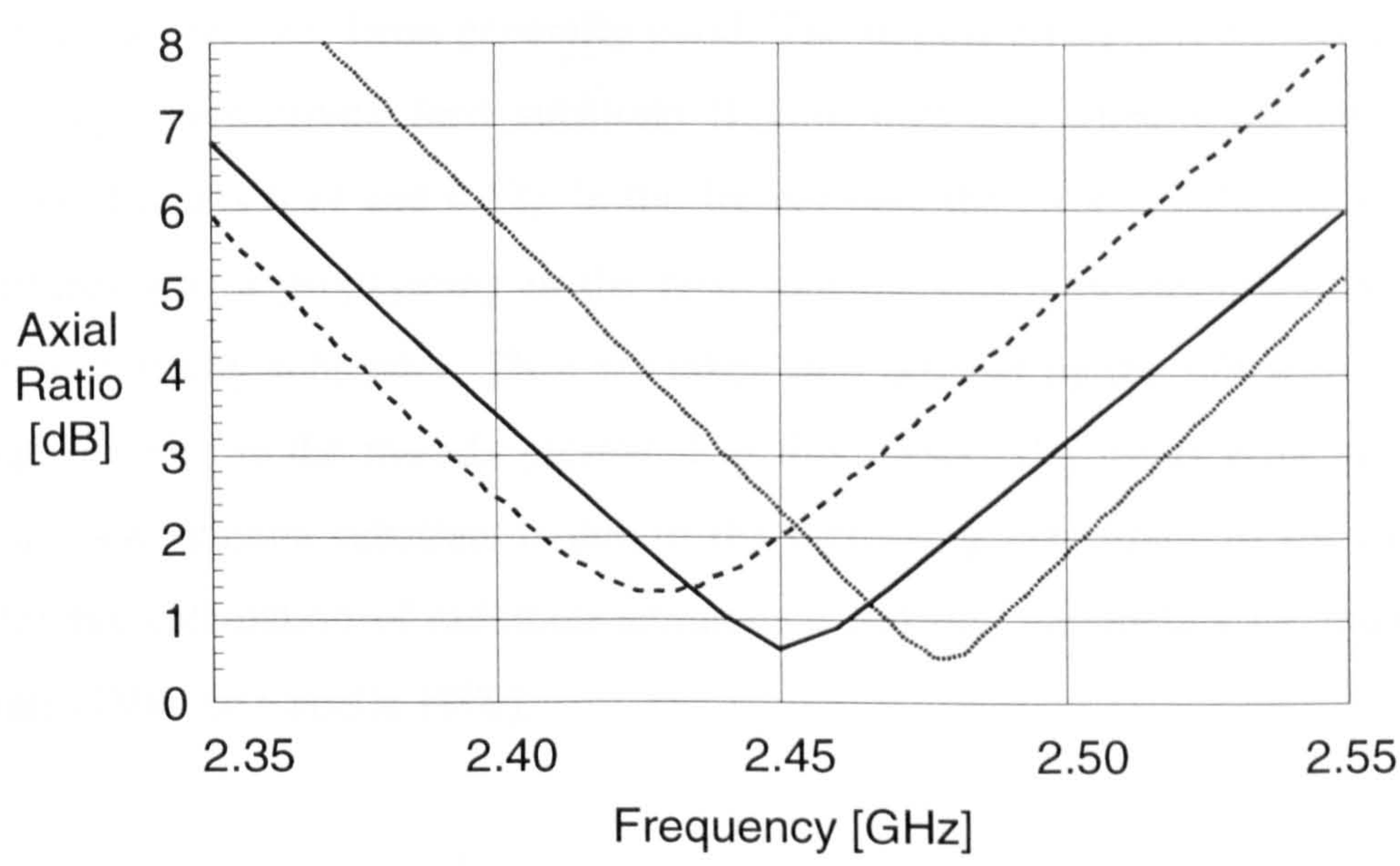

Figure 6.23. Axial ratio versus frequency.

d_a = 7.1mm, a = 29.5mm, b = 36.1mm, L_a = 22mm.

——— full wave simulation, - - - - - - transmission line method,

..... cavity model.

The impedance bandwidth of an antenna is defined as the fractional frequency range, inside which the standing wave ratio remains under a certain value, usually 2. It can be seen from Figure 6.24 that increasing the antenna thickness has a beneficial effect on the impedance bandwidth of the antenna. Figure 6.25 shows that the axial ratio bandwidth can also be increased by using a thicker antenna substrate. However, the value of the standing wave ratio increases at the centre frequency of the operating band. Therefore, when realising a cross-aperture coupled circularly polarised antenna, the antenna thickness must be appropriately chosen, so that the required bandwidth is achieved without degrading the matching of the antenna at the centre of the operating band.

6.5. ACCURACY AND VALIDITY OF THE THEORETICAL MODELS

The accuracy of the transmission line model regarding the prediction of the resonant frequency, which is defined as the frequency where the imaginary part of the input impedance is zero, has been generally good. The largest errors (3.7%), occurred when using a high permittivity feed substrate (Figure 6.9) and when using thick antenna substrates (Figures 6.11 and 6.12). In the former case the error is believed to be due to the surfaces waves propagating in the feed substrates as their amplitude is greater in higher permittivity substrates. They are taken into account by the full wave simulation package but not by the models presented in this thesis. The larger error shown when using a thick antenna substrate is due to the increasing inaccuracy of the expressions used for the calculation of radiation admittance and line parameters for thick antenna substrates [Van de Capelle 1989].

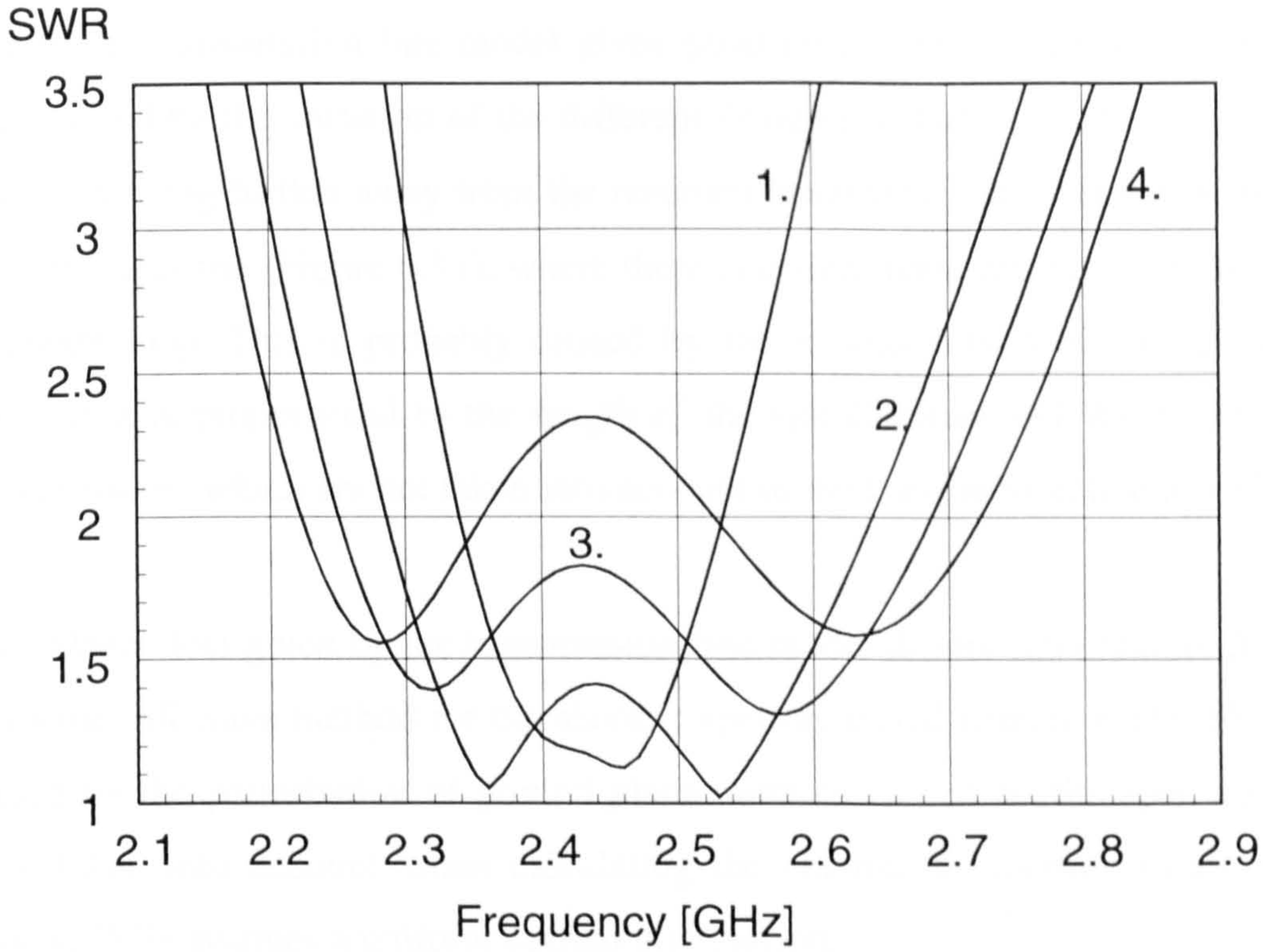

Figure 6.24. Variation of standing wave ratio with substrate thickness.

1. d_a = 3.15mm; **2.** d_a = 4.7mm; **3.** d_a = 6.3mm; **4.** d_a = 7.1mm.

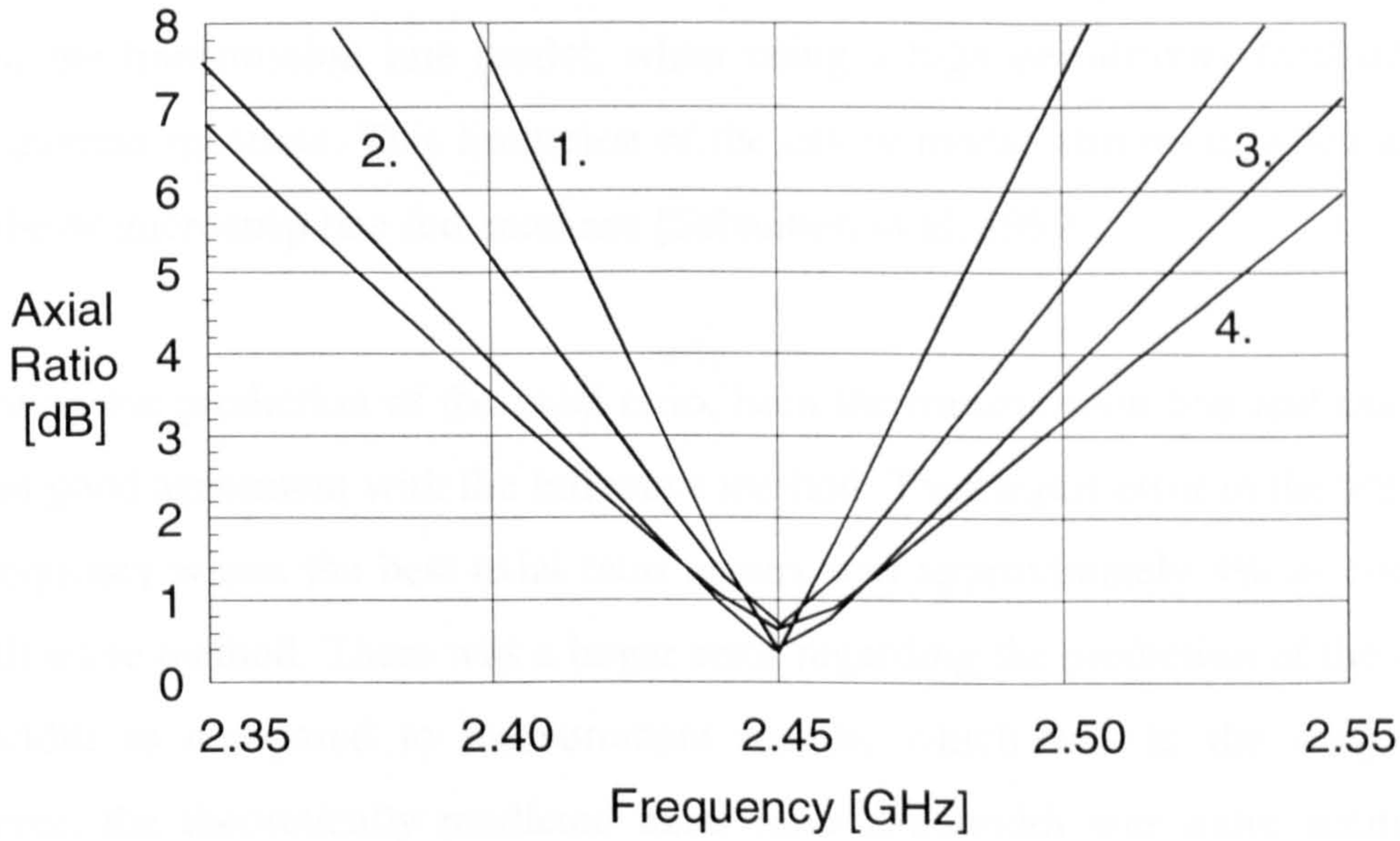

Figure 6.25 Variation of axial ratio with substrate thickness.

1. d_a = 3.15mm; **2.** d_a = 4.7mm; **3.** d_a = 6.3mm; **4.** d_a = 7.1mm.

Regarding the prediction of the input impedance at other frequencies rather than at resonance, the transmission line model gives good results and which follows well the changes caused by the variation of the different design parameters. The error is usually greater when being further away from the resonant frequency. Larger errors occur when using a long aperture (Figure 6.11), where there is a significant difference in the size of the resonant loop. This is probably caused by the increased back radiation from the aperture, as it is proportional to the length of the slot [Gronau and Wolf 1986]. This introduces losses, which are not taken into account in the transmission line model.

The impedance loci given by the transmission line model differs significantly from that given by the full wave method for the shortest aperture tested (Figure 6.11). This could be caused by the perturbation of ground plane currents caused by the aperture, which was not taken into account when calculating the antenna to aperture turns ratio, as expression (6.3) assumes a uniform current distribution.

The accuracy of the resonant frequency and the input impedance given by the cavity model is similar to that of the transmission line model. The larger errors occur, as in the case of the transmission line model, when using a high permittivity feed substrate or thick antenna substrate. This limitation of the cavity model also occur when applying it to probe or microstrip line fed antennas [Schaubert et al. 1989].

Regarding the prediction of the axial ratio, both the transmission line and cavity model were in good agreement with the full wave method. The largest error in the prediction of the frequency where the best axial ratio occurs was approximately 4% as compared to the full wave method. There was a larger error regarding the prediction of the axial ratio bandwidth as compared to measurement results, which was in the range of 10%. However, the theoretically predicted axial ratio bandwidth was more accurate when compared to the results obtained from full wave simulation. Therefore, it can be assumed that part of the difference between the theoretical and measured bandwidth is due to measurement errors.

6.6 CHAPTER SUMMARY

Initially in this chapter the input impedance and axial ratio values of two cross-aperture coupled antennas as obtained from the theoretical models, simulation and measurement were compared to each other. Good agreement has been found between the theoretical and measurement results. It was the full wave computer simulation, which gave the most accurate results, as expected.

Then the effects of a number of design parameters of the cross-aperture coupled patch antenna have been investigated using the transmission line and cavity models which were developed in the two previous chapters.

It was shown that the input impedance of the antenna can be varied by changing the length of the aperture, which allows the matching of the antenna to the feed line without the need for an external network.

It was also concluded that increasing the antenna substrate thickness improves both the impedance and the axial ratio bandwidths. However, this is limited by the standing wave ratio which can rise above an unacceptable level when using a thick substrate.

The next chapter presents an application of the cross-aperture coupled circularly polarised antenna, demonstrating the practical feasibility and good performance of this new structure.

CHAPTER 7.

APPLICATION OF THE CROSS-APERTURE COUPLED ANTENNA IN THE ON-BOARD UNIT

7.1 INTRODUCTION

In chapter six it was demonstrated how a thick low permittivity substrate increases the bandwidth of the cross-aperture coupled antenna. However, boards made from special microwave substrates, especially the thick ones have high cost. Consequently, in the on-board unit, the cross-aperture coupled antenna has been implemented using air as the antenna substrate, which is presented in this chapter. The new on-board unit antenna is designed using inexpensive fibre-glass printed circuit board. The performance of the new antenna has been tested and compared to that of the previous antenna design. The results of these tests are also discussed in this chapter. The new antenna has then been integrated with the detecting / modulating diode and the signal processing unit resulting in a new inexpensive on-board unit. Both the down- and up-link performance of the new OBU was tested and compared with that of the previous on-board unit.

The new on-board unit based on the inexpensive cross-aperture coupled microstrip antenna has also been presented at the IEE Eight International Conference on Road Traffic Monitoring and Control (23-25 April 1996, London).

7.2 THE NEW ON-BOARD UNIT ANTENNA

The design parameters of the cross-aperture coupled patch antenna with air substrate, which is to be used in the on-board unit are shown in Figure 7.1.

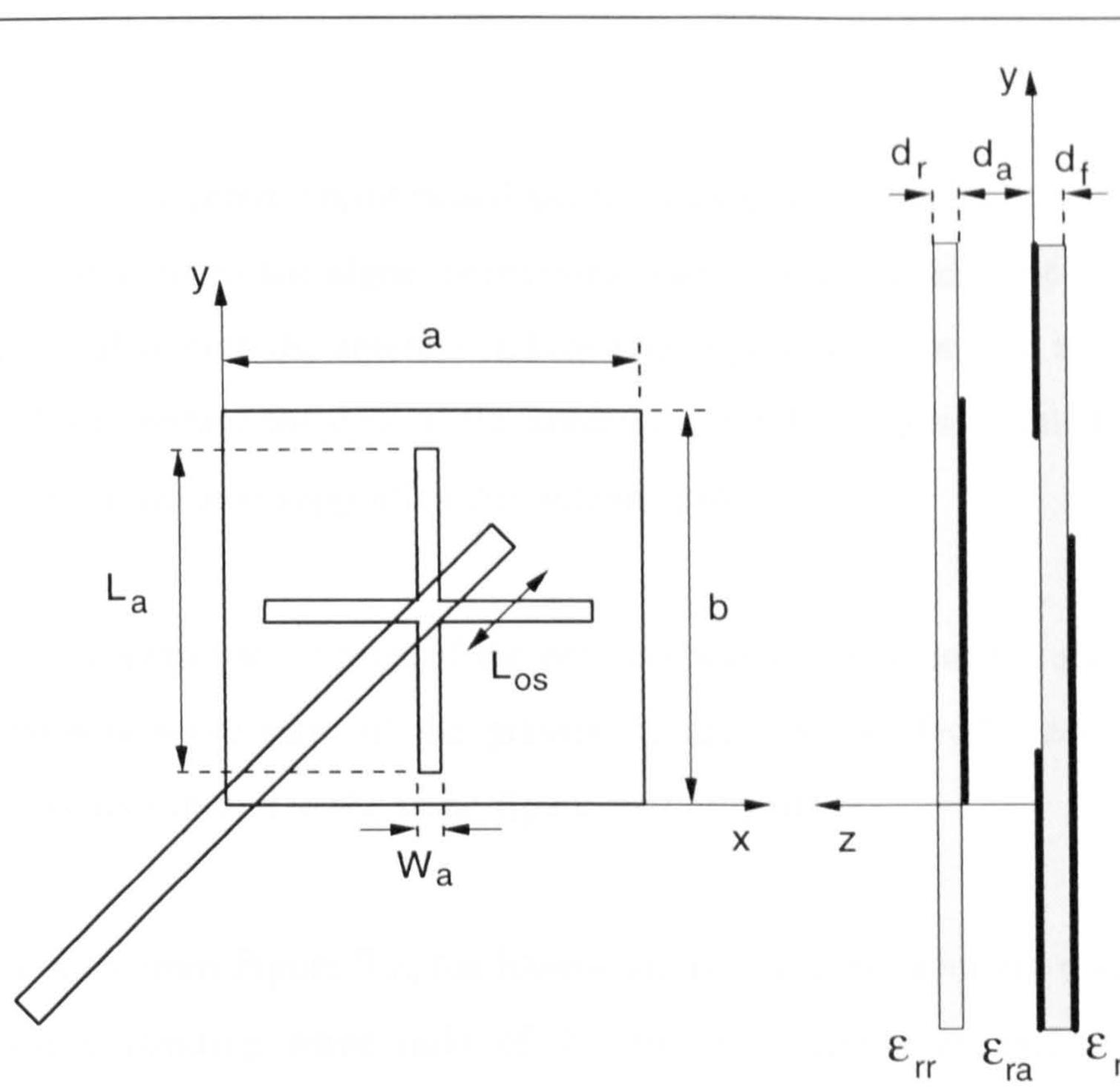

Figure 7.1. Parameters of on-board unit antenna.

a = 16.3mm, b = 18mm, W_a = 1mm, L_a = 10mm, L_{os} = 2mm, W_f = 3mm,

d_r = 0.8mm, d_a = 2.5mm, d_f = 1.5mm, ε_{rr} = 4.6, ε_{ra} = 1, ε_{rf} = 4.6.

As was demonstrated in Chapter six, the input impedance and axial ratio performance of a cross-aperture coupled antenna depends not only on the antenna dimensions (a, b), but also on the aperture dimensions (W_a, L_a) and on the thickness of the antenna substrate (d_a).

There is an infinite number of possible combinations of these design parameters, which result in an antenna generating circular polarisation at the required operating frequency of 5.8GHz. The on-board unit antenna and slot dimensions were optimised so that a suitable trade-off between the bandwidth and the standing wave ratio is obtained. How these parameters vary with the antenna thickness was demonstrated also in the previous chapter.

Normal fibre-glass printed circuit board has been used as the feed substrate of the new on-board unit antenna as the signal processing unit is built on this type of board and it was aimed to realise both the antenna and the signal processing unit on a single piece of board. In order to reduce the cost of the antenna a thin fibre-glass printed circuit board was chosen as the radome supporting the antenna patch.

The measured standing wave ratio of the new on-board unit antenna is shown in Figure 7.2. The standing wave ratio of the previously used double feed patch antenna (see Figure 2.12) is also shown in the same figure for comparison.

As it can be seen from Figure 7.2, the bandwidth of the cross-aperture coupled antenna is 13.8% for a standing wave ratio of 2. This is a significant improvement when comparing it to the 3.5% standing wave ratio bandwidth of the previous antenna design. It can also be seen from the figure that the standing wave ratio of the double feed patch antenna is less than that of the cross-aperture coupled antenna at the centre of the operating band. However, at the required operating frequency of 5.8GHz, the double feed antenna exhibits a much higher standing wave ratio than the cross-aperture coupled antenna, because of its small bandwidth and the manufacturing inaccuracy.

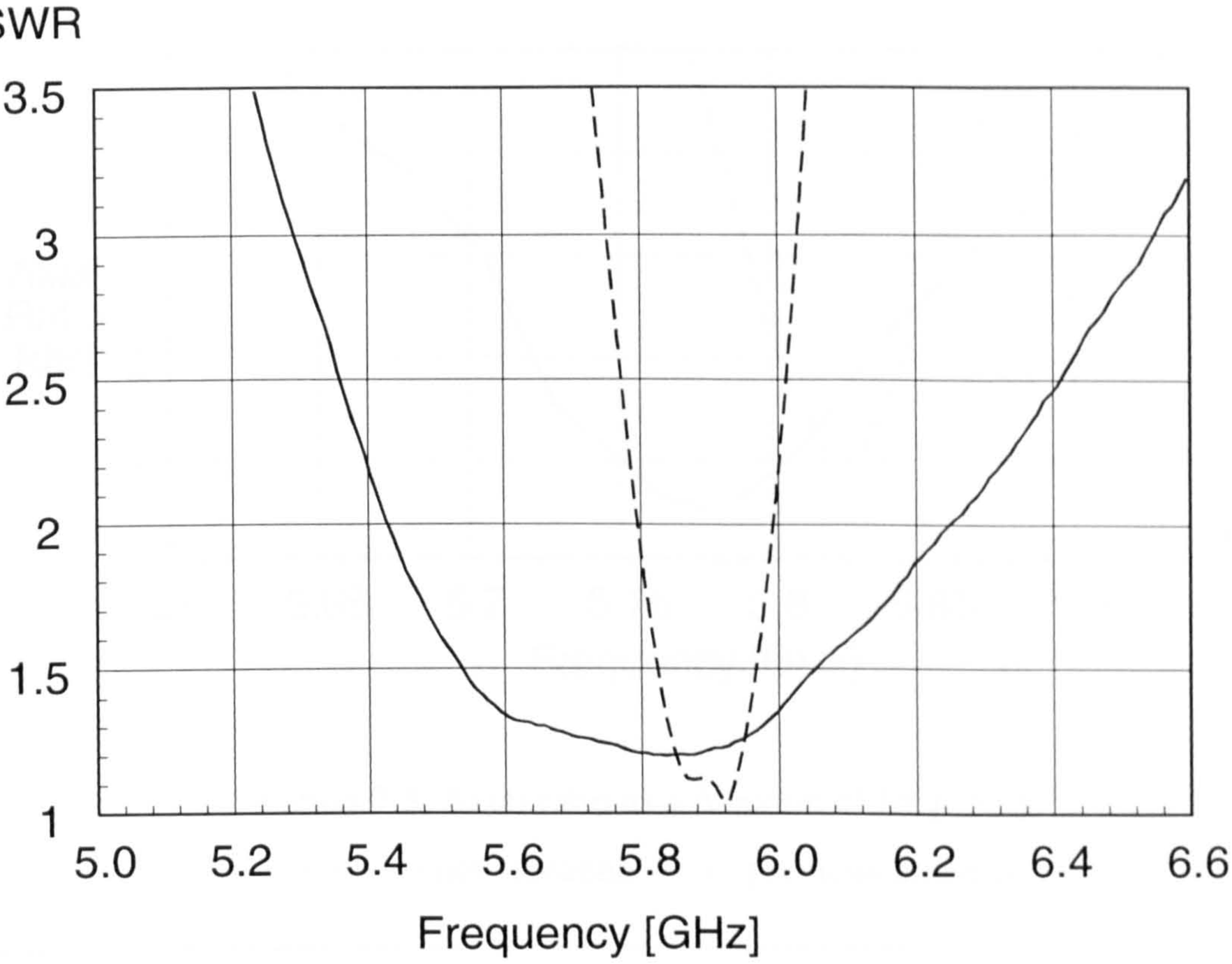

Figure 7.2. Measured standing wave ratio versus frequency.

——— new cross-aperture coupled antenna,

- - - - previous double feed antenna (Figure 2.12).

The axial ratio has also been measured in an anechoic chamber at a number of frequency points and is shown in Figure 7.3. Again, the axial ratio of the previously used antenna is shown in the same figure for comparison. The axial ratio of the new antenna is 2.7% as against 1.1% of the previous antenna design. It can be seen from the figure that the axial ratio performance of the double feed antenna is degraded at 5.8GHz, due to its small bandwidth, as in the case of standing wave ratio.

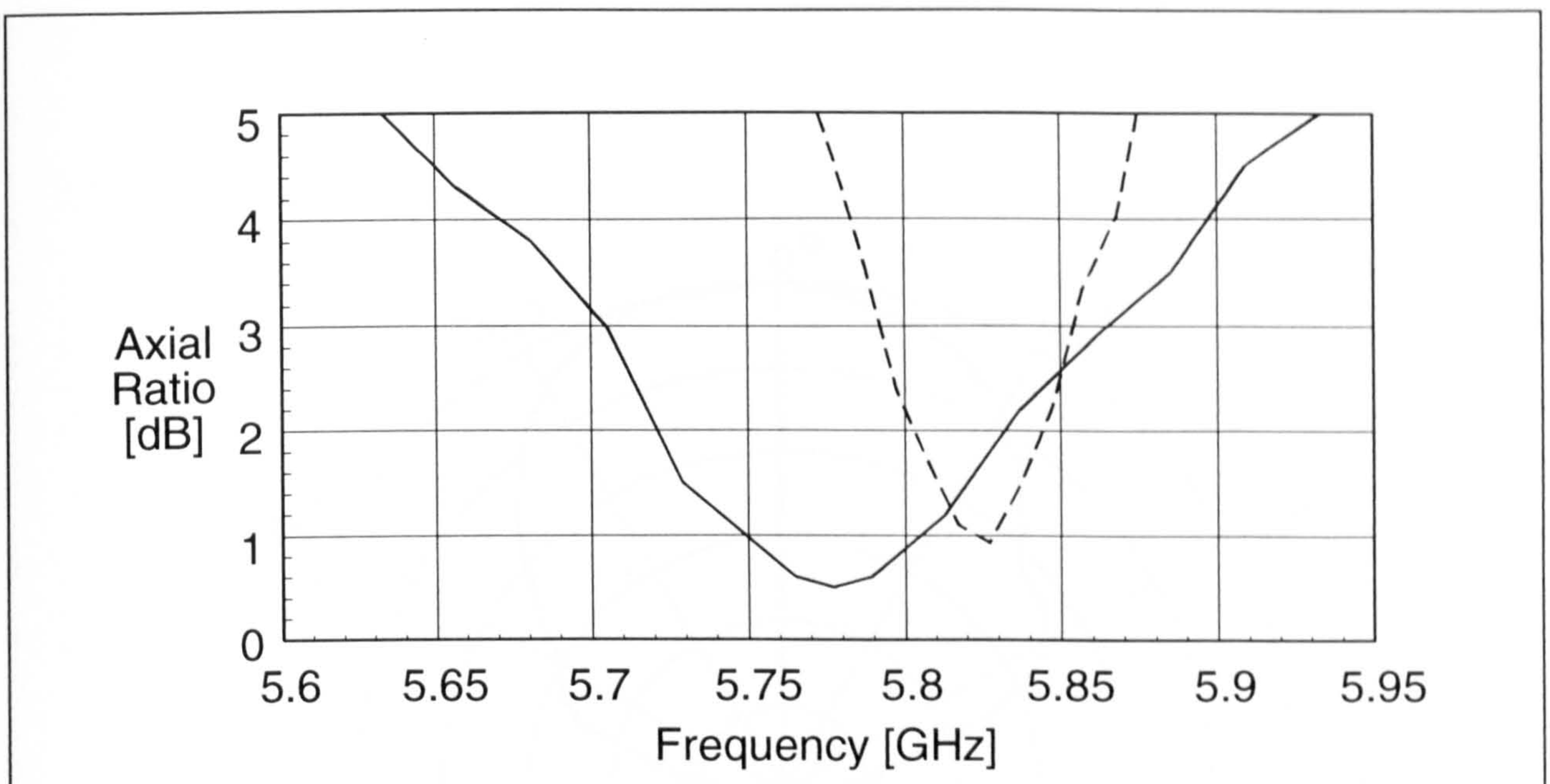

Figure 7.3. Axial ratio as a function of frequency.

——— new antenna - - - - previous antenna

The required fabrication tolerance for this antenna can be estimated using the analysis presented in chapter three, which showed that this value needs to be less than 15% of the difference between *a* and *b*, the dimension of the perturbation element. This implies a maximum fabrication tolerance of 0.26mm, which can easily be achieved with the etching process.

Finally, the radiation pattern of the prototype antenna is shown in Figure 7.4. As it can be seen the antenna has a polar pattern typical to microstrip antennas, as only the method of feeding has been changed. This result was expected and hence the radiation pattern was not theoretically modelled.

The performance characteristics, which were measured and presented in this section, confirm that the investigated novel structure of cross-aperture coupled circularly polarised antenna can be manufactured using inexpensive materials and that it can be beneficially used in practical applications.

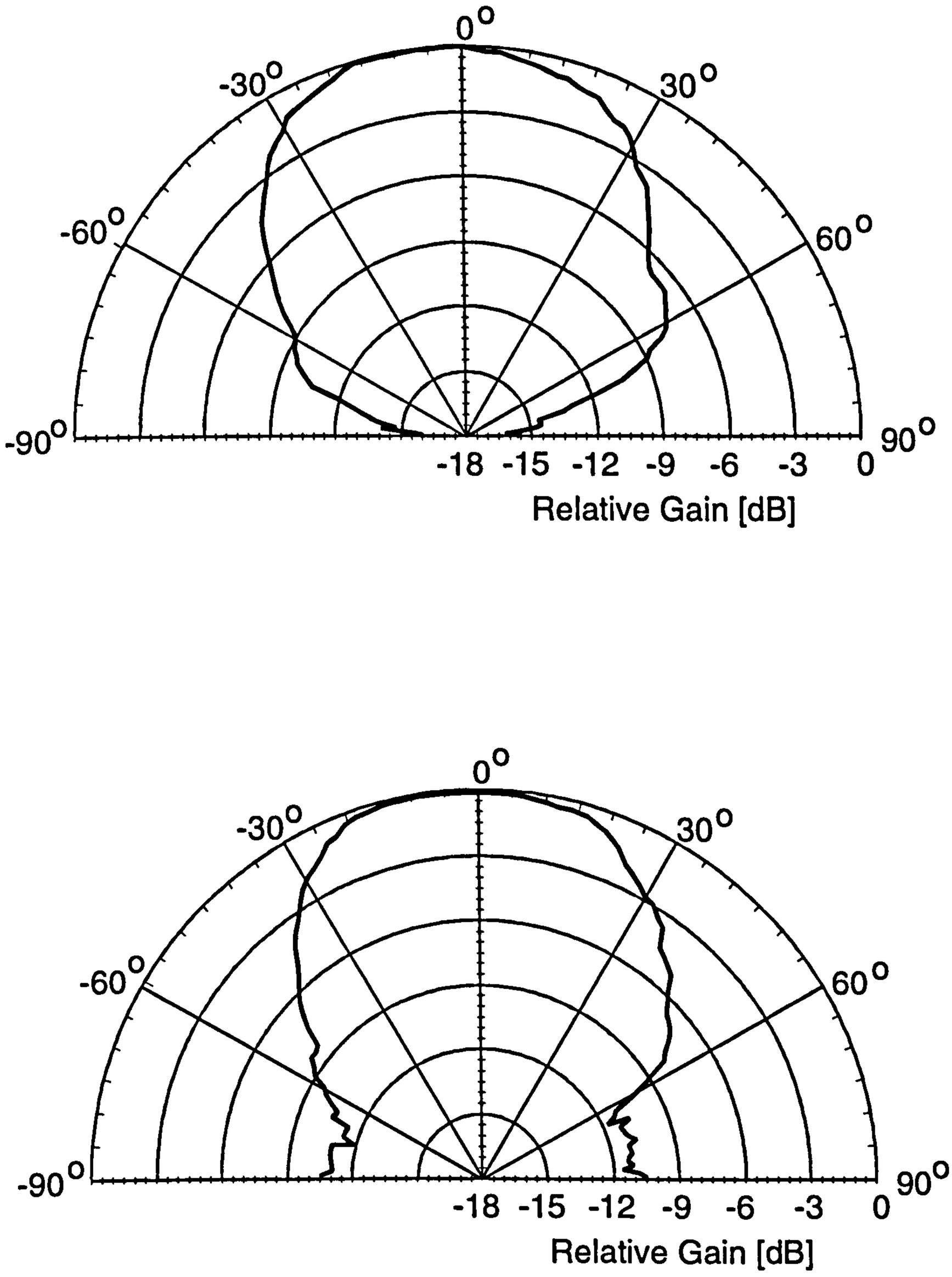

Figure 7.4. Radiation pattern of the cross-aperture coupled antenna.

7.3 THE NEW ON-BOARD UNIT

As the next step in the design of the on-board unit, the antenna has been integrated with the microwave diode. The characteristics of the HSMS8081 diode has been presented in Chapter two, showing that it can be used without any matching network as a PSK modulator when biased in either of two states, 0mA, or, 3.7mA. It can also operate as an ASK detector when the biasing current applied to is approximately 20μA. Therefore, by connecting the diode without any matching network to the antenna feed-line, a combined ASK detector / PSK modulator can be realised.

The realised on-board unit with the aperture coupled patch antenna and a single diode as ASK detector / PSK modulator is shown in Figure 7.5. The feed line between the cross-slot and the diode has been kept short in order to minimise the dielectric loss of the printed circuit board. The cathode of the diode is connected directly to the ground plane via a pin. The diode is connected to the video amplifier and DPSK modulator circuits through a high impedance quarter wavelength transmission line terminated in a radial stub.

The on-board unit shown in Figure 7.5 was fabricated in order to test the performance of the on-board unit using a cross-aperture coupled antenna. Further improvements are possible to make to this construction by using the plastic case of the OBU to support the patch which is fabricated in the form of a metal film or metal sheet. In this way the spacers holding the radome would not be required and the structure of the on-board unit could be further simplified. It is also possible to overlap the microwave circuit and the signal processing unit in order to reduce the size of the OBU, as components can be placed on the other side of the ground plane.

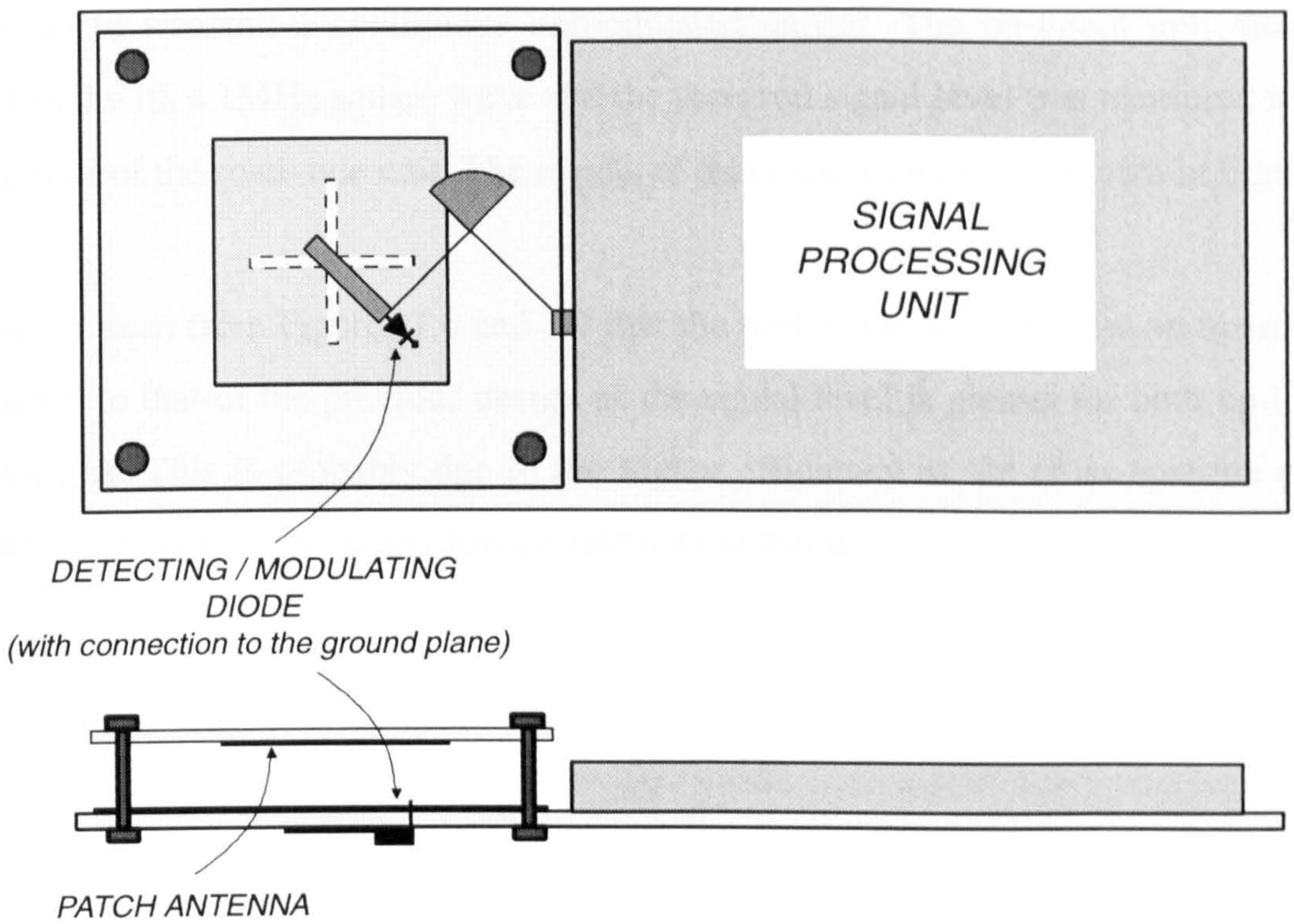

Figure 7.5. Structure of the new the on-board unit.

The performance of the fabricated new inexpensive on-board unit microwave circuit has been evaluated and compared to that of an on-board unit using the previous dual feed antenna design.

First, the down-link performance of the on-board unit has been tested. The road-side unit and the on-board unit was separated by a distance of 4.5m. The RSU was set in down-link mode to transmit continuously a 5.8GHz carrier modulated with a 125KHz square wave. The diode on the on-board unit was biased with a current of 20μA and the detected signal level was measured with an oscilloscope. The on-board unit was rotated around a vertical axis in a range of -90° to 90° with respect to facing the road-side unit and the signal level was read at 10° steps. The measurement was repeated with rotating the OBU around a horizontal axis. The detected signal levels for the new and the previous on-board units are shown in Figure 7.6.

A similar test has been carried out for up-link operation. In this case, the road-side unit was set to transmit a continuous unmodulated carrier. The on-board unit diode was switched with a 1MHz square wave and the received signal level was measured in the IF amplifier of the road-side unit. The results of this measurement are shown in Figure 7.7.

It can be seen from Figures 7.6 and 7.7 that the performance of the new on-board unit is superior to that of the previous design as the signal level is greater for both up-link and down-link. This is probably due to the higher efficiency of the cross-aperture coupled antenna because of its thicker low permittivity substrate.

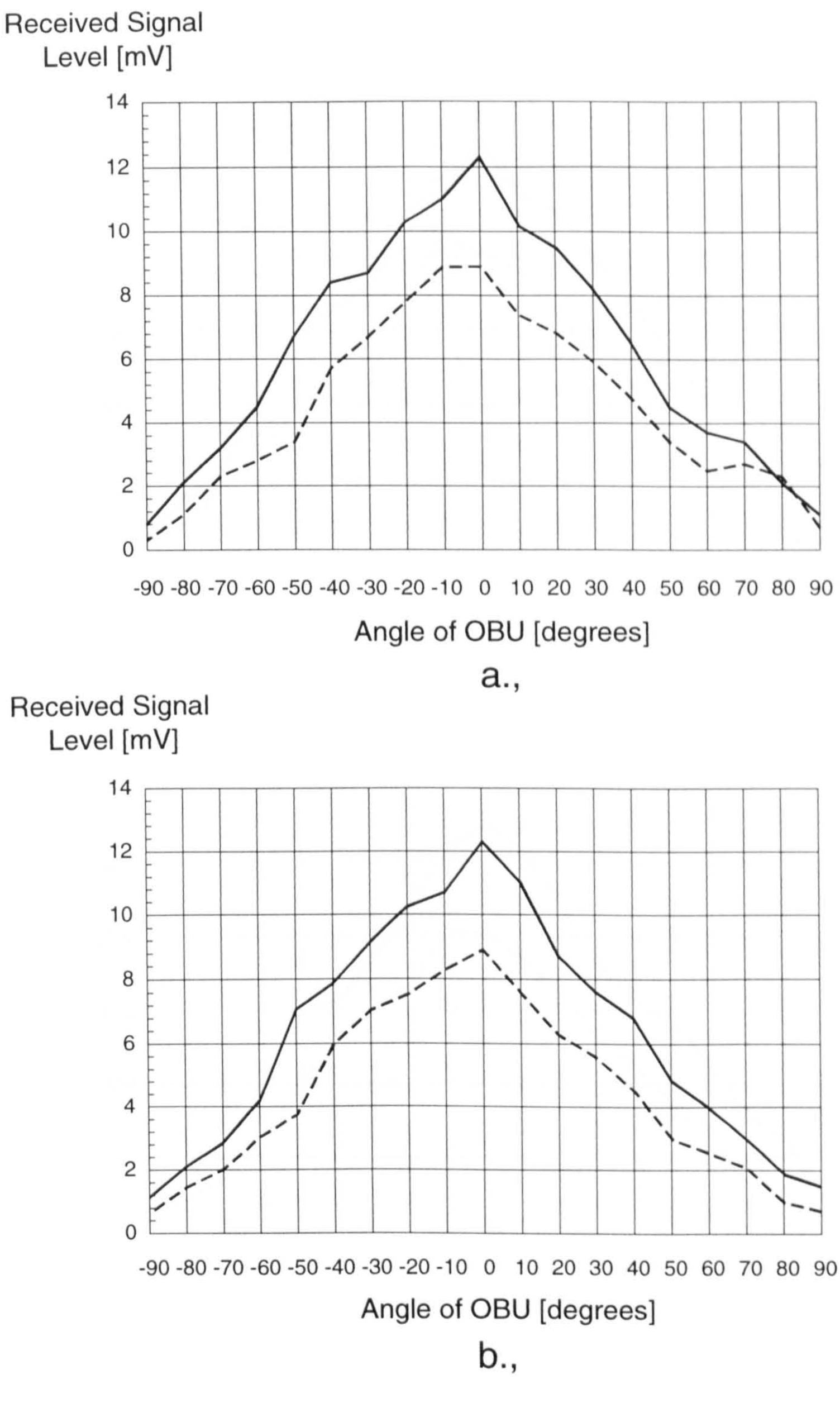

Figure 7.6. Received signal level in down-link mode with the on-board unit being rotated with respect to a vertical (a.) and a horizontal (b.) axis.

——— new OBU - - - - previous OBU

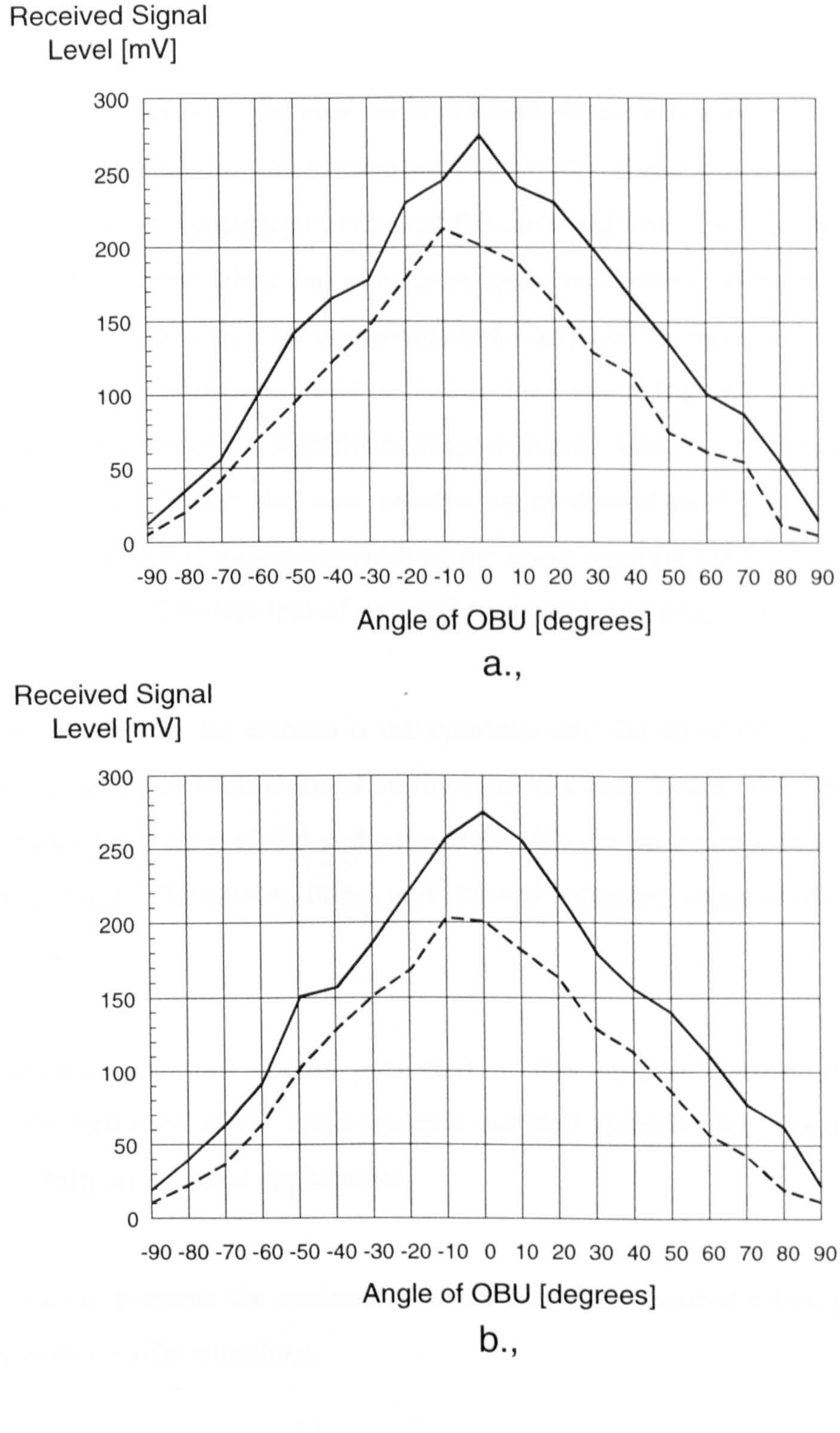

Figure 7.7. Received signal level in up-link mode with the on-board unit being rotated with respect to a vertical (a.) and a horizontal (b.) axis.

——— new OBU - - - - previous OBU

7.4 CHAPTER SUMMARY

This chapter presented how the new on-board unit antenna has been realised, which does not require any high cost microwave substrate material and which can be integrated with the rest of the low frequency circuitry of the on-board unit. The standing wave ratio and the axial ratio of the fabricated new cross-aperture coupled on-board unit antenna have been verified by practical measurements and compared to these of the previous on-board unit antenna implemented with a double feed patch fed and a T-junction. The results of these tests show a significant improvement, with the standing wave ratio bandwidth being 13.8% for the new antenna as compared to 3.5% of the previous antenna design. The axial ratio bandwidth of the cross-aperture coupled antenna is also significantly larger, 2.7% than that of the dual feed patch antenna, 1.1%.

Then it was shown how the antenna is incorporated into the on-board unit and how the microwave circuitry has been realised on the printed circuit board. The performance of the on-board unit has been tested and compared with the on-board unit using the dual feed antenna design. The new on-board unit showed increased signal levels for both up- and down-links.

The measurement and test results presented in this chapter confirm the improved bandwidth performance of the cross-aperture coupled antenna and also that it can be used successfully in practical applications.

The next chapter presents the evaluation of the 5.8GHz microwave link performed in laboratory and in traffic situations.

CHAPTER 8.

EVALUATION OF SYSTEM PERFORMANCE

8.1 INTRODUCTION

This chapter describes a number of test procedures carried out on the completed system in order to evaluate its performance. The aim of this work was to compare the practical performance of the system with that predicted by the link budget calculation (see Appendix A) and confirm that the communication system is suitable for automatic debiting and other traffic applications. These test have been carried out in co-operation with Sumitomo Electric Industries in Osaka, Japan. As at the time of the test, the new on-board unit antenna was not available, therefore these tests have been carried out using the on-board unit shown in Figure 2.12 with a double feed patch antenna. Due to the lack of test facilities simulating real traffic conditions the tests have not been repeated with the new antenna. However, as it was demonstrated in the previous chapter, the new on-board unit is superior in performance to the previous design, therefore the performance of the system with the new OBU could only be better than shown by the results presented here.

Three types of measurements have been performed, namely

- Measurement of sensitivity of road-side and on-board units in laboratory.
- Measurement of field-strength distribution above road surface with the RSU installed on a crane above the centre of the road and the on-board unit being mounted on a trolley and also behind the windscreen of a passenger car.
- Measurement of bit-error rate of data transfer for both down- and up-links when using the trolley and the car.

8.2 SENSITIVITY MEASUREMENTS

The aim of these tests was to correlate the level of the received microwave power by either the road-side or the on-board unit to the number of errors occurring in the data transfer. This allows the determination of sensitivity associated with a certain level of bit-error rate. A bit-error rate (BER) of less than 10^{-6} is required from the microwave link in order to ensure the efficient operation of the data-handling protocol [Enoksen 1993]. Therefore, the tests described in this section aimed at the measurement of the level of microwave power necessary for the on-board unit, or, road-side unit, to realise a data flow with a BER of around 10^{-6}.

8.2.1 DOWN-LINK

The measurement setup to test the bit-error rate of the down-link is shown in Figure 8.1.

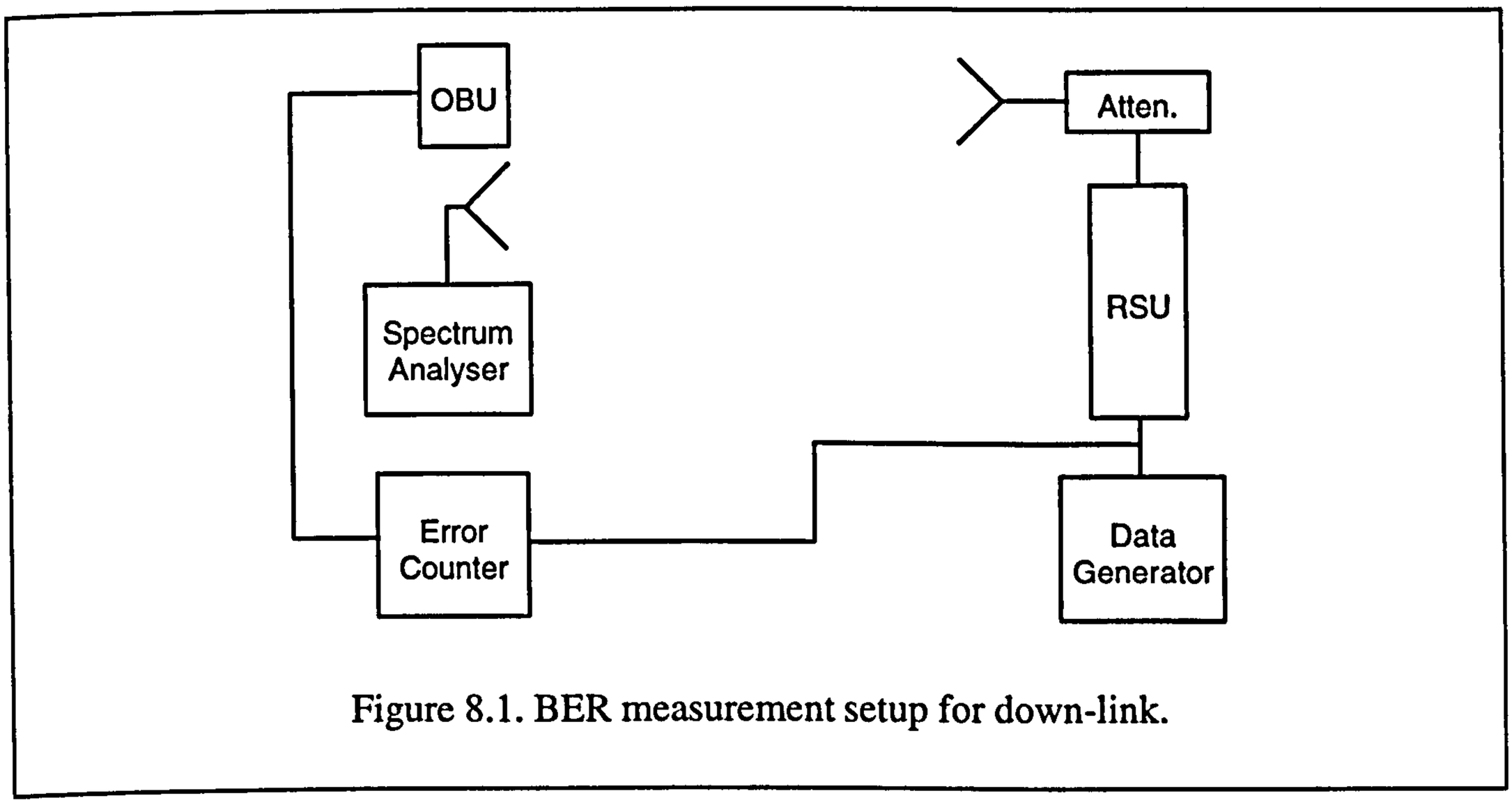

Figure 8.1. BER measurement setup for down-link.

The RSU was used to transmit the modulated signal which was fed into the antenna via attenuators. The OBU together with a reference antenna (gain: 4.5dB) was placed at 6m from the RSU. The OBU was surrounded with absorbing material in order to reduce the field-strength variations due to multipath reflections. The power output from the reference antenna was measured with a spectrum analyser from which the values of field-strength were calculated. The result of this measurement is shown in Figure 8.2.

The link budget calculation (see Appendix B) gives -43.7dBm required signal level received for a BER of 10^{-6}. Considering that the OBU antenna has a gain of 4.5dB, this means that the required field-strength must be -48.2dBm at the OBU. As it can be seen, the measured value for a BER of 10^{-6} (-49dBm) is in good agreement with the calculated value. However, the practical performance of the system is expected to be worse than the theoretically calculated performance, because of the imperfections in the realisation of the signal processing unit in the OBU. The better quality of the measured sensitivity, as against the theoretical sensitivity of the OBU could be explained by measurement errors and the fact that the tangential sensitivity value of the diode is for a large bandwidth (1MHz) while the actual baseband is approximately 250kHz.

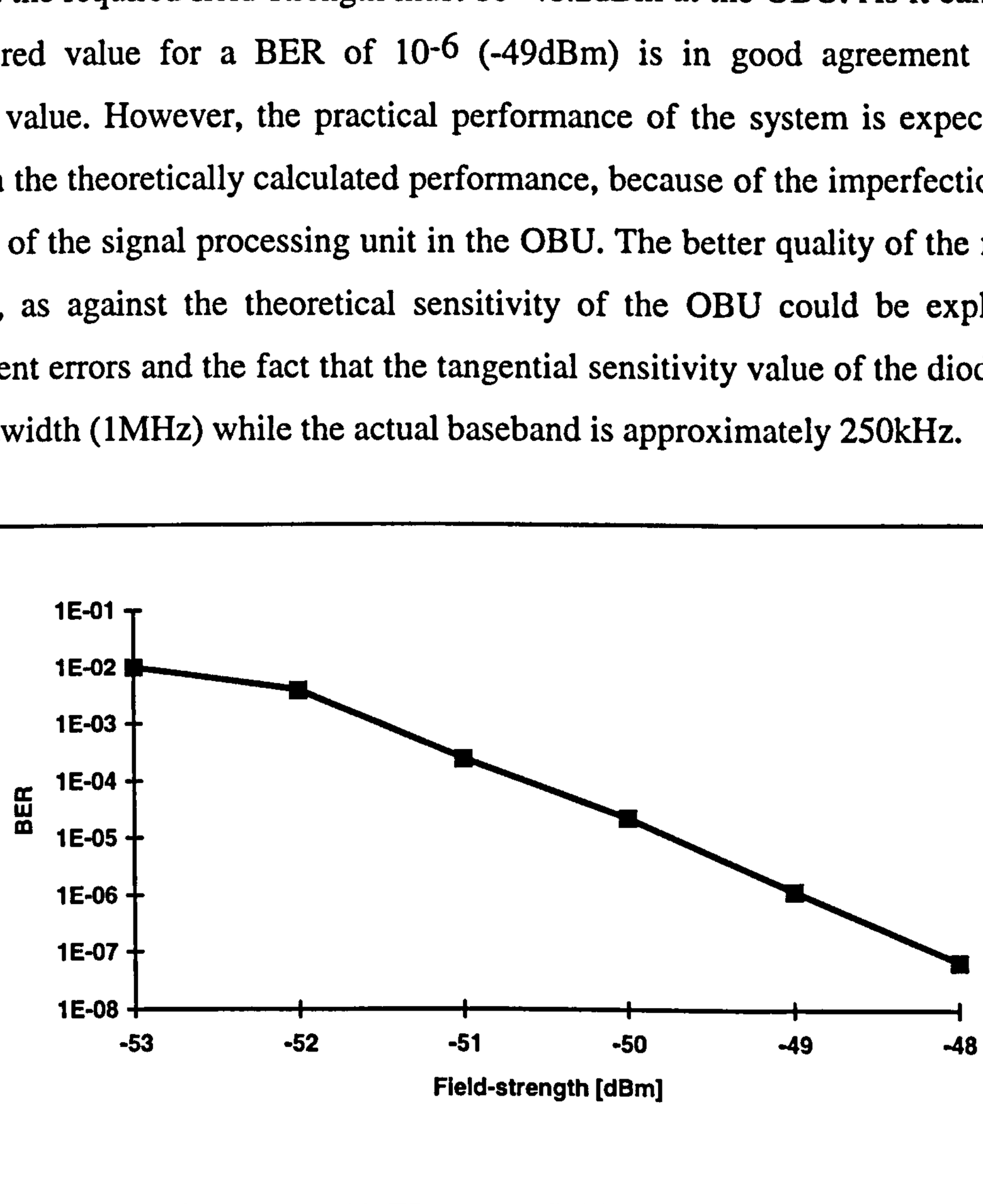

Figure 8.2. Measured BER versus field-strength for the OBU.

8.2.2 UP-LINK

The up-link BER test was performed as shown in Figure 8.3.

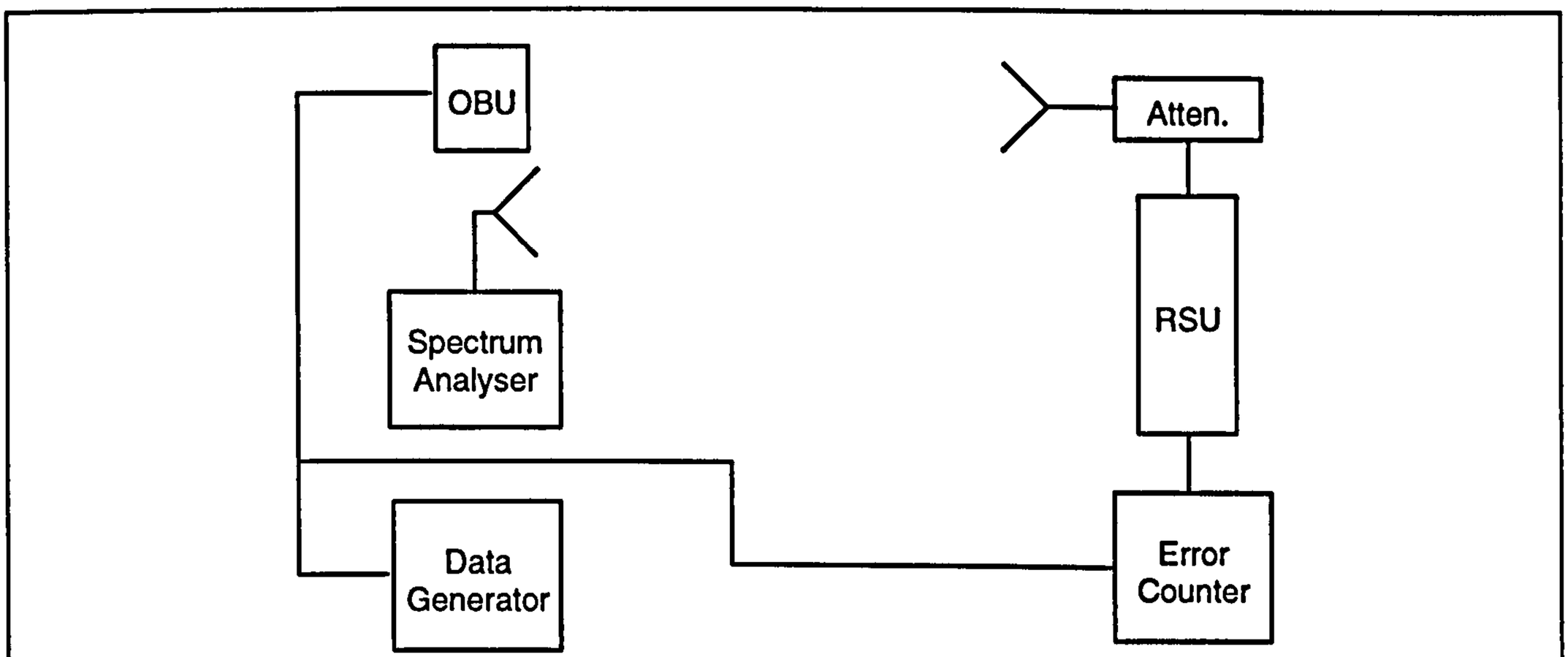

Figure 8.3. BER measurement setup for up-link.

As can be seen in Figure 8.3, the measurement of the field strength at the OBU was chosen as opposed to that at the RSU. The reason for this is that the reflected signal from the OBU would be too weak to measure it at the RSU. The level of the up-link signal at the RSU can be calculated from the received signal level at the OBU as follows [Kraus 1991]:

$$P_{UL} = P_T - 2(P_T - P_{OBU}) + 2G_{OBU} - L_{OBU} \qquad \text{[dB]}$$

where, P_{UL} is the received up-link signal at the RSU,

P_T is the transmitted EIRP from the RSU,

P_{OBU} is the measured field strength at the OBU,

G_{OBU} is the gain of the OBU antenna and

L_{OBU} is the modulation loss in the OBU.

The measured BER for the up-link versus the field-strength calculated as above is shown in Figure 8.4. The link budget calculation predicted -106.3dBm required signal level received at the RSU for a BER of 10^{-6}. Taking into account the gain of the RSU antenna, which is 16dB, the required theoretical field-strength at the RSU is -122.3dBm. The measured sensitivity of the RSU (-118dBm) is approximately 4dB worse than it was expected. This difference is probably due to measurement errors and imperfections in the realisation of the road-side unit demodulating, amplifying and detecting circuits.

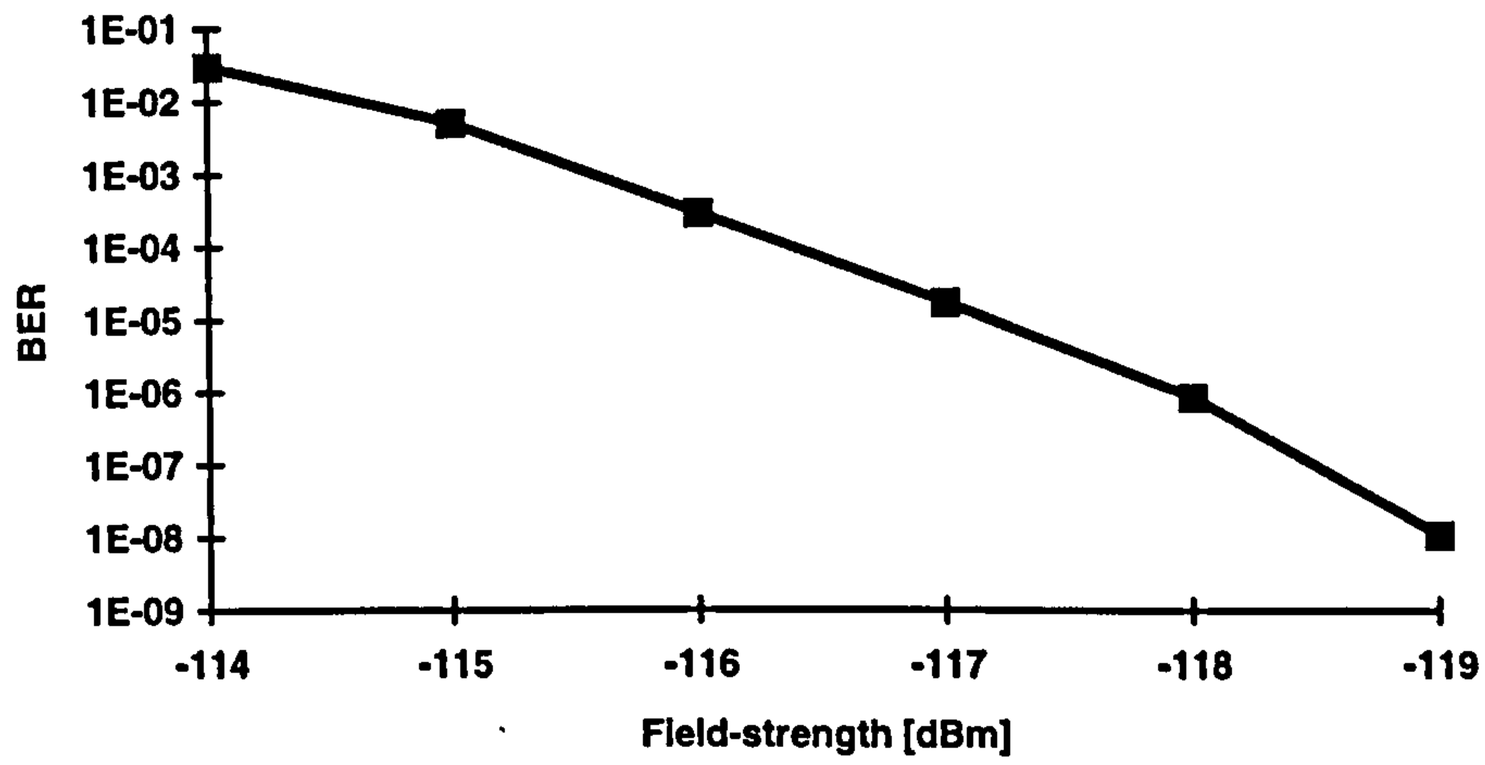

Figure 8.4. Measured BER versus field-strength for up-link.

8.3 FIELD STRENGTH MEASUREMENTS

The aim of this measurement was to obtain data on how the field-strength is varying due to reflections from the road-surface and from the vehicle bonnet, and, also to see the effect of the windscreen on the signal level.

The road-side unit was mounted on a crane at a height of 4m above the centre of the road and pointing down-wards at an angle of 30° with respect to the horizontal. During the first set of measurements the on-board unit antenna was placed on a trolley at a height of 1.2m, facing upwards at an angle of 45° with respect to the horizontal. A spectrum analyser controlled by a computer was connected to the antenna through a 50Ω coaxial cable. The computer read the level of signal strength from the spectrum analyser every 200ms while the trolley was being moved at a uniform speed. The computer was given position reference signals during the measurement through a push button at every 0.6m with the help of markings on the road surface. The trolley was then pushed along three adjacent lines, first located in the centre of the road and aligned with respect to the 'road-side unit', then with 1m offset from the centre of the road and finally with a 2m offset.

The received signal level at the on-board unit versus the horizontal distance from the road-side unit is shown in Figure 8.5. The three graphs show the variation of the power level along each of the paths used in the measurements.

The peak signal level occurs at a distance of 5m from the road-side unit corresponding to the centre of the main beam of the RSU antenna. Then on approaching the road-side unit, a drop in signal-level can be observed at 3m which corresponds to the direction between the main beam and the first side lobe of the antenna. Subsequently smaller local peaks occur corresponding to the side lobes of increasing orders.

The measurements were performed in a similar manner when the OBU was installed in the vehicle. The position of the OBU in the vehicle was such that its height above the road surface and angle with respect to the horizontal were retained when it was mounted on the trolley. The separation of the on-board unit from the windscreen was 50mm.

The received signal level at the on-board unit when it was mounted in a passenger car behind the wind-screen is shown in Figure 8.6. Comparing Figure 8.6 with 8.5 it can be seen that placing the on-board unit in the vehicle has resulted in the peak of the received signal to reduce by approximately 10dB. This is mainly due to the attenuation caused by the windscreen, which can vary between 2-8dB [Lowes 1995] depending upon the distance of the antenna from the windscreen.

It can also be seen that the variation of signal strength near the peak is greater when the on-board unit is installed in the vehicle. This is due to the combined effect of reflections from the car bonnet and the reduced axial ratio of the antenna caused by the windscreen [Lowes 1995]. The reduced axial ratio of the antenna means that it will be less able to distinguish between right and left hand polarised waves, and therefore part of the reflected wave from the car bonnet will be received, which will interfere with the direct signal.

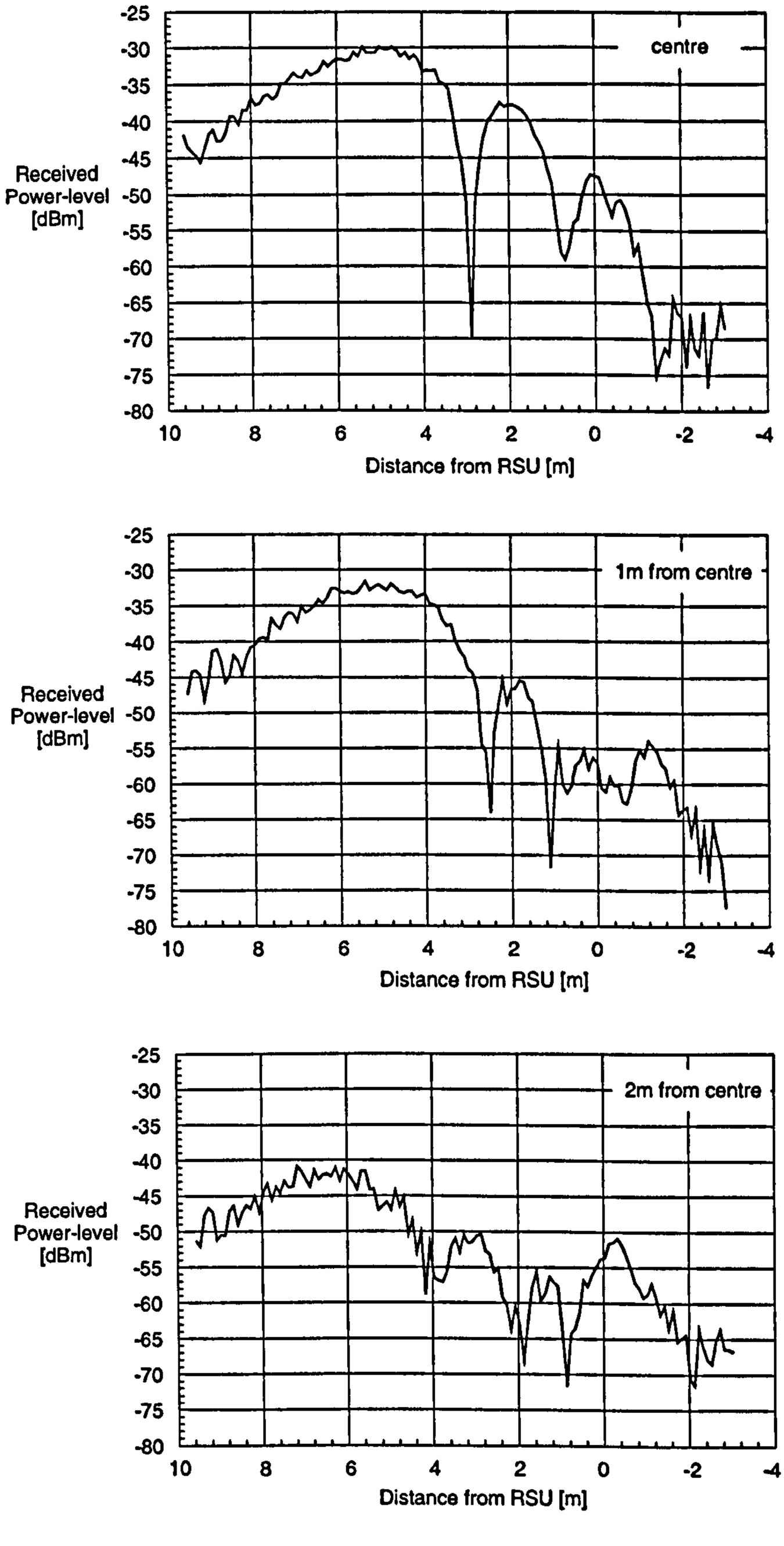

Figure 8.5. Received power-level versus distance from the road-side unit with the on-board unit on a trolley.

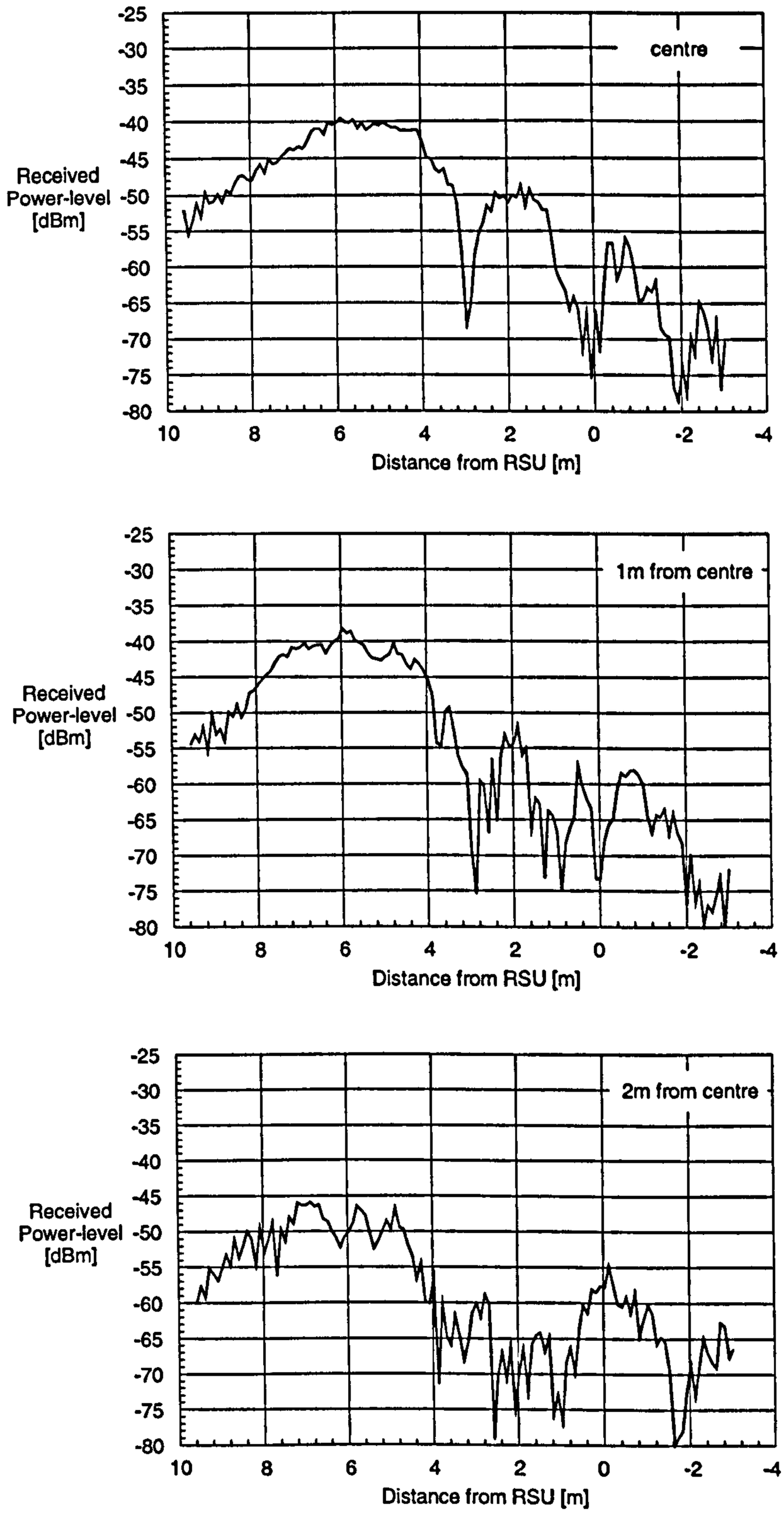

Figure 8.6. Received power-level versus distance from the road-side unit with the on-board unit installed behind the windscreen of a vehicle.

8.4 BIT-ERROR RATE MEASUREMENT

There were two sets of bit-error rate measurements performed, namely, with the OBU installed on a trolley, and, then with the OBU mounted behind the windscreen of a vehicle. The purpose of this measurement was to verify the data transfer performance of the microwave system and also to investigate how the vehicle and the windscreen affects the communication.

Figure 8.7 shows the density distribution of the bit-error rate of the communication in a horizontal plane for the down and the up-links with the on-board unit mounted on a trolley. The bit-error rate was measured on one half of the road it being assumed that the communication zone will be symmetrical with respect to the centre of the road.

In Figure 8.7, the white areas correspond to a bit-error rate of 10^{-6} or less representing the acceptable quality of data transfer. The effect of low signal level at a distance of 3m from the road-side unit (see Figure 8.5) can be seen on the bit-error rate causing a drop-out in the communication. This problem is due to the low radiated power in this particular direction as this falls between the main lobe and the first side lobe of the road-side unit antenna. This problem could be probably be corrected by modifying the road-side unit antenna array design.

The results of the bit-error rate measurements with the on-board unit positioned behind the windscreen of a vehicle are shown in Figure 8.8.

Comparing Figures 8.7 and 8.8 it can be seen that the area of acceptable communication is slightly reduced when the on-board unit is in a vehicle, as could be expected from the signal level measurements. Considering an on-board unit travelling in a vehicle along a line within 1m from the centre of the road (or traffic lane), the system will be able to communicate with a bit-error rate of less than 10^{-6} for a length of approximately 7m, which satisfies the original specification.

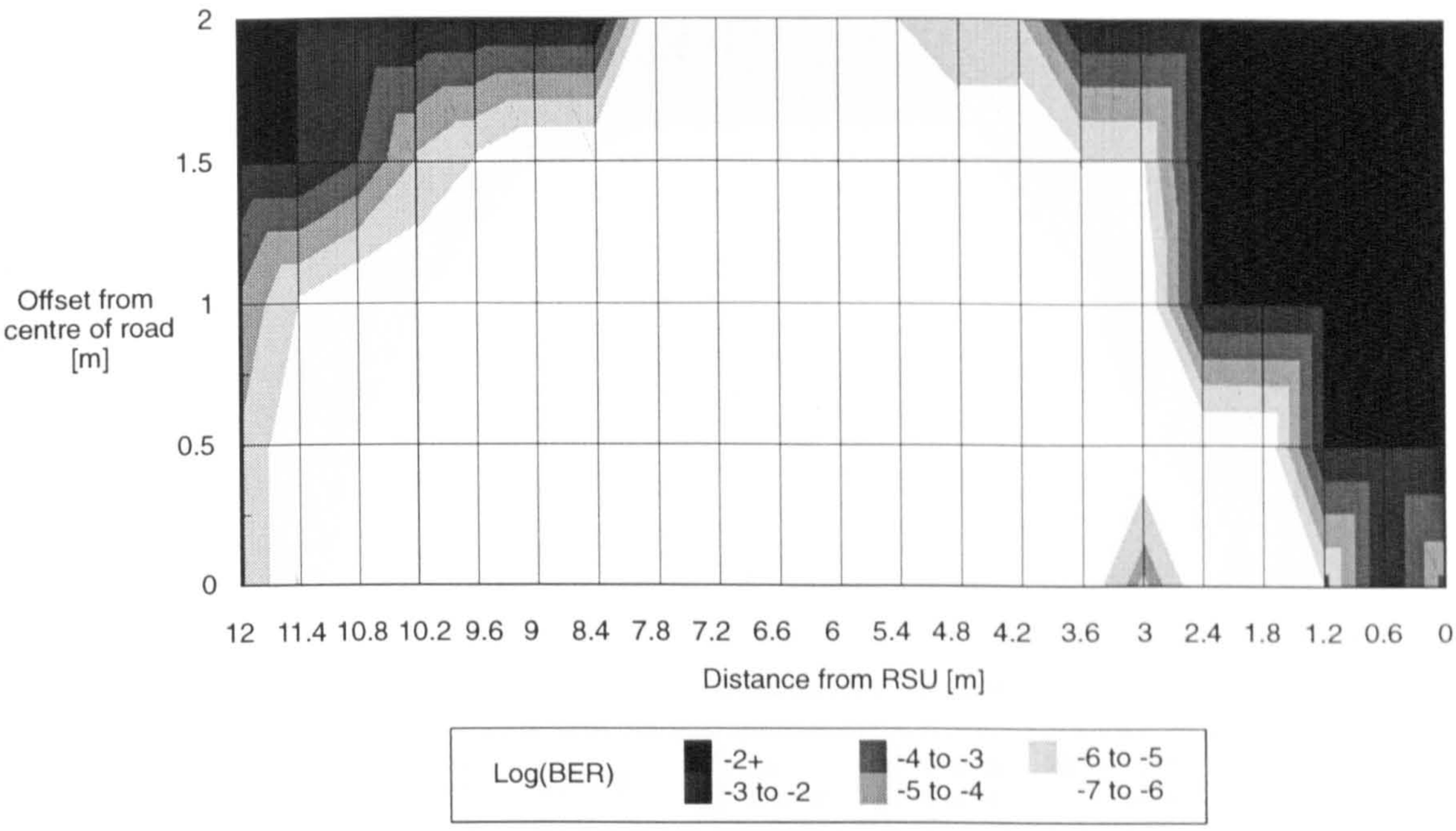

a., DOWN-LINK

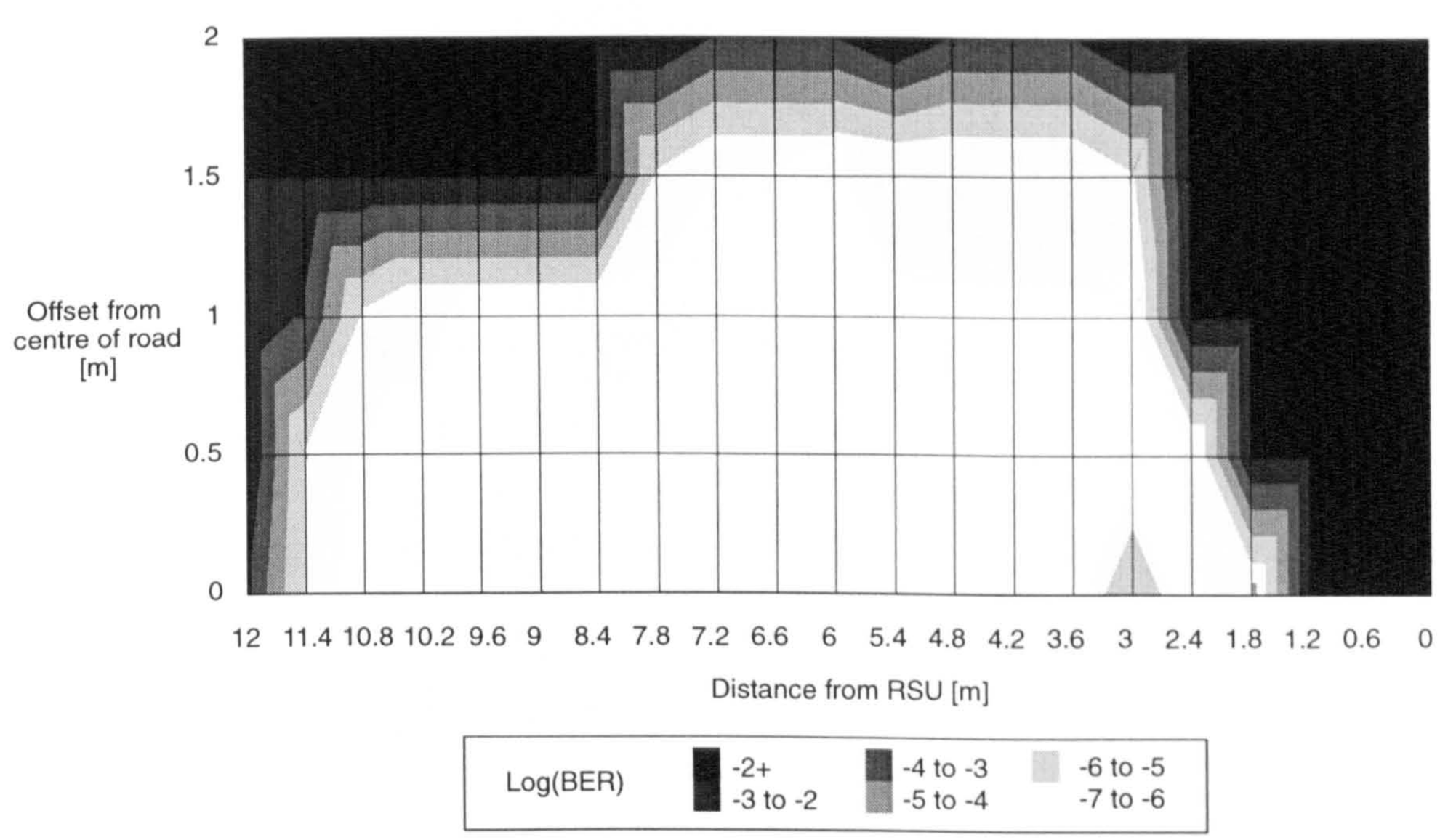

b., UP-LINK

Figure 8.7. Bit-error rate of communication with the on-board unit on a trolley.

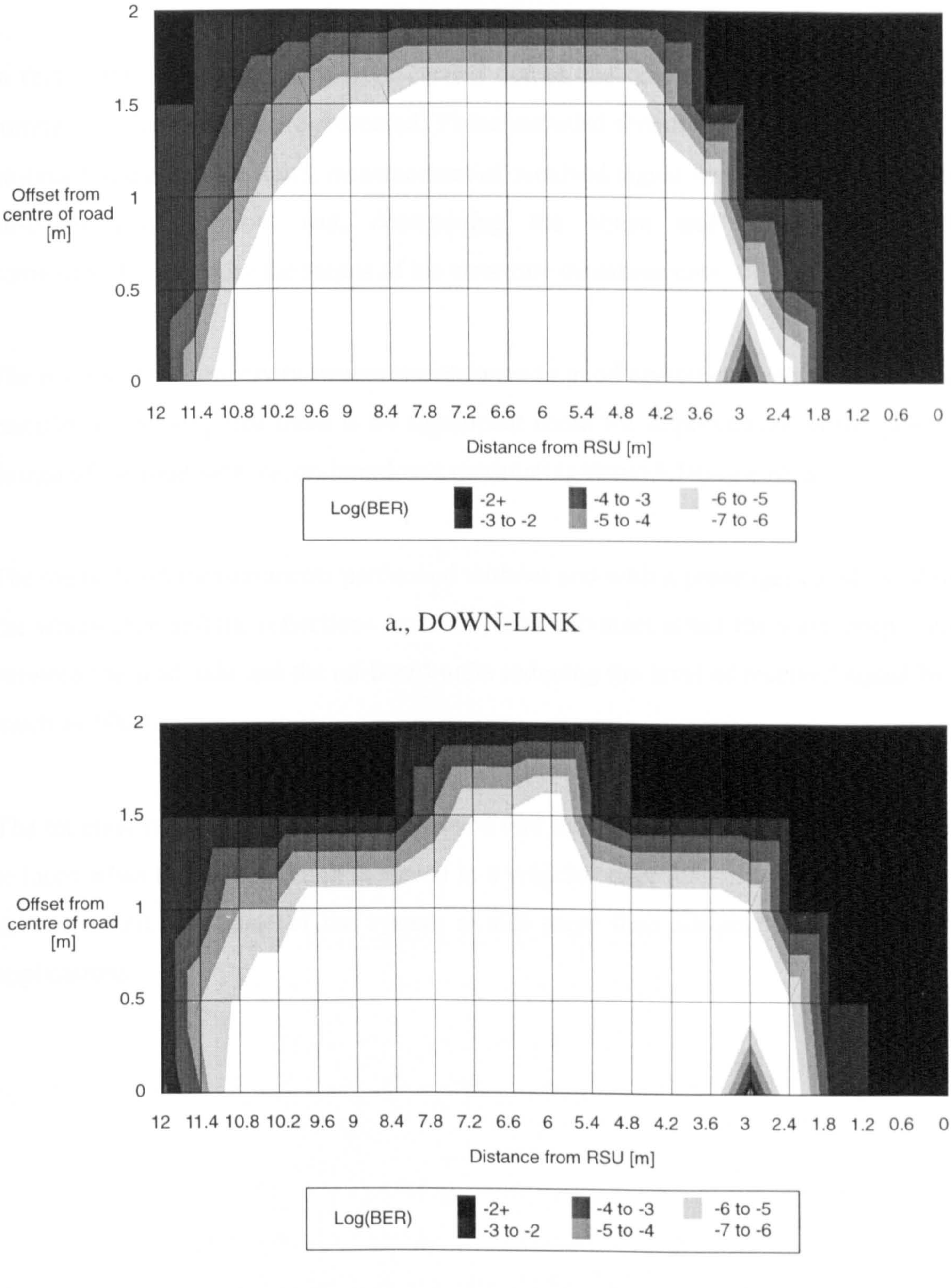

a., DOWN-LINK

b., UP-LINK

Figure 8.8. Bit-error rate of communication with the on-board unit in a passenger car.

8.5 CHAPTER SUMMARY

In this chapter the tests which were carried out on the completed 5.8GHz microwave communication system were presented. These included sensitivity measurement of both on-board and road-side units, measurement of received signal level as a function of the on-board unit position, and, determining the shape and dimensions of the communication zone by the means of bit-error rate measurements.

The results of the sensitivity measurements were in good agreement with the link budget calculation showing that there is no significant room for improvement in the practical design of the road-side, or, on-board unit modulating/demodulating circuits.

The signal level measurements performed without and with a passenger car showed that the windscreen and the reflections from the vehicle bonnet affect the wave propagation between the road-side and the on-board units reducing the level of received signal by as much as 10dB.

The bit-error rate measurements also showed that the area of the communication zone is reduced when the on-board unit is placed in a vehicle rather than in free space, however, the communication zone of the system is still more than adequate for use in traffic applications.

CHAPTER 9.

CONCLUSIONS AND FURTHER WORK

9.1 SUMMARY AND CONCLUSIONS

This thesis has described the results of the research that has been carried out in order to model theoretically a cross-aperture coupled circularly polarised antenna to be used in the on-board unit of a microwave communication link of an automatic debiting system.

Initially the specification and the design of the short-range 5.8GHz microwave system developed within the European ADEPT project (Automatic Debiting and Electronic Payment for Transport) frame-work for automatic debiting application in the Centre for Communication Systems Research at the University of Northumbria has been discussed. One of the key parameters of such a communication system is the type of polarisation used for the carrier waves. It has been determined through calculations and measurements that left-hand circular polarisation is to be used for both up- and down-links as this reduces the interfering signal levels between adjacent road-side units. Then a prototype 5.8GHz microwave system has been developed consisting of a road-side unit (RSU) and an on-board unit (OBU). The layouts of these units have been presented and it was shown how a single diode can be used for both down-link ASK detection and up-link PSK modulation in the OBU to make it small in size and inexpensive.

The on-board unit of the initial prototype system has used a double feed square patch antenna fed by a 3dB hybrid which was implemented on a microwave substrate board. The shortcomings associated with using a double feed patch antenna on a special microwave substrate, are the large surface area occupied, and the high material and manufacturing costs. Thus it was decided to develop a new OBU antenna, which would not have these defects.

A number of dual and single feed circularly polarised microstrip patch antennas have been presented and it has been shown that single feed CP patches can be built using less board space. However they are able to produce good circular polarisation only in a narrow frequency band. It was then shown by analysis and simulation that this drawback can be reduced to an acceptable level by the application of a thick air substrate. For this reason the new on-board unit antenna was chosen to be the cross-aperture coupled single feed patch antenna with air substrate.

Due to the lack of analytic methods for analysing the antenna design of the above structure to be used in the OBU, two theoretical models have been developed for the cross-aperture coupled antenna in this thesis, namely the transmission line and the resonant cavity models, which combine accurate results with numerical efficiency.

In order to apply the transmission line method, the transition between a cross-shaped aperture and a microstrip line has been investigated and it was found that the cross-aperture can be regarded as the series connection of two orthogonal slots, which excite the patch in the x and y directions independently. This allowed the representation of the patch, in the direction of its two orthogonal modes, by transmission line networks. Expressions for the input impedance and the axial ratio of the cross-aperture coupled circular polarised antenna, based on the transmission line theory, have been derived.

Then the analysis of the cross-aperture coupled circularly polarised microstrip antenna was presented in terms of the cavity resonator model. The magnetic and electric fields were determined in the cavity, and this allowed the derivation of expressions for the input impedance and axial ratio as functions of the frequency.

The results from the transmission line and resonant cavity methods have been compared to measurement and simulation results showing good agreement and supporting the validity of the theoretical models. The effects of a number of design parameters of the cross-aperture coupled patch antenna have been investigated using the transmission line and cavity models. It was shown that the input impedance of the antenna can be varied by changing the length of the aperture, thus allowing the matching of the antenna to the feed line without the need for an external network.

It was also concluded that increasing the antenna substrate thickness improves both the impedance and the axial ratio bandwidths. However, this is limited by the standing wave ratio which can rise above an unacceptable level when using a thick substrate.

A new on-board unit antenna has been then realised, which does not require any high cost microwave substrate material and which can be integrated with the rest of the low frequency circuitry of the on-board unit. The standing wave ratio, the axial ratio and the radiation parameters of the realised antenna have been verified by practical measurements. The results of these tests show improved performance as compared to the previous antenna design making the cross-aperture coupled antenna eminently suitable for use in the on-board unit. Then it was shown how the antenna is incorporated into the on-board unit and how the microwave circuitry has been realised on the printed circuit board.

Finally, the tests carried out on the completed 5.8GHz microwave communication system were presented. The results of the sensitivity measurements were in excellent agreement with the link budget calculation, showing that there is no significant room for improvement in the realisation of the road-side, or, on-board unit modulating / demodulating circuits.

The signal level measurements performed without and with a passenger car showed that the windscreen and the reflections affect the wave propagation between the road-side and the on-board units. However, the bit-error rate measurement proved that the communication zone of the system is more than adequate for use in traffic applications.

9.2 SUGGESTIONS FOR FURTHER WORK

A number of areas have been identified for further research and investigation and are discussed below.

The developed transmission line and resonant cavity models could be adapted to model similar structures to that analysed in this thesis, for example the circularly polarised cross-aperture coupled square patch antenna with unequal branches of the cross-slot [Iwasaki and Kawabata 1991]. In this configuration the phase difference of the two orthogonal modes is generated by the difference in the coupling slot length. The modelling of this structure would require the use of two different values of turns ratios between the microstrip feed line and the apertures, as this parameter depends on the length of the aperture as discussed in Chapter four. Also the two orthogonal short circuited slot-lines would have different lengths requiring the introduction of two different values for the aperture susceptances. This square patch antenna could be modelled in a simpler way, since only one set of line parameters, radiation and mutual admittances would be needed. The cavity model described in Chapter five could also be adapted in a similar manner.

The transmission line model could also be extended in order to model cross-aperture coupled circularly polarised antennas with non-linear apertures, such as the H shaped slot. This could be performed by taking into account the longitudinal slots using their self-susceptance, which loads the transversal slot line [Yazidi et al. 1992].

It could be of interest to extend the present analysis to predict the radiation pattern of the cross-aperture coupled patch antenna. This could be performed by calculating the electric field due to the equivalent magnetic currents at the edges of the patch [Lo et al. 1979].

It would be useful to design an on-board unit antenna with the plastic case of the on-board unit being the superstrate supporting the antenna. For this purpose the relative permittivity of the plastic material should be measured using the resonant cavity method described in [Lowes 1995].

A practical investigation could also be carried out in order to determine the performance of an array of the cross-aperture coupled circularly polarised antennas and to compare the performance with that of arrays of other cross-aperture feed structures [Sawamura et al. 1995, and, Rostan and Wiesbeck 1995].

REFERENCES

[Adrian and Schaubert 1987]

Adrian, A. and Schaubert, D.H., Dual Aperture-Coupled Microstrip Antenna for Dual or Circular Polarization. Electronics Letters, 1987, 23(23), p. 126-128.

[Aksun et al. 1989]

Aksun, M.I. et al., Double-slot-fed microstrip antennas for circular polarization operation. Microwave Opt. Technol. Letters, 1989, 2, p. 343-346.

[Aksun et al. 1990]

Aksun, M.I., Chuang, S.L., and Lo., Y.T., On Slot-Coupled Microstrip and their Applications to CP Operation - Theory and Experiment. IEEE Transactions on Antennas and Propagation, 1990, 38(8), p. 1224-1230.

[Antar et al. 1992]

Antar, Y.M.M., Bhattcharyya, A.K. and Ittiboon, A., Microstripline-Slotline Transition Analysis Using the Spectral Domain Technique. IEEE Transactions on Microwave Theory and Techniques, 1992, 40(3), p. 515-523.

[Bahl and Gupta 1979]

Bahl, I. and Gupta, K., Average Power-Handling Capability of Microstrip Lines. IEE Microwaves, Optics and Antennas, 1979, 3, p. 1-4.

[Balanis 1982]

Balanis, C.A. Antenna Theory: Analysis and Design. John Wiley & Sons, 1982.

[Balanis 1989]

Balanis, C., Advanced Engineering Electromagnetics. John Wiley & Sons, 1982.

[Bhattacharyya et al. 1992]

Bhattacharyya, A.K., Antar, Y.M.M. and Ittipiboon, A., Full wave analysis for the equivalent circuit of an inclined slot on a microstrip ground plane. IEE Proceedings H, 1992, 139(3), p. 245-250.

[Blythe 1989]

Blythe, P., PAMELA Deliverable - ME2 The state of art of current ADS technology and applications. University of Newcastle upon Tyne, 1989.

[Blythe 1992]

Blythe, P.T. et. al., Review of Technologies for Road-Use Pricing in London. Contract Summary, Department of Transport Research, December 1992, Report Ref. No. 02/C/5842/TTH/01.

[Blythe 1996]

Blythe, P.T. et. al., The Development of a Multi-Lane Debiting and Enforcement System for Road Tolling Applications. In: Conference Publication of the 8th International Conference on Road Traffic Monitoring & Control, London, 23-24 April 1996, Conf. Publ. No. 422, p. 158-163.

[Boulder 1995]

Boulder microwave Technologies, Ensemble. Product Information brouchure, 1995.

[Carver 1979]

Carver, K.R., Practical Analytical Techniques for the Microstrip Antenna. In: proceedings of the Workshop on Printed Circuit Antenna Technology, New Mexico State Uni., Las Cruces, 17-19 October 1979, 7, p. 1-20.

[Carver 1981]

Carver, K.R. and Mink, J.W., Microstrip Antenna Technology. IEEE Transactions on Antennas and Propagation, 1989, 29(1), p. 2-24.

[Chan 1994]

Chan, T.K., Development of a Two-Way Microwave Communications System for Traffic Applications. PhD Thesis, Department of Electrical and Electronic Engineering and Physics, University of Northumbria at Newcastle, 1994.

[Clogh 1995]

Clough, B., Beware, the Silicon Brotherhood is watching You. Traffic Technology International, Winter 1995, p. 34-38.

[Cohn 1969]

Cohn, S.B., Slot Line on a Dielectric Substrate. IEEE Transactions on Microwave Theory and Techniques, 1969, 17(10), p. 768-778.

[Daniel et al. 1993]

Daniel, J.P., Dubost, G., and Terret, C., Research on Planar Antennas and Arrays: "Structures Reyonnantes". IEEE Antennas and Propagation Magazine, 1993, 35(1), 14-38.

[Das 1993]

Das, N.K., Generalized Multiport Reciprocity Analysis of Surface-to-Surface Transitions Between Multiple Printed Transmission Lines. IEEE Transactions on Microwave Theory and Techniques, 1993, 41(6/7), p. 1164-1177.

[Derneryd 1978]

Derneryd, A.G., A Theoretical Investigation of the Rectangular Microstrip Antenna Element. IEEE Transactions on Antennas and Propagation, 1978, 26(4), p. 532-535.

[Duffy and Pozar 1995]

Duffy, S.M. and Pozar D.M., Circularly Polarised Aperture Coupled Microstrip Antenna. Electronics Letters, 1995, 31(16), p. 1303-1305.

[Enoksen 1993]

Enoksen, R., ADEPT Microwave Link Specification OSI Layer 1 Technical Explanations. DRIVE Report. Document No. MD-001. ADEPT and Standardization Body: CEN/TC278/WG9/SGL1, 1993.

[Foote 1981]

Foote, R.S., Prospects for Non-Stop Toll Collection using Automatic Vehicle Identification. Traffic Quarterly, 1981, 35, p445-460.

[Gronau and Wolf 1986]

Gronau, G., and Wolf, I, Aperture Coupling of Rectangular Microstrip Resonator. Electronics Letters, 1986, 22(10), p. 554-556.

[Hammerstad and Bekkadal 1975]

Hammerstad, E., and Bekkadal, F., Microstrip Handbook, Trondheim, Norway, Feb. 1975.

[Helszajn 1992]

Helszajn, J., Microwave Engineering: Passive, Active and Non-Reciprocal Circuits, McGraw Hill, Inc. 1992.

[Hills and Blythe 1989]

Hills, P.G. and Blythe, P., Paying Your Way, IEE Review, Nov. 1989, pp377-381.

[Himdi et al. 1989a]

Himdi, M., Daniel, J.P. and Terret, C., Transmission Line Analysis of Aperture-Coupled Microstrip Antenna. Electronics Letters, 1989, 25(18), p. 1229-1230.

[Himdi et al. 1989b]

Himdi, M., Daniel, J.P. and Terret, C., Analysis of Aperture-Coupled Microstrip Antenna Using Cavity Method. Electronics Letters, 1989, 25(18), p. 391-392.

[Himdi and Daniel 1991]

Himdi, M and Daniel, J.P, Characteristics of Sandwich-Slotlines in Front of a Parallel Metallic Strip. Electronics Letters, 1991, 27(5), p. 455-457.

[Himdi and Daniel 1992]

Himdi, M and Daniel, J.P, Analysis of Linear Slot Antenna Usig Lossy Transmission Line Model. Electronics Letters, 1992, 28(6), p. 598-601.

[Iwasaki and Kaabata 1991]

Iwasaki, H., and Kawabata, K., A Circular Microstrip Antenna with a Cross Slot for Circular Polarisation. IEICE Transactions, 1991, 74(10), p. 3274-3279.

[Kirsching et al. 1981]

Kirsching, M, Jansen, R., and Koster, N., Accurate Model for Open End Effect of Microstrip Lines. Electronics Letters, 1981, 17, p 123-125.

[Kirsching and Jansen 1982]

Kirsching, M and Jansen, R, Accurate Model for Effective Dielectric Constant of Microstrip with Validity up to Millimeter-Wave Frequencies. Electronics Letters, 1982, 18, p. 272-273.

[Korolkiewicz 1989]

Korolkiewicz, E., PAMELA Deliverable - ME4 The State of the Art of Current Technologies Applied to Road Traffic Management Systems. DRIVE Report. Polytechnic of Newcastle upon Tyne, 1989.

[Korolkiewicz 1994]

Korolkiewicz, E., ADEPT Contract Deliverable - ME-VIII Specification of the Road to Vehicle Communication Link. DRIVE Report. University of Northumbria, 1994.

[Kraus 1991]

Kraus, J.D, Electromagnetics, McGraw-Hill, Inc.

[Lim 1996]

Lim, B.W., Design and Modelling of a Corner Fed Circularly Polarised Patch Antenna, PhD Thesis, PhD Thesis, Department of Electrical and Electronic Engineering and Physics, University of Northumbria at Newcastle, 1996.

[Lo et al. 1979]

Lo, Y.T., Solomon, D. and Richards W.F., Theory and Experiment on Microstrip Antennas. IEEE Transactions on Antennas and Propagation, 1979, 27(2), p. 137-145.

[Lowes 1995]

Lowes, P., Radio Antennas on Glass. Ph.D. Thesis. Department of Electrical and Electronic Engineering and Physics, University of Northumbria at Newcastle, 1995.

[Malbrunot 1995]

Malbrunot, F., Electronic tolling: Birth of a pan-European sys-tem. Traffic Technology International, The Annual Review of Traffic Engineering and Advanced Management Systems, 1995, p. 306-309.

[Meinel 1992]

Meinel, H.H., Applications of Microwaves and Milimeterwaves for Vehicle Communications and Control in Europe. In: digest of the IEEE Transactions on Microwave Theory and Techniques Society International Symposium, Albuguerque, N.M. USA, 1992, p. 609-612.

[Micro Design 1993]

Micro Design, AS, Developing a Standard for DSRC Physical Layer Parameters. ADEPT Project Report, Micro Design AS., 1993.

[Munson 1974]

Munson, R.E., Conformal Microstrip Antennas and Microstrip Phased Arrays. IEEE Transactions on Antennas and Propagation, January 1974, 22, p. 74-78.

[Murakoshi 1995]

Murakoshi, H., Tolling system for the future. Traffic Technology International, Summer 1995, p. 76.

[Newmann and Barink 1996]

Newmann, D , Barink, B, Follow the wave (length). Traffic Technology International, June/July 1996, p. 89-91.

[Nuttal 1995a]

Nuttal, I. ed., EC Comissioner on road pricing. Traffic Technology International, Winter 1995, p. 13.

[Nuttal 1995b]

Nuttal, I. ed., Private ETC toll road opens. Traffic Technology International, Winter 1995, p. 5.

[Nuttal 1995c]

Nuttal, I. ed., New Brunswick bridge leapfrogs to RFID ETC system. Traffic Technology International, Winter 1995, p. 14.

[Nuttal 1995d]

Nuttal, I. ed., Singapore selects ETC system. Traffic Technology International, Winter 1995, p. 4.

[Nuttal 1996]

Nuttal, I. ed., Multi-lane ETC inaugurated on key trans-Alpine route. Traffic Technology International, Feb/Mar. 1996, p. 46-50.

[Owens 1976]

Owens, R., Predicted Frequency Dependence of Microstrip Characteristic Impedance Using the Planar-Waveguide Model. Electronics Letters, 1976, 12 p. 269-270.

[Palanisamy and Garg 1986]

Palanisamy, Y. and Garg, R., Analysis of Circularly Polarized Square Ring and Crossed-Strip Microstrip Antennas. IEEE Transactions on Antennas and Propagation, 1986, 34(11), p. 1340-1346.

[Pozar and Voda 1987]

Pozar, D.M. and Voda, S.M., A Rigorous Analysis of a Microstripline Fed Patch Antenna. IEEE Transactions on Antennas and Propagation, 1987, 35(12), p. 1343-1349.

[Pues and Van de Capelle 1984]

Pues, H. and Van de Capelle, A., Accurate Transmission Line Model for the Rectangular Microstrip Antenna. IEE Proceedings H, 1984, 131(6), p. 334-340.

[Rao et al. 1981]

Rao, J.S., Joshi, K.K, and Das, B.N, Analysis of Small Aperture Coupling Between Rectangular Waveguide and Microstrip Line. IEEE Transactions on Microwave Theory and Techniques, 1981, 29(2), p. 150-154.

[Richards et al. 1981]

Richards, W.F., Lo, Y-T. and Harrison D.D., An Improved Theory for Microstrip Antennas and Applications. IEEE Transactions on Antennas and Propagation, 1981, 29(1), p. 38-46.

[Rostan and Wiesbeck 1995]

Rostan, F. and Wiesbeck, W., Design Considerations for Dual Polarized Aperture-Coupled Microstrip Patch Antennas. In : digest of the IEEE Antennas and Propagation Society International Symposium, California, 18-23 June 1995, 4, p. 2086-2089.

[Sawamura et al. 1995]

Sawamura, M., Tabata, M. and Haneishi, M., Radiation Properties of Ring Microstrip Antenna Fed by Symmetrical Cross Slot. In : digest of the IEEE Antennas and Propagation Society International Symposium, California, 18-23 June 1995, 4, p. 2074-2077.

[Schaubert et al. 1989]

Schaubert D.H., Pozar, D.M. and Adrian, A., Effect of Microstrip Antenna Substrate Thickness and Permittivity: Comparison of Theories with Experiment. IEEE Transactions on Antennas and Propagation, 1989, 37(6), p. 677-682.

[Schwartz 1985]

Schwartz, M., Information Transmission, Modulation, And Noise McGraw-Hill Book Company, 1985.

[Scott 1989]

Scott, C., The Spectral Domain Method in Electromagnetics. Artech House, Inc., 1989.

[Sharma and Gupta 1983]

Sharma, P.C. and Gupta, K. C., Analysis and Optimized Design of Single Feed Circularly Polarized Mictrostrip Antennas. IEEE Transactions on Antennas and Propagation, 1983, 31(6), p. 949-955.

[Sullivan and Scaubert 1986]

Sullivan, P.L. and Schaubert, D.H, Analysis of an Aperture-Coupled Microstrip Antenna. IEEE Transactions on Antennas and Propagation, 1986, 34(8), p. 977-984.

[Svacina 1992]

Svacina, J., Analysis of Multilayer Microstrip Lines by a Conformal Mapping Method. IEEE Transactions on Antennas and Propagation, 1992, 40(4), p. 769-772.

[Targonsky and Pozar 1993]

Targonsky, S.D. and Pozar, D.M., Design of Wideband Circularly Polarized Aperture-Coupled Microstrip Antennas. IEEE Transactions on Antennas and Propagation, 1993, 41(2), p. 214-220.

[Thouroude et al. 1990]

Thouroude, D, Himdi, M, and Daniel, J.P, Cad-Oriented Cavity Model for Rectangular Patches, Electronics Letters, 1990, 26(13), p. 842-844.

[Van de Capelle 1989]

Van de Capelle, A., Transmission Line Model for Redtangular Microstrip Antennas. Handbook of Microstrip Antennas, Chapter 10. Peter Peregrinus Ltd., 1989.

[Vierth and Källström 1994]

Vierth, I., and L. Källström, "ADEPT Deliverable ME-IX - Common Evaluation Methodology and Specification of Common Experimental Design", 1994.

[Walker 1990]

Walker, J., Mobile Information Systems. Artech House, 1990.

[Wheeler 1964]

Wheeler, H.A., Transmission Line Properties of Parallel Wide Strips by a Conformal Mapping Approximation. IEEE Transactions on Microwave Theory and Techniques, 1964, 12 p. 280-287.

[Woermbke 1982]

Woermbke, J.D., Soft Substrates Conquer Hard Designs, MicroWaves, January 1982.

[Yacoubi 1994]

Yacoubi, S., An Electronic Toll and Traffic Management System. Microwave Journal, July 1994, p. 64-69, 72.

[Yazidi et al. 1992]

Yazidi, M.E., Himdi, M and Daniel, J.P, Transmission Line Analysis of Nonlinear Slot Coupled Microstrip Antenna. Electronics Letters, 1992, 28(15), p. 1406-1408.

[Yazidi et al. 1993a]

Yazidi, M.E., Himdi, M and Daniel, J.P, Aperture Coupled Antenna for Dual Frequency Operation. Electronics Letters, 1993, 29(17), p. 1506-1508.

[Yazidi et al. 1993b]

Yazidi, M.E., Himdi, M and Daniel, J.P, Analysis of Aperture-Coupled Circular Microstrip Antenna. Electronics Letters, 1993, 29(11), p. 1021-1022.

[Zhong et al. 1994]

Zhong, S. Liu, G. and Stassevich, V., Improved Transmission Line Model for Input Impedance of Rectangular Microstrip Antennas with Multi-Dielectric Layers. In: digest of the IEEE Antennas and Propagation Society International Symposium, Seattle, USA, 20-24 June 1994, 1, p. 492-495.

[Zimmermann and Neumeyer 1995]

Zimmermann, R. Dr., Neumeyer, B. Dr., Tolling: Creating a Violator-Proof System in Germany. Traffic Technology International, The Annual Review of Traffic Engineering and Advanced Management Systems, 1995, p. 302-305.

[Zurcher 1988]

Zurcher, J.-F., The SSFIP: A Global Concept for High-Performance Broadband Planar Antennas. Electronics Letters, 1988, 24(23), p. 1433-1435.

[Zurcher 1995]

Zurcher, J.-F. and Gardiol, F.E., Broadband Patch Antennas. Artech House, Inc., 1995.

APPENDIX A: LINK BUGET CALCULATION

Down-Link

The power received (P_{DR}) by the on-board unit can be obtained from the following equation [Kraus 1991]

$$P_{DR} = P_O G_T G_R \left(\frac{\lambda}{4\Pi R}\right)^2 L_1 L_2 L_3 L_4 \qquad \text{(A.1)}$$

where, P_{DR} is the received power at the OBU,

P_O is the output power of the oscillator in the RSU (20dBm),

G_T is the RSU antenna gain (16dB),

G_R is the OBU antenna gain (4.5dB),

λ is the free space wavelength at the carrier frequency,

R is the distance between the RSU and OBU,

L_1 is the insertion loss of the coupler and microwave switch in the RSU (-3dB),

L_2 is the loss due to the windscreen of the vehicle (-3dB),

L_3 is the loss due to the RSU acceptance angle (-3dB) and

L_4 is the loss due to the OBU acceptance angle (-3dB).

The received signal is detected by a diode where the bit-error rate (P_e) at the output of the detector can be calculated as [Schwartz 1985]

$$P_e = \frac{1}{2} erfc \frac{V_{\det}}{2\sqrt{2}V_n} \qquad \text{(A.2)}$$

where

$$erfc(x) \equiv 1 - \frac{2}{\sqrt{\Pi}} \int_0^x e^{-y^2} dy \qquad \text{(A.3)}$$

From the definition of the tangential sensitivity, the signal-to-noise ratio at the output of the detector (V_{det}/V_n) can be expressed as

$$\frac{V_{\text{det}}}{V_n} = \frac{2\sqrt{2}P_{DR}}{P_{TTS}} \qquad \text{(A.4)}$$

where, P_{TTS} is the tangential sensitivity of the detector with the mismatch between the diode and antenna taken into account. For a BER of 10^{-6} or less, the V_{det}/V_n ratio is required to be 9.5 or better, therefore

$$P_{DR} > 9.5\frac{P_{TTS}}{2\sqrt{2}} \qquad \text{(A.5)}$$

Substituting for the tangential sensitivity of -49dBm of the OBU ASK detector, this gives a required received power (P_{DR}) to be at least -43.7dBm in order to obtain a BER of 10^{-6} or less at the diode detector.

The received power (P_{DR}) is -43.7dBm at a distance of 15m, which is the predicted down-link range of the system.

Up-Link

The power of the received modulated up-link signal (P_{UR}) can be expressed as [Kraus 1991]

$$P_{UR} = P_O G_T{}^2 G_R{}^2 \left(\frac{\lambda}{4\Pi R}\right)^4 L_1 L_2^2 L_3^2 L_4^2 L_5 L_6 \qquad \text{(A.6)}$$

where, P_{UR} is the received up-link signal at the RSU, and

L_5 is the loss of PSK modulator at the OBU (-2dB), and

L_6 is the loss due to the unused upper harmonics in the up-link spectrum (-1dB)

The BER for coherent DPSK demodulation can be calculated as [Schwartz 1985]

$$P_{e,DPSK} = \frac{1}{2} e^{(-S/N)} \tag{A.7}$$

where S/N is the input signal-to-noise ratio (SNR). To obtain a BER of 10^{-6} or less, the SNR at the output of the image rejection mixer should be better than 11.2dB. The required input signal power to the RSU can be expressed as

$$P_{UR} = F\left(S/N\right)_o KTB \tag{A.9}$$

where, F is the noise figure of the RSU front-end,

$(S/N)_O$ is the required SNR at the IF amplifier input (>11.2dB),

K is the Boltzmann constant,

T is the noise temperature (290K) and

B is the IF Amplifier bandwidth (250KHz).

The noise figure of the RSU front-end is given by

$$F = F_1 + \left(\frac{F_2 - 1}{G_1}\right) + \left(\frac{F_3 - 1}{G_1 G_2}\right) = 2.5dB \tag{A.10}$$

where, $F_1 = 1/G_1$, the cable loss between the antenna and low noise amplifier (0.5dB),

F_2 is the LNA noise figure (2dB),

G_2 is the gain of the LNA (30dB) and

F_3 is the conversion loss of IRM (8dB).

Therefore, the required minimum input power is

$$P_{UR} > 2.5dB + 11.2dB - 120dBm = -106.3dBm \tag{A.11}$$

The received power is -106.3dBm at a distance of 15.5m, which is the predicted up-link range of the system.

APPENDIX B: CALCULATION OF SLOT-LINE PARAMETERS (k_a, Z_{ca})

Cohn's method has been used to determine the characteristic impedance (Z_{ca}) and effective permittivity (ε_{ap}) of the coupling aperture as shown in Figure B.1.

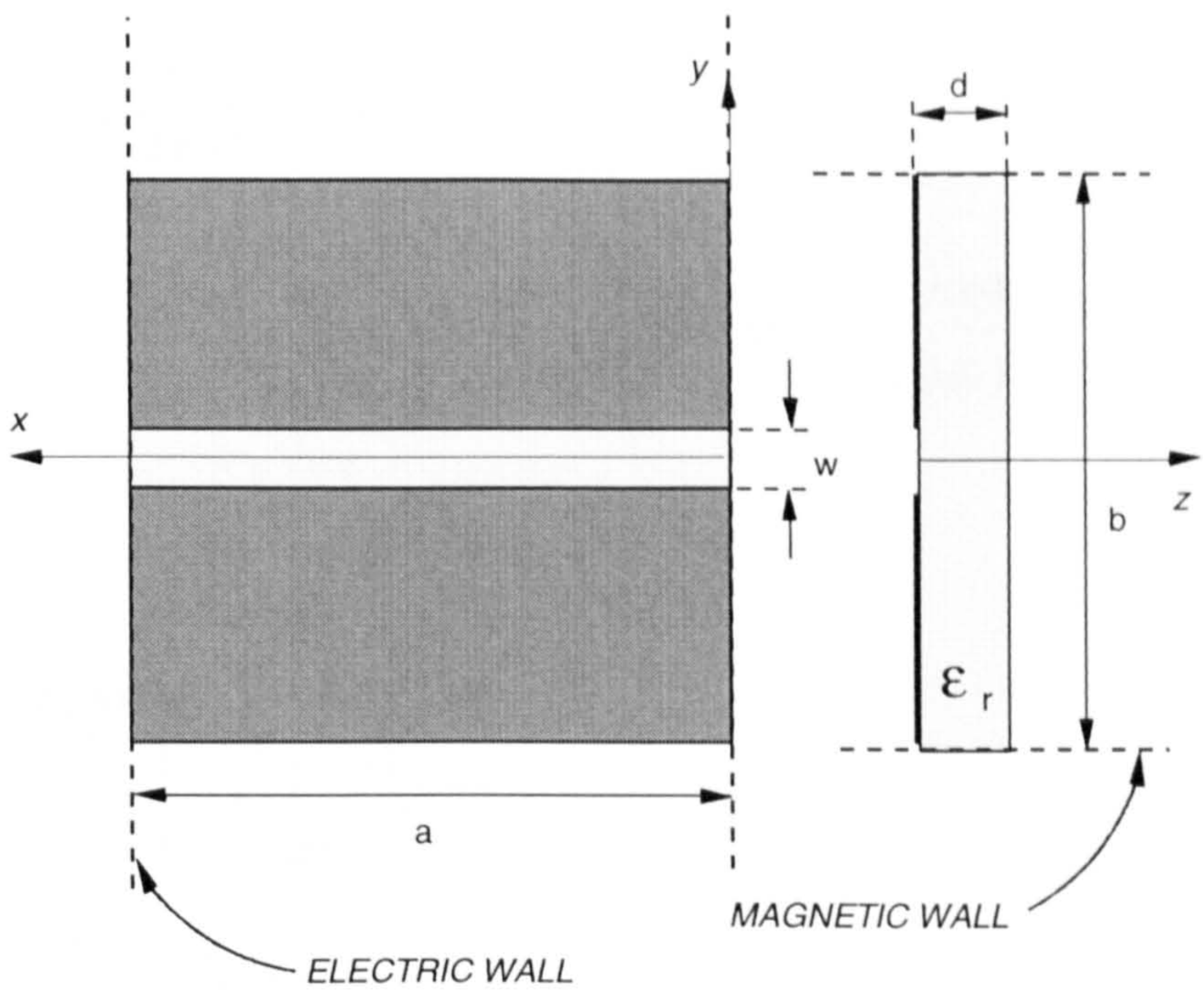

Figure B.1. Wave-guide equivalent of slot-line.

By placing infinite electric walls at $x = 0$ and at $x = \lambda_g/2 = a$ on an infinite slot-line, where λ_g is the guided wavelength, the $x < 0$ and $x > a$ regions can be eliminated. At $y = \pm b/2$, magnetic walls may be used as a boundary condition. With these electric and magnetic walls inserted, the structure can be considered as a capacitive iris in a rectangular waveguide. The total susceptance at the plane of the slot (B_t) is then expressed as a function of the effective permittivity. The value of effective permittivity is determined by the condition for resonance, as a solution of the equation

$$B_t\left(\varepsilon_{ap}\right)=0 \tag{B.1}$$

Cohn's method can not be applied directly to determine the characteristics of the slot used in the aperture-coupled antenna structure where the slot is covered with a dielectric material on both sides. The proximity of the antenna also effects the slot-line. Cohn's expression for $B_t(\varepsilon_{ap})$ has been modified [Himdi and Daniel 1991] so that it can be applied to a sandwich slot line in the proximity of a conducting parallel plate. This gives the following formula for $B_t(\varepsilon_{ap})$:

$$Z_0 B_t\left(\varepsilon_{ap}\right)=\frac{1}{2p}\left\{\left(\varepsilon_{ra}-p^2\right)\cdot\ln\frac{8}{\pi\delta}+\left(\varepsilon_{rf}-p^2\right)\cdot\ln\frac{8}{\pi\delta}+\right.$$
$$\left.+\sum_{n=\frac{1}{2},\frac{3}{2},\otimes}\left[M_{n1}\frac{\sin^2\left(n\pi\delta_1\right)}{n\left(n\pi\delta_1\right)^2}+M_{n2}\frac{\sin^2\left(n\pi\delta_2\right)}{n\left(n\pi\delta_2\right)^2}\right]\right\} \tag{B.2}$$

where,

$$M_{n1}=\frac{\varepsilon_{rf}\tanh\left(r_{n1}\right)-p^2F_{n1}^2\coth\left(q_{n1}\right)}{\left[1+\left(\frac{S}{2an}\right)^2\right]F_{n1}}-u_1^2 \tag{B.3}$$

$$M_{n2}=u_2^2\left[\frac{\coth\left(\frac{2\pi nd_aF_{n2}}{L}\right)}{F_{n2}}-1\right] \tag{B.4}$$

$$r_{n1}=\frac{2\pi nd_fF_{n1}}{S}+\tanh^{-1}\left(\frac{F_{n1}}{\varepsilon_{rf}F_n}\right) \tag{B.5}$$

$$q_{n1}=\frac{2\pi nd_fF_{n1}}{S}+\coth^{-1}\left(\frac{F_n}{F_{n1}}\right) \tag{B.6}$$

$$F_n^2=1+\left(\frac{Sv}{2an}\right)^2 \qquad F_{n1}=1-\left(\frac{Su_1}{2an}\right)^2 \qquad F_{n2}=1-\left(\frac{Su_2}{2an}\right)^2 \tag{B.7}$$

$$u_1^2=\varepsilon_{rf}-p^2 \qquad v^2=p^2-1 \qquad u_2^2=\varepsilon_{ra}-p^2 \tag{B.8}$$

$$\delta_1 = \frac{W_{ap}}{S} \qquad \delta_2 = \frac{W_{ap}}{L} \qquad p = \frac{\lambda_0}{\lambda_g} = \sqrt{\varepsilon_{ap}} \qquad a = \frac{\lambda_g}{2} \qquad \text{(B.9)}$$

Solving the equation $B_t\left(\varepsilon_{ap}\right) = 0$, for p, gives the effective permittivity (ε_{ap}) of the slot-line. The characteristic impedance of the slot-line can be calculated with the aid of the ratio of phase velocity (v) to group velocity (v_g) as given by [Cohn 1969]

$$\frac{v}{v_g} = 1 + \frac{f}{\lambda_0/\lambda_g} \cdot \frac{\Delta\left(\lambda_0/\lambda_g\right)}{\Delta f} \qquad \text{(B.10)}$$

The values of $\Delta(\lambda_0/\lambda_g)$ and Δf are computed from two separate solutions of $B_t\left(\varepsilon_{ap}\right) = 0$ for two slightly different values of a. The characteristic impedance of the slot-line then can be obtained from the expression

$$Z_{ca} = Z_0 \frac{v}{v_g} \frac{\pi}{p} \cdot \frac{1}{-Z_0} \left(\frac{dB_t\left(p_0\right)}{dp} \right)^{-1} \qquad \text{(B.11)}$$

where p_0 is the zero of $B_t(p)$. The numerical value of $\left(dB_t\left(p_0\right)/dp\right)^{-1}$ is estimated by the central difference approximation about the point $p = p_0$.

APPENDIX C: DERIVATION OF EXPRESSION FOR THE TURNS RATIO OF AN INCLINED APERTURE-MICROSTRIP LINE TRANSITION

$$\Delta v = \frac{V_0 \cos\theta_s}{W_a \sqrt{Dh}\sin\left(k_a \frac{L_a}{2}\right)} \iint_{slot} \sin\left[k_a\left(\frac{L_a}{2} - |u|\right)\right] du dv \qquad \text{(C.1)}$$

The integral in (C.1) must be performed over the overlapping area of the aperture and the equivalent parallel plate microstrip line as shown in Figure C.1.

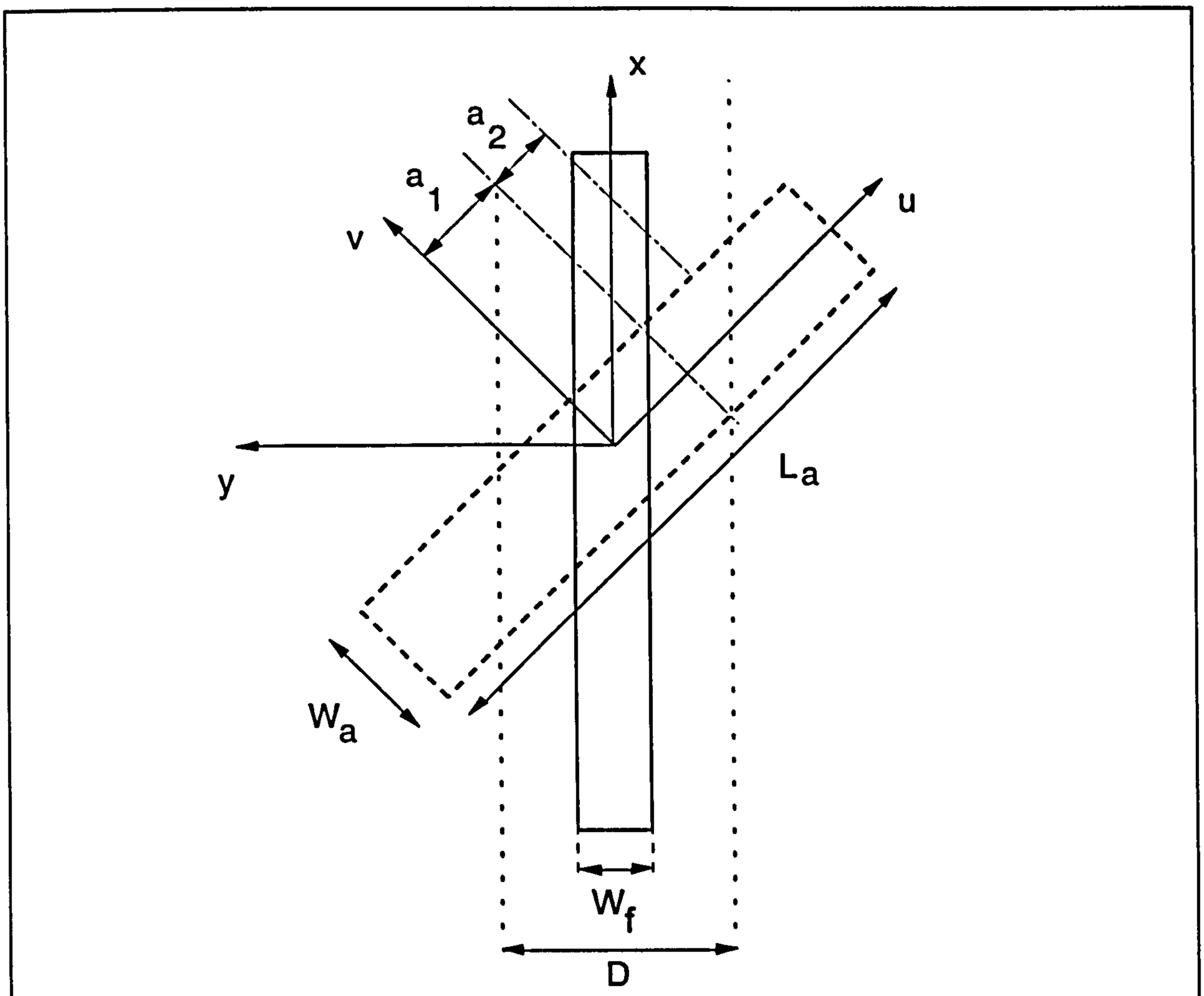

Figure C.1. Aperture to microstrip line transition.

The integration is performed in two parts. Initially the integration over the area bounded by the v axis and a_1 is carried out as given by

$$I_1 = 2W_a \int_0^{a_1} \sin\left[k_a\left(\frac{L_a}{2}-u\right)\right]du$$

$$= \frac{2W_a}{k_a}\left[-\cos\left[k_a\left(\frac{L_a}{2}-u\right)\right]\right]_0^{U_1}$$

$$= \frac{2W_a}{k_a}\left[\cos\left[k_a\left(\frac{L_a}{2}-a_1\right)\right]-\cos\left[k_a\left(\frac{L_a}{2}-U_1\right)\right]\right] \qquad \text{(C.2)}$$

Then the integration is performed over the triangular area bounded by a_1 and a_2

$$I_2 = 2W_a \int_{a_1}^{U_2} \sin\left[k_a\left(\frac{L_a}{2}-u\right)\right] fc(u)\,du \qquad \text{(C.3)}$$

where,

$$fc(u) = \frac{a_1 + a_2 - u}{a_2} \qquad \text{(C.4)}$$

Hence,

$$I_2 = W_a \int_{a_1}^{U} \sin\left[k_a\left(\frac{L_a}{2}-u\right)\right]\frac{a_1 + a_2 - u}{a_2}du$$

$$= \frac{W_a}{k_a}\left[\frac{u-a_1-a_2}{a_2}\cos\left[k_a\left(\frac{L_a}{2}-u\right)\right]\right]_{a_1}^{U_2} - \frac{W_a}{k_a a_2}\int_{a_1}^{U_2}\cos\left[k_a\left(\frac{L_a}{2}-u\right)\right]du$$

$$= \frac{W_a}{k_a}\left[\frac{U_2-a_1-a_2}{a_2}\cos\left[k_a\left(\frac{L_a}{2}-U_2\right)\right]+\cos\left[k_a\left(\frac{L_a}{2}-a_1\right)\right]\right]$$

$$+\frac{W_a}{k_a a_2}\int_{U_2}^{a_1}\cos\left[k_a\left(\frac{L_a}{2}-u\right)\right]du$$

$$= \frac{W_a}{k_a}\left[\frac{U_2 - a_1 - a_2}{a_2}\cos\left[k_a\left(\frac{L_a}{2} - U_2\right)\right] + \cos\left[k_a\left(\frac{L_a}{2} - a_1\right)\right]\right]$$

$$+ \frac{W_a}{k_a^2 a_2}\left[\sin\left[k_a\left(\frac{L_a}{2} - u\right)\right]\right]_{U_2}^{a_1}$$

$$= \frac{W_a}{k_a}\left[\frac{U_2 - a_1 - a_2}{a_2}\cos\left[k_a\left(\frac{L_a}{2} - U_2\right)\right] + \cos\left[k_a\left(\frac{L_a}{2} - a_1\right)\right]\right]$$

$$+ \frac{W_a}{k_a^2 a_2}\left[\sin\left[k_a\left(\frac{L_a}{2} - a_1\right)\right] - \sin\left[k_a\left(\frac{L_a}{2} - U_2\right)\right]\right] \qquad \text{(C.5)}$$

The integration limits U_1 and U_2 depend on the length of the aperture as given by

$$U_1 = \begin{cases} a_1 & \mathrm{L}_a < a_1 \\ \\ L_a & L_a \geq a_1 \end{cases} \qquad \text{(C.6)}$$

$$U_2 = \begin{cases} a_1 & \mathrm{L}_a < a_1 \\ L_a & a_1 \leq L_a < a_2 \\ a_2 & L_a \geq a_2 \end{cases} \qquad \text{(C.7)}$$

The values of a_1 and a_2 can be determined from the geometry of the structure as shown in Figure C.1 as given by

$$a_1 = \left|\frac{D}{\sqrt{2}} - \frac{W_a}{2}\right| \qquad \text{(C.8)}$$

$$a_2 = \begin{cases} a_1 + W_a & \sqrt{2}D \geq W_a \\ \\ a_1 + D\sqrt{2} & \sqrt{2}D < W_a \end{cases} \qquad \text{(C.9)}$$

If $\sqrt{2}D < W_a$ then a correction factor must be introduced as the integration with respect to variable v is not performed along the whole width of the aperture. Hence, the value of discontinuity voltage can finally be written as

$$\Delta v = AB\left(I_1 + I_2\right)$$

$$A = \frac{V_{0u}}{W_a\sqrt{2Dh}\sin\left(k_a\frac{L_a}{2}\right)} \qquad B = \begin{cases} 1 & \sqrt{2}D \le W_a \\ \dfrac{\sqrt{2}D}{W_a} & \sqrt{2}D < W_a \end{cases}$$

$$I_1 = \frac{2W_a}{k_a}\left[-\cos\left[k_a\left(\frac{L_a}{2}-u\right)\right]\right]_0^{U_1}$$

$$U_1 = \begin{cases} a_1 & \mathrm{L_a} < a_1 \\ L_a & L_a \ge a_1 \end{cases}$$

$$I_2 = \frac{W_a}{k_a}\left[\frac{U_2 - a_1 - a_2}{a_2}\cos\left[k_a\left(\frac{L_a}{2}-U_2\right)\right] + \cos\left[k_a\left(\frac{L_a}{2}-a_1\right)\right]\right]$$

$$+\frac{W_a}{k_a^2 a_2}\left[\sin\left[k_a\left(\frac{L_a}{2}-a_1\right)\right] - \sin\left[k_a\left(\frac{L_a}{2}-U_2\right)\right]\right]$$

$$U_2 = \begin{cases} a_1 & \mathrm{L_a} < a_1 \\ L_a & a_1 \le L_a < a_2 \\ a_2 & L_a \ge a_2 \end{cases}$$

$$a_1 = \left|\frac{D}{\sqrt{2}} - \frac{W_a}{2}\right| \qquad a_2 = \begin{cases} a_1 + W_a & \sqrt{2}D \ge W_a \\ a_1 + D\sqrt{2} & \sqrt{2}D < W_a \end{cases} \qquad \text{(C.10)}$$

APPENDIX D: EXPRESSIONS FOR TRANSMISSION LINE PARAMETERS OF THE PATCH ANTENNA

EFFECTIVE PERMITTIVITY

For a microstrip line having a width of W, printed on a substrate with a thickness of h and relative permittivity of ε_r, the effective width can be calculated as given by [Kirsching and Jansen 1982]

$$\varepsilon_{eff}(f) = \varepsilon_r - \frac{\varepsilon_r - \varepsilon_{eff}(0)}{1 + P(f)} \tag{D.1}$$

where $\varepsilon_{eff}(0)$ is the quasi-static value of the effective permittivity given by

$$\varepsilon_{eff}(0) = \frac{1}{2}\{\varepsilon_r + 1 + (\varepsilon_r - 1)G\} \tag{D.2}$$

$$G = (1 + 10h/W)^{-AB} - \frac{\ln 4}{\pi}\frac{t}{\sqrt{Wh}} \tag{D.3}$$

$$A = 1 + \frac{1}{49}\ln\left\{\frac{(W/h)^4 + W^2/(52h)^2}{(W/h)^4 + 0.432}\right\} + \frac{1}{18.7}\ln\left\{1 + \left(\frac{W}{18.1h}\right)^3\right\} \tag{D.4}$$

$$B = 0.564\exp\left(-\frac{0.2}{\varepsilon_r + 0.3}\right) \tag{D.5}$$

and the frequency dependent term $P(f)$ is given by

$$P(f) = P_1 P_2\{(0.1844 + P_3 P_4) f_n\}^{1.5673} \tag{D.6}$$

$$P_1 = 0.27488 + \{0.6315 + 0.525/(1 + 0.0157 f_n)^{20}\}u - 0.065683\exp(-8.7513u) \tag{D.7}$$

$$P_2 = 0.33622\{1 - \exp(-0.03442)\varepsilon_r\} \tag{D.8}$$

$$P_3 = 0.0363\exp(-4.6u)\left\{1-\exp\left[-(f_n/38.7)^{4.97}\right]\right\} \tag{D.9}$$

$$P_4 = 1+2.751\left\{1-\exp\left[-(\varepsilon_r/15.916)^8\right]\right\} \tag{D.10}$$

$$f_n = fh \qquad \text{in [GHz mm]} \tag{D.11}$$

$$u = \left\{W+(W'-W)/\varepsilon_r\right\}/h \tag{D.12}$$

$$W' = W+\frac{t}{\pi}\left\{1+\ln\left(4\Big/\sqrt{(t/h)^2+(1/\pi)^2/(W/t+1.1)^2}\right)\right\} \tag{D.13}$$

EFFECTIVE WIDTH

The formula for calculating the effective width of a microstrip line has been proposed by Owens [Owens 1976]

$$W_{eff}(f) = W+\frac{W_{eff}(0)-W}{1+(f/f_0)^2} \tag{D.14}$$

where

$$f_0 \cong \frac{c}{2\sqrt{\varepsilon_{eff}(0)}W_{eff}(0)} \tag{D.15}$$

The quasi-static value of the effective permittivity, $\varepsilon_{eff}(0)$ is given by equations (D.2) to (D.5). In (D.14), $W_{eff}(0)$ is the quasi-static value of the effective width, which is given by

$$W_{eff}(0) = 2\pi h/\ln\left\{hF/W'+\sqrt{1+(2h/W')^2}\right\} \tag{D.16}$$

$$F = 6+(2\pi-6)\exp\left\{-\frac{4\pi^2}{3}\left(\frac{h}{W'}\right)^{3/4}\right\} \tag{D.17}$$

OPEN-END EXTENSION

The open-end extension of a microstrip line can be calculated using the following formulas [Kirsching et al. 1981]

$$\Delta l = h\xi_1\xi_3\xi_5 / \xi_4 \tag{D.18}$$

$$\xi_1 = 0.434907 \cdot \frac{\varepsilon_{eff}^{0.81} + 0.26}{\varepsilon_{eff}^{0.81} - 0.189} \cdot \frac{(W/h)^{0.8544} + 0.236}{(W/h)^{0.8544} + 0.87} \tag{D.19}$$

$$\xi_2 = 1 + \frac{(W/h)^{0.371}}{2.358\varepsilon_r + 1} \tag{D.20}$$

$$\xi_3 = 1 + \frac{0.5274 \ \arctan\left\{0.084(W/h)^{1.9413/\xi 2}\right\}}{\varepsilon_{eff}^{0.9236}} \tag{D.21}$$

$$\xi_4 = 1 + 0.0377 \ \arctan\left\{0.067(W/h)^{1.456}\right\}\left\{6 - 5\exp\left[0.036(1-\varepsilon_r)\right]\right\} \tag{D.22}$$

$$\xi_5 = 1 - 0.218\exp(-7.5W/h) \tag{D.23}$$

EXPRESSIONS FOR THE ATTENUATION CONSTANT

The attenuation constant (α) includes the dielectric losses in the substrate (α_d), conductor losses in the strip (α_{cs}) conductor and in the ground plane (α_{cg}) as given by

$$\alpha = \alpha_d + \alpha_{cs} + \alpha_{cg} \tag{D.24}$$

The dielectric losses can be calculculated as given by [Hammerstadt and Bekkadal 1975]

$$\alpha_d = 0.5\beta \frac{\varepsilon_r}{\varepsilon_{eff}(f)} \frac{\varepsilon_{eff}(f) - 1}{\varepsilon_r - 1} \tan\delta \tag{D.25}$$

The conducting losses are given by [Bahl and Gupta 1979]

$$\alpha_{cs} = \alpha_n R_{ss} F_{\Delta s} F_s \tag{D.26}$$

$$\alpha_{cg} = \alpha_n R_{sg} F_{\Delta g} \tag{D.27}$$

$$R_{ss} = \sqrt{\pi f \mu_0 / \sigma_s} \tag{D.28}$$

$$R_{sg} = \sqrt{\pi f \mu_0 / \sigma_g} \tag{D.29}$$

$$\alpha_n = \begin{cases} \dfrac{1}{4\pi h Z_c(0)} \dfrac{32 - (W'/h)^2}{32 + (W'/h)^2}; & W'/h < 1 \\ \dfrac{\sqrt{\varepsilon_{eff}(0)}}{2\eta_0 W_{eff}(0)} \left(W'/h + \dfrac{0.667 W'/h}{W'/h + 1.444} \right) & W'/h \geq 1 \end{cases} \tag{D.30}$$

$$F_{\Delta s} = 1 + \frac{2}{\pi} \arctan\left\{ 1 \cdot 4 \left(R_{ss} \Delta_s \sigma_s \right)^2 \right\} \tag{D.31}$$

$$F_{\Delta g} = 1 + \frac{2}{\pi} \arctan\left\{ 1 \cdot 4 \left(R_{sg} \Delta_g \sigma_g \right)^2 \right\} \tag{D.32}$$

$$F_s \cong 1 + \frac{2h}{W'} \left(1 - \frac{1}{\pi} + \frac{W' - W}{t} \right) \tag{D.33}$$

In order to calculate the parameters α_x, α_y, ε_{effx}, ε_{effy}, Δl_x, Δl_y, a_{eff} and b_{eff}, one needs to substitute the design parameters of the antenna d_a, a or b in the above equations in place of h and W.

APPENDIX E. CALCULATION OF PATCH ADMITTANCE AT THE APERTURE

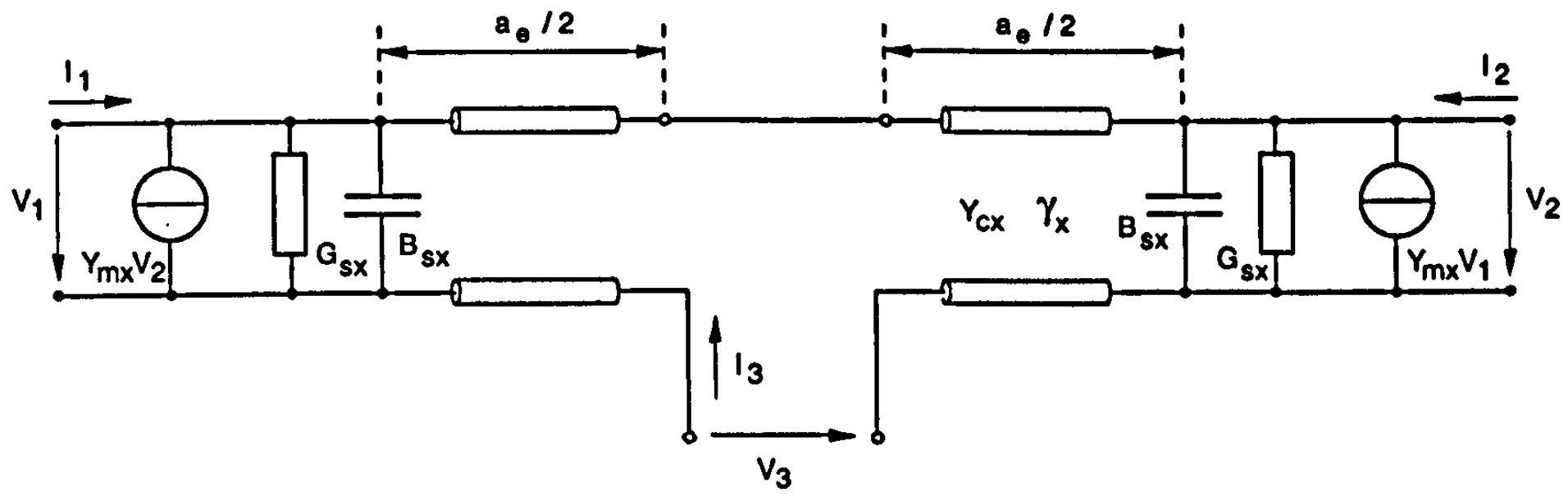

Figure E.1. Equivalent circuit of the patch antenna for the x direction.

The patch admittance at the aperture is the input admittance of the transmission line network shown in Figure E.1, at port 3. In order to obtain the value of the input impedance, the admittance matrix must first be determined.

The elements of the admittance matrix can be determined as given by

$$Y_{px,mn} = \frac{I_m}{V_n}\Bigg| \qquad V_{m'} = 0 \quad m' \neq m \tag{E.1}$$

With

$$Y_{sx} = G_{sx} + jB_{sx} \tag{E.2}$$

and taking into account the symmetry of the network, the elements of the admittance matrix are as follows

$$Y_{px,11} = Y_{px,22} = Y_{sx} + Y_{cx}\coth(\gamma a_e)$$

$$Y_{px,33} = \frac{Y_{cx}}{2}\coth\left(\gamma\frac{a_e}{2}\right)$$

$$Y_{px,12} = Y_{px,21} = -Y_{mx} - \frac{Y_{cx}}{\sinh(\gamma a_e)}$$

$$Y_{px,13} = Y_{px,31} = -Y_{px,23} = -Y_{px,32} = \frac{Y_{cx}}{2\sinh\left(\gamma\frac{a_e}{2}\right)} \qquad \text{(E.3)}$$

Hence the admittance matrix of the transmission line network shown in Figure E.1 is given by

$$Y_{px} = \begin{bmatrix} Y_{sx} + Y_{cx}\coth(\gamma a_e) & -Y_{mx} - \frac{Y_{cx}}{\sinh(\gamma a_e)} & \frac{Y_{cx}}{2\sinh\left(\gamma\frac{a_e}{2}\right)} \\ -Y_{mx} - \frac{Y_{cx}}{\sinh(\gamma a_e)} & Y_{sx} + Y_{cx}\coth(\gamma a_e) & \frac{-Y_{cx}}{2\sinh\left(\gamma\frac{a_e}{2}\right)} \\ \frac{Y_{cx}}{2\sinh\left(\gamma\frac{a_e}{2}\right)} & \frac{-Y_{cx}}{2\sinh\left(\gamma\frac{a_e}{2}\right)} & \frac{Y_{cx}}{2}\coth\left(\gamma\frac{a_e}{2}\right) \end{bmatrix} \qquad \text{(E.4)}$$

The admittance matrix relates the currents and voltages at the three ports of the network as given by

$$\begin{bmatrix} I_1 \\ I_2 \\ I_3 \end{bmatrix} = \begin{bmatrix} Y_{px,11} & Y_{px,12} & Y_{px,13} \\ Y_{px,21} & Y_{px,22} & Y_{px,23} \\ Y_{px,31} & Y_{px,32} & Y_{px,33} \end{bmatrix} \cdot \begin{bmatrix} V_1 \\ V_2 \\ V_3 \end{bmatrix} \qquad \text{(E.5)}$$

The input admittance at port 3 is defined as

$$Y_{PX} = \frac{I_3}{V_3}\Bigg| \qquad I_1 = I_2 = 0 \tag{E.6}$$

Substituting this condition into (E.5) and multiplying the equation with the inverse of the admittance matrix gives

$$\begin{bmatrix} V_1 \\ V_2 \\ V_3 \end{bmatrix} = \left[Y_{px} \right]^{-1} \cdot \begin{bmatrix} 0 \\ 0 \\ I_3 \end{bmatrix} \tag{E.7}$$

Hence

$$\frac{I_3}{V_3} = \frac{\left|\left[Y_{px} \right]\right|}{Y^c_{px,33}} \tag{E.8}$$

where $\left|\left[Y_{px} \right]\right|$ is the determinant of the matrix $\left[Y_{px} \right]$ and

$Y^c_{px,33}$ is the cofactor of element $Y_{px,33}$

Using the identities in (E.3)

$$\left|\left[Y_{px} \right]\right| = Y_{px,33}\left(Y^2_{px,11} - Y^2_{px,12}\right) - 2Y^2_{px,13}\left(Y_{px,11} + Y_{px,12}\right) \tag{E.9}$$

$$Y^c_{px,33} = Y_{px,33}\left(Y^2_{px,11} - Y^2_{px,12}\right) \tag{E.10}$$

Therefore

$$Y_{PX} = 1 - 2\frac{Y^2_{px,13}\left(Y_{px,11} + Y_{px,12}\right)}{Y_{px,33}\left(Y^2_{px,11} - Y^2_{px,12}\right)}$$

$$= 1 - 2\frac{Y_{px,13}^2}{Y_{px,33}\left(Y_{px,11} - Y_{px,12}\right)} \tag{E.11}$$

Hence, the input impedance of the transmission line network, which is the patch impedance at the aperture is given by

$$Y_{PX} = 1 - \frac{Y_{cx}}{\sinh\left(\gamma\frac{a_e}{2}\right)\cosh\left(\gamma\frac{a_e}{2}\right)\left[Y_{sx} + Y_{cx}\coth\left(\gamma a_e\right) + Y_{mx} + \frac{Y_{cx}}{\sinh\left(\gamma a_e\right)}\right]} \tag{E.12}$$

Similarly

$$Y_{PY} = 1 - \frac{Y_{cx}}{\sinh\left(\gamma\frac{b_e}{2}\right)\cosh\left(\gamma\frac{b_e}{2}\right)\left[Y_{sy} + Y_{cy}\coth\left(\gamma b_e\right) + Y_{my} + \frac{Y_{cy}}{\sinh\left(\gamma b_e\right)}\right]} \tag{E.13}$$

APPENDIX F: CALCULATION OF MODE COEFFICIENTS ($B_{x,mn}$, $B_{y,mn}$)

$$B_{x,mn} = \frac{j\omega\varepsilon}{\left(k^2 - k_{mn}^2\right)\cdot k_n^2} \int_0^a \int_0^b J_{mx} \Psi_{x,mn} dxdy \tag{F.1}$$

where

$$\Psi_{x,mn} = A_{mn} \cdot k_n \cdot \cos(k_m x)\sin(k_n y) \tag{F.2}$$

and

$$J_{mx} = \frac{-2V_{0x}}{d_a W_a} \frac{\sin\left[k_a\left(\frac{L_a}{2} - \left|x - \frac{a}{2}\right|\right)\right]}{\sin\left(k_a \frac{L_a}{2}\right)}; \qquad \begin{matrix} \frac{b-W_a}{2} \le y \le \frac{b+W_a}{2} \\ \frac{a-L_a}{2} \le y \le \frac{a+L_a}{2} \\ 0 \le z \le d_a \end{matrix}$$

$$= 0\ ; \qquad \text{otherwise} \tag{F.3}$$

Substituting (F.1) and (F.2) into (F.3) gives

$$B_{x,mn} = \frac{-2\, j\omega\varepsilon A_{mn} V_{ox}}{d_a k_n \left(k^2 - k_{mn}^2\right) W_a} \cdot$$

$$\int_{\frac{a-L_a}{2}}^{\frac{a+L_a}{2}} \int_{\frac{b-W_a}{2}}^{\frac{b+W_a}{2}} \frac{\sin\left[k_a\left(\frac{L_a}{2} - \left|x - \frac{a}{2}\right|\right)\right]}{\sin\left(k_a \frac{L_a}{2}\right)} \cos(k_m x)\sin(k_n y)\, dxdy \tag{F.4}$$

The integration with respect to the x and the y variables can be separated, which gives

$$B_{x,mn} = \frac{-2\,j\omega\varepsilon A_{mn} V_{ax}}{d_a k_n \left(k^2 - k_{mn}^2\right) W_a} \cdot \frac{1}{\sin\left(k_a \frac{L_a}{2}\right)} \cdot$$

$$\underbrace{\int_0^a \sin(k_n y)\,dy}_{I_1} \cdot \underbrace{\int_0^b \sin\left[k_a\left(\frac{L_a}{2} - \left|x - \frac{a}{2}\right|\right)\right]\cos(k_m x)\,dx}_{I_2} \qquad \text{(F.5)}$$

where the value of the first integral, I_1 is

$$I_1 = -\frac{1}{k_n}\left[\cos\left(k_n \frac{b}{2} + k_n \frac{W_a}{2}\right) - \cos\left(k_n \frac{b}{2} - k_n \frac{W_a}{2}\right)\right] \qquad \text{(F.7)}$$

That is

$$I_1 = \frac{2}{k_n}\sin\left(k_n \frac{W_a}{2}\right)\sin\left(\frac{n\pi}{2}\right) \qquad \text{(F.8)}$$

Replacing x by $x + a/2$ in the second integral gives

$$I_2 = \int_{-\frac{L_a}{2}}^{\frac{L_a}{2}} \sin\left[k_a\left(\frac{L_a}{2} - |x|\right)\right]\cos\left[k_m\left(\frac{a}{2} + x\right)\right]dx$$

$$= \int_0^{\frac{L_a}{2}} \sin\left[k_a\left(\frac{L_a}{2} - x\right)\right]\cos\left[k_m\left(\frac{a}{2} + x\right)\right]dx +$$

$$+ \int_{L_a}^{0} \sin\left[k_a\left(\frac{L_a}{2} + x\right)\right]\cos\left[k_m\left(\frac{a}{2} + x\right)\right]dx$$

$$-\frac{}{2}$$

$$= \int_0^{\frac{L_a}{2}} \sin\left[k_a\left(\frac{L_a}{2}-x\right)\right]\cos\left[k_m\left(\frac{a}{2}+x\right)\right]dx +$$

$$+ \int_0^{\frac{L_a}{2}} \sin\left[k_a\left(\frac{L_a}{2}-x\right)\right]\cos\left[k_m\left(\frac{a}{2}-x\right)\right]dx$$

$$= \int_0^{\frac{L_a}{2}} \sin\left[k_a\left(\frac{L_a}{2}-x\right)\right]\left\{\cos\left[k_m\left(\frac{a}{2}+x\right)\right]+\cos\left[k_m\left(\frac{a}{2}-x\right)\right]\right\}dx$$

$$= 2\cos\left(k_m\frac{a}{2}\right)\int_0^{\frac{L_a}{2}} \sin\left[k_a\left(\frac{L_a}{2}-x\right)\right]\cos\left(k_m x\right)dx$$

$$= 2\cos\left(k_m\frac{a}{2}\right)\cdot$$

$$\int_0^{\frac{L_a}{2}}\left\{\sin\left[k_a\frac{L_a}{2}+\left(k_m-k_a\right)x\right]+\sin\left[k_a\frac{L_a}{2}-\left(k_m+k_a\right)x\right]\right\}dx$$

(F.9)

Hence, the value of the second integral is

$$I_2 = \frac{2k_a\cos\left(k_m\frac{a}{2}\right)}{k_a^2-k_m^2}\left[\cos\left(k_m\frac{L_a}{2}\right)-\cos\left(k_a\frac{L_a}{2}\right)\right] \qquad \text{(F.10)}$$

Therefore, the mode coefficients ($B_{x,mn}$) are given by

$$B_{x,mn} = \frac{-j\omega\varepsilon\cdot A_{mn}V_{0x}}{d_a k_n\cdot\left(k^2-k_{mn}^2\right)}\cdot\frac{4\,\mathrm{sinc}\left(k_n\frac{W_a}{2}\right)\sin\left(\frac{n\pi}{2}\right)\cos\left(\frac{m\pi}{2}\right)}{\sin\left(k_a\frac{L_a}{2}\right)}\cdot\frac{k_a\left[\cos\left(k_m\frac{L_a}{2}\right)-\cos\left(k_a\frac{L_a}{2}\right)\right]}{k_a^2-k_m^2}$$

(F.11)

Similarly, the mode coefficients ($B_{y,mn}$) are given by

$$B_{y,mn} = \frac{j\omega\varepsilon \cdot A_{mn} V_{0y}}{d_a k_m \cdot \left(k^2 - k_{mn}^2\right)} \cdot \frac{4\text{sinc}\left(k_m \frac{W_a}{2}\right)\sin\left(\frac{m\pi}{2}\right)\cos\left(\frac{n\pi}{2}\right)}{\sin\left(k_a \frac{L_a}{2}\right)} \cdot \frac{k_a\left[\cos\left(k_n \frac{L_a}{2}\right) - \cos\left(k_a \frac{L_a}{2}\right)\right]}{k_a^2 - k_n^2} \quad \text{(F.12)}$$

.

APPENDIX G: CALCULATION OF THE INPUT IMPEDANCE OF THE PATCH ANTENNA AT THE APERTURES ($Y_{x,ant}$, $Y_{y,ant}$)

$$Y_{x,ant} = \frac{\iiint H_x^* J_{mx} dv}{|V_{0x}|^2} \tag{G.1}$$

where

$$H_x = \sum_m \sum_n A_{mn} B_{x,mn} k_n \cos(k_m x) \sin(k_n y) \tag{G.2}$$

and

$$J_{mx} = \frac{-2V_{0x}}{d_a W_a} \frac{\sin\left[k_a\left(\frac{L_a}{2} - \left|x - \frac{a}{2}\right|\right)\right]}{\sin\left(k_a \frac{L_a}{2}\right)}; \quad \begin{matrix} \frac{b-W_a}{2} \le y \le \frac{b+W_a}{2} \\ \frac{a-L_a}{2} \le y \le \frac{a+L_a}{2} \\ 0 \le z \le d_a \end{matrix}$$

$$= 0; \quad \text{otherwise} \tag{G.3}$$

Substituting (G.1) and (G.2) into (G.3) gives

$$Y_{x,ant} = \frac{-2V_{0x}}{d_a W_a |V_{0x}|^2 \sin\left(k_a \frac{L_a}{2}\right)} \cdot$$

$$\int_{\frac{a-L_a}{2}}^{\frac{a+L_a}{2}} \int_{\frac{b-W_a}{2}}^{\frac{b+W_a}{2}} \int_0^{d_a} \sum_m \sum_n A_{mn} B_{x,mn}^* k_n \cos(k_m x) \sin(k_n y) \cdot$$

$$\sin\left[k_a\left(\frac{L_a}{2} - \left|x - \frac{a}{2}\right|\right)\right] dx dy dz \tag{G.5}$$

Performing the integration with respect to variable z and changing the order of summation and integration gives

$$Y_{x,ant} = \sum_m \sum_n \frac{-2V_{0x} A_{mn} B^*_{x,mn} k_n}{W_a |V_{0x}|^2 \sin\left(k_a \frac{L_a}{2}\right)} \cdot$$

$$\int_0^a \int_0^b \cos(k_m x) \sin(k_n y) \cdot \sin\left[k_a \left(\frac{L_a}{2} - \left|x - \frac{a}{2}\right|\right)\right] dx dy$$

$$= \sum_m \sum_n \frac{-2V_{0x} A_{mn} B^*_{x,mn} k_n}{W_a |V_{0x}|^2 \sin\left(k_a \frac{L_a}{2}\right)} \underbrace{\int_0^a \sin(k_n y)\, dy}_{I_1} \cdot \underbrace{\int_0^b \sin\left[k_a \left(\frac{L_a}{2} - \left|x - \frac{a}{2}\right|\right)\right] \cos(k_m x)\, dx}_{I_2} \tag{G.6}$$

The value of integrals I_1 and I_2 have been evaluated in Appendix E and are given by

$$I_1 = \frac{2}{k_n} \sin\left(k_n \frac{W_a}{2}\right) \sin\left(\frac{n\pi}{2}\right) \tag{G.7}$$

$$I_2 = \frac{2 k_a \cos\left(\frac{m\pi}{2}\right)}{k_a^2 - k_m^2} \left[\cos\left(k_m \frac{L_a}{2}\right) - \cos\left(k_a \frac{L_a}{2}\right)\right] \tag{G.8}$$

Substituting I_1, I_2 and the expression for $B_{x,mn}$ which is given by

$$B_{x,mn} = \frac{-j\omega\varepsilon \cdot A_{mn} V_{0x}}{d_a k_n \cdot \left(k^2 - k_{mn}^2\right)} \cdot \frac{4 \operatorname{sinc}\left(k_n \frac{W_a}{2}\right) \sin\left(\frac{n\pi}{2}\right) \cos\left(\frac{m\pi}{2}\right)}{\sin\left(k_a \frac{L_a}{2}\right)} \cdot \frac{k_a \left[\cos\left(k_m \frac{L_a}{2}\right) - \cos\left(k_a \frac{L_a}{2}\right)\right]}{k_a^2 - k_m^2} \tag{G.9}$$

into (G.6), the expression for the input impedance is given by

$$Y_{x,ant} = \sum_m \sum_n \frac{16 \cdot j\omega\varepsilon \cdot A_{mn}^2}{d_a\left((k^*)^2 - k_{mn}^2\right)} \cdot$$

$$\left\{ \frac{\operatorname{sinc}\left(k_n \frac{W_a}{2}\right) \sin\left(\frac{n\pi}{2}\right) \cos\left(\frac{m\pi}{2}\right)}{\sin\left(k_a \frac{L_a}{2}\right)} \cdot \frac{k_a\left[\cos\left(k_m \frac{L_a}{2}\right) - \cos\left(k_a \frac{L_a}{2}\right)\right]}{k_a^2 - k_m^2} \right\}^2 \quad \text{(G.10)}$$

Similarly, the input impedance $Y_{y,ant}$ is given by

$$Y_{y,ant} = \sum_m \sum_n \frac{16 \cdot j\omega\varepsilon \cdot A_{mn}^2}{d_a\left[\omega^2 - \omega_{mn}^2\left(1 + j\delta_{eff} \frac{\omega^2}{\omega_{mn}^2}\right)\right]} \cdot$$

$$\left\{ \frac{\operatorname{sinc}\left(k_m \frac{W_a}{2}\right) \sin\left(\frac{m\pi}{2}\right) \cos\left(\frac{n\pi}{2}\right)}{\sin\left(k_a \frac{L_a}{2}\right)} \cdot \frac{k_a\left[\cos\left(k_n \frac{L_a}{2}\right) - \cos\left(k_a \frac{L_a}{2}\right)\right]}{k_a^2 - k_n^2} \right\}^2 \quad \text{(G.11)}$$

APPENDIX H: CALCULATION OF EQUIVALENT EFFECTIVE AND RELATIVE PERMITTIVITY

In order to account for the effect of the radome in the theoretical models of the cross-aperture coupled patch antenna, the quasi static value of the effective permittivity of a single equivalent homogeneous dielectric representing the substrate-superstrate double layer, must first be calculated. As the effective permittivity is also dependent on the width of the microstrip line, the calculation has to be performed separately with respect to both the x and y directions resulting in $\varepsilon_{effx}'(0)$ and $\varepsilon_{effy}'(0)$. The calculation of these values can be carried out by the application of the conformal mapping technique [Wheeler 1964 and Svacina 1992].

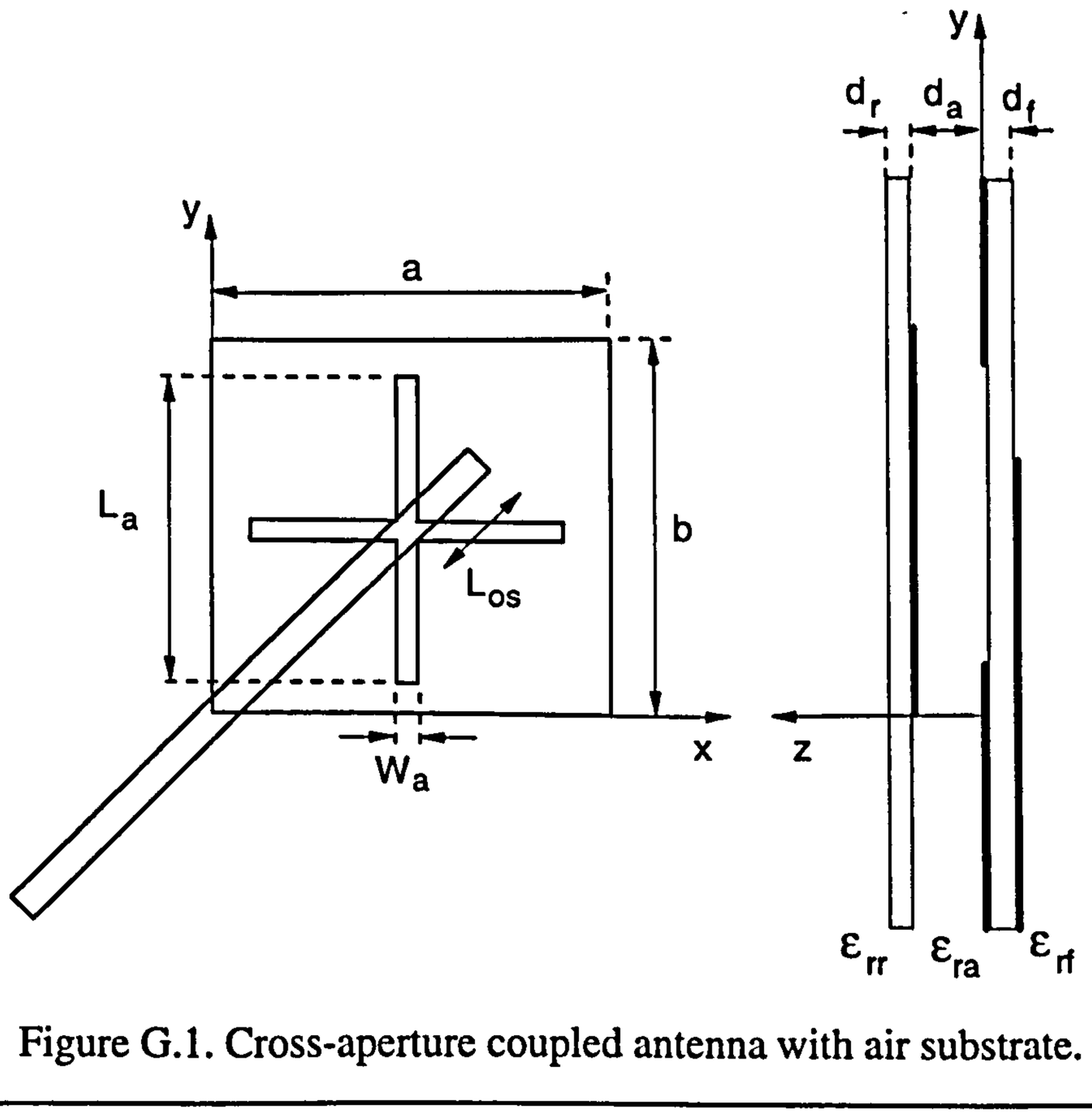

Figure G.1. Cross-aperture coupled antenna with air substrate.

Using the notation for the design parameters as shown in Figure H.1, this method gives the following expression for the quasi-static effective permittivity of the homogeneous single layer in the x direction:

$$\varepsilon_{effx}^{'}(0)=\varepsilon_{ra}q_{1x}+\varepsilon_{rr}\frac{(1-q_{1x})^2}{\varepsilon_{rr}(1-q_{1x}-q_{2x})+q_{2x}} \tag{H.1}$$

where q_{1x} and q_{2x} are the filling factors as given by

$$q_{1x}=1-\frac{1}{2}\cdot\frac{\ln\left(\frac{\pi}{d_a}w_x-1\right)}{\frac{w_x}{d_a}} \tag{H.2}$$

$$q_{2x}=1-q_{1x}-\frac{1}{2}\cdot\frac{h-v_x}{w_x}\cdot\ln\left[\pi\frac{w_x}{d_a}\frac{\cos\left(\frac{v_x}{2}\cdot\frac{\pi}{d_a}\right)}{\pi\left(\frac{1}{2}+\frac{d_r}{d_a}\right)+\frac{v_x}{2}\cdot\frac{\pi}{d_a}}+\sin\left(\frac{v_x}{2}\cdot\frac{\pi}{d_a}\right)\right] \tag{H.3}$$

where w_x and v_x are given by the following formulas

$$w_x=b+\frac{2d_a}{\pi}\ln\left[17.08\cdot\left(\frac{b}{2d_a}+0.92\right)\right] \tag{H.4}$$

$$v_x=2\frac{d_a}{\pi}\arctan\left(\frac{\pi\cdot\frac{d_r}{d_a}}{\frac{\pi}{2}\frac{w_x}{d_a}-2}\right) \tag{H.5}$$

The value of effective permittivity at a certain frequency is given by [Kirschning and Jansen 1982]

$$\varepsilon_{effx}^{'}=\varepsilon_{ra}^{'}-\frac{\varepsilon_{ra}^{'}-\varepsilon_{effx}^{'}(0)}{1+P(f)} \tag{H.6}$$

where ε'_{ra} is an equivalent relative permittivity of the antenna substrate-superstrate double layer. The expression for the function *P(f)* is given in Appendix D. The value of the quasi static equivalent effective permittivity ($\varepsilon'_{effy}(0)$) in the *y* direction can be similarly calculated by substituting *a* into the above expressions in place of *b*.

The equivalent relative permittivity (ε'_{ra}) can be calculated based on the equivalence between a multi-layer microstrip line and a normal line using the value of the equivalent effective permittivity [Zhong et al. 1994]. In order to avoid having two values of equivalent relative permittivity depending upon the direction, the average of $\varepsilon'_{effx}(0)$ and $\varepsilon'_{effy}(0)$ is used to obtain ε'_{ra} as given by

$$\varepsilon'_{ra} = \frac{\varepsilon'_{effx}(0) + \varepsilon'_{effy}(0) - 1 + A}{1 + A} \qquad A = \left(1 + \frac{24 d_a}{a+b}\right)^{-\frac{1}{2}} \tag{H.7}$$

Once the values of equivalent effective and relative permittivity are known, the transmission line method and the cavity resonator model, as described in Chapters four and five, can be adapted to the structure shown in Figure H.1 by using ε'_{effx}, ε'_{effy}, and ε'_{ra} in the expressions in place of ε_{effx}, ε_{ffy} and ε_{ra}.